NATIONAL CENTER FOR EARTHQUAKE
ENGINEERING RESEARCH
State University of New York at Buffalo

1:4 SCALE MODEL STUDIES OF ACTIVE TENDON SYSTEMS AND ACTIVE MASS DAMPERS FOR ASEISMIC PROTECTION

by

A. M. Reinhorn, T. T. Soong, R. C. Lin and Y. P. Wang
Department of Civil Engineering
State University of New York at Buffalo
Buffalo, NY 14260

Y. Fukao, H. Abe and M. Nakai
Takenaka Komuten Construction Co.
21-1, 8 Chome, Ginza
Chuo-ku, Tokyo, Japan

Technical Report NCEER-89-0026

November 22, 1989

This research was conducted at the State University of New York at Buffalo and Takenaka Komuten Construction Co. and was partially supported by the National Science Foundation under Grant No. ECE 86-07591.

NOTICE

This report was prepared by State University of New York at Buffalo and Takenaka Komuten Construction Co. as a result of research sponsored by the National Center for Earthquake Engineering Research (NCEER). Neither NCEER, associates of NCEER, its sponsors, State University of New York at Buffalo, Takenaka Komuten Construction Co., nor any person acting on their behalf:

a. makes any warranty, express or implied, with respect to the use of any information, apparatus, method, or process disclosed in this report or that such use may not infringe upon privately owned rights; or

b. assumes any liabilities of whatsoever kind with respect to the use of, or the damage resulting from the use of, any information, apparatus, method or process disclosed in this report.

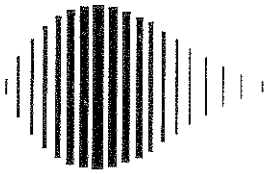

1:4 SCALE MODEL STUDIES OF ACTIVE TENDON SYSTEMS AND ACTIVE MASS DAMPERS FOR ASEISMIC PROTECTION

by

A.M. Reinhorn[1], T.T. Soong[2], R.C. Lin[3], Y.P. Wang[4],

and

Y. Fukao[5], H. Abe[6], M. Nakai[7]

November 22, 1989

Technical Report NCEER-89-0026

NCEER Contract Numbers 87-2001 and 88-2001

NSF Master Contract Number ECE 86-07591

1 Associate Professor, Dept. of Civil Engineering, State University of New York at Buffalo
2 Professor, Dept. of Civil Engineering, State University of New York at Buffalo
3 Research Associate, Dept. of Civil Engineering, State University of New York at Buffalo
4 Graduate Student, Dept. of Civil Engineering, State University of New York at Buffalo
5 Chief Research Engineer, Takenaka Komuten Construction Co., Tokyo, Japan
6 Research Engineer, Takenaka Komuten Construction Co., Tokyo, Japan

NATIONAL CENTER FOR EARTHQUAKE ENGINEERING RESEARCH
State University of New York at Buffalo
Red Jacket Quadrangle, Buffalo, NY 14261

PREFACE

The National Center for Earthquake Engineering Research (NCEER) is devoted to the expansion and dissemination of knowledge about earthquakes, the improvement of earthquake-resistant design, and the implementation of seismic hazard mitigation procedures to minimize loss of lives and property. The emphasis is on structures and lifelines that are found in zones of moderate to high seismicity throughout the United States.

NCEER's research is being carried out in an integrated and coordinated manner following a structured program. The current research program comprises four main areas:

- Existing and New Structures
- Secondary and Protective Systems
- Lifeline Systems
- Disaster Research and Planning

This technical report pertains to Program 2, Secondary and Protective Systems, and more specifically, to protective systems. Protective Systems are devices or systems which, when incorporated into a structure, help to improve the structure's ability to withstand seismic or other environmental loads. These systems can be passive, such as base isolators or viscoelastic dampers; or active, such as active tendons or active mass dampers; or combined passive-active systems.

In the area of active systems, research has progressed from the conceptual phase to the implementation phase with emphasis on experimental verification. As the accompanying figure shows, the experimental verification process began with a small single-degree-of-freedom structure model, moving to larger and more complex models, and finally, to full-scale models.

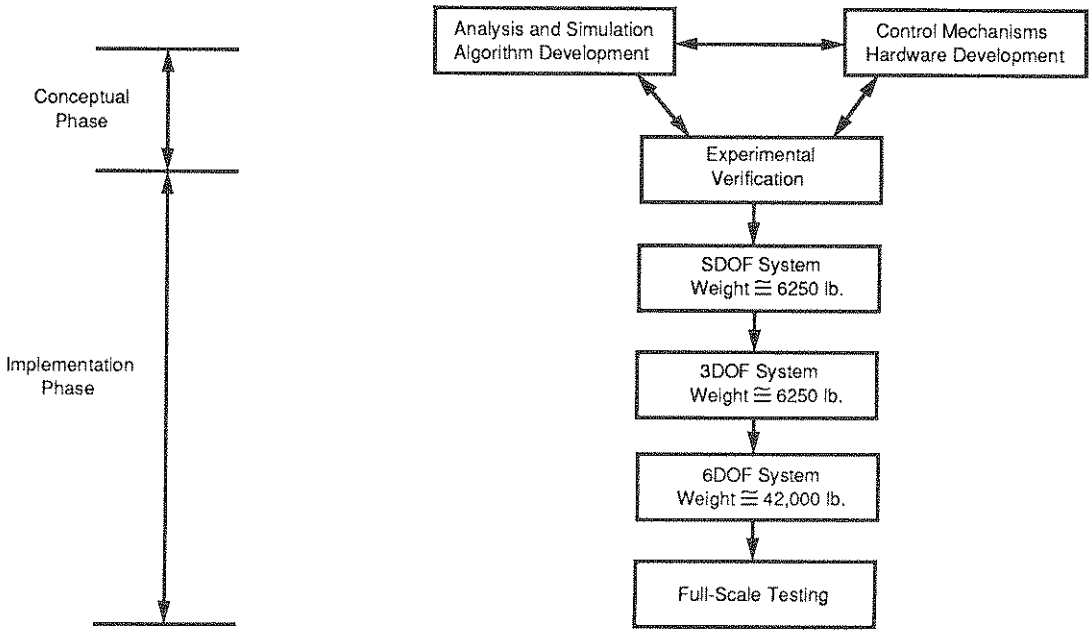

In the area of active systems, research has progressed from the conceptual phase to the implementation phase with emphasis on experimental verification. As the accompanying figure shows, the experimental verification process began with a small single-degree-of-freedom structure model, moving to larger and more complex models, and finally, to full-scale models.

The control experiments involving the 42,000 pound six-degree-of-freedom structural model were completed in February, 1989. Two active control systems, an active tendon system and an active mass damper, were tested and their performance compared. The results of this work are presented in this report which represent a considerably expended effort in comparison with earlier experiments. Additionally, a large number of investigators were involved; they represent researchers from Takenaka Corporation, Kayaba Industry, and MTS Systems Corporation as well as from the University at Buffalo.

As the preceding figure indicates, the next step in this research program is full-scale testing. Efforts in this direction are underway and more details of the full-scale testing plan are described in this report.

ABSTRACT

The feasibility of control of structures during transient disturbances, such as earthquakes or wind has been investigated intensively for almost two decades. Following the initial steps of J.T.P. Yao, a large number of researchers have suggested various control algorithms which can be implemented by mechanical devices attached to building structures. Comprehensive reviews of active structural control have shown that among most prominent devices are the active tendon system (ATS) and the active mass damper (AMD).

The ATS uses either prestressed cables or diagonal bracings which can be activated axially by servo-controlled hydraulic or electromagnetic actuators. The system seems attractive to engineers since it is based on diagonal structural elements which already exist in many structures or are added usually for passive stiffening or strengthening. Extensive analyses showed that the active tendon system provides a feasible solution in reducing the vibrations of *slender structures*, *tall buildings*, *cable stayed bridges*, and *off-shore structures*.

The active mass damper (AMD) is a derivation of passive devices, i.e., the tuned mass dampers (TMD), which are presently used in several tall building structures for motion control during strong winds. A large mass is placed on an upper story of a building, is connected to the structure via actuators or springs and is free to slide on a smooth surface. A hydraulic power source moves the mass which in turn transmits forces to the structure which reduces structural vibrations. Experimental studies of AMD systems were performed in which model structures of three to four stories were bolted to shaking tables and controlled using experimental reduced scale dampers during simulated earthquake motions, thus proving the applicability of such dampers to aseismic protection in addition to wind vibration reductions.

Since 1982, a comprehensive experimental study has been designed and carried out, by the first two authors and their associates, to study the feasibility of active tendon control, (ATS), using a series of carefully calibrated structural models. The model structures increased in weight and complexity as the experiments progressed from stage 1 to stage 3, so that more control features could be incorporated into the experiments.

As a further step in the comprehensive study, a substantially larger and heavier six-story model structure was fabricated for stage 3 of the experiment and was used for a simultaneous experimental and analytical study of ATS and AMD controls. The six-story structure is also

a 1:4 scale welded space frame utilizing artificial mass simulation. Multiple tendon control was possible in this case, and the following arrangements were included in this phase of the experiment:

(1) A single actuator is placed at the base with diagonal tendons connected to a single floor.
(2) A single actuator is placed at the base with tendons connected simultaneously to two floors, thus applying proportional control to the structure.
(3) Two actuators are placed at different locations of the structure with two sets of tendons acting independently.

The important feature at this stage was the testing of the second control system developed by Takenaka Corporation and Kayaba Industries, an active mass damper (AMD) on the same model structure, thus allowing a performance comparison of the two systems. Several control algorithms were considered and modifications of the initial AMD were implemented to reduce the energy consumption, to improve recentering capability and to increase performance in the higher modes.

This report presents the control systems considered in this stage, the test set-up, the specific optimal closed loop algorithms used in the control, and the theoretical and experimental results. Extensive discussions accompany the response results for the systems considered. The report concludes with a comparison of the two systems, which proves again the feasibility of active control using either one of them.

ACKNOWLEDGEMENTS

The studies carried in this report were supported by grants from the National Center for Earthquake Engineering Research which in turn is supported by U.S. National Science Foundation and the State of New York, from MTS, Machine Testing Systems Corp., Minneapolis, U.S.A., and from Takenaka Construction Company and Kayaba Industries, Tokyo, Japan. All the support is greatly acknowledged.

The authors wish to express their gratitude to the participants in the test preparation and evaluations, **Mr. Haniuda** from Kayaba Industries, Japan, and **Mr. A. Clark, Mr. R. Pulkrabek, Mr. N. Peterson** from MTS Corp., U.S.A. Special acknowledgments are due to **Mr. M. Pitman**, Head Technical Operator, **Mr. D.Walch** and **Mr. R. Cizdziel**, for their knowledgeable performances in carrying the preparation of tests set up, instrumentation, and operation of the complicated equipment. The authors acknowledge the thorough work of **Ms. M. Chastain** who typed and produced this report.

TABLE OF CONTENTS

SECTION	TITLE	PAGE
1	INTRODUCTION	1-1
2	TEST SET-UP	2-1
2.1	Overview	2-1
2.2	Test Components	2-1
2.3	Base Motion	2-19
2.4	Experimental Program	2-26
3	CONTROL ALGORITHMS	3-1
3.1	Control Algorithm for Active Tendon System (ATS)	3-1
3.1.1	Time Delay Compensation	3-3
3.2	Control Algorithm for the Active Mass Damper (AMD) System	3-7
4	EXPERIMENTAL STUDY	4-1
4.1	Identification of Structure's Parameters	4-1
4.2	Evaluation of Time Delays (ATS)	4-7
4.3	Response of Controlled Structure	4-9
4.3.1	Response In "Strong" Direction	4-9
4.3.1.1	Response With ATS Control	4-9
4.3.1.1.1	Control Parameters	4-9
4.3.1.1.2	Structural Response of Controlled Structure	4-11
4.3.1.1.3	Comparison of Experimental Response With Analytical Studies	4-11
4.3.1.1.4	Comparison of Various Tendons Configurations	4-22
4.3.1.1.5	ATS Control Efficiency	4-22
4.3.1.2	Response With AMD Control	4-23
4.3.1.2.1	Samples of Experimental Results	4-23
4.3.1.2.2	Efficiencies of Various Control Cases	4-29
4.3.1.2.3	Comparison of Experimental Results With Theoretical Results For AMD	4-41
4.3.2	Response in "Weak" Direction	4-44
4.3.2.1	Response With ATS Control	4-44
4.3.2.1.1	Control Parameters	4-59
4.3.2.1.2	Structural Response and Comparison to Analytical Predictions	4-59
4.3.2.1.3	Comparison of Single Tendon System Versus Two Tendon System (Independent Control)	4-59
4.3.2.1.4	Control Efficiency	4-78
4.3.2.2	Response With AMD Control	4-78
4.3.2.2.1	Samples of Experimental Result	4-78
4.3.2.2.2	Efficiency of Various Control Cases	4-87
4.3.2.2.3	Comparison of Controlled Responses With Theoretical Prediction (in the weak direction)	4-94

SECTION	TITLE	PAGE
5	ACTIVE MASS DAMPER - ACTIVE TENDON PERFORMANCE COMPARISONS	5-1
6	CONCLUDING REMARKS	6-1
7	REFERENCES	7-1
	APPENDIX A - SERVO-CURRENT IN AMD ALGORITHM	A-1
	APPENDIX B - SAMPLE COMPUTER PROGRAM FOR ATS	B-1

LIST OF ILLUSTRATIONS

FIGURE	TITLE	PAGE
2.1	The Model Structure	2-2
2.2	Model Structure	2-3
2.3	View of Active Tendon Systems	2-5
2.4	Typical Arrangements of Tendons (ATS)	2-6
2.5	ATS with Actuator, Transverse Frame and Cables	2-7
2.6	Block Diagrams of Control for Active Tendon Systems	2-9
2.7	Set-Up of AMD System	2-10
2.8	The AMD System	2-11
2.9	View of AMD System	2-12
2.10	Block Diagram of AMD Control System	2-14
2.11	View of University at Buffalo Shaking Table	2-16
2.12	View of Measurements Set-Up	2-18
2.13	Earthquake Acceleration in Strong Direction (25% El Centro)	2-21
2.14	Earthquake Acceleration in Weak Direction	2-22
2.15	Comparison of Base Acceleration Input in Frequency Domain (El Centro)	2-23
2.16	Comparison of Base Acceleration Input in Frequency Domain (Hachinohe)	2-24
2.17	Comparison of Base Acceleration Input Frequency Domain (Miyagioki)	2-25
3.1	Phasor Diagram of Feedback Forces and Responses	3-5
3.2	Schematic Illustration of AMD System	3-8
3.3	Equivalent Models of the Structure	3-12
4.1	Absolute Acceleration Frequency Transfer Functions Under White Noise Input	4-3
4.2	Identification of Time Delay From Slope of Phase Lag	4-8
4.3	Comparisons of Values β Values	4-10
4.4	First Floor Relative Displacement Responses	4-12
4.5	Second Floor Relative Displacement Responses	4-13
4.6	Third Floor Relative Displacement Responses	4-14
4.7	Fourth Floor Relative Displacement Responses	4-15
4.8	Fifth Floor Relative Displacement Responses	4-16
4.9	Sixth Floor Relative Displacement Responses	4-17
4.10	Absolute Acceleration Responses in Frequency Domain (Experimental)	4-18
4.11	Peak Values of Relative Displacement in Strong Direction (25% El Centro Excitation)	4-19

FIGURE	TITLE	PAGE
4.12	Comparisons of Single Force Control in Strong Direction	4-20
4.13	Comparisons of Proportional Control in Strong Direction	4-21
4.14	Absolute Acceleration Responses in Frequency Domain (Theoretical)	4-24
4.15	Relative Displacement Response With AMD Control (El Centro 25% Excitation	4-25
4.16	Absolute Acceleration Response With AMD Control (El Centro 25% Excitation)	4-26
4.17	Control Resources For KYB-M Regulator	4-27
4.18	Transfer Functions of the Absolute Acceleration (White Noise 0.04G Excitation)	4-28
4.19	The Peak Values of Relative Displacement (El Centro 25% Excitation)	4-30
4.20	Time Histories of the Relative Displacement at the Top Floor and the Percentages of the Displacements Reductions (El Centro 25% Excitation)	4-31
4.21	Comparison by the Regulators Depending on the Weighting Magnitudes (El Centro 25% Excitation)	4-33
4.22	Relationships Between the Displacement Reductions and the Maximum Control Forces and the Maximum Mass Stroke (El Centrol 25% Excitation)	4-34
4.23	Effects of Using the Middle (3rd) Floor Information (El Centro 25% Excitation)	4-35
4.24	Effects of Added Mass Weight to the AMD (El Centro 25% Excitation)	4-36
4.25	Effects of Adding the Stiffness to the AMD (El Centro 25% Excitation)	4-38
4.26	Comparison of Efficiencies Versus the Objective Variables (El Centro 25% Excitation)	4-39
4.27	Comparison Between the Absolute Displacement Control and the Relative Displacement Control (El Centro 25% Excitation)	4-40
4.28	Experimental and Theoretical Results Without Control (El Centro 25% Excitation)	4-42
4.29	Comparison Between Experimental and Theoretical Results With Control (25% El Centrol Excitation)	4-43
4.30(a)	The Peak Relative Displacement Under 25% El Centro Excitation	4-47
4.30(b)	The Peak Relative Displacement Under 25% El Centro Excitation	4-48
4.31	First Floor Relative Displacement (25% El Centro)	4-49
4.32	Second Floor Relative Displacement (25% El Centro)	4-50
4.33	Third Floor Relative Displacement (25% El Centro)	4-51
4.34	Fourth Floor Relative Displacement (25% El Centro)	4-52
4.35	Fifth Floor Relative Displacement (25% El Centro)	4-53

FIGURE	TITLE	PAGE
4.36	Sixth Floor Relative Displacement (25% El Centro)	4-54
4.37	Fourier Spectrum of Acceleration Responses	4-55
4.38	Fourier Spectrum of Acceleration Responses (Simulation Under 25% El Centro)	4-56
4.39	Control Force (Experimental Under 25% El Centro)	4-57
4.40	Control Force (Simulation Under 25% El Centro)	4-58
4.41	Sixth Floor Relative Displacement in Weak Direction (El Centro)	4-62
4.42	Sixth Floor Relative Displacement in Weak Direction (Hachinohe)	4-63
4.43	Sixth Floor Relative Displacement in Weak Direction (Miyagioki)	4-64
4.44	Peak Relative Displacement For Case W1C1	4-65
4.45	The Peak Relative Displacement For 20% El Centro, $\beta = 4$	4-66
4.46	The Peak Relative Displacement For 20% El Centro, $\beta = 8$	4-67
4.47	The Peak Relative Displacement For 30% Hachinohe, $\beta = 4$	4-68
4.48	The Peak Relative Displacement For 30% Hachinohe, $\beta = 8$	4-69
4.49	The Peak Relative Displacement For 40% Miyagioki, $\beta = 4$	4-70
4.50	The Peak Relative Displacement For 40% Miyagioki, $\beta = 9$	4-71
4.51	Frequency Transfer Function of Absolute Acceleration in Weak Direction	4-72
4.52	Frequency Transfer Function of Sixth Floor Absolute Acceleration in Weak Direction For 30% Hachinohe	4-73
4.53	Frequency Transfer Function of Sixth Floor Absolute Accelertion in Weak Direction For 40% Miyagioki	4-74
4.54	Comparison of 1TS vs 2TS in Weak Direction For 20% El Centro	4-75
4.55	Comparison of 1TS vs 2TS in Weak Direction For 30% Hachinohe	4-76
4.56	Comparison of 1TS vs 2TS in Weak Direction For 40% Miyagioki	4-77
4.57	Time Histories of the Relative Displacement (20% El Centro Excitation)	4-80
4.58	Time Histories of the Absolute Acceleration (20% El Centro Excitation)	4-81
4.59	Time Histories Under Control (20% El Centro Excitation)	4-83
4.60	Time Histories of the Relative Displacement at the Top Floor	4-84
4.61	The Peak Relative Displacements in Weak Direction	4-85

FIGURE	TITLE	PAGE
4.62	Transfer Functions of the Absolute Acceleration in Weak Direction (White Noise 0.02G Excitation)	4-86
4.63	Time Histories of the Relative Displacement at the Top Floor (20% El Centro Excitation)	4-88
4.64	Comparison by the Regulators Depending on the Weighting Magnitudes (20% El Centro Excitation)	4-91
4.65	Relationships Between the Displacement Reduction and the Maximum Control Forces or the Maximum Mass Stroke (20% El Centro Excitation)	4-89
4.66	Effects of Using Both the Top (Sixth) and the Middle (Third) Floor Information	4-90
4.67	Effects of Changing the Mass Weight (20% El Centro Excitation)	4-91
4.68	Effects of Adding the Stiffness to the AMD (20% El Centro Excitation)	4-92
4.69	Comparison by the Objective Variables (20% El Centro Excitation)	4-93
4.70	Comparison Between Experimental and theoretical Results Without Control (20% El Centro Excitation)	4-95
4.71	Comparison Between Experimental and Theoretical Results Without Control (30% Hachinohe Excitation)	4-96
4.72	Comparison Between Experimental and Theoretical Results Without Control (40% Miyagioki Excitation)	4-97
4.73	Comparison Between Experimental and Theoretical Results With Control (20% El Centro Excitation)	4-98
4.74	Comparison Between Experimental and Theoretical Results With Control (30% Hachinohe Excitation)	4-99
4.75	Comparison Between Experimental and Theoretical Results With Control (40% Miyagioki Excitation)	4-100
4.76(a)	The Peak Relative Displacement Under 20% El Centro Excitation	4-101
4.76(b)	The Peak Relative Displacement Under 20% El Centro Excitation	4-102
4.77	The Peak Relative Displacement Under 30% Hachinohe Excitation	4-103
4.78	The Peak Relative Displacement Under 40% Miyagioki Excitation	4-104
4.79	First Floor Relative Displacement (20% El Centro)	4-110
4.80	Second Floor Relative Displacement (20% El Centro)	4-111
4.81	Third Floor Relative Displacement (20% El Centro)	4-112
4.82	Fourth Floor Relative Displacement (20% El Centro)	4-113
4.83	Fifth Floor Relative Displacement (20% El Centro)	4-114
4.84	Sixth Floor Relative Displacement (20% El Centro)	4-115
4.85	Fourier Spectrum of Acceleration Responses (Experiment Under 20% El Centro)	4-116
4.86	Fourier Spectrum of Acceleration Responses (Simulation Under 20% El Centro)	4-117
4.87	Control Force (Experiment Under 20% El Centro)	4-118

FIGURE	TITLE	PAGE
4.88	Control Force (Simulation Under 20% El Centro)	4-119
5.1	Response Parameters In Strong Direction	5-2
5.2	Control Parameter In Strong Direction	5-3
5.3	Response Parameters in Weak Direction	5-4
5.4	Control Parameters in Weak Direction	5-5

LIST OF TABLES

TABLE	TITLE	PAGE
2.1	Base Motion	2-20
2.2	Experimental Study in Strong Direction for ATS	2-27
2.3	Experimental Study in Weak Direction for ATS	2-28
2.4	Experimental Conditions in Both Directions for AMD	2-29
3.1	Numerical Data for the Structural Model (With AMD)	3-16
3.2	Properties of AMD System	3-17
4.1	Properties of Model Structure in Strong Direction	4-4
4.2	Properties of Model Structure in Weak Direction	4-5
4.3	Summary of Identification Tests of Model Structure	4-6
4.4	Summary of Experimental Results in Strong Direction (25% El Centro)	4-6
4.5	Experimental Responses to 25% El Centro Excitation (Strong Direction)	4-45
4.6	Theoretical Responses to 25% El Centro Excitation (Strong Direction)	4-46
4.7	Summary of Results in Weak Direction for One Actuator - On Tendon at First Floor (W1C1)	4-60
4.8	Summary of Results in Weak Direction (W2) for 20% El Centro	4-60
4.9	Summary of Results in Weak Direction (W2) for 30% Hachinohe	4-61
4.10	Summary of Results in Weak Direction (W2) for 40% Miyagioki	4-61
4.11	Experimental Responses to 20% El Centro Excitation (Weak Direction)	4-105
4.12	Theoretical Responses to 20% El Centro Excitation (Weak Direction)	4-106
4.13	Experimental Responses to 30% Hachinohe EW Excitation (Weak Direction)	4-107
4.14	Theoretical Responses to 30% Hachinohe EW Excitation (Weak Direction)	4-107
4.15	Experimental Responses to 40% Miyagioki EW Excitation (Weak Direction)	4-108
4.16	Theoretical Responses to 40% Miyagioki EW Excitation (Weak Direction	4-108

SECTION 1
INTRODUCTION

The feasibility of control of structures during transient disturbances, such as earthquakes or wind has been investigated intensively for almost two decades. Following the initial steps of Yao (1972), a large number of researchers have suggested various control algorithms which can be implemented by mechanical devices attached to building structures. Comprehensive reviews of active structural control [Reinhorn, Manolis (1985, 1989) and Soong (1988)] have shown that among most prominent devices are the active tendon system (ATS) and the active mass damper (AMD).

The ATS uses either prestressed cables or diagonal bracings which can be activated axially by servo-controlled hydraulic or electromagnetic actuators. The system seems attractive to engineers since it is based on diagonal structural elements which already exist in many structures or are added usually for passive stiffening or strengthening. Extensive analyses showed that the active tendon system provides a feasible solution in reducing the vibrations of *slender structures* [Roorda (1975), Nissim (1976), Yang and Giannopoulos (1978)], *tall buildings* [Roorda (1975), Yang and Giannopoulos (1978), Yang (1982), Yang and Samali (1983), Abdel-Rohman and Leipholz (1983), Yang and Lin (1983), Abdel-Rohman and Leipholz (1983), Yang and Lin (1983), Samali, Yang and Lin (1985), Samali, Yang and Yeh (1985), Abdel-Rohman (1987), Chung, Reinhorn and Soong (1988)], *cable stayed bridges* [Yang and Giannopoulos (1979) a, and b] and *off-shore structures* [Prucz, and Soong (1983), Reinhorn, Manolis and Wen (1985, 1987), Reinhorn, Soong and Manolis (1986) Reinhorn and Soong (1988)].

Research on active control has been performed continuously since 1976 at the State University of New York at Buffalo, when the practicability of active control for structures against wind and earthquake loads was first investigated. The first five years focused on analytical and simulation studies of control algorithms and related implementation problems such as time delay, on-line computation, inelastic structural behavior and the problem of modal control.

Since 1982, a comprehensive experimental study has been designed and carried out, by the first two authors and their associates, to study the feasibility of active tendon control, (ATS),

using a series of carefully calibrated structural models. The model structures increased in weight and complexity as the experiments progressed from stage 1 to stage 3, so that more control features could be incorporated into the experiments.

The model structure studied during the first stage was a three-story steel frame modeling a shear building by the method of mass simulation, with the top two floors rigidly braced to simulate a single-degree-of-freedom system. The model was similar in geometry, material properties and boundary conditions to a structural model extensively tested in several laboratories, and was approximately a 1:4 scaled model of a prototype structure (1:2 scaled model) that has also been extensively tested [Soong et.al., (1987)].

The model was mounted on the University at Buffalo's shaking table which supplied the base excitation. The control force was transmitted to the structure through two sets of diagonal prestressed tendons mounted on the side frames. In the experiment, the classical optimal closed-loop control algorithm was employed with time delay compensation.

Several significant features of the experiments are noteworthy: (i) they were carefully designed so that a realistic structural control situation could be investigated. Efforts towards this goal included making the model structure dynamically similar to a real structure, working with a carefully calibrated model, using realistic base excitation and requiring more realistic control forces, (ii) these experiments permitted a realistic comparison between analytical and experimental results, which made it possible to perform extrapolation to real structural behavior. Furthermore, important practical considerations such as time delay, robustness of control algorithms, modeling errors and structure-control system interactions could be identified and realistically assessed. Results of the studies performed in this stage were published in a report by Lin et. al. (1987).

At stage 2, rigid bracings on the top two floors of the model structure were removed in order to simulate a three-degree-of-freedom system. This multi-degree-of-freedom model provided opportunities for study and verification of a number of control features which were not possible in the stage 1 study. These included modal control, time delay in the modal space and control and observation spillover compensation. Moreover, further verification of simulation procedures could be carried out which gave added confidence in using simulation for extrapolating active control results to more complex situations. The control algorithms tested in this series of experiments included instantaneous optimal control and discrete-time control

algorithms, as well as the classical closed-loop optimal control. Experimental results compared favorably with analytical results obtained under the same conditions, and they showed that the motion of all three floors can be effectively controlled using a single actuator when control design is carefully carried out by accounting for the aforementioned practical consideration. Results of this stage were reported by Chung et. al. (1988).

The experimental studies of active tendon systems performed on small models have shown that the computational algorithms can be implemented using electrohydraulic actuators or pneumatic cushions and active tendons [Roorda (1980), Bouten and Meyr (1987), Chung, Reinhorn and Soong, (1986, 1988), Lin, Soong and Reinhorn (1987), Rodellar, Chung, Soong and Reinhorn (1987, 1989), Chung, Lin, Soong and Reinhorn (1989)]. However these implementations are conditionally feasible provided that a good identification of structural parameters can be performed and that the time delay which appear in the control mechanisms and electronic computations can be compensated [Chung, Reinhorn and Soong (1986, 1988), Lin, Soong and Reinhorn (1987), McGreevy, Soong and Reinhorn (1988)]. Several methods of compensation were suggested and implemented in experiments including a modification of control gains, by performing a phase shift of the measured state variables in the modal domain [Chung et. al. (1986, 1988, 1989), Lin et. al. (1987)] and by methods of updating the measured quantities kinematically and dynamically [McGreevy et. al. (1988)]. Among all the methods, the phase shift compensation in the modal domain proved to be most efficient and stable solution [McGreevy et. al. (1989)].

The inevitable errors from control and observation spillover have also been extensively analyzed and tested in the laboratory experiments. Methods of compensation were suggested to be used with the reduced order systems and found efficient in actual experiments [Chung (1989)]. The experiments using reduced scale structural models [Chung et. al. (1986), (1988) and (1989)] showed that the active tendon systems, using various algorithms, is adequate to reduce seismic response of the building structure. The tendon system has not been tested, however, for wind vibration reduction.

The active mass damper (AMD) is a derivation of passive devices, i.e., the tuned mass dampers (TMD), which are presently used in several tall building structures for motion control during strong winds [Petersen (1980), ENR (1977), McNamara (1977))]. A large mass is placed on an upper story of a building, is connected to the structure via actuators or springs and is free to slide on a smooth surface. A hydraulic power source moves the mass which in turn transmits

forces to the structure which reduces structural vibrations. A series of feasibility studies of semi-active dampers and fully active dampers were performed by Chang and Soong (1980), Abdel-Rohman (1984), Hrovat, Barek and Robins (1983) and Lund (1980).

Experimental studies of AMD systems were reported by Kuroiwa and Aizawa (1987) and Kobori (1987). Model structures of three to four stories were bolted to shaking tables and controlled using experimental reduced scale dampers during simulated earthquake motions, thus proving the applicability of such dampers to aseismic protection in addition to wind vibration reductions. Among initial problems encountered in the reduced model testing were the large power requirements and lack of recentering capabilities of the mass dampers.

Comparative analytical studies have also been carried out concerning relative merits associated with active tendon systems and active mass dampers for specific applications [(Abdel-Rohman (1987), Juang, Sae-Ung and Yang (1980), Samali, Yang and Lin (1985), Yang (1982), Sae-Ung and Yao (1978), Wiesner (1986)]. Yang and Lin (1983) concluded that both the active mass damper and the active tendon systems are equally efficient in reducing the seismic response, however, while the tendon system is insensitive to errors in damping and stiffness estimates, the AMD is sensitive to uncertainties in stiffness estimates. Yang and Lin (1982) showed analytically that under the same control objectives in an optimal critical-mode scheme, the ATS reduces the responses and the base shears better than the AMD in the higher modes of vibration. As indicated in [Yang (1982)], one of the inherent limitations associated with an AMD is that, since only one is likely to be used for economical reasons, it provides only a single point of control action and it usually acts at the top of a structure. Simulation results show that, under practical constraints, its effectiveness is mostly felt at the first fundamental frequency but less so at higher frequencies. A comparative study was made between an active tendon system and an active mass damper using the eight-story structure under an earthquake-like ground excitation [Yang (1982)]. When the tendons are attached at all floors, the results show that while the active tendon system is capable of suppressing peak amplitudes at several modal frequencies, the effect of the active mass damper is only felt at the first frequency. Abdel-Rohman (1987) noticed that while the ATS is very efficient in reducing the response, its performance is extremely sensitive to the time delay effect. At the same time the AMD seem to be efficient for free vibration control and less efficient for force vibrations due to an apparent reduction of the building stiffness, due to sensitivity of control parameters and due to the large strokes of mass movements and

associated power consumption. Using performance indexes, based on force efficiency and structure energy, Abdel-Rohman concluded that a combination of ATS and AMD are most desirable. All the comparisons made until now were analytical only and based on limited number of variables which influence the control efficiency.

As a further step in the comprehensive study at University of Buffalo, a substantially larger and heavier six-story model structure was fabricated for stage 3 of the experiment and was used for a simultaneous experimental and analytical study of ATS and AMD controls. There has been a significant industrial participation in this stage of the project. The main contributors are Takenaka Corporation and Kayaba Industries, Ltd. in Japan, and MTS Systems Corporation in the U.S. The six-story structure is also a 1:4 scale welded space frame utilizing artificial mass simulation. Multiple tendon control was possible in this case, and the following arrangements were included in this phase of the experiment:

(1) A single actuator is placed at the base with diagonal tendons connected to a single floor.

(2) A single actuator is placed at the base with tendons connected simultaneously to two floors, thus applying proportional control to the structure.

(3) Two actuators are placed at different locations of the structure with two sets of tendons acting independently.

The important feature at this stage was the testing of the second control system developed by Takenaka Corporation and Kayaba Industries, an active mass damper (AMD) on the same model structure, thus allowing a performance comparison of the two systems. Several control algorithms were considered and modifications of the initial AMD were implemented to reduce the energy consumption, to improve recentering capability and to increase performance in the higher modes.

This report presents the control systems considered in this stage, the test set-up, the specific optimal closed loop algorithms, used in the control and the theoretical and experimental results. Extensive discussions accompany the response results for the systems considered. The report concludes with a comparison of the two systems. The analytical study shows some

superiority for the ATS related to the kinematic reductions and power consumption while the experimental results show mixed results, i.e., the kinematic reduction is superior for the AMD and the power required for the ATS is much smaller than for the AMD.

SECTION 2
TEST SET-UP

2.1 Overview

The series of tests, for comparison of the two systems, was carried out in University at Buffalo laboratories using a scaled model structure which was shaken with various base motions on the earthquake simulator. This section describes the experimental components, the test set-up with the instrumentation, the base motion, and all the devices required for the implementation of the active control.

2.2 Test Components

The test set-up includes the model structure, the active tendon system (ATS), the active mass damper (AMD), the earthquake simulator (the shaking table), and necessary instrumentation to monitor the experiments.

(A) **The model structure** is a 1:4 scale, six-story, space frame as shown in Fig. 2.1. The three-bay frame in one direction and one bay in the other represent a typical "slice" of a full-scale prototype of a moment resisting frame of a building structure. The welded space frame was scaled utilizing the artificial mass simulation method for a total weight of 19,100 kgs (42,000 lbs). Fig. 2.2 shows several details of the 5.49m (18'-0") high model and its ballast concrete blocks used in the mass simulation. The long direction of the **slice** model 3.66m (12'-0") was designated as the **strong direction**, and the short one 1.22m (4'-0") was designated as the **weak direction**. Experiments were carried out in both directions to capture both the actual behavior of the prototype (**strong direction**) and the behavior of an extremely flexible hypothetical structure (**weak direction**). Removable diagonal bracings were installed in the plane frames parallel to one direction when the other direction was the major axis of shaking. With such bracings the structure behaves as a planar structure with very little or no transverse and torsional coupling. The frame was rigidly bolted through a rigid steel foundation to a heavy concrete block, placed on the shaking table to accommodate oversized models (see Fig. 2.1).

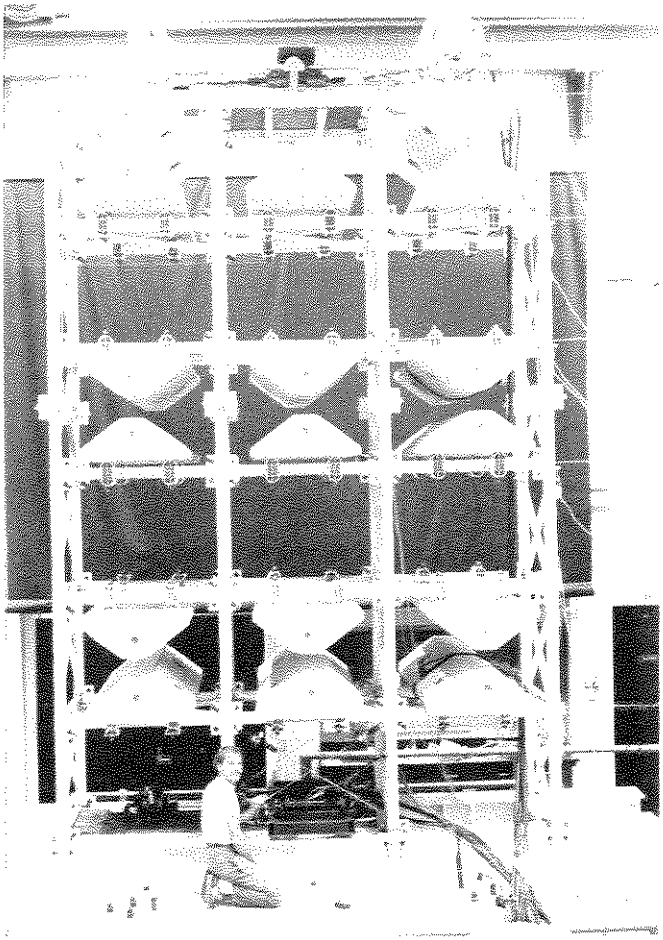

Figure 2.1 - The Model Structure.

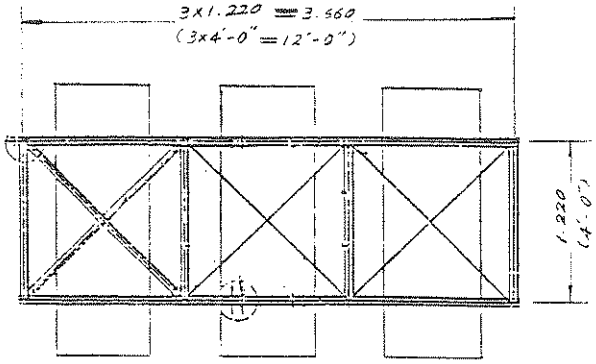

a) Top View

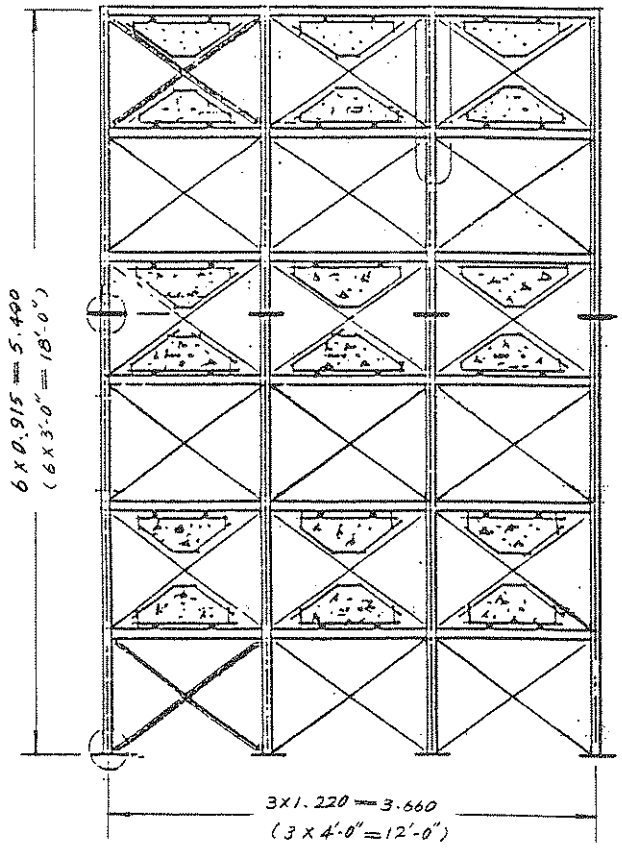

b) Side View

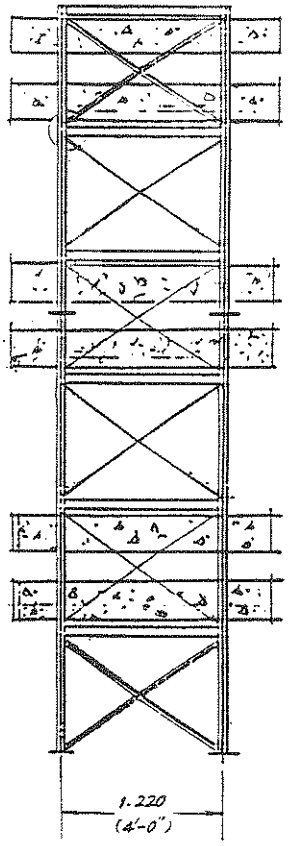

c) Front View

Specifications:

1. All structural bars are S3 x 5.7
2. All horizontal braces are L2 x 1 x 1/4, and all vertical braces are L1-1/2 x 1-1/2 x 1/4.
3. All ballast blocks are concrete 0.900 tons (Avg.) (2000lbs)

Figure 2.2 - Model Structure.

(B) **The active tendon system (ATS)** consisted of pretension diagonal tendon cables attached in the frame structure similar with the diagonal bracings (see Fig. 2.3) and continuously tensioned by a servo-controlled hydraulic actuator receiving its commands from a microcomputer.

The tendon system was installed in various bays of the frame to study the efficiency of the system (see Fig. 2.4). The system installed in one bay consists of two parallel active X-bracings, each installed in one of the parallel frames in the direction of shaking. The hydraulic actuator was installed in the center, between the two plane X-bracings, and was connected to the tendons through a horizontal transverse frame as shown in Fig. 2.5. The tendons, 7x9 - ϕ1/4" Stainless Aircord Cables were pretensioned to 910kgs (2,000 lbs) such that they remained in tension at all stages of operation of the control system.

The stiffness of the cables was measured under monotonically increasing load and under cyclic loading. The *cyclic stiffness*, relevant for the control case, is 3,245 kg/mm (28.11 kips/inch) for a 30.5mm/1 ft sample. The tendons were mounted in various configurations which provided the basic cases of investigation.

(1) A single tendon system with one actuator and the set of diagonal tendons was mounted at a single floor as shown in Figs. 2.4 (a) and 2.4 (c).

(2) A single actuator was placed at the base and two sets of tendons were braced to two different floors, thus applying proportional control forces (i.e., *proportional control*) as shown in Fig. 2.4 (b).

(3) Two actuators with two sets of tendons are placed at different stories acting independently (i.e., *independent control*) as shown in Fig. 2.4 (d).

The arrangements in Fig. 2.4 are all typical and representative for similar arrangements which were used in the testing program.

The actuators used in the ATS were sized to provide force capacity of 2.5 tons (5.5 kips) and a force rate of 5.6 tons/sec (12.3 kips/sec). The actuators, provided by MTS Systems Corporation, were provided with a servo-controlled system using a 3.95 liter/min (15 gpm) servo-valve providing a maximum piston velocity of 59 cm/sec (15 in/sec). The sizing of the actuators used a safety factor of 1.5 to 1.8 in respect to the expected requirements.

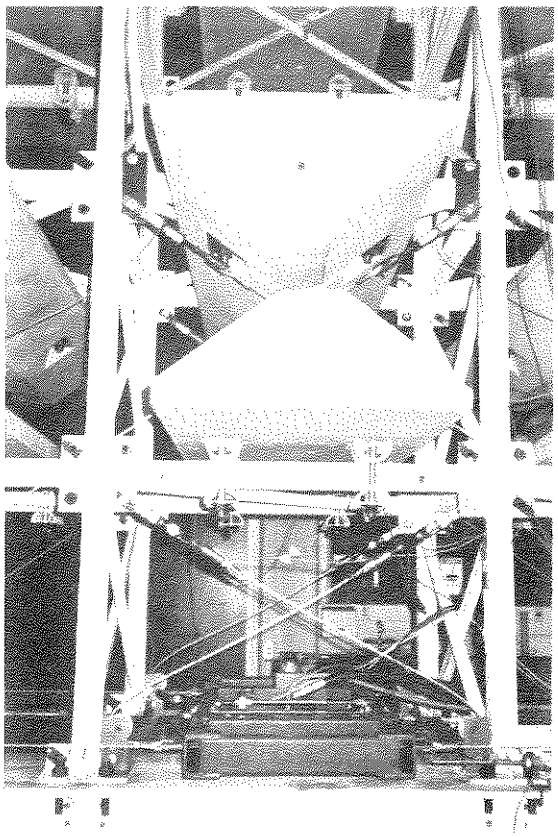

a) In Strong Direction

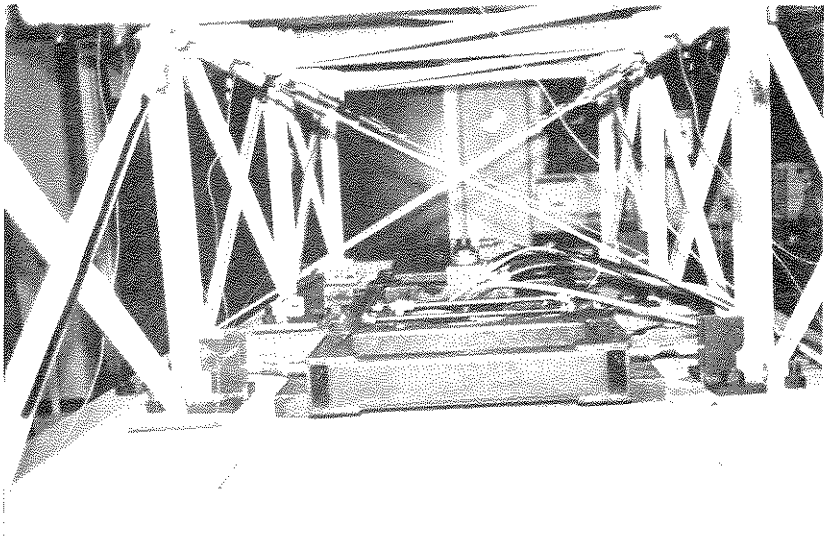

b) In Weak Direction

Figure 2.3 - View of Active Tendon System.

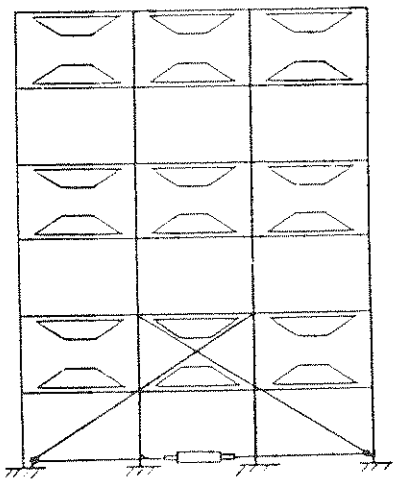

a) Single Force Control in Strong Direction

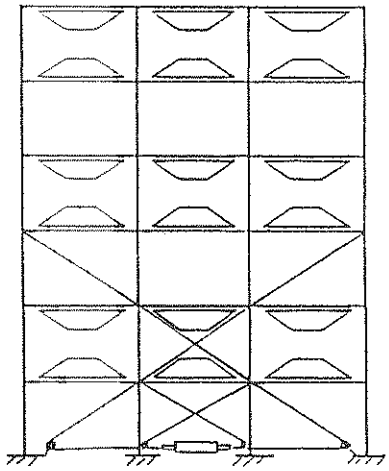

b) Proportional Control in Strong Direction

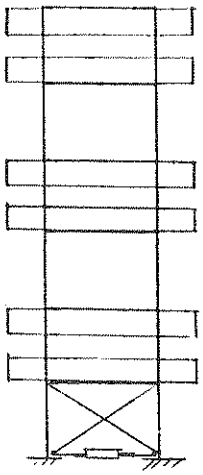

c) Single Force Control in Weak Direction

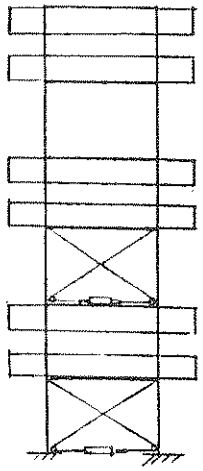

d) Two Controllers Independently Controlled in Weak Direction

Figure 2.4 - Typical Arrangements of Tendons (ATS).

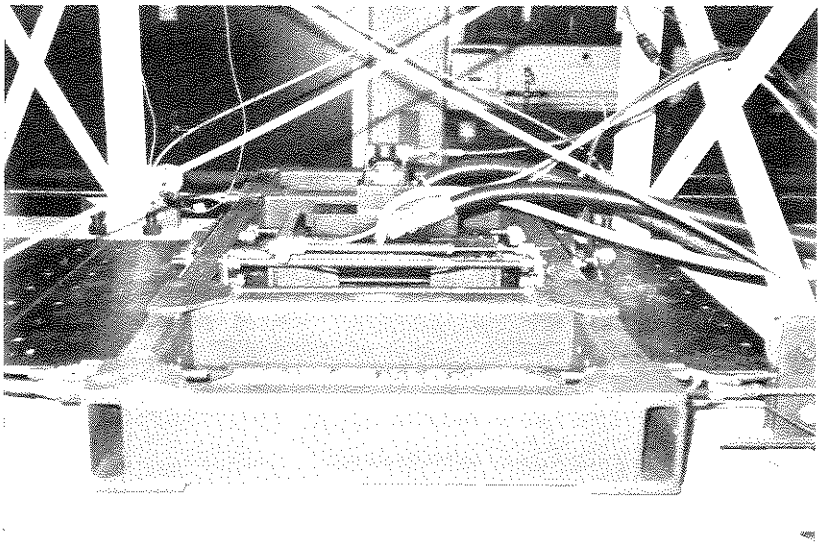

Figure 2.5 - ATS with Actuator, Transverse Frame and Cables.

The control system for the ATS is shown schematically in Fig. 2.6. The system includes besides the tendons and the hydraulic actuator the following:

(a) Displacement sensors attached at all six floors and velocity differentiates.
(b) A microcomputer (PC-Limited 286) equipped with A/D and D/A boards.
(c) A servo-valve controller for the hydraulic actuator.

The sensing devices included displacement transducers which are described in detail in the section on Instrumentation. The velocities required for the implementation of the control algorithms were obtained from the displacement measurements using generic analog differentiators.

The microcomputer, PC-Limited 286 used an 80286-12 MHz processor and an 80287-10 MHz co-processor. The unit used two Data Translation, DT-2801A boards with 16 floating (differential) A/D conversion channels and four D/A converters. The board can operate the 16 channels of A/D and the four D/A channels up to a speed of 1,964 samples per second. The actual operation speed was reduced to 200 samples per second dictated by the on-line computations. The analog signals were prefiltered by anti-aliasing, low pass filters, PCB Piezotronics, with a band of 0-50 Hz.

The performance of the on-line computing system were verified experimentally and adjusted to match the response time of the servo-valve of the control actuators, i.e. 12 msec., update.

(C) **The Active Mass Damper (AMD)** is a heavy mass guided on linear bearings and moved by a hydraulic actuator following commands from a microcomputer in a similar manner as the tendon system (ATS). The system is placed on the sixth floor of the model frame (top of the structure) as shown in Fig. 2.7. The system actually includes a moving mass which can be adjusted by addition or removal of steel plates, linear bearings, driving hydraulic cylinders, oil accumulators, and gas springs (made with gas accumulators). The details are shown in Fig. 2.8 and in the close-up picture in Fig. 2.9.

The assembly was bolted rigidly to the upper floor of the model in the strong direction or in the weak direction for the various stages of the project.

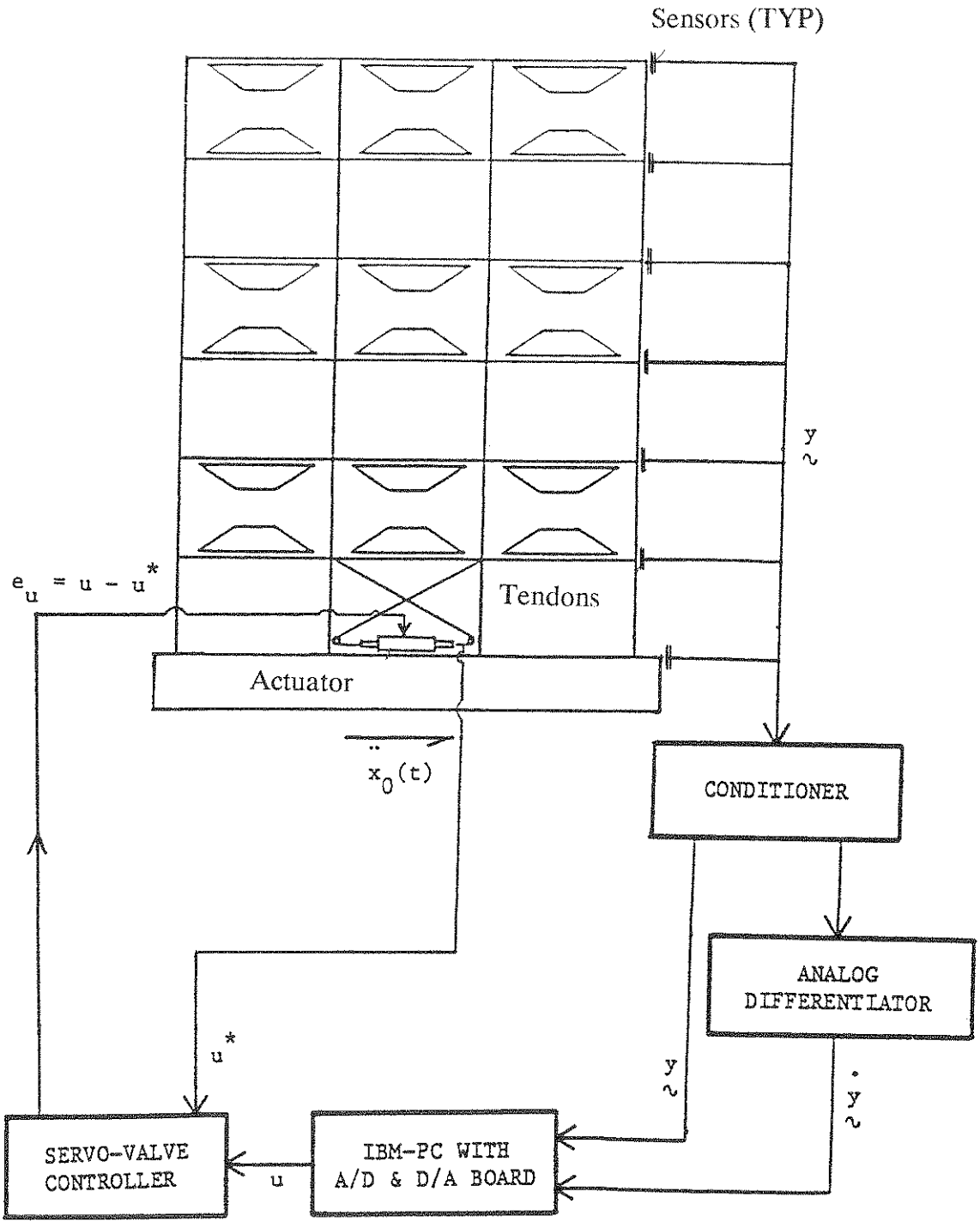

Figure 2.6 - Block Diagrams of Control for Active Tendon System.

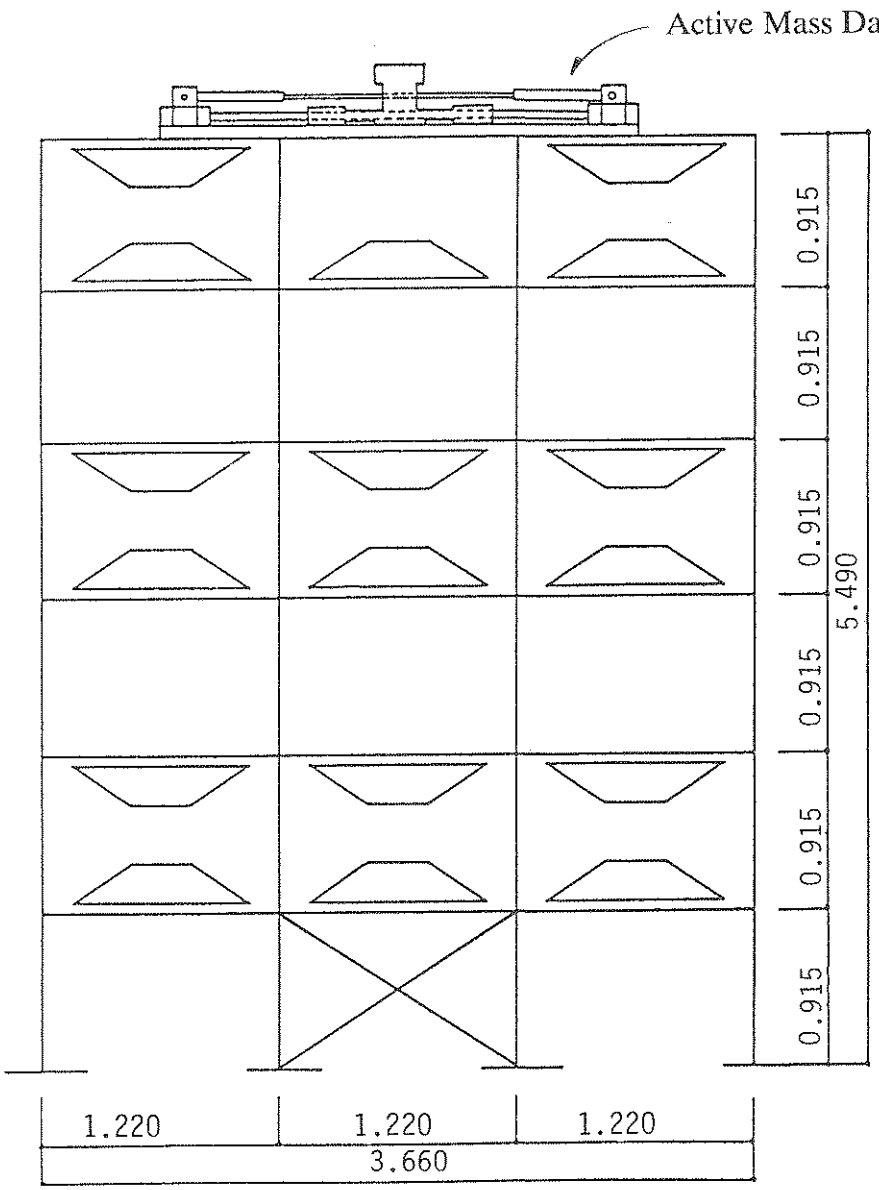

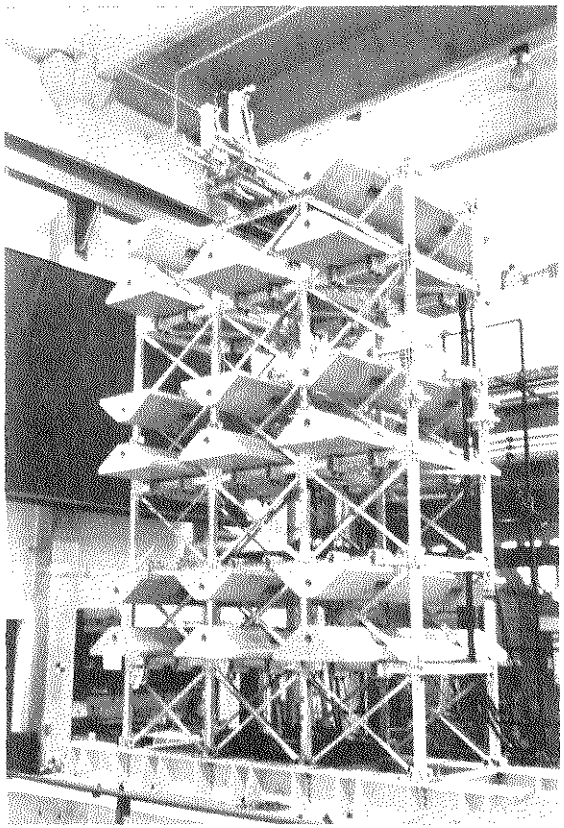

Figure 2.7 - Set-Up of AMD System.

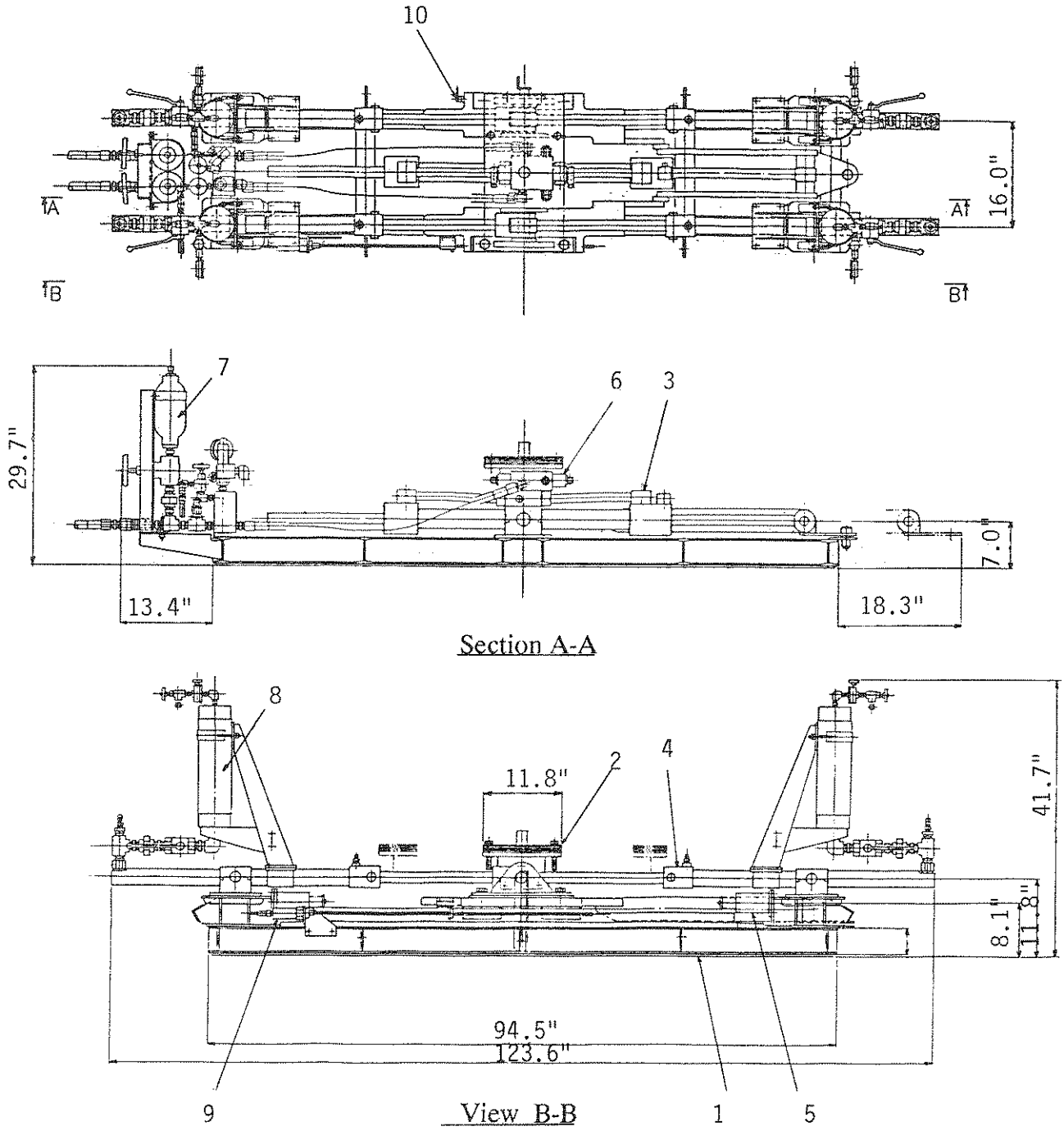

1. Base Frame
2. Added Mass
3. Driving Cylinder
4. Gas Spring
5. Buffer
6. Servo-Valve
7. Oil Accumulator
8. Gas Accumulator
9. Stroke Sensor
10. Accelerometer

Figure 2.8 - The AMD System.

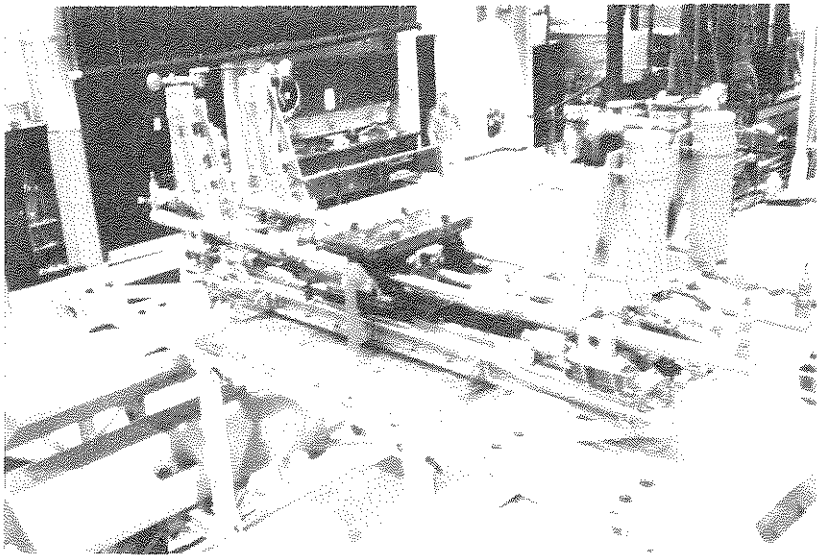

Figure 2.9 - View of AMD System.

The moving mass was adjusted during the testing program in increments of 50 kgs (110 lbs) from 150 kgs to 250 kgs (330 to 550 lbs). Most of the experiments were carried out with a 200 kgs (440 lbs) added mass, and this case serves as a benchmark for comparisons with other tests.

The gas springs were attached to the AMD system to provide the necessary stiffness. The spring can be tuned according to the required structural characteristics.

The AMD system operates similarly with the ATS as shown in the block diagram in Fig. 2.10. The components of the control systems includes acceleration and displacement.

(a) Acceleration and displacement sensors attached at the top and third floor.

(b) A microcomputer system (NEC/PC9801) equipped with A/D and D/A boards.

(c) A servo-amplifier unit for the dectrohydraulic valves attached to the hydraulic cylinders.

The measurement system for control used acceleration and displacement measurements of the moving map as well as of the floor system. The velocities required as state variables were obtained by digital integration in the microcomputer.

The microcomputer system (NEC/PC9801) used A/D and D/A converters for the input/output to the control system. The computer was used to process on-line operations, determine velocity states, and vary test parameters.

(D) **The earthquake simulator** at University at Buffalo has been used to perform the experiments. The system developed by the MTS System Corporation includes a shaking table of 3.66 x 3.66m (12 ft x 12 ft) with a capacity of 50 mtons (110 kips) and an advanced control system. The shaking table has five degrees of freedom (DOF) actively controlled, with three DOF programmable directions (horizontal, vertical, and roll) and the other two DOF corrected for cross coupling only. The sixth degree of freedom (horizontal-transverse) is restrained by hydrostatic bearings which provide free sliding with lateral displacement/force control.

The system has two horizontal actuators with a capacity of 32 mtons (70 kips), which can provide a horizontal acceleration of 0.625 g with maximum payload. Four vertical actuators with a total capacity of 100 tons (220 kips) can accelerate the system with 1.05 g at maximum

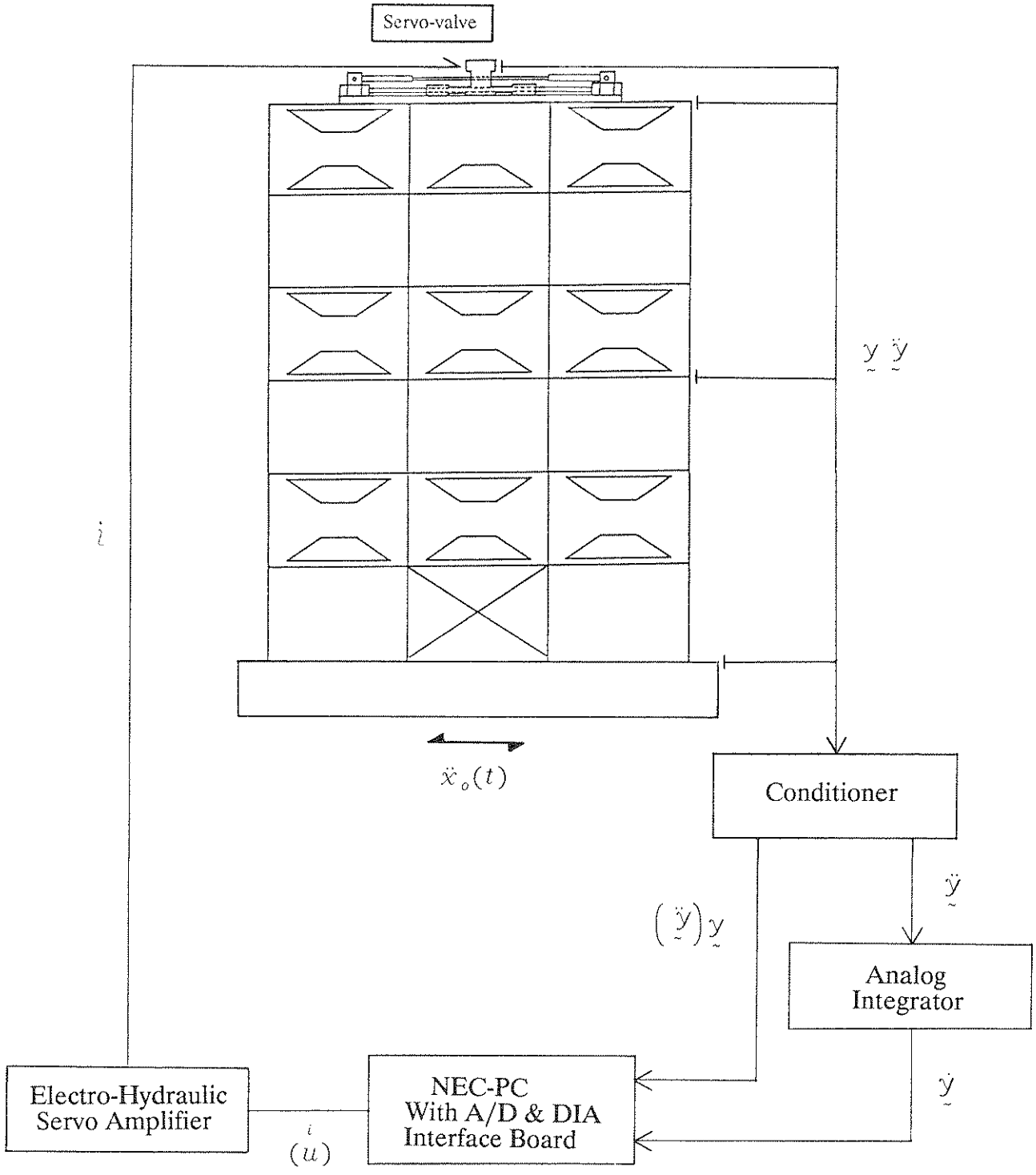

Figure 2.10 - Block Diagram of AMD Control System.

payload. At lower size models as payloads the system can produce larger accelerations (up to 4.0 g horizontally and 8.0 g vertically). Fig. 2.11 shows the artistic views of the shaking system. The system is driven by hydraulic power supplies of 1,061 liter/minute (280 gpm) and accumulators which can provide double flow capacity at peak velocity requirements. The system can, therefore, provide velocities of 1.828 m/sec (72 in/sec) and 0.864 m/sec (34 in/sec) in the horizontal and the vertical direction, respectively. At low frequency the system is limited by actuators' stroke, ±15.3 cm (6 in) and ±7.6 cm (3 in) in the horizontal and vertical direction, respectively.

The analog control system is based on the state-of-the art, three variable feedback control system. Such system using simultaneous displacement, velocity, and acceleration feedback allows for a better tracking between the shaking table and the command signal over a wide range of frequencies.

In addition, an off-line compensation system using the measured frequency characteristics of the table model system allows correction of the drive signals to produce a final reproduction of desired motions.

The shaking system operates over a frequency range of 0 to 50 Hz being limited by the shaking table's anticlastic mode of 62 Hz and by the oil column resonant frequency of 58 Hz. A series of prestressing tendons are mounted in the shaking table to allow detaining in the vicinity of the resonant frequencies.

The shaking table is driven by either analog or digital signals:

(a) harmonic analog signals (sinusoidal, square, triangular, sweep)

(b) random analog motion (pseudo of periodic random)

(c) recorded or simulated accelerograms (provided by a database of more than 3,000 accelerograms records in digital form (Caltech database) and other)).

As all imperfect systems, model-structure interaction is unavoidable and a certain amount of errors is always present. Actual obtained motion is recorded automatically by an electronic digital data acquisition system (52 channels) which allow accurate tracking of information.

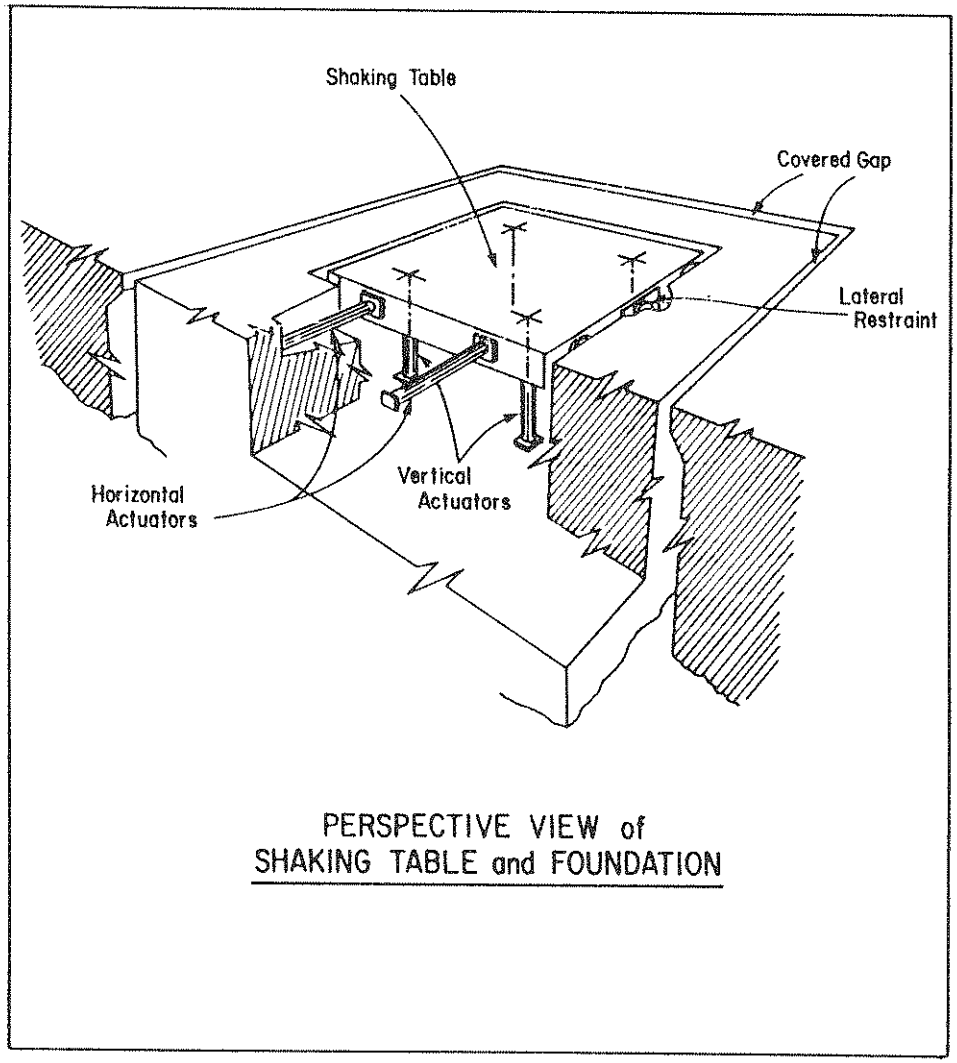

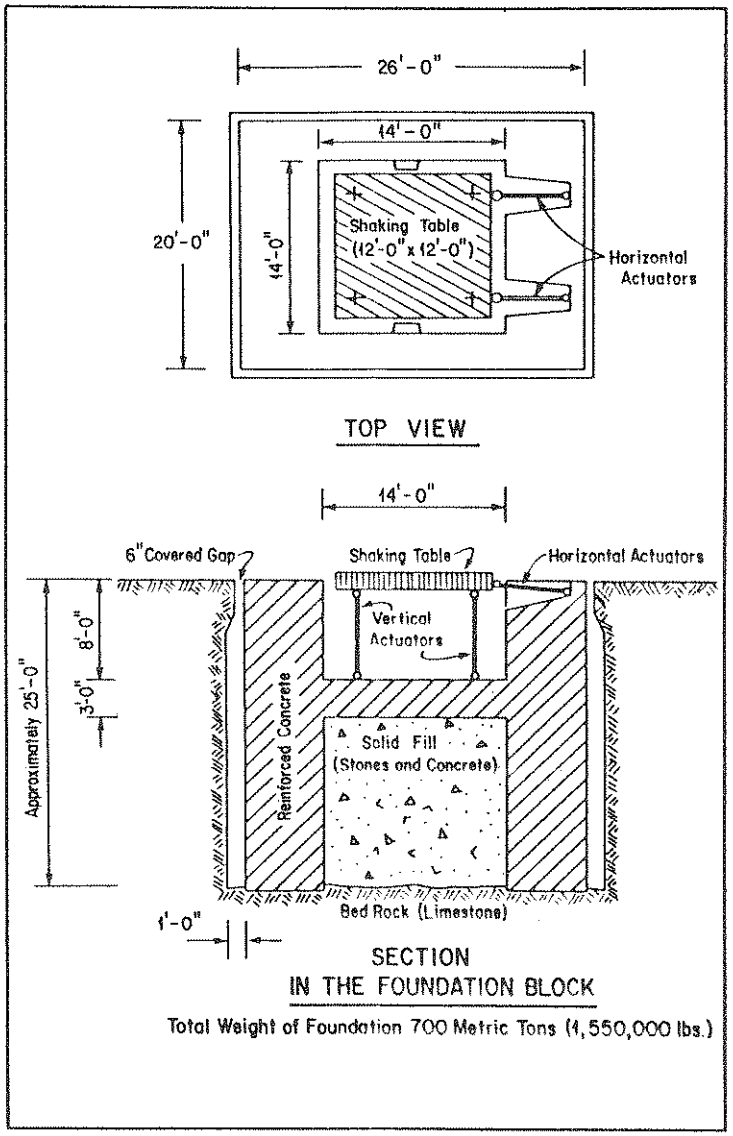

Figure 2.11 - View of University at Buffalo Shaking Table.

(E) **Instrumentation** plays a critical role in the active control experiments. The sensing equipment includes accelerometers, displacement transducers and load cells, and provides information for control operation and for performance evaluation of the system. A schematic of the sensors used in the experiment is shown in Fig. 2.12. This instrumentation includes:

(1) Linear position-displacement sonic transducers (Temposonic-TM) conditioned by a generic power supply and manufacturer amplifiers-decoders. The transducers were all calibrated to provide 2.0-2.3v/cm (5-6 v/in).

(2) Accelerometers (Bruel & Kyaer #4702 and Endevco 25 g) conditioned by PCB Piezotronics power supplies and VISHEY 2200 conditioner/amplifier/filters. The accelerometers were calibrated to a sensitivity of 5V/g within a frequency range of 0-50 Hz.

(3) Accelerometers (KYOWA-ASQ-1BL) conditioned by VAQ-500A conditioner with a sensitivity of 33.3 V/g in a frequency range of 0-100Hz.

(4) Load cells (generic) with a capacity of 10 kips conditioned by a VISHEY 2200 conditioner/amplifier/filter with a sensitivity of 0.45 ton/V (1,000 lbs/V). The load cells are used for the ATS system to monitor the prestressing forces and its variations.

The state variables were obtained by computations of the absolute displacements measured by the seven linear postion-displacement sonic transducers mounted at each floor and at the base. The displacement transducers used a reference frame mounted outside of the shaking system. The velocities at each level were obtained by a battery of differentiates attached to the displacement transducer. These signals are used for the ATS control and overall monitoring of response.

The accelerometers (B&K and Endevko) were used at each floor to monitor the structural response, and for the calibrations of the model structure (i.e., correction of torsional response, local bending of columns and actuator's adjustments). The high sensitivity accelerometers (Kyowa ASQ-1BL) were installed at selective floors (base, third, and six floor) and were used for the AMD control as well as for response tracking.

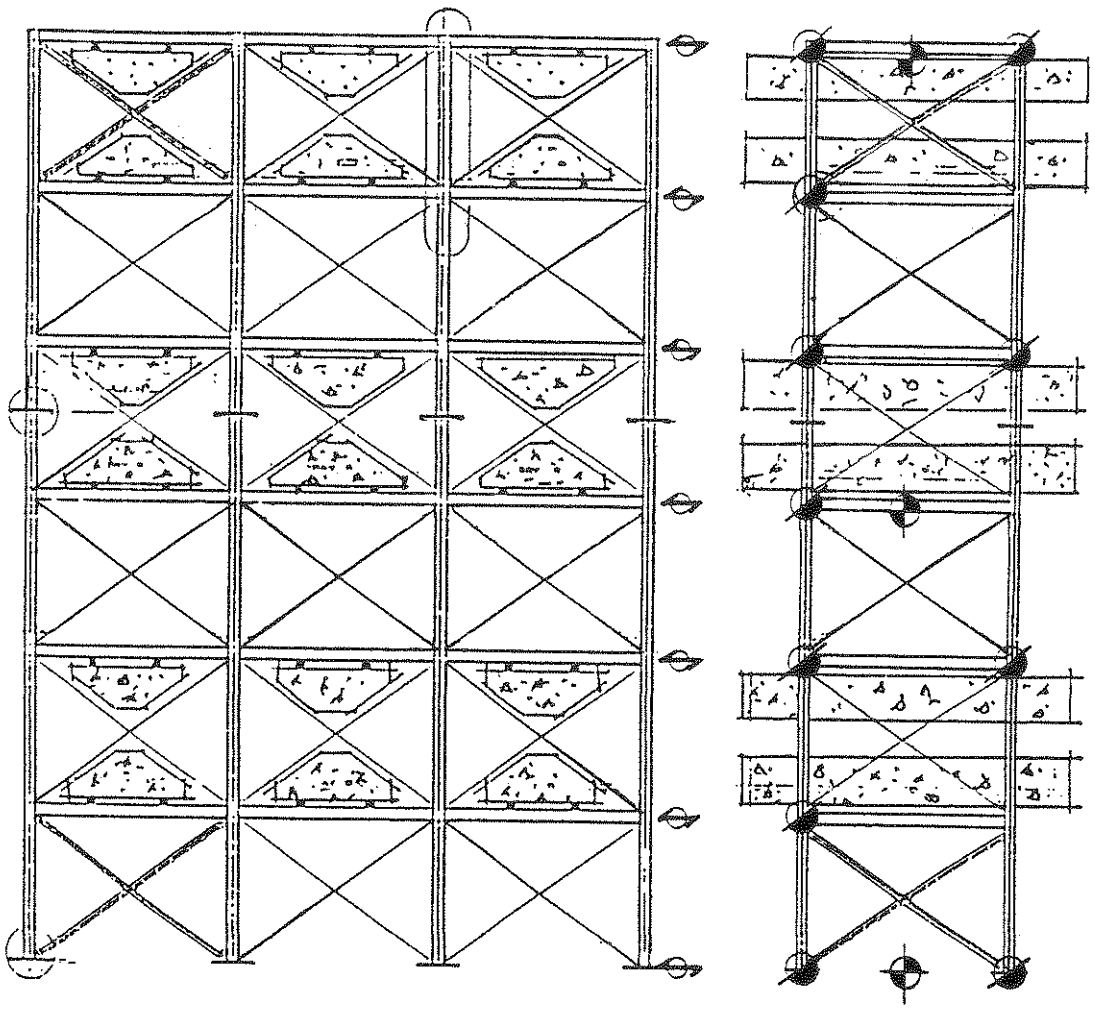

Figure 2.12 - View of Measurement Set-Up.

The analog information produced by the sensors was simultaneously recorded by two data acquisition systems, MEGADAC 5533 - 128 channel system and MTS/DIGITAL-52 channel system. The first system has a throughput of 256,000 samples per second and allowed a high speed recording and on-line plotting using a HP/LASERJET printer and an HP7475 plotter. The MTS/DIGITAL system complemented by a custom made processing package MTS/STEX was used to monitor the experiment calculate and filter the response and plot it using a TEKTRONIX 4025A terminal and a TEKTRONIX plotter.

In addition to the recording system, a four channel SPECTRAL DYNAMICS SD380 Signal Analyzer and a NICOLETT/PACKARD 7090A Digital Oscilloscop were used to obtain immediate experimental information in time and frequency domain for continuous test monitoring.

2.3 Base Motion

The model was subjected to a series of base motions intended to excite the system for parameters identification, calibration of control system and evaluation of the control algorithms.

The structure was tested in both the **strong** and **weak directions** using white noise for identification and calibration of controllers and with earthquake motions for evaluation of control efficiency. The base motions used in the testing program include white noise, El Centrol 1940 acceleogram, Hachinohe 1968 and Miyagioki 1978 earthquake and are listed in Table 2.1. The time histories for the earthquake base motion achieved by the shaking table is shown in Figs. 2.13 and 2.14.

In spite of the high fidelity corrections of the drive motion and of the *off-line compensation* of the drive signals, the achieved motion showed a strong interaction with the control system in the tests performed with the ATS control. This interaction is visible in the frequency transforms of the ground motions as shown in Figs. 2.15 and 2.16, and 2.17. The interaction was pronounced in the vicinity of 7.5 Hz and 12.5 Hz which correspond with either the second or the third mode of vibration of the structure in the **strong** and **weak** direction, respectively. In particular, the interaction which was present in the Hachinohe and Miyagioki earthquakes in this range is substantial and produces a resonant input to the structure. Such interaction will not appear in real systems since the ground is not driven by control systems.

Table 2.1

Base Motion

Structural cases	Base Motion	Peak values (g's)	Frequency Range (Hz)
Strong Direction	White Noise	0.040	0-50
	25% El Centro	0.0871	0-50
Weak Direction	White Noise	0.020	0-50
	20% El Centro	0.0697	0-50
	30% Hachinohe	0.0560	0-50
	40% Miyagioki	0.0658	0-50

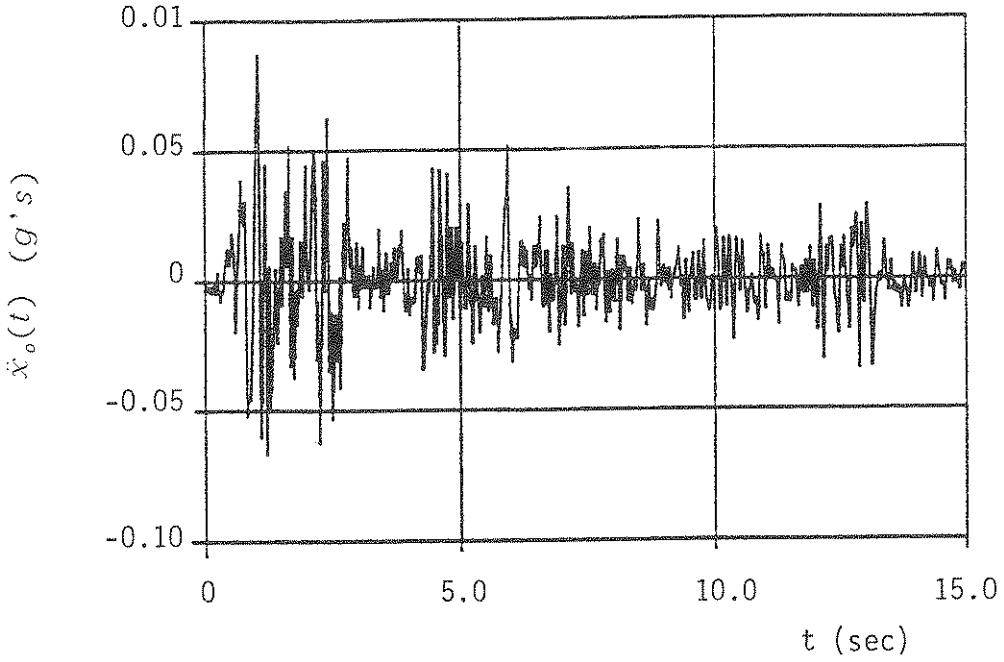

Figure 2.13 - Earthquake Acceleration in Strong Direction (25% El Centro).

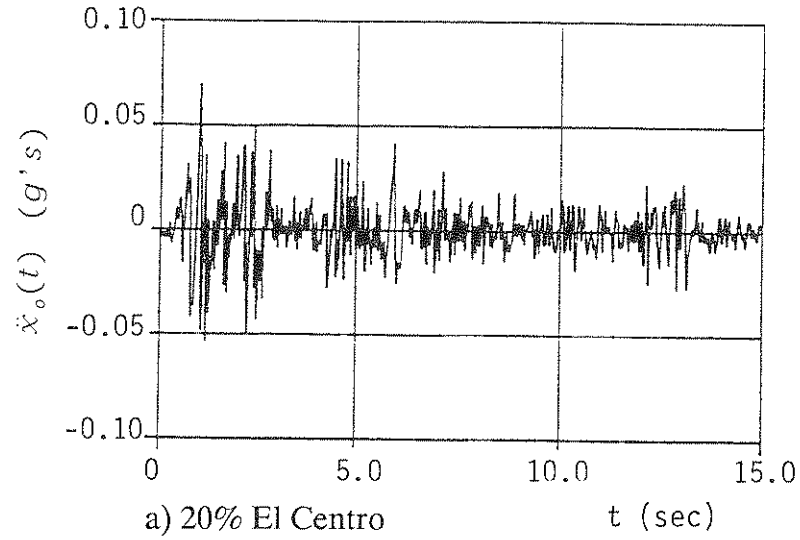

a) 20% El Centro

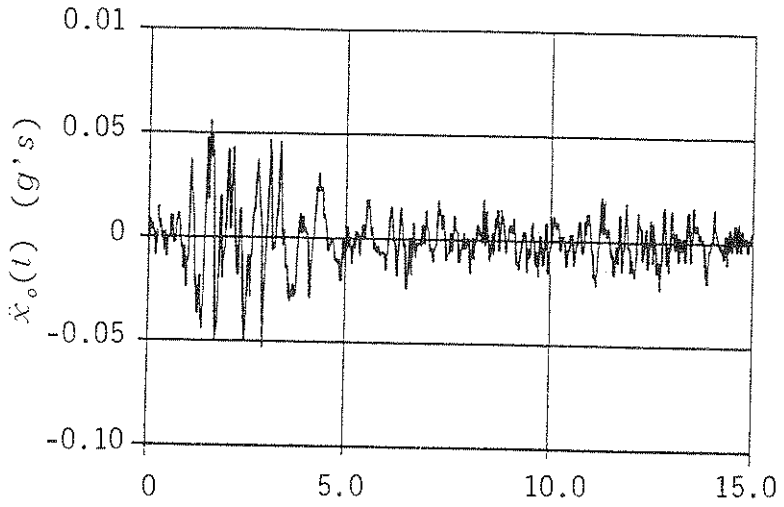

b) 30% Hachinohe

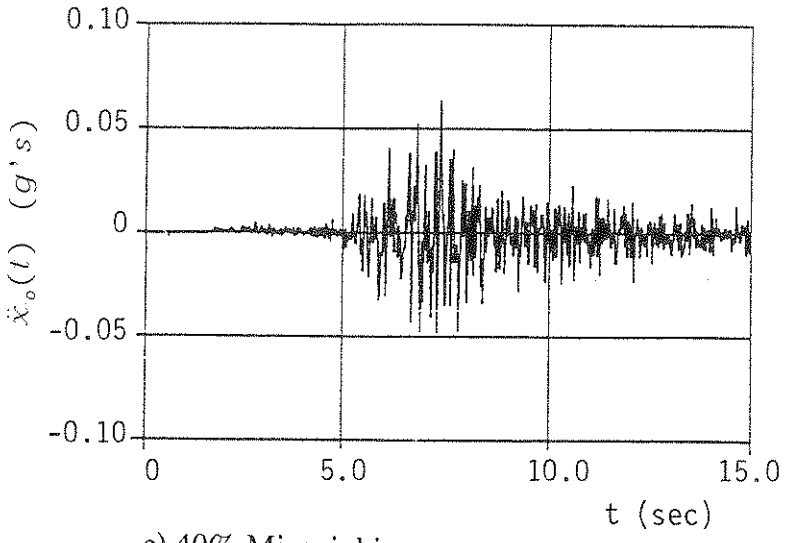

c) 40% Miyagioki

Figure 2.14 - Earthquake Acceleration in Weak Direction.

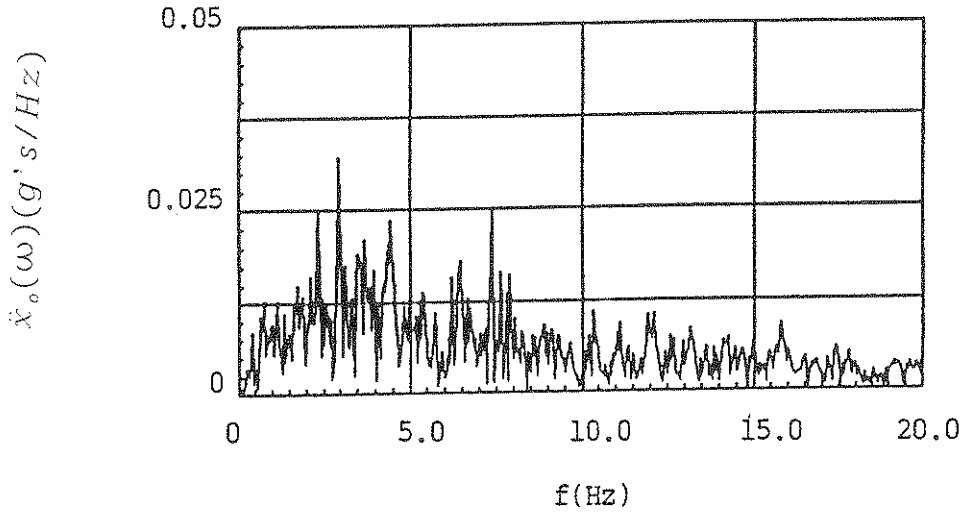

a) No Control Case

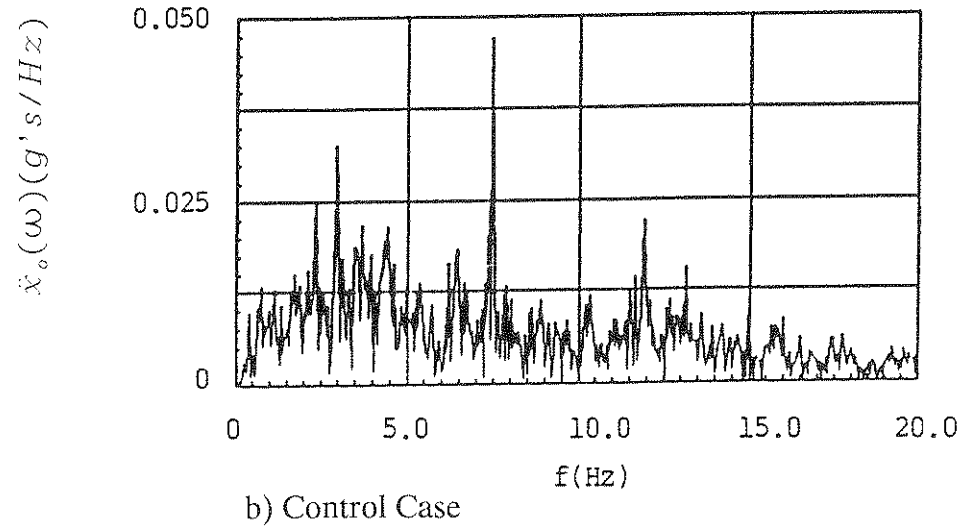

b) Control Case

Figure 2.15 - Comparison of Base Acceleration Input in Frequency Domain (El Centro).

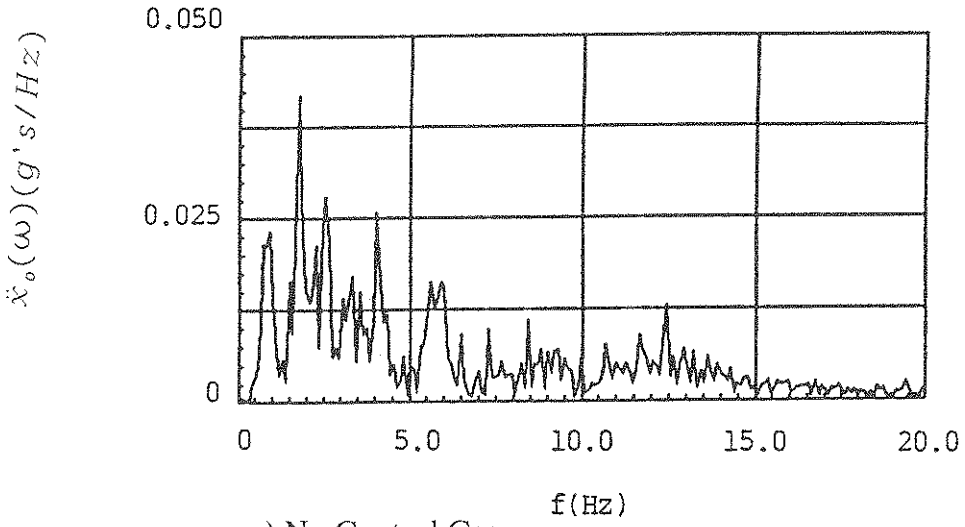

a) No Control Case

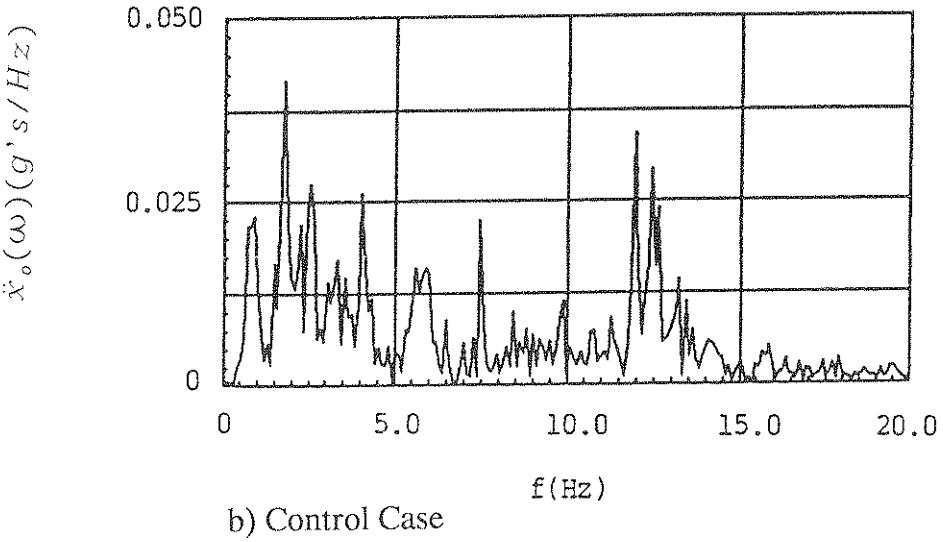

b) Control Case

Figure 2.16 - Comparison of Base Acceleration Input in Frequency Domain (Hachinohe).

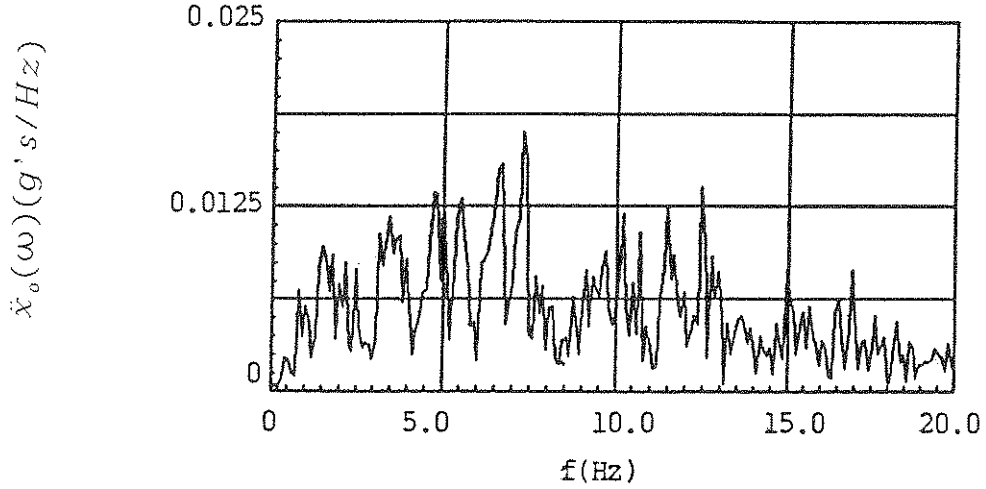

a) No Control Case

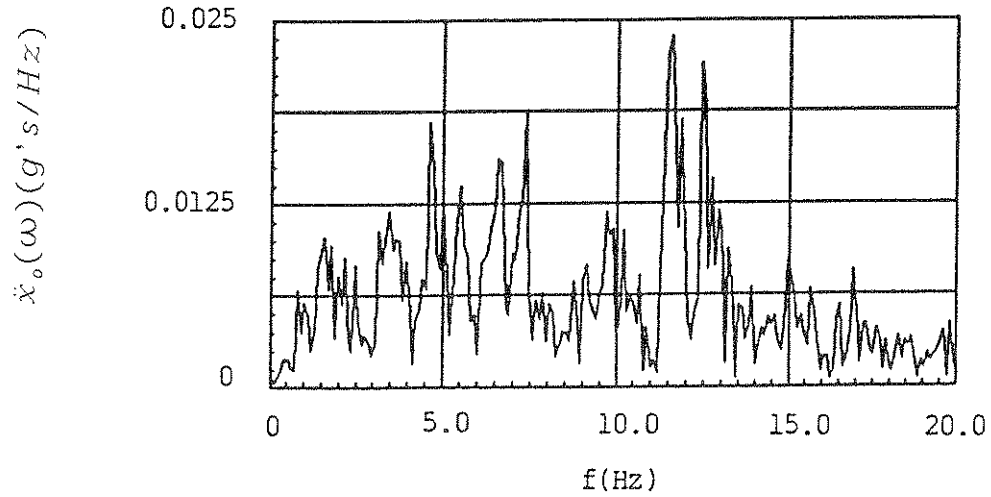

b) Control Case

Figure 2.17 - Comparison of Base Acceleration Input Frequency Domain (Miyagioki).

2.4 Experimental Program

The experiments for the evaluation of the two control systems were designed to consider the most important parameters which influence the efficiency of the controllers.

(A) **Testing programs for the ATS** includes changes of the structural configuration using the tendons attached at various places in the frame and changing the control parameter for the control economy, β (for definition of this parameter see detailed developments in Section 3.1). A complete list of tests shown in Tables 2.2 and 2.3 indicate all the tests performed and their symbolic notation.

The control configuration included:

(a) Single actuator with one tendon at the base of the structure in the **strong direction** and respected in the **weak direction.**

(b) Single actuator at the base with one tendon connected to second or third floor in the **strong direction.**

(c) Single actuator at the base with two tendons attached at different floors, i.e., proportionally control, in the **strong direction.**

(d) Two actuators and two tendons applied at different floors, i.e., independent control, in the **weak direction.**

All tests were performed with earthquake ground motion described in the previous section with and without control (a common benchmark case used for evaluation of control efficiency).

(B) **Testing program for the AMD** includes two control algorithm **TAK** and **KYB** (described in detail in the next section), with the damper installed at the top floor. The testing program includes experiments in both directions, in which the AMD system was operated under different conditions, in terms of (1) the measured quantities used for control, (2) the magnitude of the added mass, (3) the AMD stiffness, and (4) the objective variables. The details of the experimental program including test conditions used for both directions are listed in Table 2.4, in which three types of regulators, **S** (strong), **M** (medium), and **W** (weak), indicate the selection of the weighting magnitude.

Table 2.2

Experimental Study in Strong Direction for ATS

Structural Configuration	Control case	Control Force Location	Control Parameter β	Excitation Input	
				White Noise 0.04g	El Centro 25 %
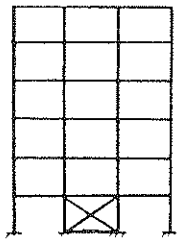	SC1	1st floor only	β = ∞	SC1 WUN	SC1 EUN
			β = 2	SC1 WB2	SC1 EB2
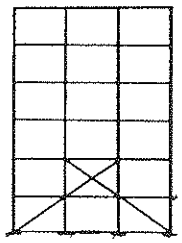	SC2	2nd floor only	β = ∞	SC2 WUN	SC2 EUN
			β = 2	SC2 WB2	SC2 EB2
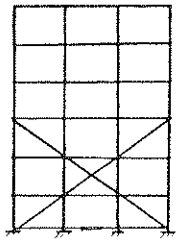	SC3	3rd floor only	β = ∞	SC3 WUN	SC3 EUN
			β = 2	SC3 WB2	SC3 EB2
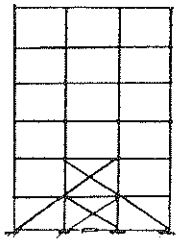	SC12	Proportional 1st & 2nd	β = ∞	SC12 WUN	SC12 EUN
			β = 2	SC12 WB2	SC12 EB2
			β = 1	SC12 WB1	SC12 EB1
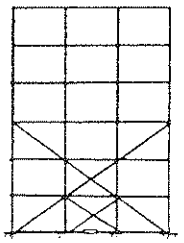	SC13	Proportional 1st & 3rd	β = ∞	SC13 WUN	SC13 EUN
			β = 2	SC13 WB2	SC13 EB2

Table 2.3

Experimental Study in Weak Direction for ATS

Structural Configuration	Control case	Control Force Location	Control Parameter β	Excitation Input			
				W. Noise 0.02g	El Centro 20 %	Hachinohe 30 %	Miyagioki 40 %
	W1C1	No control	β = ∞	W1C1 WUN	W1C1 EUN	W1C1 HUN	W1C1 MUN
		1st floor only	β = 4	W1C1 WB4	W1C1 EB4	W1C1 HB4	W1C1 MB4
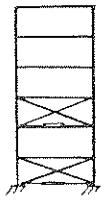	W2UN	No Control	β = ∞	W2WUN	W2EUN	W2HUN	W2MUN
	W2C1	1st floor only	β = 4	W2C1 WB4	W2C1 EB4	W2C1 HB4	W2C1 MB4
			β = 8	W2C1 WB8	W2C1 EB8	W2C1 HB8	W2C1 MB8
	W2C3	3rd floor only	β = 8	W2C3 WB8	W2C3 EB8	W2C3 HB8	W2C3 HB8
	W2C13	1st & 3rd Independent	β = 4	W2C13 WB4	W2C13 EB4	W2C13 HB4	W2C13 MB4
			β = 8	W2C13 WB8	W2C13 EB8	W2C13 HB8	W2C13 MB8

Table 2.4

Experimental Conditions in Both Directions for AMD

Test #	Sensor Position	Objective Variables	Added Mass	AMD Stiffness	Regulator Type	Remarks
0	-	-	-	-	-	Without Control
1	Top Floor	Relative Displacement	200 kg	-	TAK-S KYB-S	
2					TAK-M KYB-M	
3					TAK-W KYB-W	
4		Relative Velocity			TAK-M	
5		Relative Acceleration			TAK-M	
6		Absolute Displacement			TAK-M(S)	
7		Absolute Acceleration			TAK-M(S)	
8	Top & 3rd Floor	Relative Displacement	200 kg	-	TAK-S KYB-S	
9					TAK-M KYB-M	
10					TAK-W KYB-W	
11		Story Drift			TAK-M	* Q_1:Q_2=9:1
12					TAK-M(S)	Q_1:Q_2=9:1 **
13					TAK-M	Q_1:Q_2=1:1
14					TAK-M	Q_1:Q_2=1:9
15	Top Floor	Relative Displacement	150 kg	-	TAK-M(S) KYB-M	
16					KYB-M(S)	Designed for 200 kg mass
17			250 kg		TAK-M(S) KYB-M	
18					KYB-M(S)	Designed for 200 kg mass
19			200 kg	Connected	TAK-M KYB-M	[Added mass is connected to gas spring]
20				Optimum	KYB-S(S)	
21					KYB-M	
22					KYB-M(S)	Designed for no stiffness
23					TAK-M	
24				Half of Optimum	KYB-M	
25					TAK-M(W)	
26				1.1 x Optimum	KYB-M(W)	
27					TAK-M(W)	

Notes:

* Q_1,Q_2 shows the weighting magnitudes for the story drift between the base and the 3rd floor, or that between the 3rd and the top floor, respectively.

** The feedback coefficients for the 3rd floor are omitted.

(S) and (W) indicate the regulator types only for the strong direction and the weak direction, respectively.

(Note: 1kg = 2.20459 lb.)

The same types of excitations used for the ATS experiments were used for the AMD experiments, i.e., white noise excitation and El Centro in both directions and Hachinohe and Miyagioki (see Section 2.3 and Table 2.1) in the weak direction only. The experimental cases shown in Table 2.4 were performed in both directions using same designations.

SECTION 3
CONTROL ALGORTHMS

Both system, ATS and AMD, were designed to use classical linear optimal control law which were previously developed and discussed by [Chung et. al. (1988) (1989) and Fukao et. al (1988) (1989)]. The algorithms, however, were adjusted to fit the specific information used in the control system, the hardware requirements and controllers configuration. In the present section, the specific algorithms used in the experimental study are described in detail.

3.1 Control Algorithm for Active Tendon System (ATS)

The Classical Linear Optimal Control Law was used in this study. The equation of motion of a discrete-parameter structure under earthquake excitation, $\ddot{x}_0(t)$, , and active control vector, $\underset{\sim}{u}(t)$, , is described in the state-space representation as:

$$\dot{\underset{\sim}{z}}(t) = A\,\underset{\sim}{z}(t) + B\,\underset{\sim}{u}(t) + \underset{\sim}{w}\,\ddot{x}_0(t) \qquad (3.1)$$

where:

$$\underset{\sim}{z}(t) = \begin{pmatrix} \underset{\sim}{x}(t) \\ \dot{\underset{\sim}{x}}(t) \end{pmatrix}, A = \begin{pmatrix} 0 & I \\ -M^{-1}K & -M^{-1}C \end{pmatrix}, B = \begin{pmatrix} 0 \\ -M^{-1}B_1 \end{pmatrix}, \underset{\sim}{w} = \begin{pmatrix} 0 \\ \underset{\sim}{w}_1 \end{pmatrix},$$

where $\underset{\sim}{z}(t)$ is the state vector of order 2n consisting of vectors $\underset{\sim}{x}(t)$ and $\dot{\underset{\sim}{x}}(t)$ which

are the relative displacement and relative velocity vectors of order n, respectively. n being the number of DOF of structure (in the present case n = 6); $\underset{\sim}{u}(t)$ is the control vector of

order r consisting of the actuator displacements in Active Tendon System, r being the number of actuators; M, C and K are the mass, the damping and the stiffness matrices, respectively. For different position of the tendon system K and C will be different and have to be determined during the experiments by identification tests; B_1 is the control force location matrix of order n x r. The elements of this matrix are $4k_c\cos\alpha$ for the corresponding floors where the active tendon are attached and zero otherwise, where k_c

is the stiffness of the active tendon and α is the tendons inclination angle from the horizontal. $\underset{\sim}{w}_1$ is a vector of order n with all elements equal to -1, indicating the contribution of the ground acceleration.

In this study, the observed variables, $\underset{\sim}{y}(t)$, consists of the absolute displacements and absolute velocities at each floor and base, so $\underset{\sim}{y}(t)$ is a vector of order 2 (n + 1). The state vector $\underset{\sim}{z}(t)$ can be obtained from $\underset{\sim}{y}(t)$ by:

$$\underset{\sim}{z}(t) = \mathrm{E}\,\underset{\sim}{y}(t) \tag{3.2}$$

where E is a 2n x 2 (n + 1) transfer matrix of unities.

According to the classical quadratic performance criterion, the control vector, $\underset{\sim}{u}(t)$, is found such that the integral:

$$J = \frac{1}{2}\int_0^{t_f}\left[\underset{\sim}{z}^T(t)\mathrm{Q}\,\underset{\sim}{z}(t) + \underset{\sim}{u}^T(t)\mathrm{R}\,\underset{\sim}{u}(t)\right]dt \tag{3.3}$$

is minimized for the duration of ground motion excitation t_f . Q is a positive semi-definite weighting matrix for the responses, and R is a positive definite weighting matrix for the control vector.

For the present case of Active Tendon System control, the matrix Q was chosen to be:

$$\mathrm{Q} = \begin{pmatrix} \mathrm{K} & 0 \\ 0 & 0 \end{pmatrix} \tag{3.4}$$

so that the first term of Eq. (3.3) characterizes the potential energy of the structure.

The matrix R was chosen to be a r x r diagonal matrix, where the diagonal elements are:

$$R(i,i) = \beta \sum_{j=1}^{n_1} 4(k_c)_{ij} \tag{3.5}$$

where $(k_c)_{ij}$ is the tendon stiffness for the j-th set of tendons of i-th actuator; n_1 is the number of tendon sets: a) $n_1 = 1$ for single force control; b) $n_1 = 2$ for the proportional control. Thus, the second term in Eq. (3.3) characterizes the applied control energy; β is a control parameter which determines the relative importance between safety and economy. $\beta = \infty$ represents the uncontrolled case. From the above derivation, the value of β is the only parameter which should be determined in the design of the Active Tendon System Control.

Using a linear feedback control approach and a variational procedure to minimize the performance index J, given in Eq. (3.3), the active control vector is obtained to be linearly related to the state vector, $\underset{\sim}{z}(t)$, as [Sage (1977), Chung (1988), (1989)]:

$$\underset{\sim}{u}(t) = -\mathbf{G}\,\underset{\sim}{z}(t) = -\mathbf{R}^{-1}\mathbf{B}^T\mathbf{P}\mathbf{E}\,\underset{\sim}{y}(t) \tag{3.6}$$

where $\mathbf{P}$ is obtained from the approximated time invariant Riccati matrix Eq. (3.3)

$$\mathbf{P}\mathbf{A} + \mathbf{A}^T\mathbf{P} - \mathbf{P}\mathbf{B}\mathbf{R}^{-1}\mathbf{B}^T\mathbf{P} + \mathbf{Q} = 0 \tag{3.7}$$

3.1.1 Time Delay Compensation

In algorithm for the Active Tendon System, the time delay generated by the on-line computations and by the generation of the control forces is considered using the phase compensation method [Chung (1988), McGreevy (1988)]. The development of the same method for an MDOF system [Chung et. al. (1989)] is presented here for the sake of completion.

If the displacement feedback force lags the displacement by τ_x in time while velocity feedback force lags the velocity by $\tau_{\dot{x}}$ their corresponding phase lags for the i-th mode are $\omega_i\tau_x$ and $\omega_i\tau_{\dot{x}}$, respectively. Fig. 3.1 shows the relationship between feedback forces and responses in the phase space. With the phase shift, the displacement feedback force may be resolved to produce positive active stiffness and negative active damping while the velocity feedback force may be resolved to produce positive active stiffness and positive active damping. Due to the existence of negative active damping, control effects are diminished for the real system as compared to the ideal one. Even worse, time delay will cause instability if the resultant damping force is negative. Since phase lag is proportional to the delay time and modal frequency, the effect of time delay may be very serious for higher modes even with small amounts of time delay.

For a MDOF system, time delay can be compensated in the modal domain by phase shift method which was developed for single-degree-of-freedom systems [McGreevy et. al. (1988)] and previously compared experimentally with several other methods [Chung et. al. (1988)]. The control force contributed by the i-th mode can be expresses as [Chung et. al. (1989)]:

$$u_i(t) = -g_{1i}\eta_i(t) - g_{2i}\dot{\eta}_i(t) = -g'_{1i}\eta_i(t-\tau_x) - g'_{2i}\dot{\eta}_i(t-\tau_x) \qquad (3.8)$$

where g'_{1i} and g'_{2i} are the modified displacement and velocity feedback gain factors, respectively, with time delay compensation. The modified feedback gain factors are determined so that the same control effect can be achieved.

Due to phase shift, the displacement feedback forces contributed by the i-th mode can be resolved into the displacement and velocity components as $(g'_{1i}\cos\omega_i\tau_x)\eta_i$ and $(-g'_{1i}\sin\omega_i\tau_x)\dot{\eta}_i/\omega_i$, respectively. Similarly, the displacement and velocity components of the velocity feedback force contributed by the i-th mode are, respectively, $(g'_{2i}\sin\omega_i\tau_x)\omega_i\eta_i$ and $(g'_{2i}\cos\omega_i\tau_x)\dot{\eta}_i$. In order to make the real system equivalent to the ideal one, the relationship between feedback gains for the real system and those for the ideal system can be established such that both systems have the same active stiffness and active damping. Thus, the modified feedback gains are obtained:

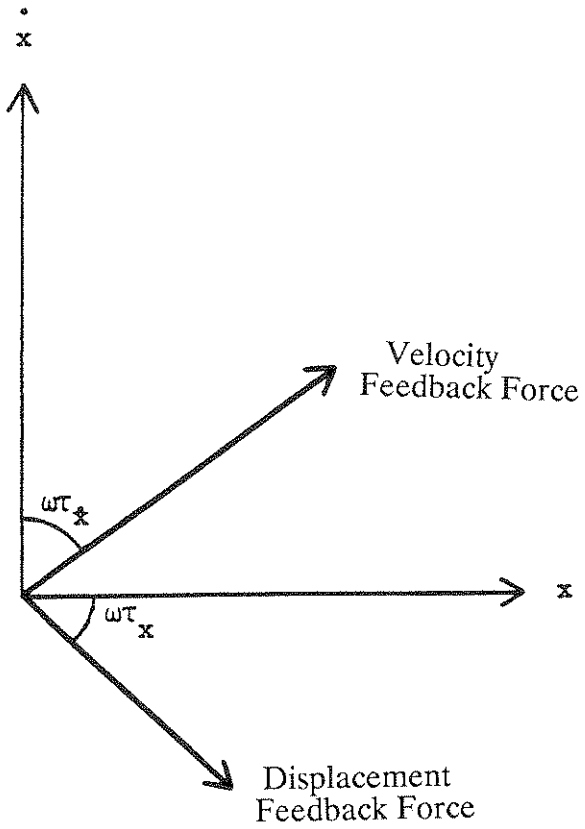

Figure 3.1 - Phasor Diagram of Feedback Forces and Responses.

$$[g'_{1i} g'_{2i}] = [g_{1i} g_{2i}] \begin{pmatrix} \cos\omega_i \tau_x & -(1/\omega_i)\sin\omega_i \tau_x \\ \omega_i \sin\omega_i \tau_{\dot{x}} & \cos\omega_i \tau_{\dot{x}} \end{pmatrix}^{-1} \tag{3.9}$$

Equation (3.9) can be rewritten shortly for the i-th mode:

$$\underset{\sim}{g}'^{T}_{i} = \underset{\sim}{g}'^{T}_{i} D_i \tag{3.10}$$

where D_i is a 2 x 2 compensation matrix for each mode given by:

$$D_i = \frac{1}{\cos\omega_i(\tau_x - \tau_{\dot{x}})} \begin{pmatrix} \cos\omega_i \tau_{\dot{x}} & (1/\omega_i)\sin\omega_i \tau_x \\ -\omega_i \sin\omega_i \tau_{\dot{x}} & \cos\omega_i \tau_x \end{pmatrix} \tag{3.11}$$

The compensation matrix, D_e, for the system in modal space can be obtained by aggregating Eq. 3.11. D_e, therefore, will be a 2n x 2n matrix consisting of 4 x (n x n) diagonal submarine given by the following relations:

$$D_e(i,i) = \frac{\cos\omega_i \tau_{\dot{x}}}{\cos\omega_i(\tau_x - \tau_{\dot{x}})} \tag{3.12}$$

$$D_e(i, i+n) = \frac{\sin\omega_i \tau_x}{\omega_i(\cos\omega_i(\tau_x - \tau_{\dot{x}})}$$

$$D_e(i, i+n, i) = \frac{-\omega_i \sin\omega_i \tau_{\dot{x}}}{\cos\omega_i(\tau_x - \tau_{\dot{x}})}$$

$$D_e(i+n, i+n) = \frac{\cos\omega_i \tau_x}{\cos\omega_i(\tau_x - \tau_{\dot{x}})}$$

i = 1, 2, ..., n, where n is the number of DOF observed, and all other components equal to zero.

Transforming D_e to the time domain from the modal space the compensation matrix D for the real system is obtained as:

$$D = \Phi_s D_e \Phi_s^{-1} \tag{3.13}$$

where

$$\Phi_s = \begin{pmatrix} \Phi & 0 \\ 0 & \Phi \end{pmatrix} \tag{3.14}$$

where Φ is the modal (shapes) matrix of the system.

The compensated feedback gain matrix G' for the real system is obtained, therefore,

$$G' = G D \tag{3.15}$$

Using G' instead of G in the control force evaluation (Eq. (3.6), the actuator motion will be, therefore, compensated for the delay.

3.2 Control Algorithm for the Active Mass Damper (AMD) System

In the case of the AMD system, like in the tendon case, the classical linear optimal closed-loop control law with a quadratic performance index is used. Two kinds of control algorithms based on the optimization of the control force and the servo-current, denoted by TAK and KYB, respectively, are utilized.

In order to determine the optimal feedback vector, it is assumed that the six-story model structure can be approximated by (a) an equivalent single-degree-of-freedom (SDOF) system or by (b) a two-degrees-of-freedom (2DOF) system. A schematic illustration of the AMD system is shown in Fig. 3.2.

The state equation of the SDOF system under the ground acceleration $\ddot{x}_0(t)$, including the terms of the added mass, is given by Eq. (3.1), where the state vector has the following components:

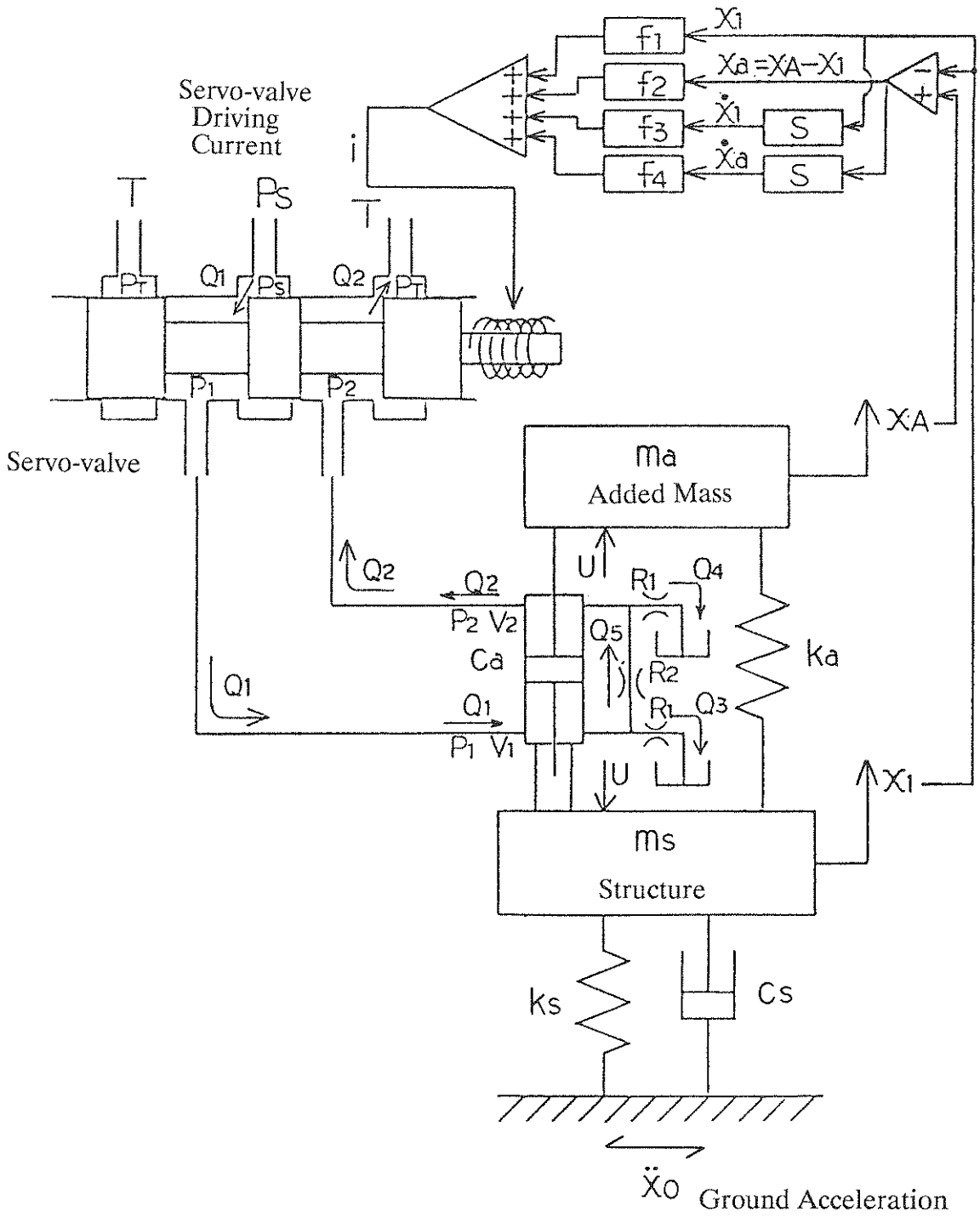

Figure 3.2 - Schematic Illustration of AMD System.

$$\underset{\sim}{z}(t) = \begin{pmatrix} x_s \\ x_\alpha \\ \dot{x}_s \\ \dot{x}_\alpha \end{pmatrix} \tag{3.16a}$$

The components x_s and x_α are the relative displacement of the structure and the added mass stroke, respectively. The dots indicate time derivative. The contribution of the ground motion is given by the vector:

$$\underset{\sim}{w} = \begin{pmatrix} 0 \\ 0 \\ -1 \\ 0 \end{pmatrix} \tag{3.16b}$$

The matrices A and B in Eq. (3.1) are given by:

$$A = \begin{bmatrix} 0 & 0 & 1 & 0 \\ 0 & 0 & 0 & 1 \\ -\frac{k_s}{m_s} & \frac{k_\alpha}{m_s} & -\frac{c_s}{m_s} & \frac{c_\alpha}{m_s} \\ \frac{k_s}{m_s} & -\frac{k_\alpha}{m_s} - \frac{k_\alpha}{m_\alpha} & \frac{c_s}{m_s} & -\frac{c_\alpha}{m_s} - \frac{c_\alpha}{m_\alpha} \end{bmatrix} \tag{3.17a}$$

$$B = \begin{pmatrix} 0 \\ 0 \\ -\frac{1}{m_s} \\ \frac{1}{m_s} + \frac{1}{m_a} \end{pmatrix} \qquad (3.17b)$$

for TAK algorithm case, and

$$A = \begin{bmatrix} 0 & 0 & 1 & 0 \\ 0 & 0 & 0 & 1 \\ -\frac{k_s}{m_s} & \frac{k_a}{m_s} & -\frac{c_s}{m_s} & \frac{c_a}{m_s} + \frac{D}{m_s} \\ \frac{k_s}{m_s} & -\frac{k_a}{m_s} - \frac{k_a}{m_a} & \frac{c_s}{m_s} & -\frac{c_a + D}{m_s} - \frac{c_a + D}{m_a} \end{bmatrix} \qquad (3.18a)$$

$$B = \begin{pmatrix} 0 \\ 0 \\ -\frac{\alpha D}{m_s A_c} \\ \frac{\alpha D}{m_s A_c} + \frac{\alpha D}{m_a A_c} \end{pmatrix} \qquad (3.18b)$$

for KYB algorithm case.

As shown in Fig. 3.3 (a), $m_s, k_s,$ and c_s are, respectively, the mass, stiffness and damping coefficient of the structure, which are determined based on the identification results of the model structure, and $m_a, k_a,$ and c_a represent the added mass, AMD stiffness and damping coefficient, respectively.

In the case of KYB algorithm, the control force vector $\underset{\sim}{u}(t)$ in Eq. (3.1) can be expressed as the scalar $u(t)$, related to $i(t)$, the servo-current driving the actuator's valve, by the following formula:

$$u(t) = \underset{\sim}{g}^T \underset{\sim}{z}(t) + \frac{\alpha D}{A_c} i(t) \tag{3.19}$$

where $\underset{\sim}{g}^T = \{0, -k_a, 0, -(c_a + D)\}$. (see Appendix A).

The elements of Eqs. (3.18) and (3.19) are given in the following:

$$D = \frac{2A_c^2}{\beta + R_1 + 2R_2}, \quad \alpha = \frac{k}{\sqrt{2}}, \quad k = \frac{Q_r}{I_r}\sqrt{\frac{P_s}{35}}, \quad \beta = \frac{kI_0}{\sqrt{2}P_s}$$

where A_c is the effective area of cylinder; Q_r and I_r are, respectively, the rated flow and the rated current of the servo-value; P_s is the supplied pressure; I_o is the current at equilibrium; R_1 and R_2 show the coefficient for inner and outer leaking of the cylinder, respectively.

For these algorithms, TAK and KYB, the output vector $\underset{\sim}{y}(t)$ is defined according to the selected objective variables, i.e., the relative or absolute displacement, velocity and acceleration of the structure, mass stroke and their combinations.

a) SDOF System

b) 2DOF System

Figure 3.3 - Equivalent Models of the Structure.

The classical optimal close-loop control is based on the minimization of a quadratic performance index J given by Eq. [3.3], where $u(t)$ is replaced by $i(t)$ for the case of KYB algorithm.

The optimal control force $u^*(t)$ or servo-current $i^*(t)$ minimizing the performance index J is obtained using the optimal feedback vector $\underset{\sim}{f}^*$.

$$u^*(t) = \underset{\sim}{f}^{*T} \underset{\sim}{z}(t) \tag{3.20}$$

or

$$i^*(t) = \underset{\sim}{f}^{*T} \underset{\sim}{z}(t)$$

where,

$$\underset{\sim}{f}^{*T} = -\mathrm{R}^{-1}\mathrm{B}^T\mathrm{P} \tag{3.21}$$

In Eq. (3.21), P is a positive definite matrix satisfying the Ricatti matrix equation given by Eq. (3.7).

Similarly to the developments for the SDOF approximation, in the case in which the feedback vector is regulated by the signals of the added mass, the top and the third floor measurements, i.e., a 2DOF system approximation, the control algorithm can be developed from Eqs. (3.1) and (3.3) using the system matrices as follows.

The matrices and vectors used for 2DOF system are given by:

$$\underset{\sim}{z}(t) = \begin{pmatrix} x_1 \\ x_2 \\ x_a \\ \dot{x}_1 \\ \dot{x}_2 \\ \dot{x}_a \end{pmatrix}, \qquad \underset{\sim}{w} = \begin{pmatrix} 0 \\ 0 \\ 0 \\ -1 \\ -1 \\ 0 \end{pmatrix},$$

$$A = \begin{bmatrix} 0 & 0 & 0 & 1 & 0 & 0 \\ 0 & 0 & 0 & 0 & 1 & 0 \\ 0 & 0 & 0 & 0 & 0 & 1 \\ -\frac{k_1 + k_2}{m_1} & \frac{k_2}{m_1} & 0 & -\frac{c_1 + c_2}{m_1} & \frac{c_2}{m_1} & 0 \\ \frac{k_2}{m_2} & -\frac{k_2}{m_2} & \frac{k_a}{m_2} & \frac{c_2}{m_2} & -\frac{c_2}{m_2} & \frac{c_a}{m_2} \\ -\frac{k_2}{m_2} & \frac{k_2}{m_2} & -\frac{k_a}{m_2} - \frac{k_a}{m_a} & -\frac{c_2}{m_2} & \frac{c_2}{m_2} & -\frac{c_a}{m_2} - \frac{c_a}{m_a} \end{bmatrix}$$

$$B = \begin{pmatrix} 0 \\ 0 \\ 0 \\ 0 \\ -\frac{1}{m_2} \\ \frac{1}{m_2} + \frac{1}{m_a} \end{pmatrix}$$

for TAK algorithm case, and

$$A = \begin{bmatrix} 0 & 0 & 0 & 1 & 0 & 0 \\ 0 & 0 & 0 & 0 & 1 & 0 \\ 0 & 0 & 0 & 0 & 0 & 1 \\ -\frac{k_1+k_2}{m_1} & \frac{k_2}{m_1} & 0 & -\frac{c_1+c_2}{m_1} & \frac{c_2}{m_1} & 0 \\ \frac{k_2}{m_2} & -\frac{k_2}{m_2} & \frac{k_a}{m_2} & \frac{c_2}{m_2} & -\frac{c_2}{m_2} & \frac{c_a}{m_2}+\frac{D}{m_2} \\ -\frac{k_2}{m_2} & \frac{k_2}{m_2} & -\frac{k_a}{m_2}-\frac{k_a}{m_a} & -\frac{c_2}{m_2} & \frac{c_2}{m_2} & -\frac{c_a+D}{m_2}-\frac{c_a+D}{m_a} \end{bmatrix}$$

$$B = \begin{pmatrix} 0 \\ 0 \\ 0 \\ 0 \\ -\frac{\alpha D}{m_2 A} \\ \frac{\alpha D}{m_2 A}+\frac{\alpha D}{m_a A} \end{pmatrix}$$

for KYB algorithm case.

where x_1 and x_2 are the relative displacements of the damped mass, and m_i, k_i and $c_i (i = 1, 2)$ are the damped mass, stiffness and damping coefficient of the model as shown in Fig. 3.3(b).

Numerical data used for the control design of the AMD system are summarized in Tables 3.1 and 3.2.

Table 3.1
Numerical Data for the Structural Model (With AMD)

(a) SDOF System

	Strong Direction	Weak Direction
m_s $\left[\frac{lb\cdot sec^2}{inch}\right]\left(\left[\frac{t\cdot sec^2}{cm}\right]\right)$	56.77 (1.014x10^{-2})	54.89 (9.803x10^{-3})
k_s $\left[\frac{lb}{inch}\right]\left(\left[\frac{t}{cm}\right]\right)$	12270 (2.192)	4651 (0.8306)
c_s $\left[\frac{lb\cdot sec}{inch}\right]\left(\left[\frac{t\cdot sec}{cm}\right]\right)$	21.70 (3.876x10^{-3})	10.41 (1.859x10^{-3})
m_a^* $\left[\frac{lb\cdot sec^2}{inch}\right]\left(\left[\frac{t\cdot sec^2}{cm}\right]\right)$	1.143 (2.041x10^{-4})	1.143 (2.041x10^{-4})
k_a^{**} $\left[\frac{lb}{inch}\right]\left(\left[\frac{t}{cm}\right]\right)$	236.3 (4.220x10^{-2})	75.04 (1.340x10^{-2})
c_a $\left[\frac{lb\cdot sec}{inch}\right]\left(\left[\frac{t\cdot sec}{cm}\right]\right)$	0	0

(b) 2DOF System

	Strong Direction	Weak Direction
m_1 $\left[\frac{lb\cdot sec^2}{inch}\right]$ $\left(\left[\frac{t\cdot sec^2}{cm}\right]\right)$ m_2	54.60 (9.752x10^{-3}) 54.60 (9.752x10^{-3})	54.60 (9.752x10^{-3}) 54.60 (9.752x10^{-3})
k_1 $\left[\frac{lb}{inch}\right]$ $\left(\left[\frac{t}{cm}\right]\right)$ k_2	26710 (4.770) 56610 (10.11)	10770 (1.924) 18670 (3.334)
C $\left[\frac{lb\cdot sec}{inch}\right]$ x10^{-3} $\left[\frac{t\cdot sec}{cm}\right]$	$\begin{bmatrix} 24.30 & -2.713 \\ -2.713 & 23.02 \end{bmatrix}$ $\begin{bmatrix} 4.340 & -0.4845 \\ -0.4845 & 4.110 \end{bmatrix}$	$\begin{bmatrix} 15.49 & -3.866 \\ -3.866 & 13.26 \end{bmatrix}$ $\begin{bmatrix} 2.767 & -0.6904 \\ -0.6904 & 2.368 \end{bmatrix}$
m_a^* $\left[\frac{lb\cdot sec^2}{inch}\right]\left(\left[\frac{t\cdot sec^2}{cm}\right]\right)$	1.143 (2.041x10^{-4})	1.143 (2.041x10^{-4})
k_a $\left[\frac{lb}{inch}\right]\left(\left[\frac{t}{cm}\right]\right)$	236.3 (4.220x10^{-2})	75.04 (1.340x10^{-2})
c_a $\left[\frac{lb\cdot sec}{inch}\right]\left(\left[\frac{t\cdot sec}{cm}\right]\right)$	0	0

m_a^* = 200 kg (changable to 150 and 250 kg) ** Optimal Sitffness

Table 3.2
Properties of AMD System

A_c [cm^2]	7.07
R_1	0
R_2	0
P_S [kg/cm^2]	140.0
Q_R [cm^3/sec]	1893.4
I_R [mA]	200.0
I_0 [mA]	50.0

SECTION 4
EXPERIMENTAL STUDY

The experimental study followed the program described in Section 2.4. This program included first the identification of structural parameters and the testing of efficiency of various control cases. This section describes the experimental results and presents a comparison with theoretical predictions.

4.1 Identification of Structure's Parameters

The structure parameters were determined using the frequency domain response described below:

For an MDOF system subjected to base acceleration, the equation of motion is:

$$\mathrm{M}\,\underset{\sim}{\ddot{x}}(t) + \mathrm{C}\,\underset{\sim}{\dot{x}} + \mathrm{K}\,\underset{\sim}{x}(t) = -\underset{\sim}{m}\,\ddot{x}_0(t) \qquad (4.1)$$

where $\underset{\sim}{m}$ is the mass vector consisting of the floor masses as components.

In the frequency domain, the absolute acceleration transfer function of the j-th DOF contributed by the k-th mode, ($\mathrm{H}_{jk}(i\omega))_a$ is obtained by a:

$$\mathrm{H}_{jk}(i\omega))_a = \frac{-\Gamma_k(2i\zeta_k\omega_k\omega + \omega_k^2)}{\omega_k^2 - \omega^2 + 2i\zeta_k\omega_k\omega}\phi_{jk} \qquad (4.2a)$$

where $\Gamma_k = -\underset{\sim}{\phi}_k^T \underset{\sim}{m}$, $\underset{\sim}{\phi}_k$ is the k-th modal vector of structure, i.e., the k-th column of modal shape matrix Φ which was orthgonally normalized such that $\Phi^T \mathrm{M}\Phi = \mathrm{I}$. ω_k and ζ_k are the natural frequency and damping factor of the k-th mode, respectively.

The peak values of the j-th transfer function is a superposition contribution of all modes, that is:

$$(H_j(i\omega))_a = \sum_{k=1}^{n} (H_{jk}(i\omega))_a \qquad (4.2b)$$

However, for small damping and well separated modes, the k-th peak of the j-th transfer function becomes equal to $(H_{jk}(i\omega))_a$. When the structure is lightly damped, the peaks in the transfer function occurs precisely at $\omega = \omega_k$ with its amplitude determined by:

$$|(H_{jk}(i\omega))_a| = \frac{\Gamma_k\sqrt{1+4\zeta_k^2}}{2\zeta_k}\phi_{jk} \qquad (4.3)$$

From Eq. (4.3), it is shown that the k-th peak value of the j-th transfer function, $|(H_{jk}(i\omega))_a|$, is proportional to the j-th component of the k-th modal shape. Therefore, by measuring the absolute acceleration transfer function at each DOF, the modal shapes can be determined from the ratio of the peak values for the same frequency corresponding to one mode of vibration. The frequency is the natural frequency of the k-th mode. Moreover, the damping factor of each mode can be estimated by solving Eq. (4.3).

The identification tests of the model structure were carried out on the shaking table. The banded (0-50 Hz) white noise, specified in Table 2.2 and 2.3, were used as the input excitations. A set of typical absolute acceleration transfer function in identification tests of model structure are shown in Fig. 4.1.

To permit the comparison between the ATS and the AMD Systems, the system configuration was maintained the same. Therefore, a basic structural configuration was considered, in which the AMD system was fixed on the top floor and the pretensioned tendons were attached only at the first floor. For this configuration, the model's properties are given in Table 4.1 for the strong direction and Table 4.2 for the weak direction.

In the testing program of the ATS Control, various structural configurations resulted from the attachments of the tendons. Identification tests were performed for each case and the identified structure parameters are listed in Table 4.3.

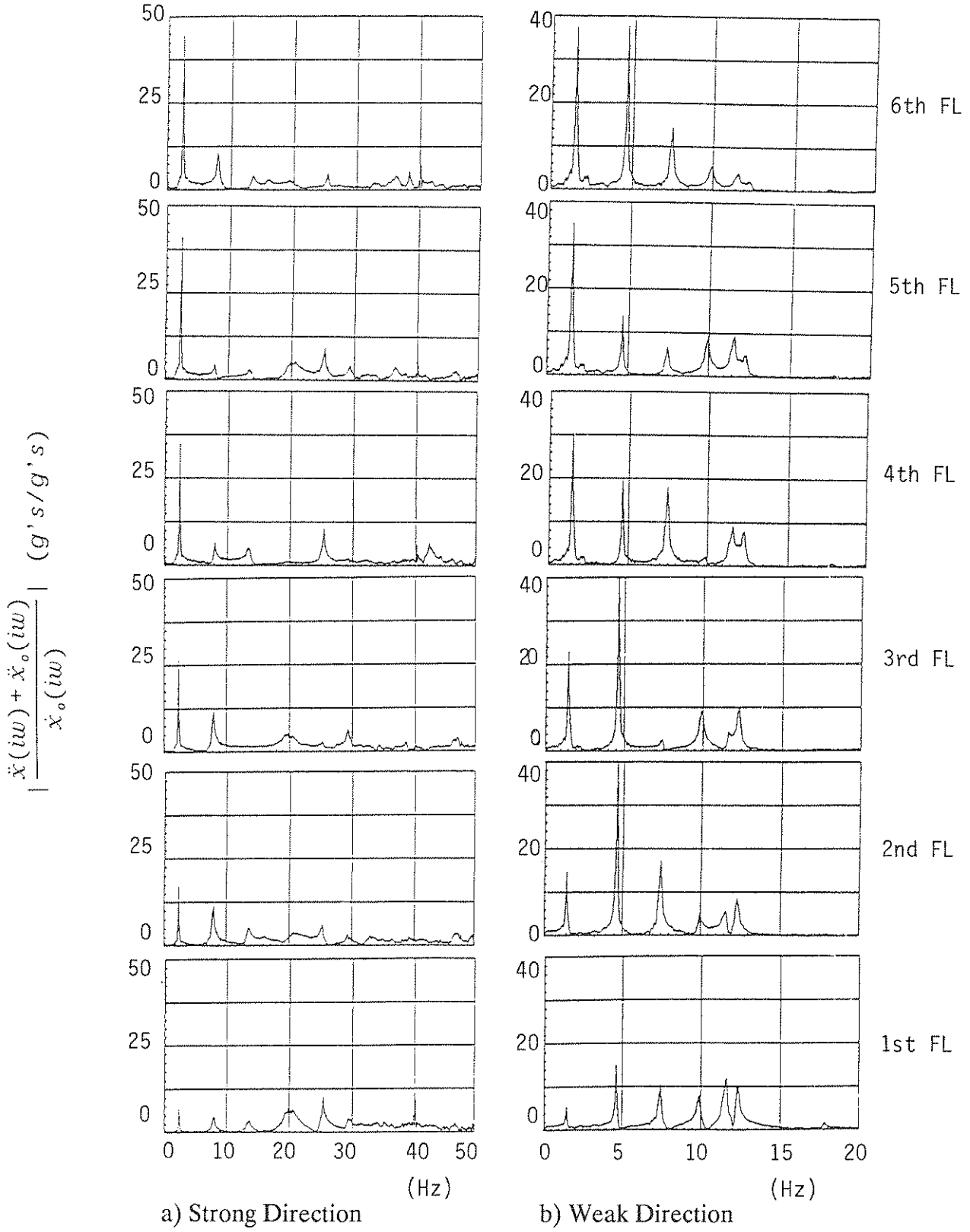

Figure 4.1 - Absolute Acceleration Frequency Transfer Functions Under White Noise Input

Table 4.1
Properties of Model Structure in Strong Direction

Height (ft)	18					
Width (ft)	12					
Weight (kips)	42					
Mode	1	2	3	4	5	6
Modal Shapes	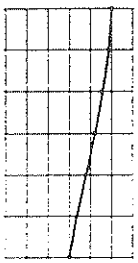	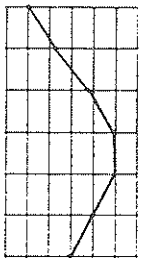	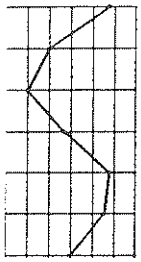	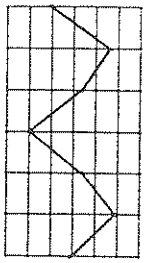	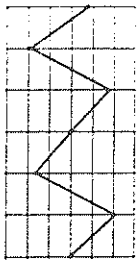	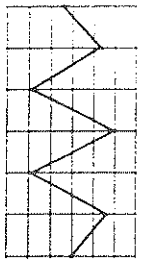
Modal Frequency (Hz)	2.44	7.91	13.48	20.51	25.29	29.20
Modal Damping factor (%)	1.42	2.04	2.35	1.55	0.59	0.86
Mass Matrix ($lb \cdot sec^2/inches$)	$\begin{bmatrix} 18.2 & & & & & \\ & 18.2 & & & 0 & \\ & & 18.2 & & & \\ & & & 18.2 & & \\ & 0 & & & 18.2 & \\ & & & & & 18.2 \end{bmatrix}$					
Stiffness Matrix $10^3 \cdot (lb/inches)$	$\begin{bmatrix} 3.446 & -1.731 & 0.217 & -0.098 & 0.154 & -0.095 \\ -1.731 & 2.786 & -1.615 & 0.253 & 0.009 & -0.013 \\ 0.217 & -1.615 & 2.758 & -1.602 & 0.211 & 0.016 \\ -0.098 & 0.253 & -1.602 & 2.849 & -1.727 & 0.273 \\ 0.154 & 0.009 & 0.211 & -1.727 & 2.714 & -1.254 \\ -0.095 & 0.013 & 0.016 & 0.273 & -1.254 & 0.990 \end{bmatrix}$					
Damping Matrix ($lb \cdot sec/inches$)	$\begin{bmatrix} 56.114 & 5.329 & -9.988 & -11.453 & 7.325 & -2.001 \\ 5.329 & 48.242 & -11.341 & -6.321 & -10.131 & 4.363 \\ -9.988 & -11.341 & 51.396 & -10.200 & -10.952 & -2.106 \\ -11.453 & -6.321 & -10.200 & 46.059 & -2.272 & -17.153 \\ 7.325 & -10.131 & -10.952 & -2.272 & 40.959 & -19.143 \\ -2.001 & 4.363 & -2.106 & -17.153 & -19.143 & 38.776 \end{bmatrix}$					

Table 4.2
Properties of Model Structure in Weak Direction

Height (ft)	18					
Width (ft)	4					
Weight (kips)	42					
Mode	1	2	3	4	5	6
Modal Shapes	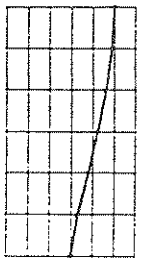	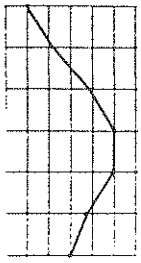	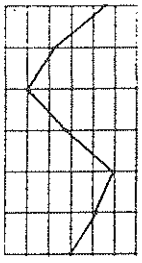	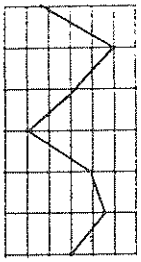	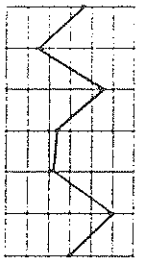	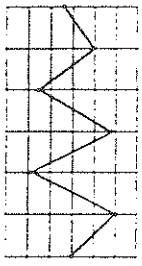
Modal Frequency (Hz)	1.46	4.59	7.42	9.96	11.62	12.30
Modal Damping factor (%)	1.70	0.47	0.76	1.02	1.00	0.67
Mass Matrix ($lb \cdot sec^2/inches$)	$\begin{bmatrix} 18.2 & & & & & \\ & 18.2 & & & 0 & \\ & & 18.2 & & & \\ & & & 18.2 & & \\ & 0 & & & 18.2 & \\ & & & & & 18.2 \end{bmatrix}$					
Stiffness Matrix $10^4 \cdot (lb/inches)$	$\begin{bmatrix} 8.553 & -2.637 & -0.072 & 0.075 & -0.095 & -0.098 \\ -2.637 & 5.283 & -2.790 & 0.076 & 0.026 & -0.003 \\ -0.072 & -2.790 & 5.613 & -2.929 & 0.048 & 0.057 \\ 0.075 & 0.076 & -2.929 & 5.583 & -2.842 & 0.082 \\ -0.095 & 0.026 & 0.048 & -2.842 & 5.579 & -2.840 \\ -0.098 & -0.003 & 0.057 & 0.082 & -2.840 & 2.726 \end{bmatrix}$					
Damping Matrix ($lb \cdot sec/inches$)	$\begin{bmatrix} 21.397 & -3.480 & -3.643 & 2.474 & -0.886 & 0.191 \\ -3.480 & 13.158 & -4.972 & -1.997 & 2.273 & 0.079 \\ -3.643 & -4.972 & 14.811 & -4.926 & -1.480 & 2.196 \\ 2.474 & -1.997 & -4.926 & 15.253 & -4.976 & 0.459 \\ -0.886 & 2.273 & -1.480 & -4.976 & 17.260 & -6.730 \\ 0.191 & 0.079 & 2.196 & 0.459 & -6.730 & 10.215 \end{bmatrix}$					

Table 4.3
Summary of Identification Tests of Model Structure

	Control case	Natural Frequency (f) & Damping Factors(ζ)	Mode					
			1	2	3	4	5	6
Strong direction	SC1	f (Hz)	2.44	7.91	13.48	20.51	25.29	29.20
		ζ (%)	1.42	2.04	2.35	1.55	0.59	0.86
	SC2	f (Hz)	2.54	8.30	13.38	19.92	24.80	28.42
		ζ (%)	1.76	3.16	1.32	1.09	0.68	0.76
	SC3	f (Hz)	2.63	7.91	13.28	19.82	25.00	28.71
		ζ (%)	1.90	2.54	1.00	1.24	0.59	0.63
	SC12	f (Hz)	2.54	8.30	13.57	20.02	25.00	28.52
		ζ (%)	2.00	2.75	2.03	2.11	0.86	1.96
	SC13	f (Hz)	2.64	8.01	13.28	19.92	25.00	28.81
		ζ (%)	1.50	4.00	1.59	1.64	0.55	0.36
Weak direction	W1C1	f (Hz)	1.46	4.59	7.42	9.96	11.62	12.30
		ζ (%)	1.70	0.47	0.76	1.02	1.00	0.67
	W2C13	f (Hz)	1.56	4.59	7.91	10.45	11.52	13.38
		ζ (%)	2.34	0.59	0.61	2.16	0.81	1.11

Table 4.4
Summary of Experimental Results in Strong Direction (25% El Centro)

Control cases		One Ctrl. Force						Prop. Ctrl.			
Case No.		SC 1		SC 2		SC 3		SC 12		SC 13	
Control parameter β		β = 2		β = 2		β = 2		β = 2		β = 2	
		Exp.	Theo.	Exp.	Theo.	Exp.	Theo.	Exp.	Theo.	Exp.	Theo.
Ave. Reduction of Structural Response (%)	Relative Dspl.	38.9	44.7	29.9	27.6	35.6	34.2	24.3	30.3	20.9	33.0
	Storydrift	33.5	41.7	14.0	23.3	21.7	30.9	19.7	24.4	7.0	28.7
	Absolute Acc.		34.8		19.5		18.3		22.9		24.0
Max. Control Force (Kips)		4.012	2.927	2.477	1.553	1.768	1.331	4.420	3.118	3.662	3.208
Max. Base Shear (kips)	Uncontrol	7.620	7.929	6.105	6.512	6.512	6.054	6.385	6.206	5.656	6.139
	Controlled	5.360	4.652	5.615	4.514	5.778	3.994	5.589	4.301	5.210	3.996
	Reduction (%)	29.7	41.3	8.0	26.5	11.3	34.0	12.5	30.7	7.9	34.9
Max. Power Supply (Kw)		1.064	0.565	2.340	0.465	1.218	0.456	0.978	0.491	0.822	0.507

4.2 Evaluation of Time Delays (ATS)

In ATS, the feedback control force lags the state variables by the time τ_x and $\tau_{\dot{x}}$. The delay time of control force is mostly contributed by the phase lags in conditioners, filters, on-line computations and the generation of the control force in the hydraulic system.

The time delay is determined from the phase lag measured between the signal input and signal output from any component. In an identification test, the banded (0-20 Hz) white noise was used as input. The output signals were measured from each one of components of the control system. The phase lag angle was determined from the imaginary and the real parts of the frequency transfer functions of the input and output signals. The delay time is then determined for each component of system by:

$$T_d = \frac{1}{360} \frac{\theta^\circ}{f} \tag{4.4}$$

where T_d is the time delay, θ° is the phase lag in degree and f is the frequency in hertz.

To minimize the time delay in the real time computations performed by the microprocessor from 14 channels of data a more rapid form of data transfer was used, i.e., a direct memory access (DMA). Data from all channels of the A/D board can be acquired almost simultaneously (i.e., at 36μsec. intervals). The real time control is performed by the microprocessor (computer) using a procedure coded using Microsoft/Quick Basic TM 4.0 using the DMA approach. A sample program for real time control is shown in Appendix B.

A set of typical experimental results were shown in Fig. 4.2. The time delay for real time computations was determined to be 7.1 ~ 7.5 msec. The time delay during the generation of the control forces by the hydraulic system was 11 ~ 15 msec. The total delay time, therefore, was 20 - 23 msec.

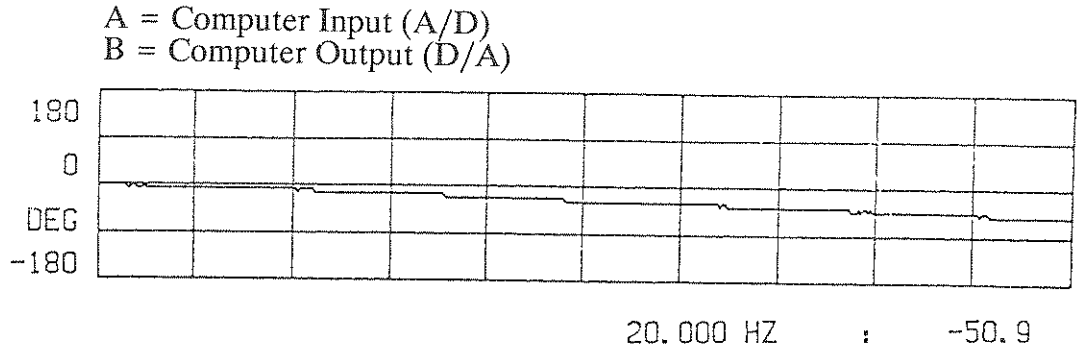

a) Computation Phase Lag

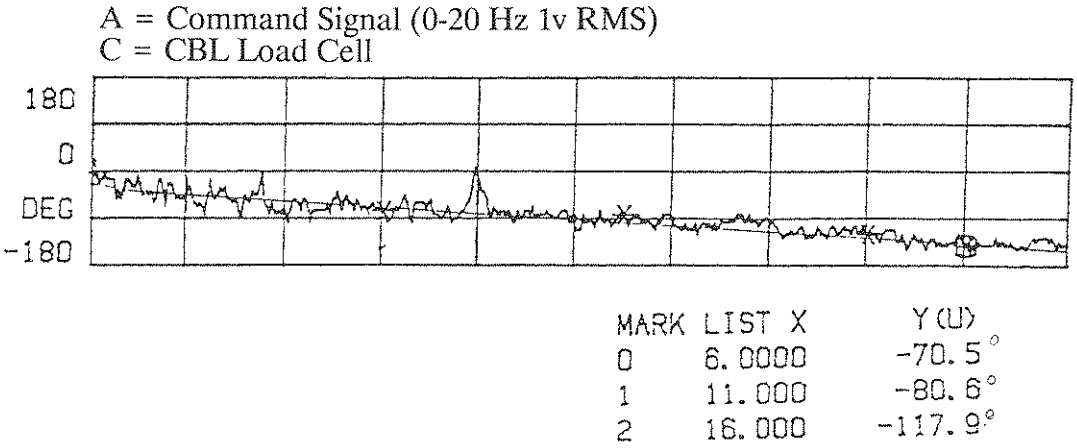

b) Phase Lag in Generation of Control Force

Figure 4.2 - Identification of Time Delay From Slope of Phase Lag.

4.3 Response of Controlled Structure

4.3.1 Response In "Strong" Direction

According to the experimental program (Section 2.4) the following excitation were used in the strong direction: (1) Banded (0-50 Hz) white noise with maximum acceleration 0.04g, and (2) the N-S component of El Centro 1940 earthquake acceleration. The accelerogram was scaled to 25% of its actual intensity (see Fig. 2.13) to prevent inelastic deformations in the model structure during the uncontrolled vibrations.

The white noise excitation was used only to check the experimental set-up and the calibration of the real-time computations. The experimental and the theoretical results presented in this report are for the seismic excitations only.

4.3.1.1 Response With ATS Control

According to the experimental program, only one actuator, installed at the base, was used. The tendons were connected to a single floor to produce a single control force, or to two floors simultaneously in order to produce a proportional control. The results of the experimental study were listed in Table 4.4.

4.3.1.1.1 Control Parameters

The design of the ATS control depends only on one parameter, β, therefore only this parameter should be determined in the design of the ATS control. Based on computer simulations performed prior to the experiments for the case SC1 (see Table 2.2), the average reductions of displacement responses, control force, base shear reduction and maximum power requirements were determined and are shown in Figs. 4.3 (a) through (d), respectively. From these simulations, it was shown that as the β value was decreased, the control efficiency was increased, however, the control force and power requirements were simultaneously increased.

To obtain the best control efficiency, a smaller β value had to be chosen. However, the β value cannot be too small due to limitation in the mechanical resources, such as the

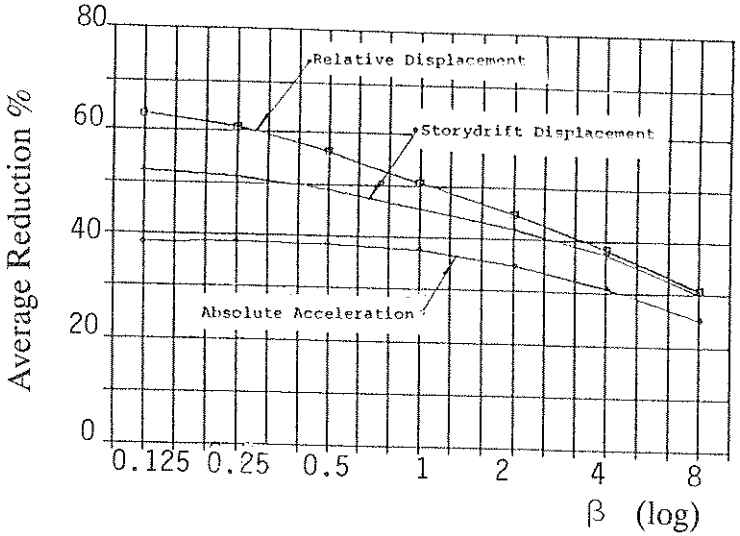

a) Reductions of Structural Responses

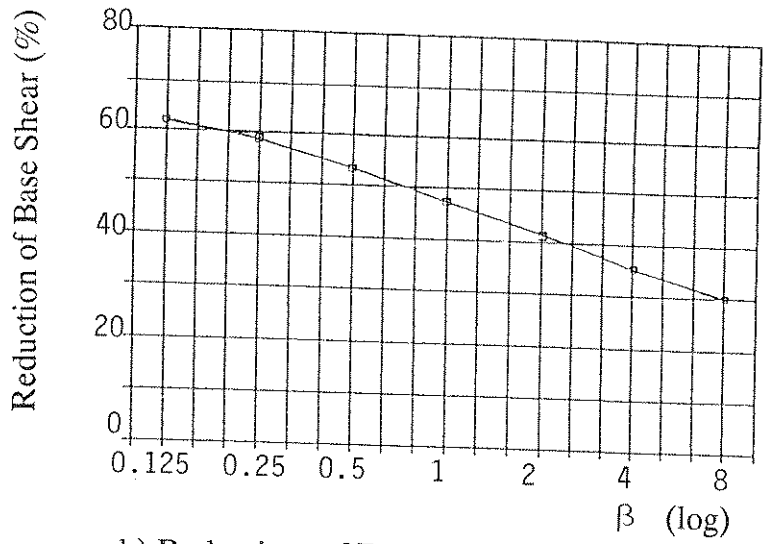

b) Reductions of Base Shear

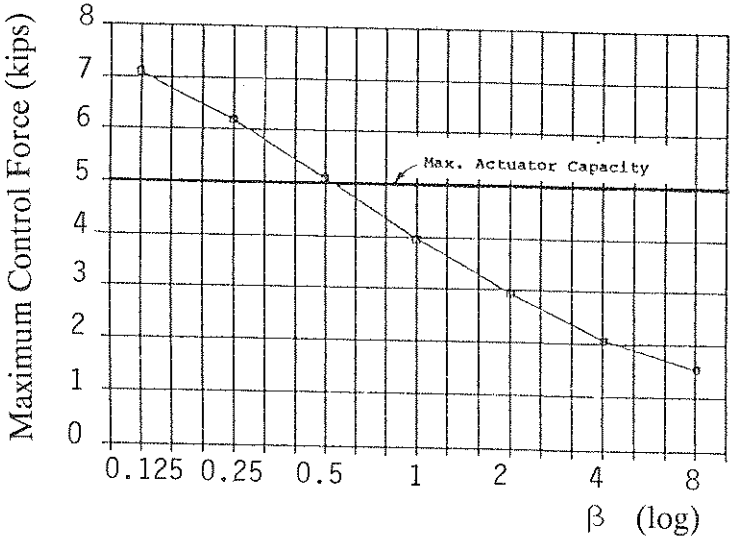

c) Maximum Control Forces

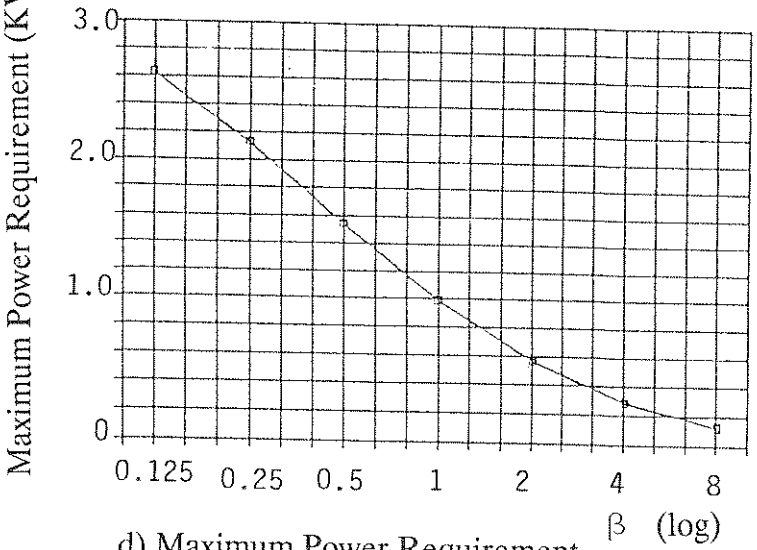

d) Maximum Power Requirement

Figure 4.3 - Comparisons of β Values

control force which cannot exceed 2.27 ton (5000 lbs). Similar simulations had to be done for all other cases. The control parameter β was determined to be 2.0 for all cases and was used in the experimental verification.

4.3.1.1.2 Structural Response of Controlled Structure

Typical response of the structure with active control for the case SC1 are shown in Figs. 4.4 through 4.9. The displacement response is clearly reduced at all floors similarly with the predicted theoretical values. At the same time the absolute acceleration is shown in Fig. 4.10. The reduction of the first dominant mode is visible. However the second mode and in part (but much less) the third mode are somewhat amplified particularly due to the interaction between the active controller and the driving system of the shaking table. The increase is insignificant, however, and influences only weakly the displacement response as shown in Figs. 4.4 through 4.9.

4.3.1.1.3 Comparison of Experimental Response With Analytical Studies

Using the model structure's parameters obtained in identification test, the theoretical results were calculated by computer simulations. The experimental and theoretical results are summarized in Table 4.4, in which the reductions of the relative displacements, story drifts, and base shear were calculated based on the peak response values obtained in time domain. Average reductions were calculated to emphasize the general efficiency of the control schemes.

The comparisons of experimental and theoretical results based on the peak values are shown in Figs. 4.11 through 4.13. The plots show similar experimental and theoretical influences of the control configurations, however, differences of up to 50% appear in the actual results. These discrepancies are originated by:

(1) The interaction between the model structure and shaking table, as explained in Section 2.3. The higher frequency components which were introduced to the base excitation input caused an increase in the response of the second mode which in turn produced discrepancies in both displacement and accelerations. The experimental response shows pronounced increases due to the second mode (see Fig. 4.11), which in turn cause reduction of the control efficiency (see

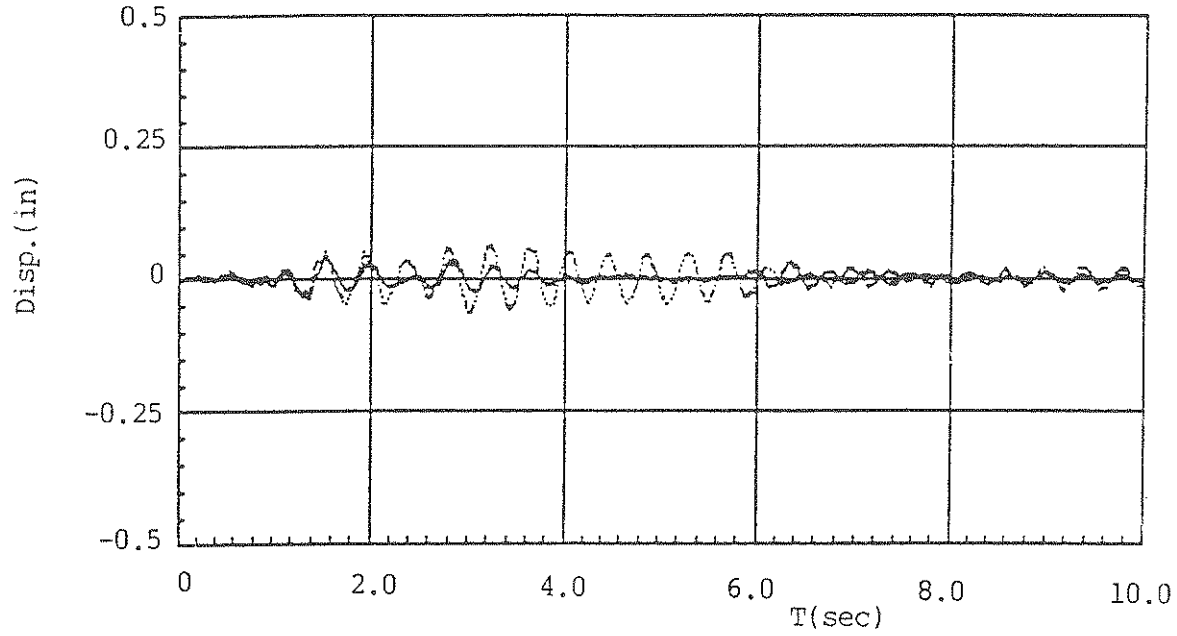

a) Experimental

..... No Control

——— With Control

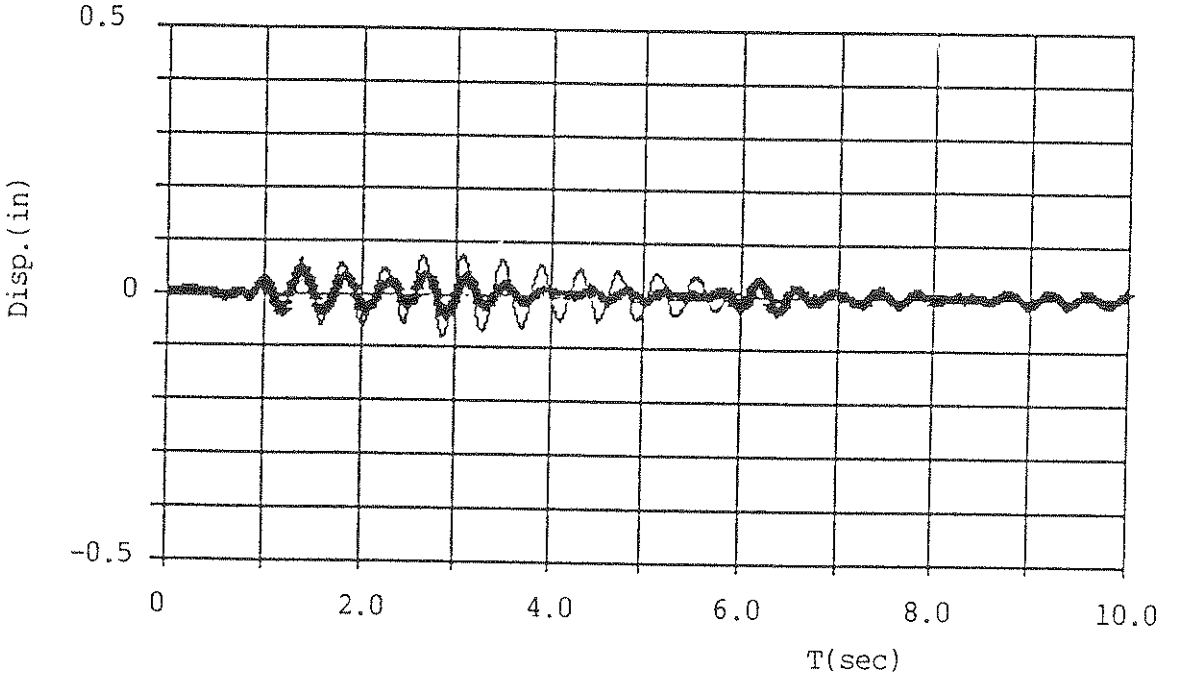

b) Theoretical

——— No Control

++++++++ With Control

Figure 4.4 - First Floor Relative Displacement Responses.

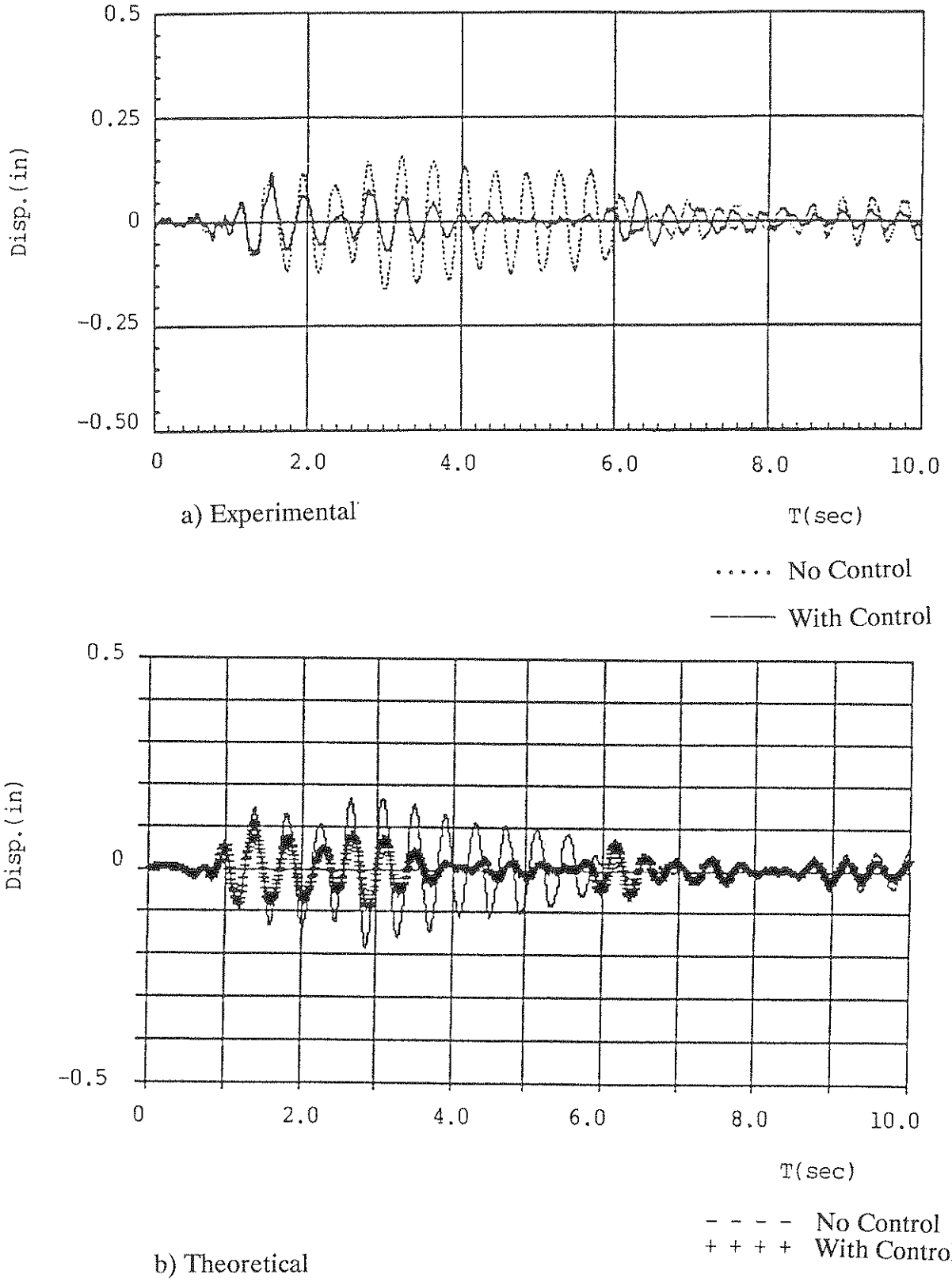

Figure 4.5 - Second Floor Relative Displacement Responses.

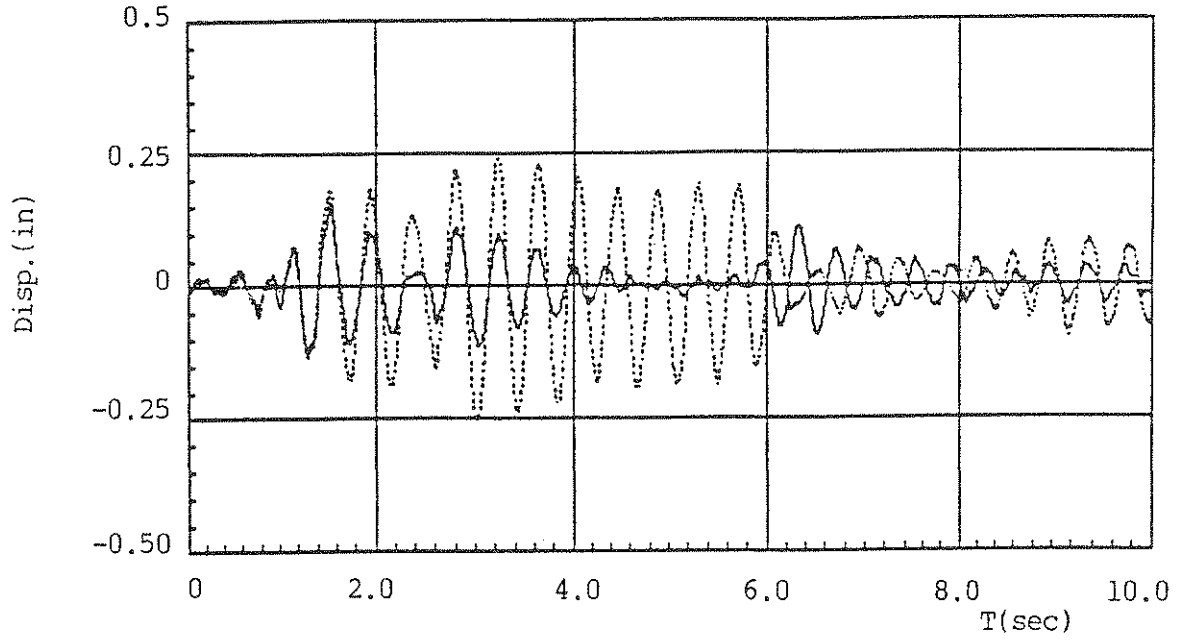

a) Experimental

····· No Control

—— With Control

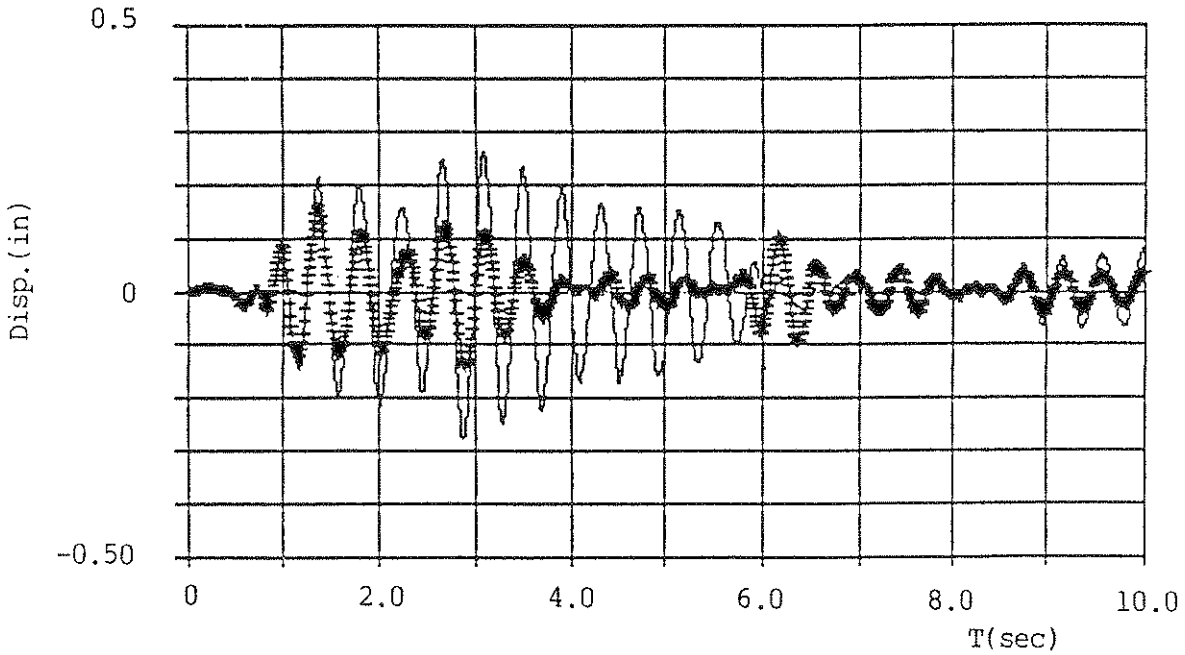

b) Theoretical

– – – – No Control

+ + + + With Control

Figure 4.6 - Third Floor Relative Displacement Responses.

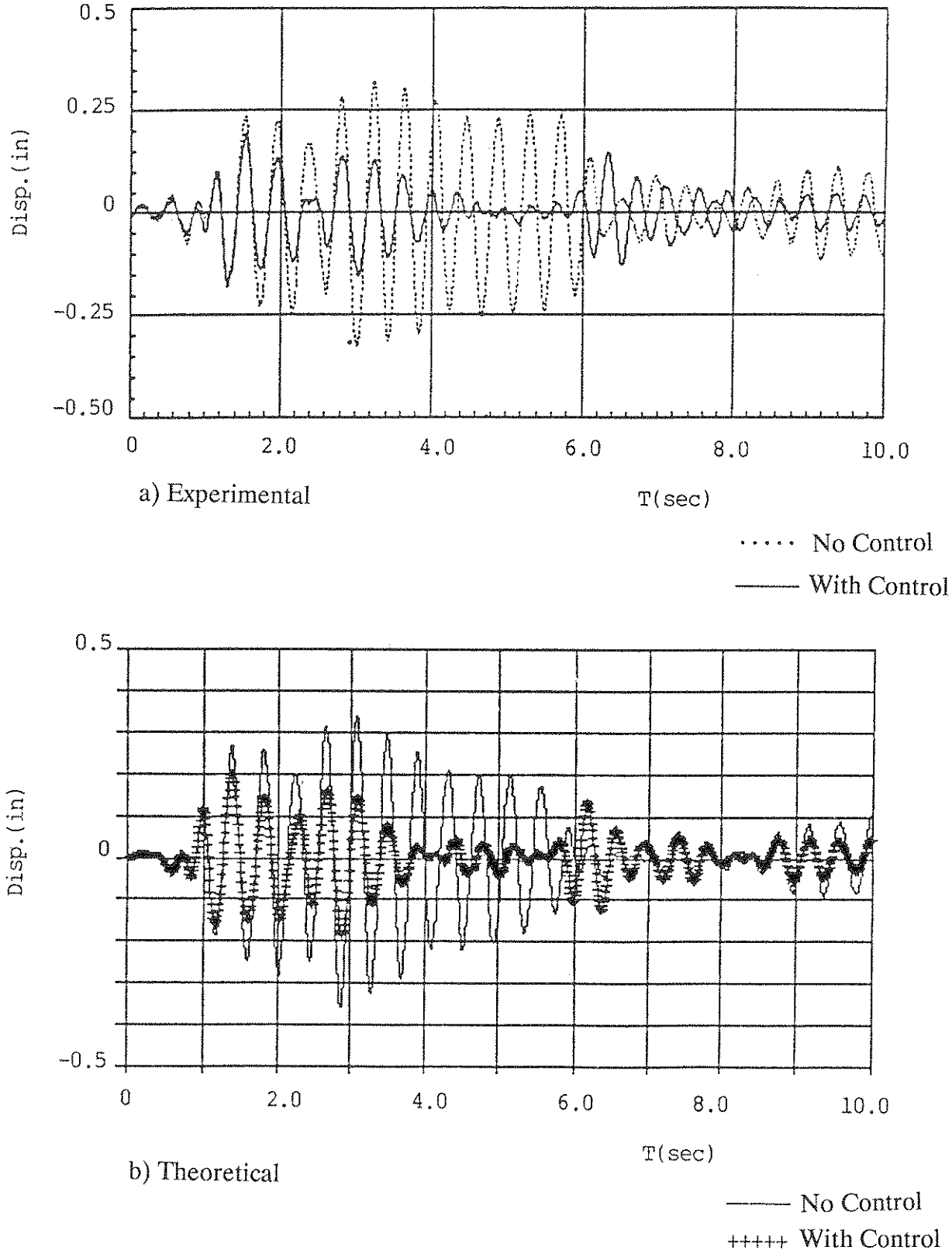

Figure 4.7 - Fourth Floor Relative Displacement Responses.

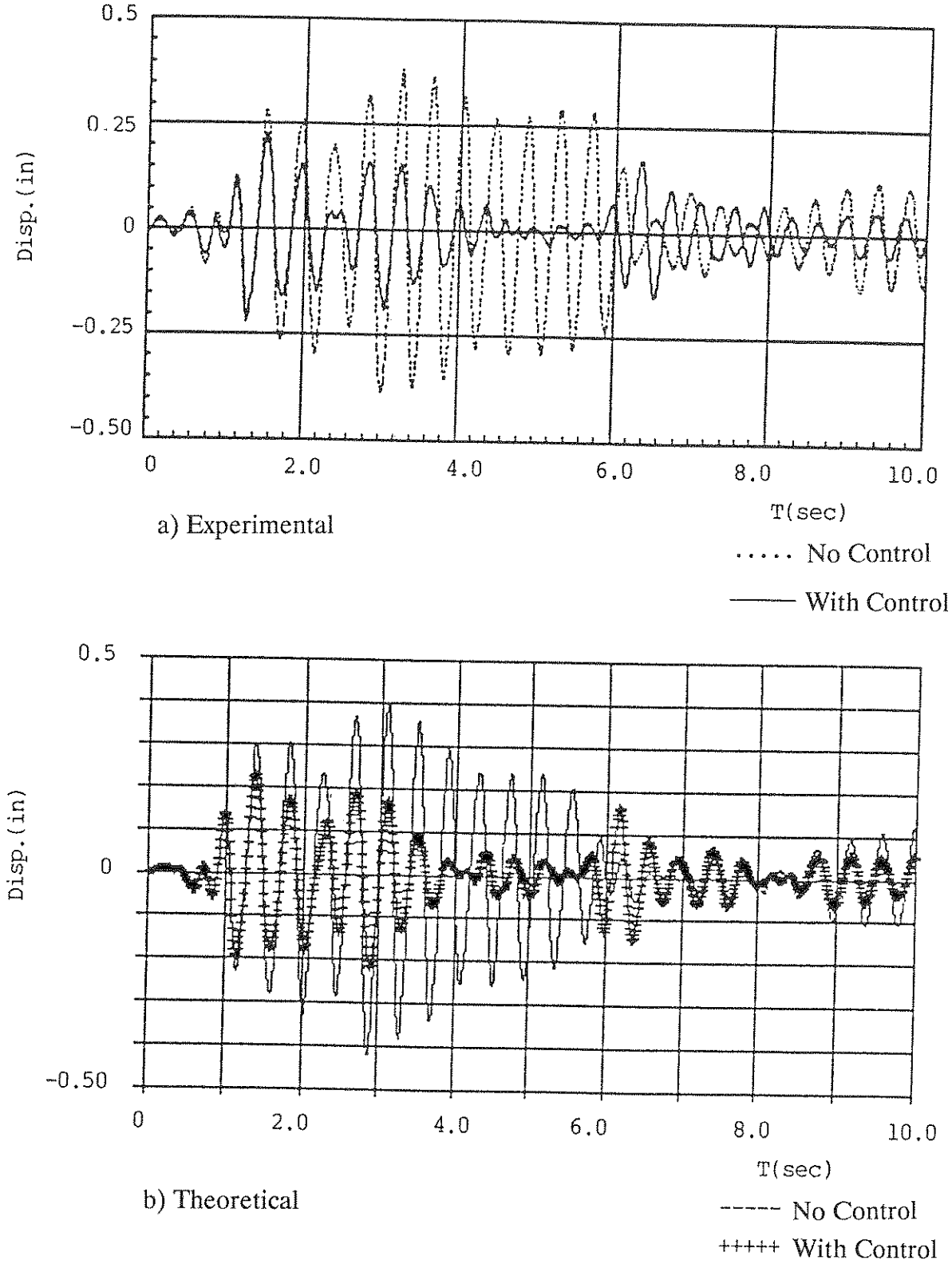

Figure 4.8 - Fifth Floor Relative Displacement Responses.

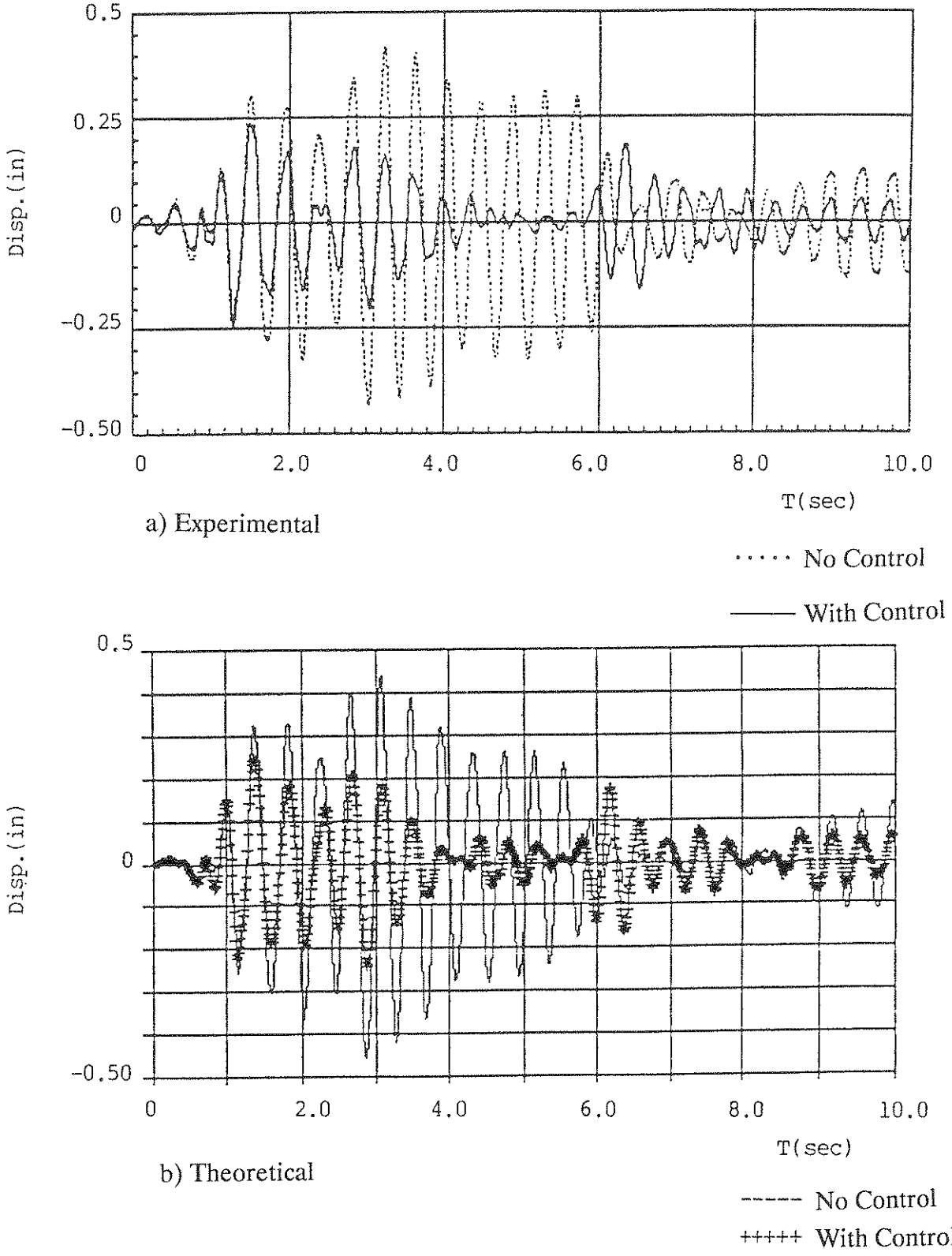

Figure 4.9 - Sixth Floor Relative Displacement Responses.

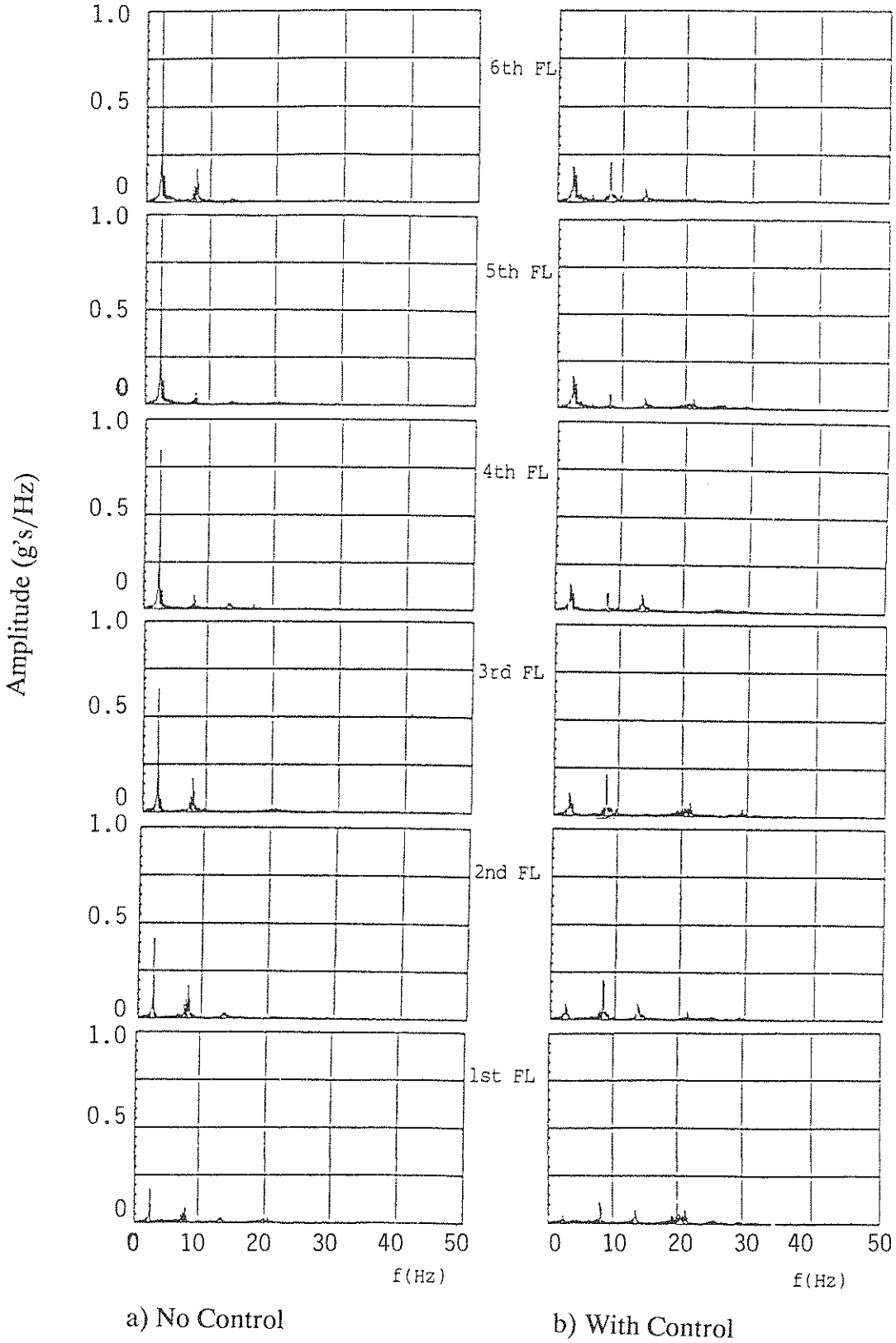

Figure 4.10 - Absolute Acceleration Responses in Frequency Domain (Experimental)

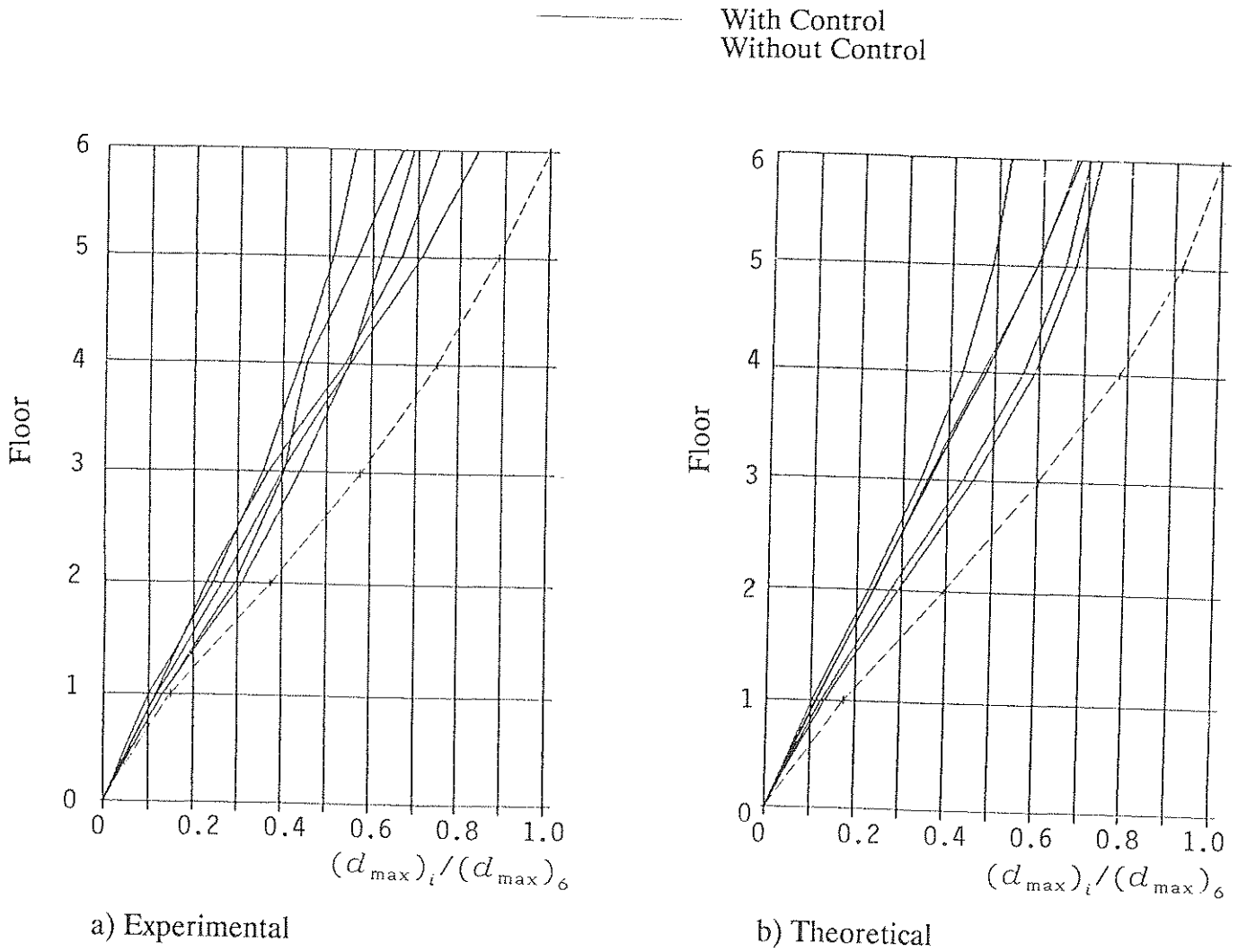

Figure 4.11 - Peak Values of Relative Displacement in Strong Direction (25% El Centro Excitation).

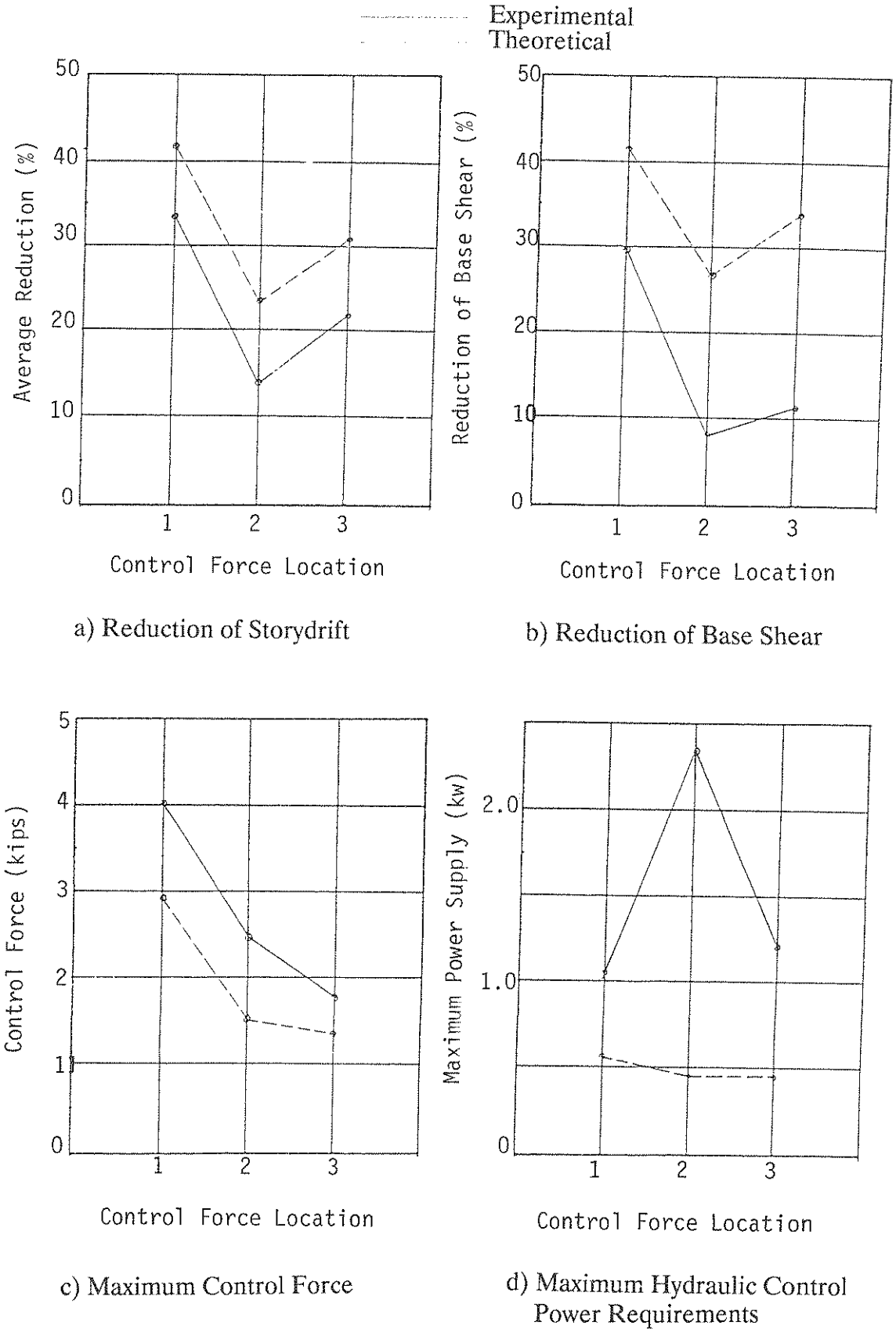

Figure 4.12 - Comparisons of Single Force Control in Strong Direction.

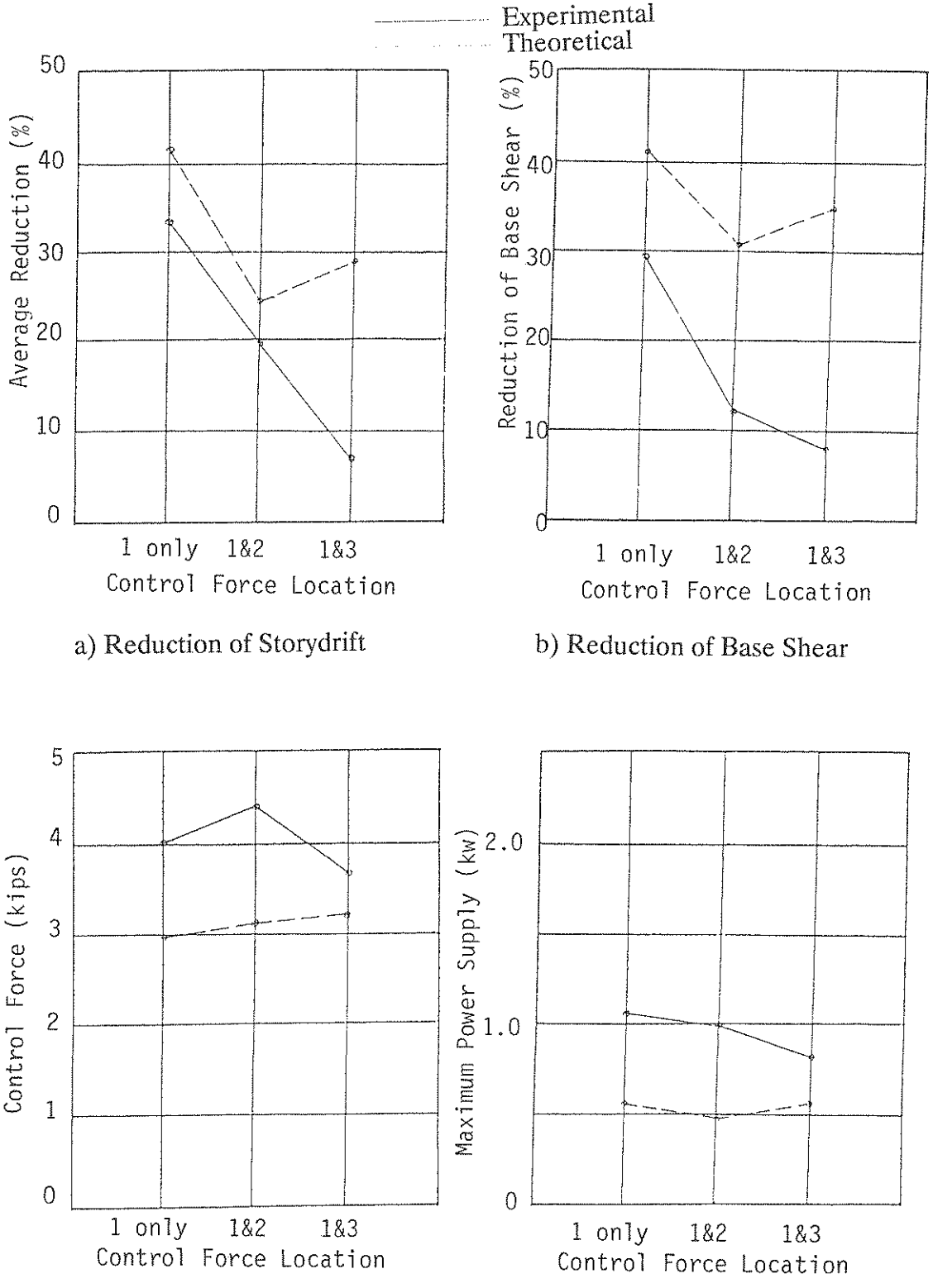

a) Reduction of Storydrift

b) Reduction of Base Shear

c) Maximum Control Force

d) Maximum Hydraulic Control Power Requirements

Figure 4.13 - Comparisons of Proportional Control in Strong Direction.

Fig. 4.11), which in turn cause reduction of the control efficiency (see Figs. 4.12 and 4.13). At the same time this distorted input, resonant to the second mode, increased the power requirements, the control forces, and the total base shear.

(2) The errors in estimating the damping factors which were determined from the peak values of absolute acceleration transfer function are not negligible. Due to the interaction between modes, which can be seen from Fig. 4.1, the errors are unavoidable. These errors influenced the theoretical results.

In spite of the discrepancies in the peak amplitudes in the time response, a regular in pattern can be noticed in Figs. 4.4 through 4.9, which show the comparisons of relative displacement response for each floor.

4.3.1.1.4 Comparison of Various Tendons Configurations

The maximum relative displacement, storydrift, control forces, base shear and power requirements are plotted in Figs. 4.11 through 4.13 for all single force and proportional forces controls. The results are produced in terms of reductions in respect to the uncontrolled case. As it can be noticed in Fig. 4.11 (a), that the single actuator single tendon case (SC1) produces the largest reduction throughout the height of the structure. At the top, the reduction reaches 45%. All other response quantities are also reduced, mostly in the case SC1 (i.e., 30%-35%). The power requirements for this case are about the same as for the other control configurations.

4.3.1.1.5 ATS Control Efficiency

The control efficiency is emphasized in Table 4.4 and in Figs. 4.11 through 4.13 in the best control case, the average reductions of relative displacement achieved are 39% in experimental and 45% in theoretical results. The average reductions of story drifts were 34% in the experimental and 42% in the theoretical results. The reductions of base shear were 30% in experimental and 41% in theoretical results.

In the experimental results, the reduction of absolute acceleration was not calculated (and not shown in Table 4.4), since several peak values of the absolute acceleration response were increased due to the interaction between the control system and the shaking systems in the second and third mode. These high frequency peaks make the comparisons meaningless. The

absolute acceleration peaks in the frequency domain (Fig. 4.10) emphasize the increase in the peak of second mode. The experimental acceleration response shows, therefore, a reduction of the dominant mode (under control) and the higher modes in addition to some sporadic increases contributed by the second mode.

At the same time the theoretical response (Fig. 4.14) shows first mode reduction like the experimental, and in addition shows the expected reductions in the higher modes (in absence of base motion errors). The theoretical results indicated that the average reduction of absolute acceleration of 35% can be achieved in perfect experimental conditions or in real operation.

Moreover, from reductions of maximum base shear (see Figs. 4.12 (b)) and 4.13 (b) calculated based on the absolute accelerations, it is clear that effects of the absolute acceleration responses were well controlled in the experiments.

A detailed discussion of feasibility of control using the ATS control is presented in Section 5.

4.3.1.2 Response With AMD Control

4.3.1.2.1 Samples of Experimental Results

Following the experimental program emphasized in Section 2.4, the structure was tested with various control parameters. Only several results, most representative, are presented in this section.

The experimental results with and without control in terms of time histories of the relative displacement and the absolute acceleration at the top and at the third floors under 25% El Centro excitation are displayed in Figs. 4.15 and 4.16, respectively. In this controlled case, KYB-M regulator (Type 2 in Table 2.4) was used.

As shown in Figs. 4.15 and 4.16, significant reductions of the relative displacement and the absolute accelerations are obtained. The corresponding time histories of the mass stroke, the mass acceleration and the control force are shown in Fig. 4.17.

Transfer functions of the absolute acceleration at the top and the third floor under the banded white noise input are shown in Fig. 4.18. For three kinds of experimental results, which are obtained from the uncontrolled case, i.e., the controlled case with the top floor information only, and the controlled case with both the top and the third floor information.

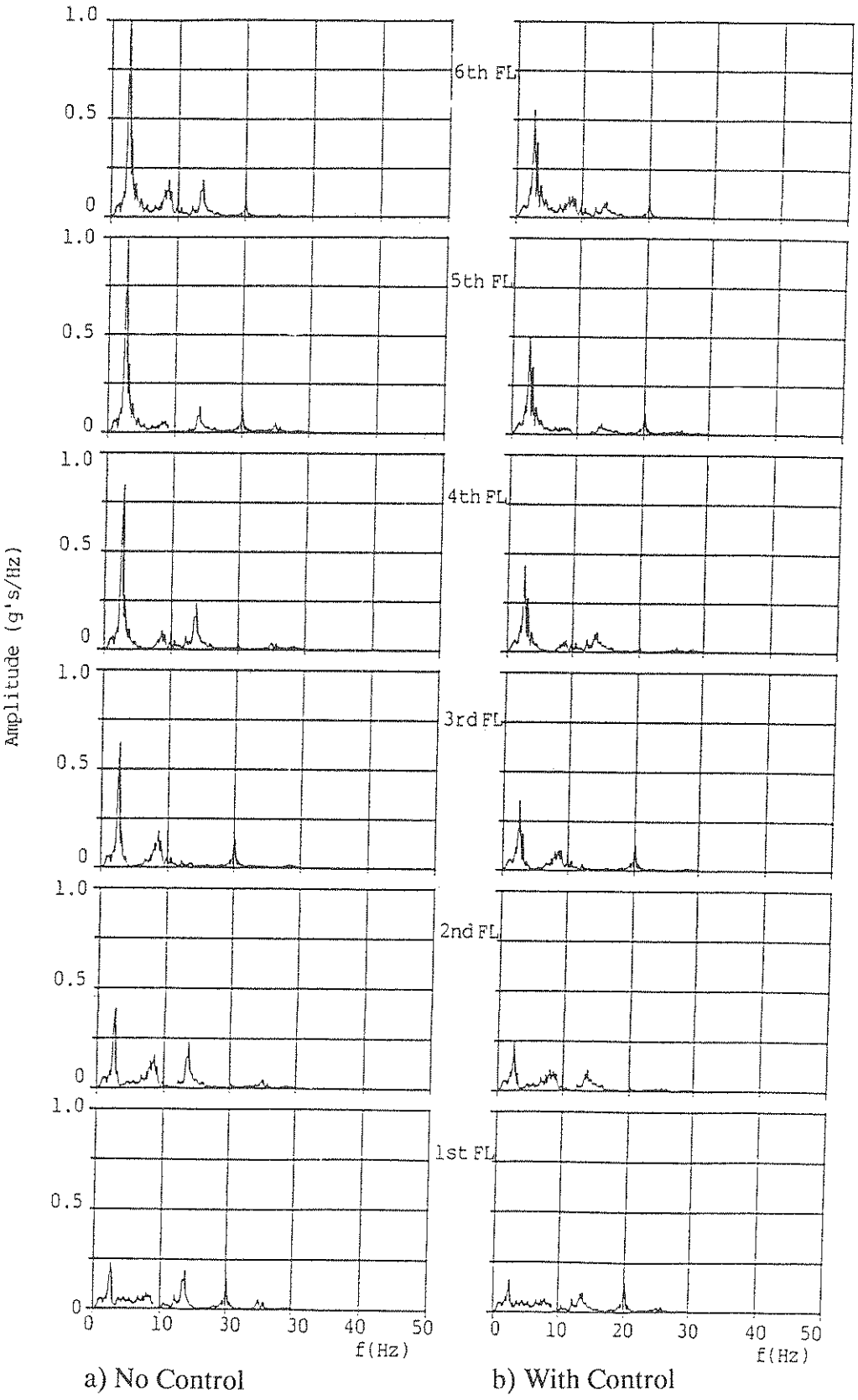

Figure 4.14 - Absolute Acceleration Responses in Frequency Domain (Theoretical)

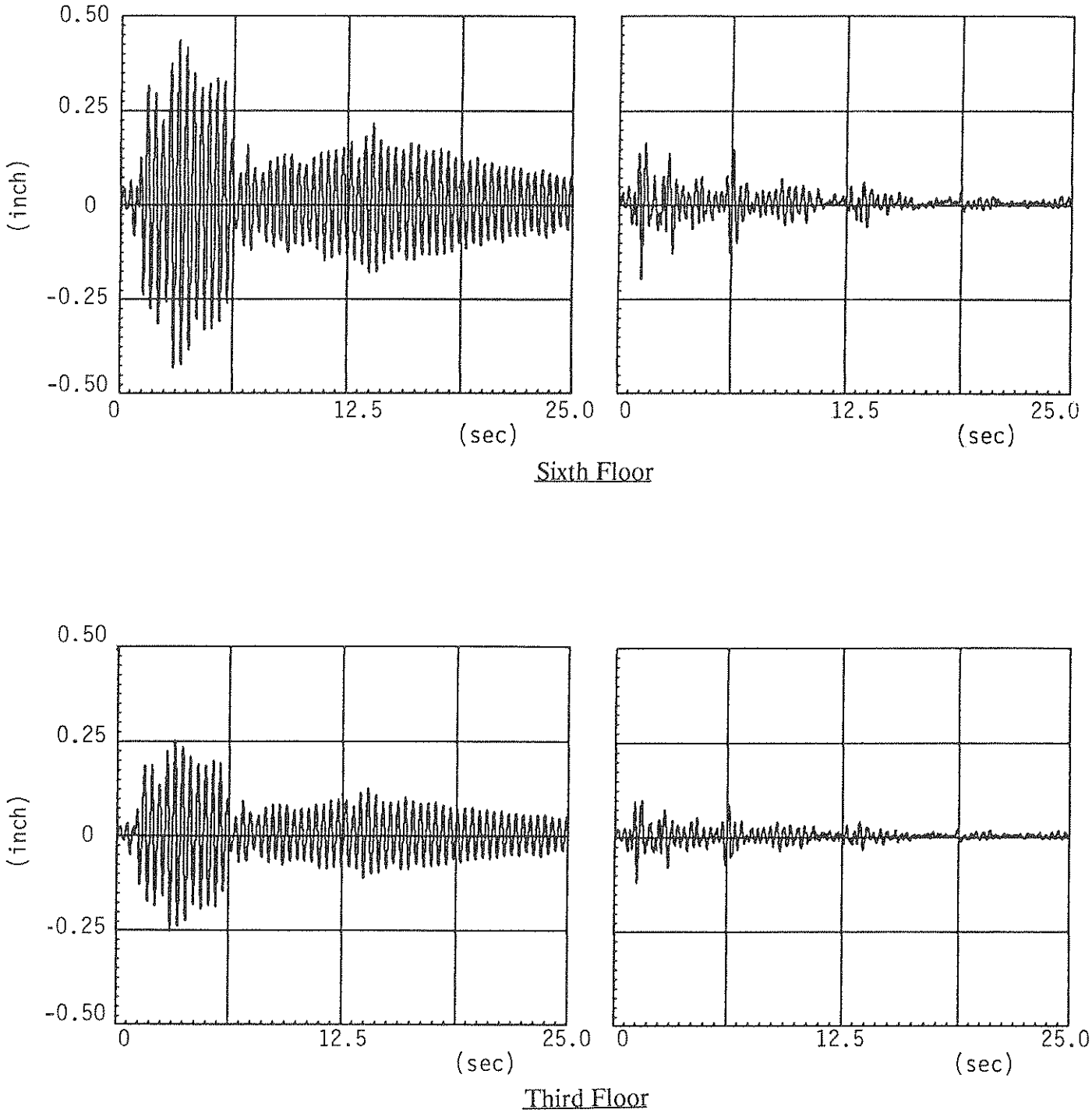

Figure 4.15 - Relative Displacement Response With AMD Control (El Centro 25% Excitation).

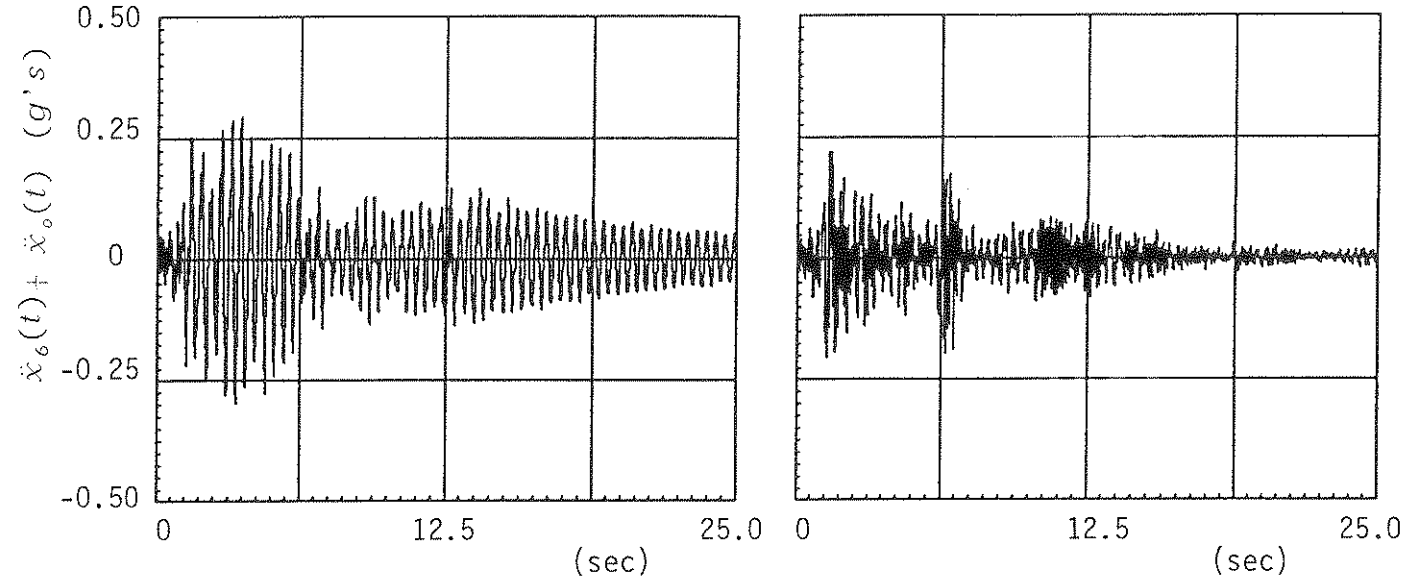

Sixth Floor

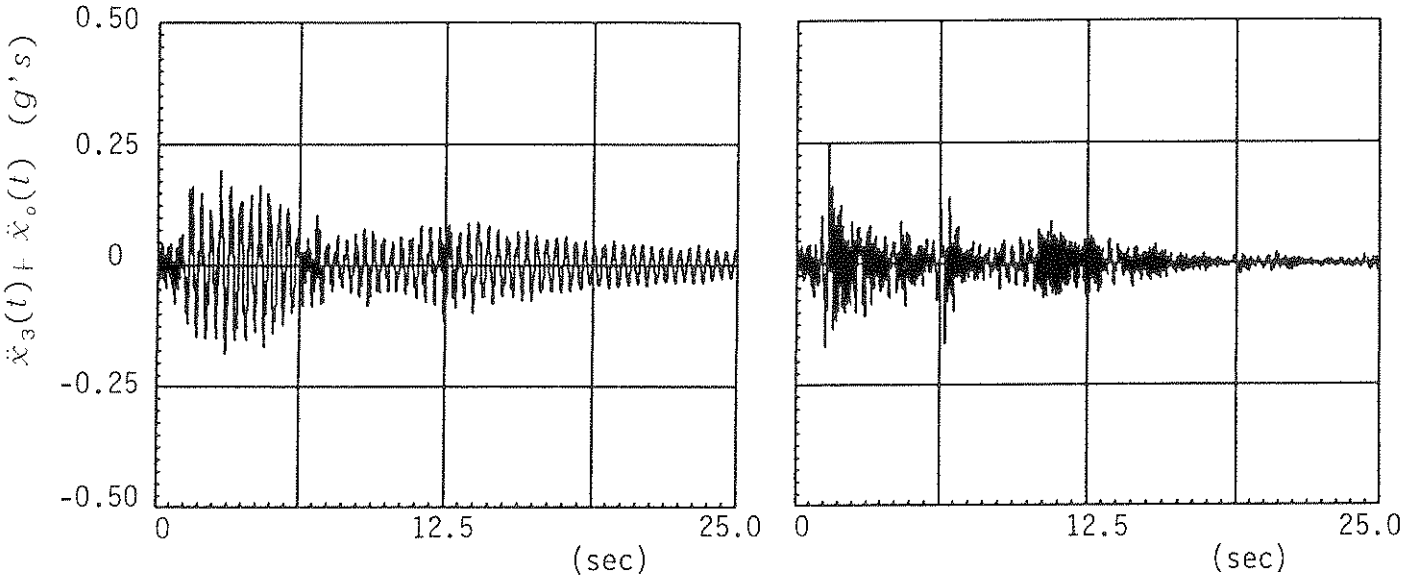

Third Floor

a) Without Control

b) With Control

Figure 4.16 - Absolute Acceleration Response With AMD Control (El Centrol 25% Excitation).

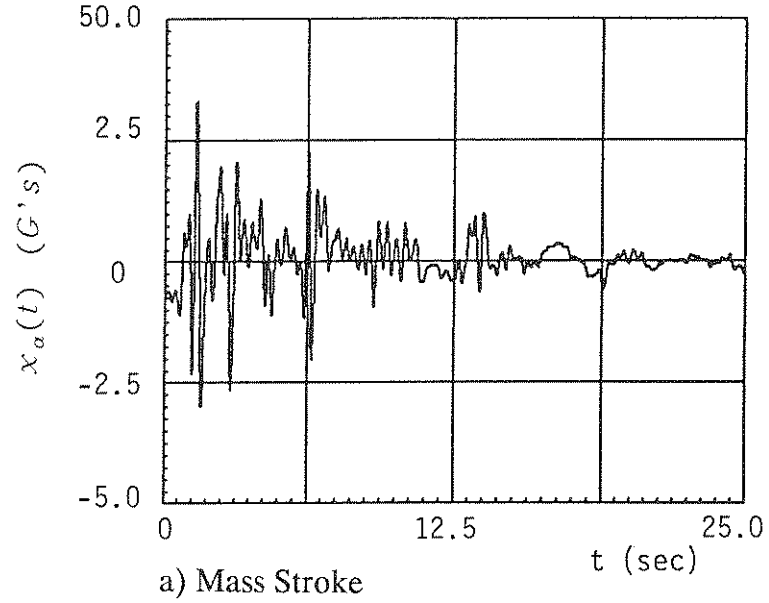

a) Mass Stroke

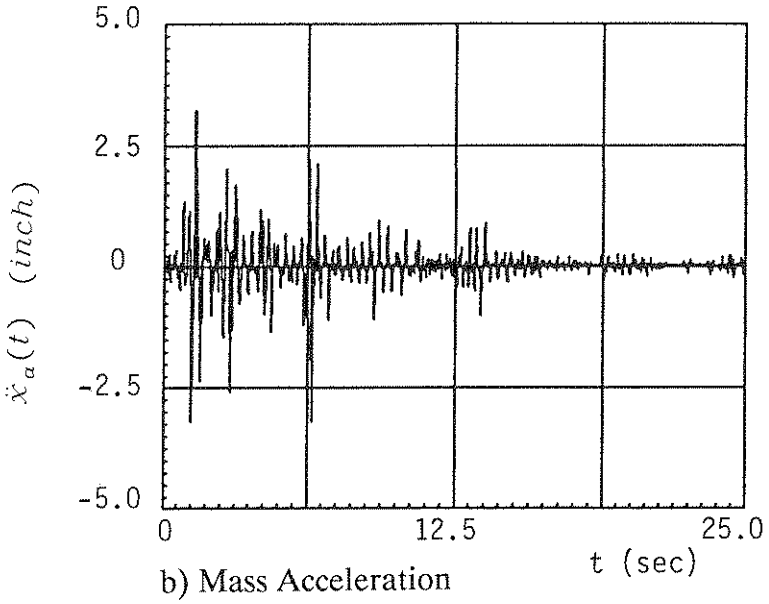

b) Mass Acceleration

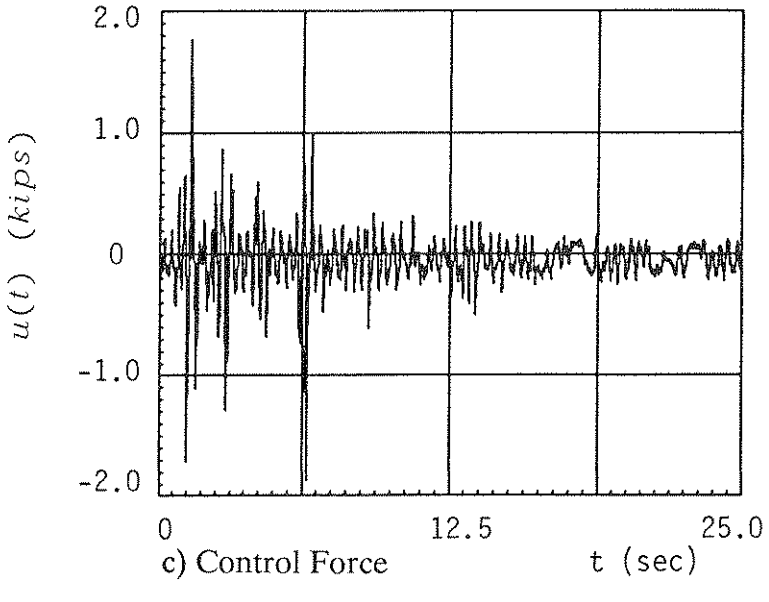

c) Control Force

Figure 4.17 - Control Resources For KYB-M Regulator.

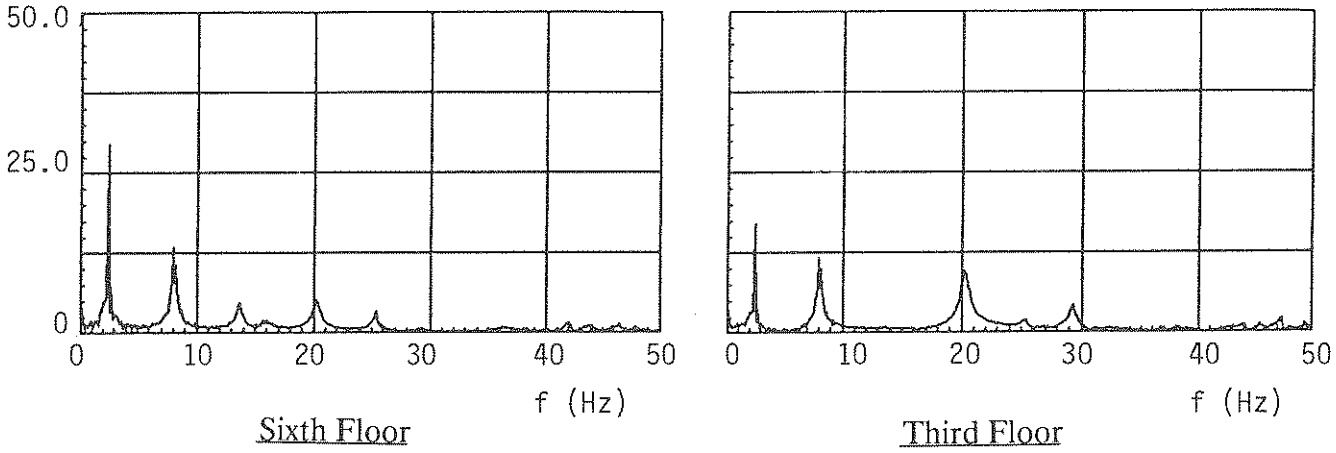

a) Uncontrolled

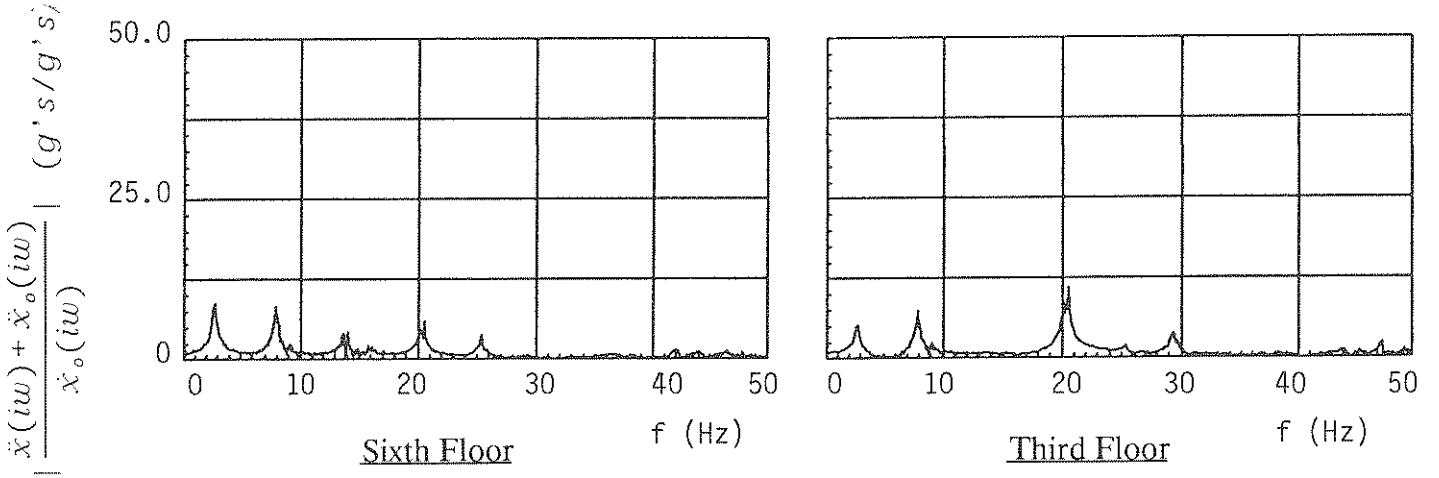

b) Controlled With the Top Floor Information

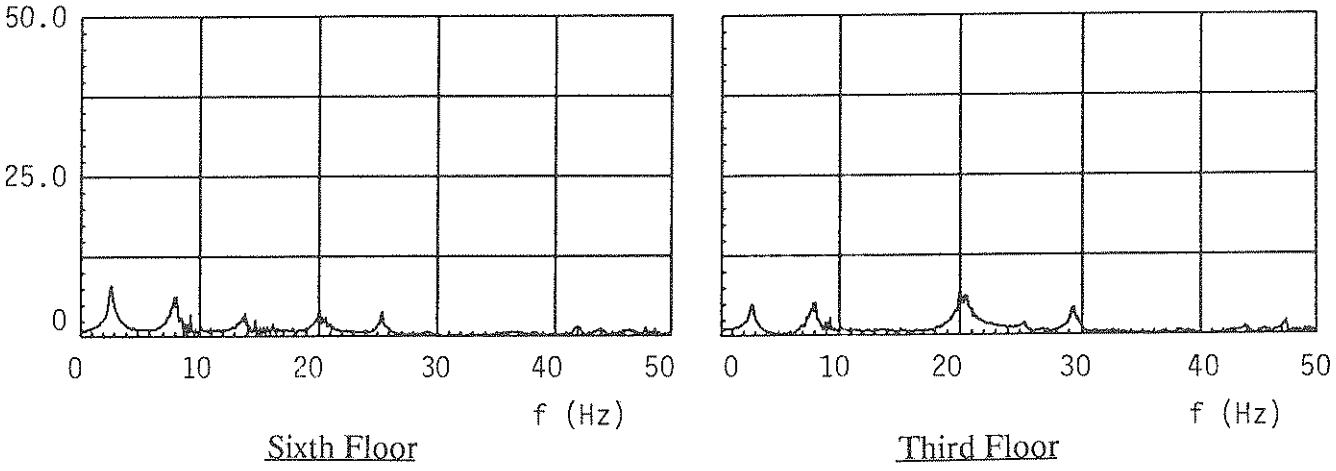

c) Controlled With the Top and the Third Floor Information.

Figure 4.18 - Transfer Functions of the Absolute Acceleration (White Noise 0.04G Excitation).

The controlled results show significant reductions on the second and the third components of acceleration response as well as the first one. In the case with both the top and the third floor information, the control effects for the higher components are obviously better.

The maximum experimental relative displacements at each floor with various regulators are plotted in Fig. 4.19. At the top floor, a reduction of 20% to 60% is achieved. The percentage of reduction is primarily dependent on the weighting magnitude used in the control algorithms. The percentage of the reduction of the displacement response at each peak is shown in Fig. 4.20 (b), in which the top floor displacement responses with and without control are compared for KYB-M regulator (Type 2 in Table 2.4). For the uncontrolled case, the occurrence of the maximum relative displacement response or maximum absolute acceleration response at each floor is about four cycles behind that of the peak acceleration of the El Centro excitation. The maximum value of the controlled case occurs at the same time as that of the input ground motion.

Throughout all the experimental programs, as shown in this typical example, the control was less effective at the initial few steps, however, in the following steps the control efficiency was substantially improved. In spite of their brief occurrence, the maximum response quantities are used further in the evaluation to indicate the control effects, because they are the important factors for the actual structural design, even though the time factors are not taken into account. Moreover, to evaluate the control efficiencies, the maximum mass stroke and the maximum control force, which are the important factors for the design of the AMD system, are further used for comparisons. The reduced values of the maximum displacement and acceleration responses divided by the required mass stroke or control force are defined as the *characteristic magnitudes*.

4.3.1.2.2 Efficiencies of Various Control Cases

The efficiency of various control regulators tested in the present experimental programs (see Section 2.6) is dependent on the control weighting magnitudes, on the mass stroke, on the control force, on the mass weight, on the added stiffness, and on the objective variables. The various influences are compared in the following:

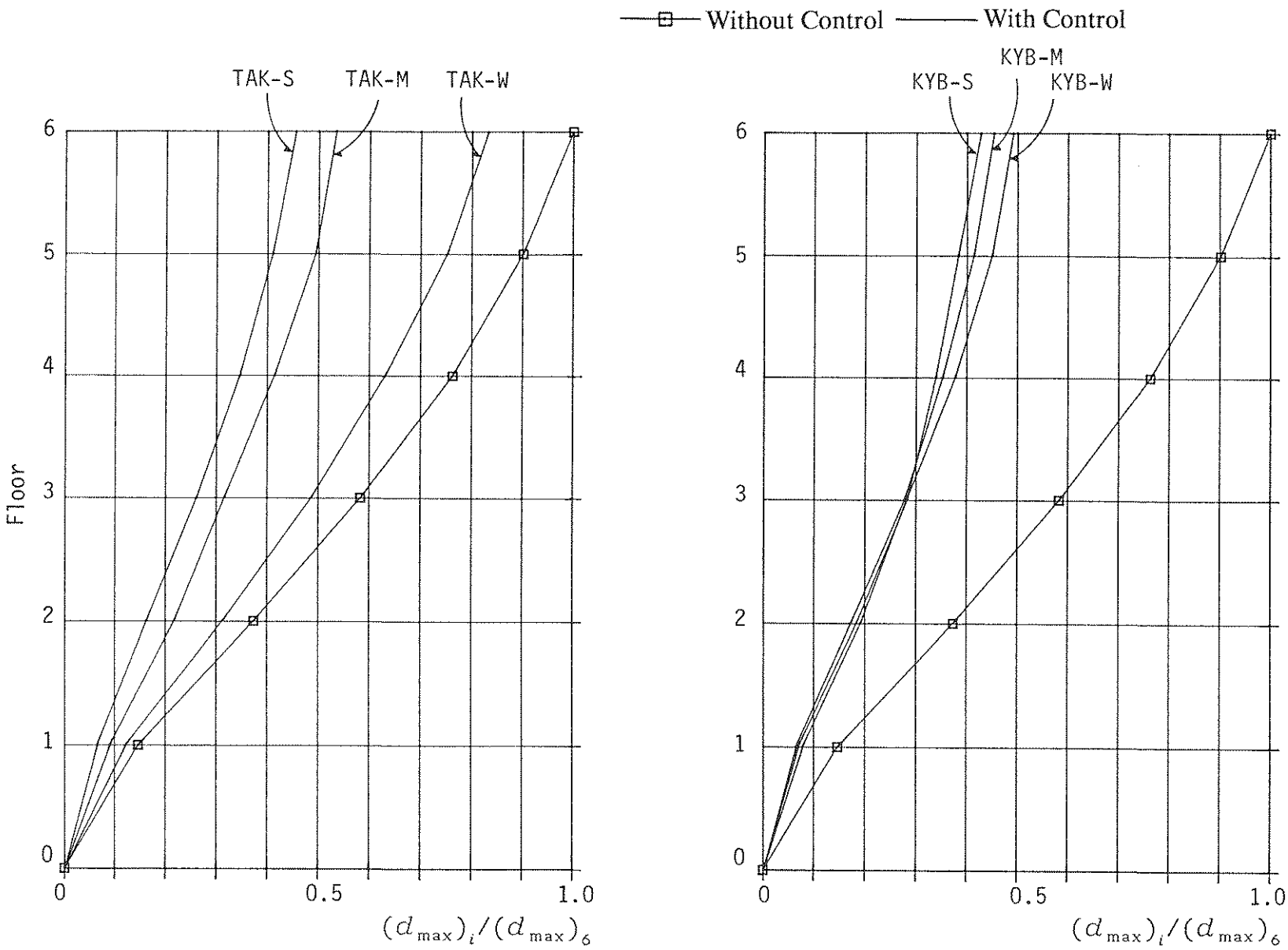

[Regulator Type: No. 1, 2, and 3 in Table 1]

Figure 4.19 - The Peak Values of Relative Displacement (El Centro 25% Excitation).

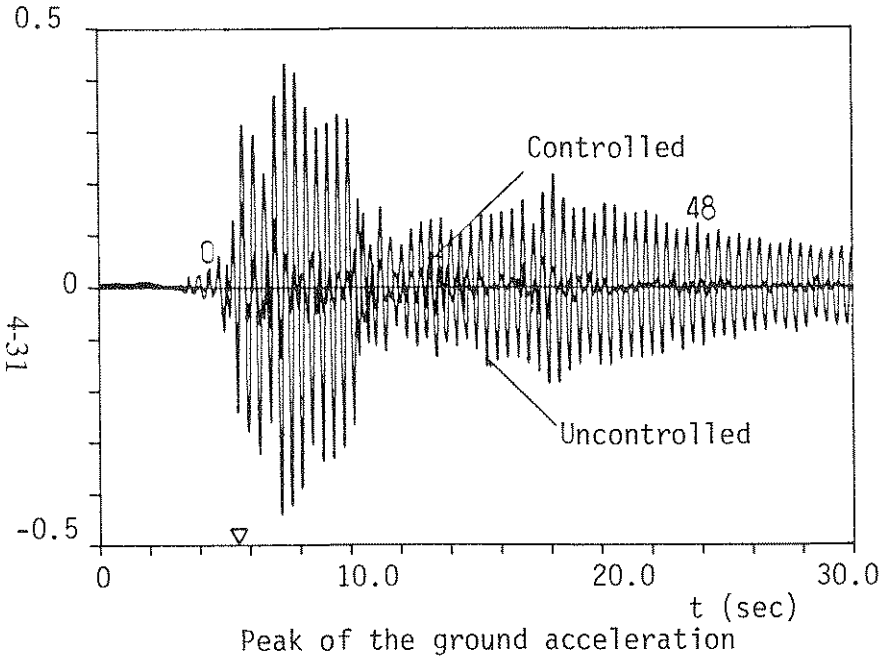

a) Top Relative Displacement

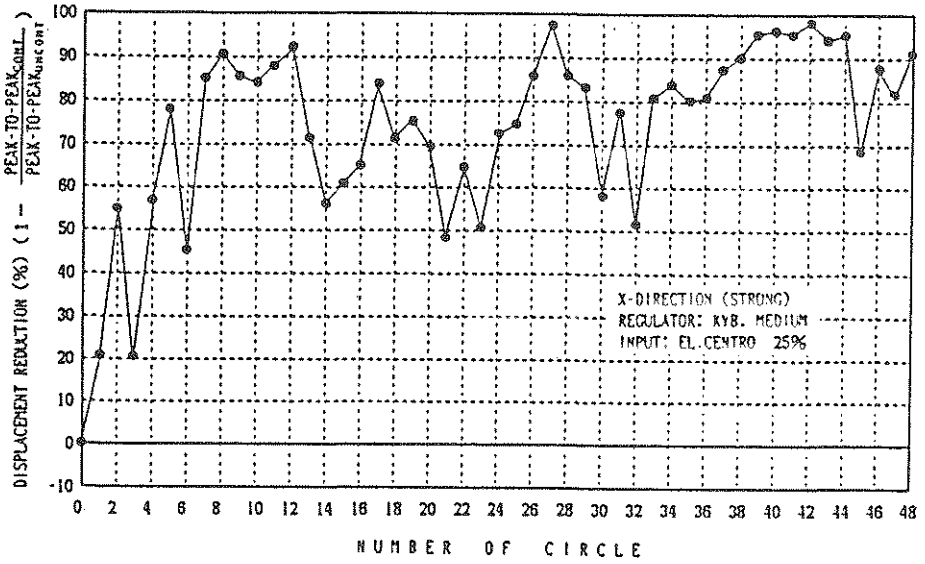

b) Time History of Displacement Reduction at Sixth Floor Approximation Estimate.

Figure 4.20 - Time Histories of the Relative Displacement at the Top Floor and the Percentages of the Displacements Reductions (El Centrol 25% Excitation).

(A) *Dependency on weighting magnitude is reflected in Fig. 4.21 for various regulators.* As shown in Fig. 4.21 (a), the control of the maximum displacement is more efficient with increasing weighting factors. The control per unit mass stroke and per unit control force is less efficient with the increase of weighting factors as noticed in Figs. 4.21 (b) and (c). The tendencies shown in the displacement reductions are almost the same for the maximum acceleration. However, the control efficiency for the maximum acceleration is considerably less than that for the maximum displacement. A reduction of more than 30% at the top floor is achieved only with certain kinds of regulators. Several sources may account for this trend: (1) the feedback delay due to the use of the measured information one-step previous to the current step; (2) the time delay in performing computations and executing the control forces as required; and (3) the higher components of acceleration caused by the movement of AMD.

(B) *Relationships between the control efficiencies and the maximum mass stroke or maximum control forces.* The control efficiencies for the reduction of maximum displacement are approximately proportional to the maximum mass stroke (see Fig. 4.22 (b)), and they are not significantly affected by the method of design of the control system. However, the relations between the control efficiencies in reducing the maximum displacement and the required maximum control forces vary according to the regulator used, i.e., they depend greatly on the design method (Fig. 4.22 (a)).

(C) *Effects of number of observers on the control efficiency.* When the control algorithm is based on measurements of responses at the top (sixth) floor and at the third floor, the mass stroke efficiency and the control force efficiency are improved (see Fig. 4.23) in comparison to those controlled without the third floor information (see Fig. 4.21). Moreover, the acceleration response at the third floor tends to become slightly smaller. However, those effects are small compared to the additional effort required by measurements and processing power.

(D) *Effects of changing the mass weight.* According to the experimental results using any of the mass weights, 150, 200 or 250 kg, produce almost identical reductions of maximum displacement and acceleration responses, when the regulators are designed for the corresponding mass weights (Fig. 4.24). However, the *mass stroke* is reduced and the mass stroke efficiency is improved when the additional mass is increased.

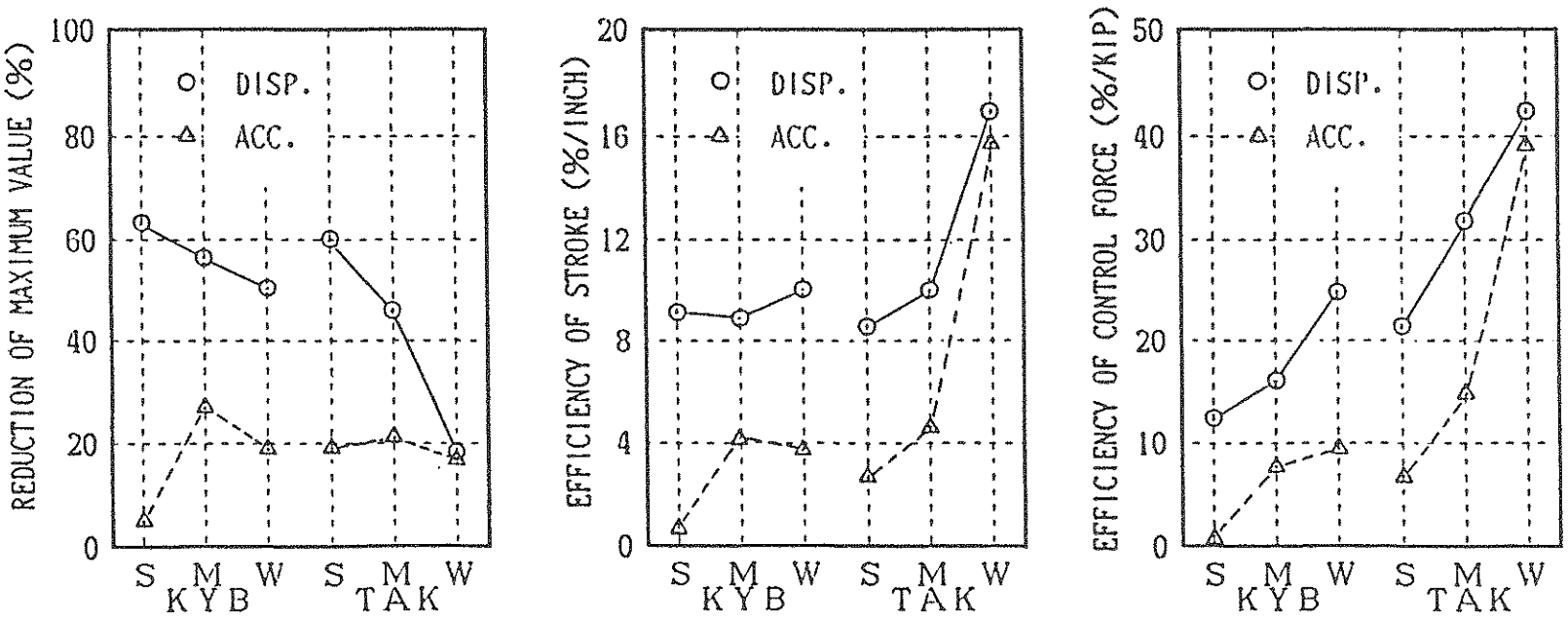

a) Maximum Response Reduction b) Maximum Unit Mass Stroke c) Maximum Unit Control Force

Sensor Position: The top floor

Objective Variable: The Relative Displacement at the Top Floor

Mass Weight: 200 (kg)

AMD Stiffness: None

Figure 4.21 - Comparison by the Regulators Depending on the Weighting Magnitudes (El Centro 25% Excitation).

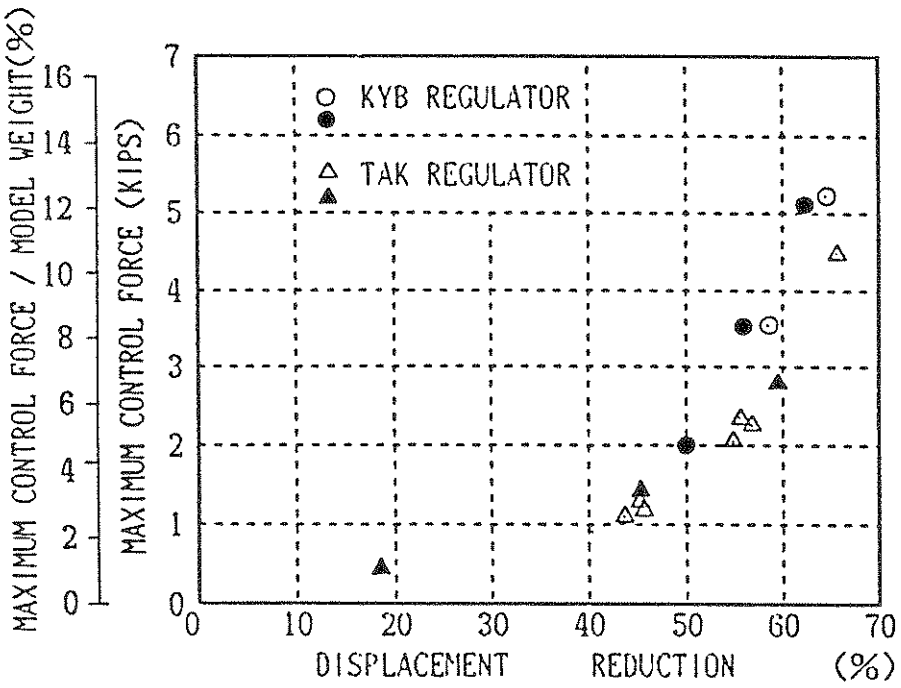

a) Maximum Control Force Influence

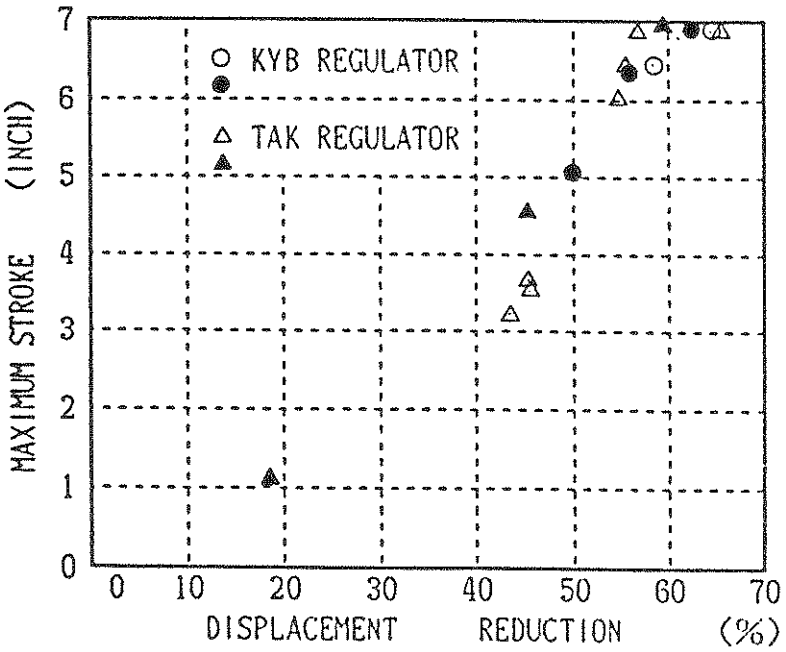

b) Maximum Mass Stroke Influence

Figure 4.22 - Relationships Between the Displacement Reductions and the Maximum Control Forces and the Maximum Mass Stroke (El Centrol 25% Excitation).

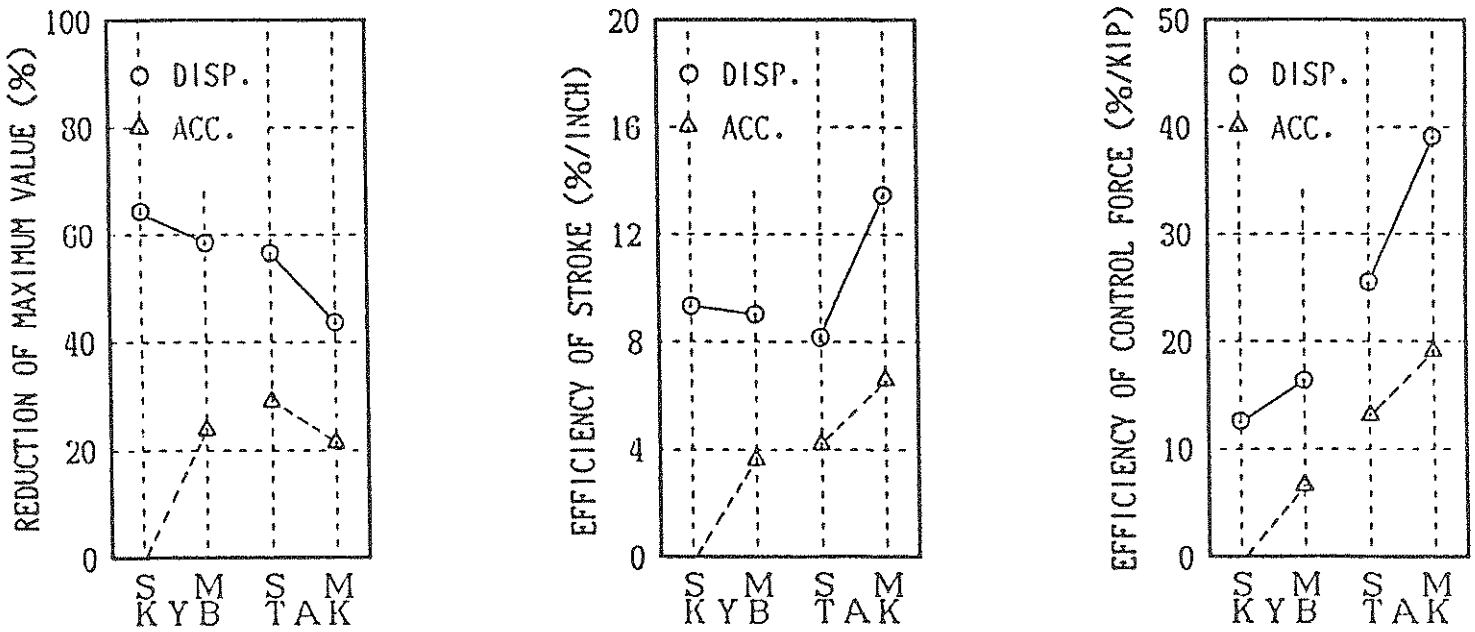

Sensor Position: The top and the third floors

Objective Variable: The Relative Displacements at the Top and Third Floor

Mass Weight: 200 (kg)

AMD Stiffness: None

Figure 4.23 - Effects of Using the Middle (3rd) Floor Information (El Centrol 25% Excitation).

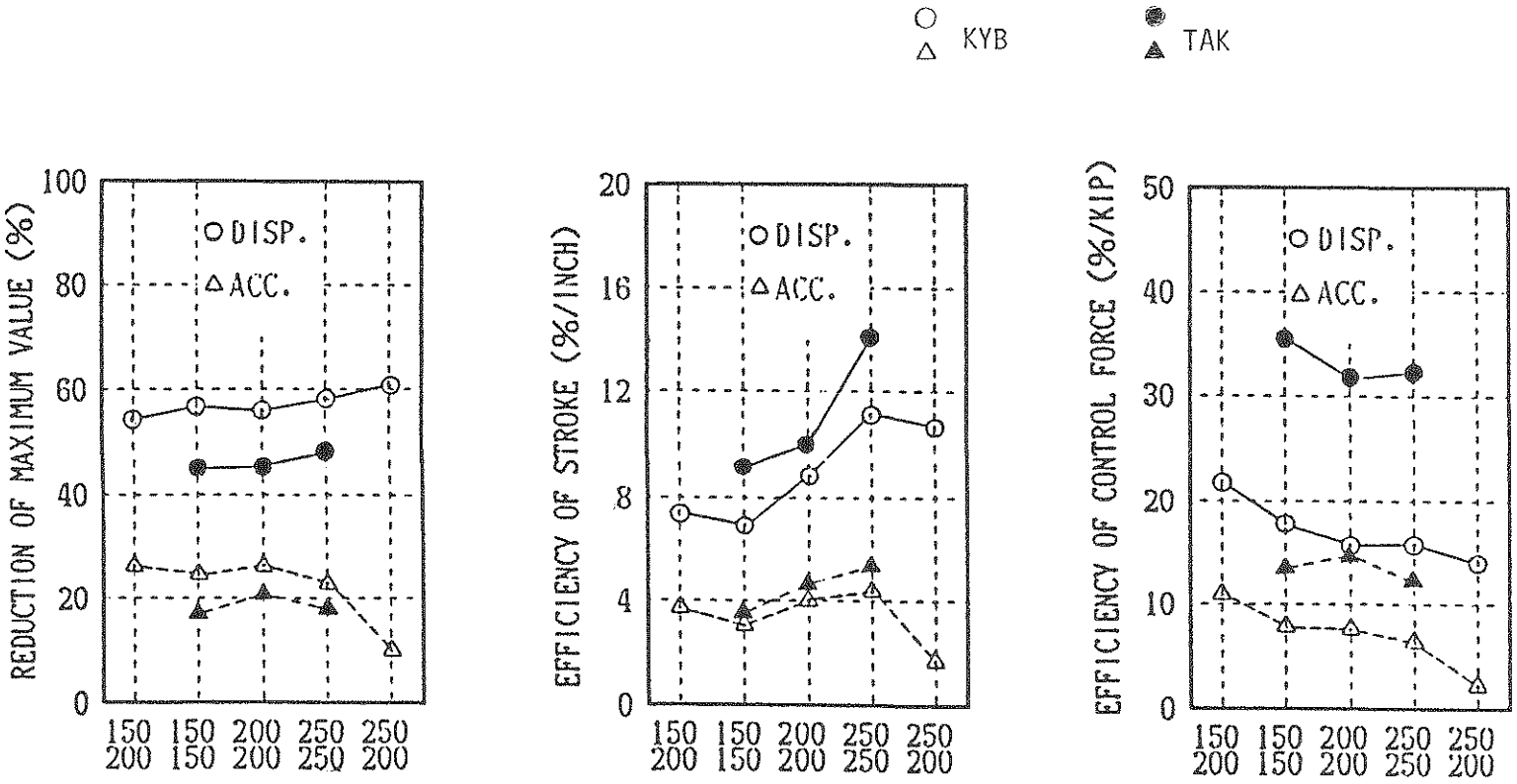

Sensor Position: The top floor

Objective Variables: The Relative Displacement at the Top Floor

AMD Stiffness: None

Figure 4.24 - Effects of Added Mass Weight to the AMD (El Centro 25% Excitation).

(E) *Effects of adding springs to the AMD.* When the gas spring is added to the AMD, the maximum control force produced by the actuator becomes apparently smaller (Fig. 4.25). However, since the direction of oil flow in the actuator used in this study is determined by the sign (plus/minus) of the servo-current and since the gas spring influences the differential pressure between both sides of the piston, it cannot always regulate the direction of mass movement. Therefore, the control force becomes smaller when the direction of the reaction in the spring corresponds to that of the mass movement, otherwise the gas spring increases the pressure. According to the experimental results using half of the optimal additional stiffness, the maximum control forces required for control are reduced. Moreover, the advantage of adding such a gas spring eliminates the necessity of tuning accurately the AMD. This is extremely important in the design of the AMD since small fluctuations in tuning will not influence the response.

(F) *Comparison of the objective variables.* When the control is applied using the measurements of either relative accelerations, velocities or displacements, the control efficiently in reducing the maximum response does not change (see Fig. 4.26 (a)). However, the mass stroke and the control force efficiencies are improved when the relative accelerations are used, while they worsen when the measurement of relative displacements are used.

(G) *Comparison of control of the absolute displacement and of the relative displacement.* Apparently controlling the *absolute states* (displacements, velocities) of the structure rather than the *relative states*, it requires more resources (twice the mass stroke and one and the half times the control force) in order to obtain the same control effects (Fig. 4.27). This can be explained by the fact that when the *absolute* control is used, the states measurements include also the components of the ground motion along with the structure response. For this control, the mass travels much larger stroke because of the lower frequencies of the components of the earthquake displacements (Fig. 4.27). Furthermore, the controlled absolute displacements at the top floor are the same for both control approaches. The meaning of this observation is that the effect of the control on the absolute displacement is negligible, independent on the control algorithm used. Therefore, controlling the absolute states require resources, control force and mass stroke which are essentially wasted (see Figs 4.27 (a) and (b)).

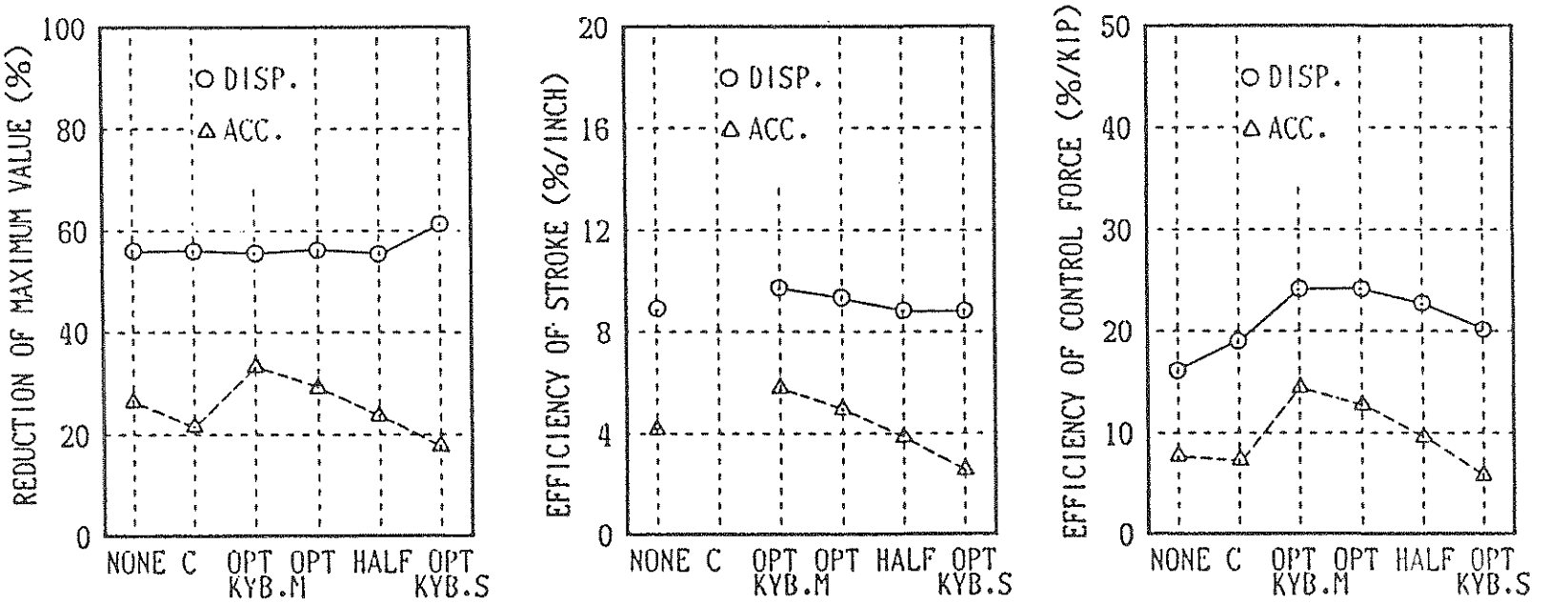

a) Maximum Response Reduction b) Maximum Unit Mass Stroke c) Maximum Unit Control Force

Sensor Position: The top floor

Objective Variable: The Relative Displacement at the Top Floor

Mass Weight: 200 (kg)

Figure 4.25 - Effects of Adding the Stiffness to the AMD (El Centro 25% Excitation).

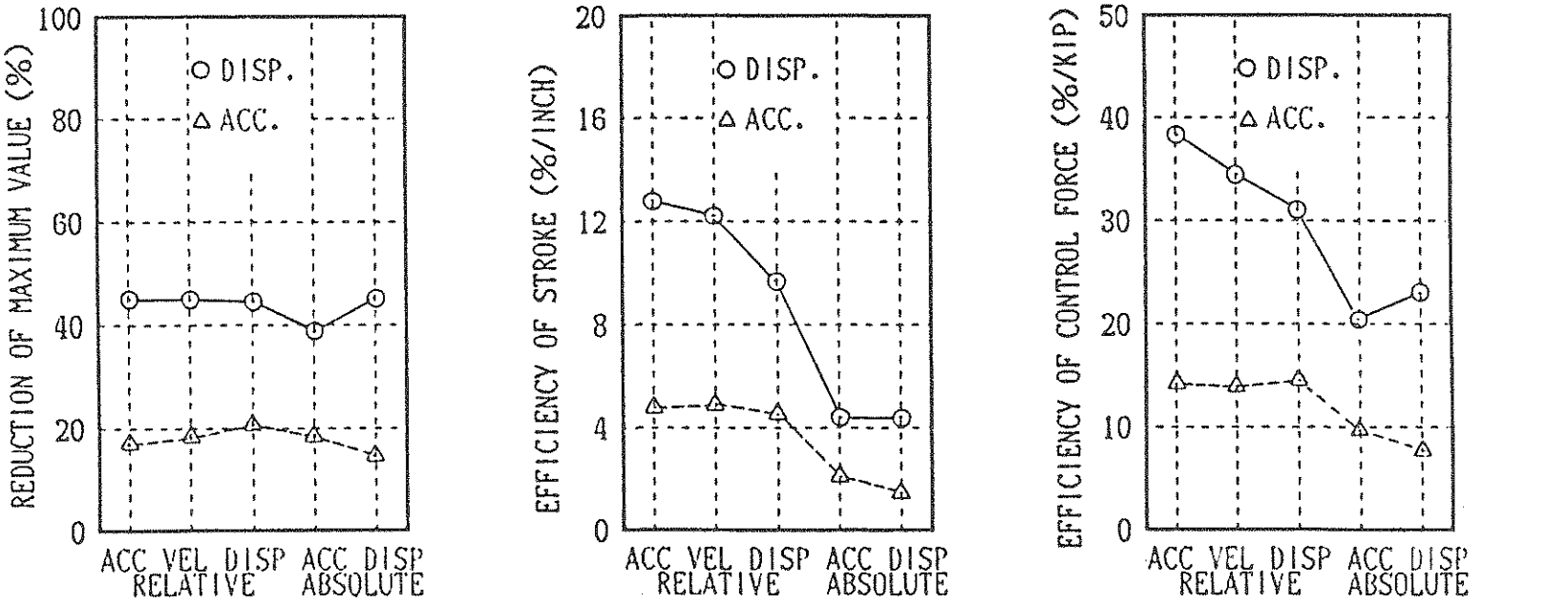

a) Maximum Response Reduction

b) Maximum Unit Mass Stroke

c) Maximum Unit Control Force

Sensor Position: The top floor

Mass Weight: 200 (kg)

AMD Stiffness: None

Figure 4.26 - Comparison of Efficiencies Versus the Objective Variables (El Centro 25% Excitation)

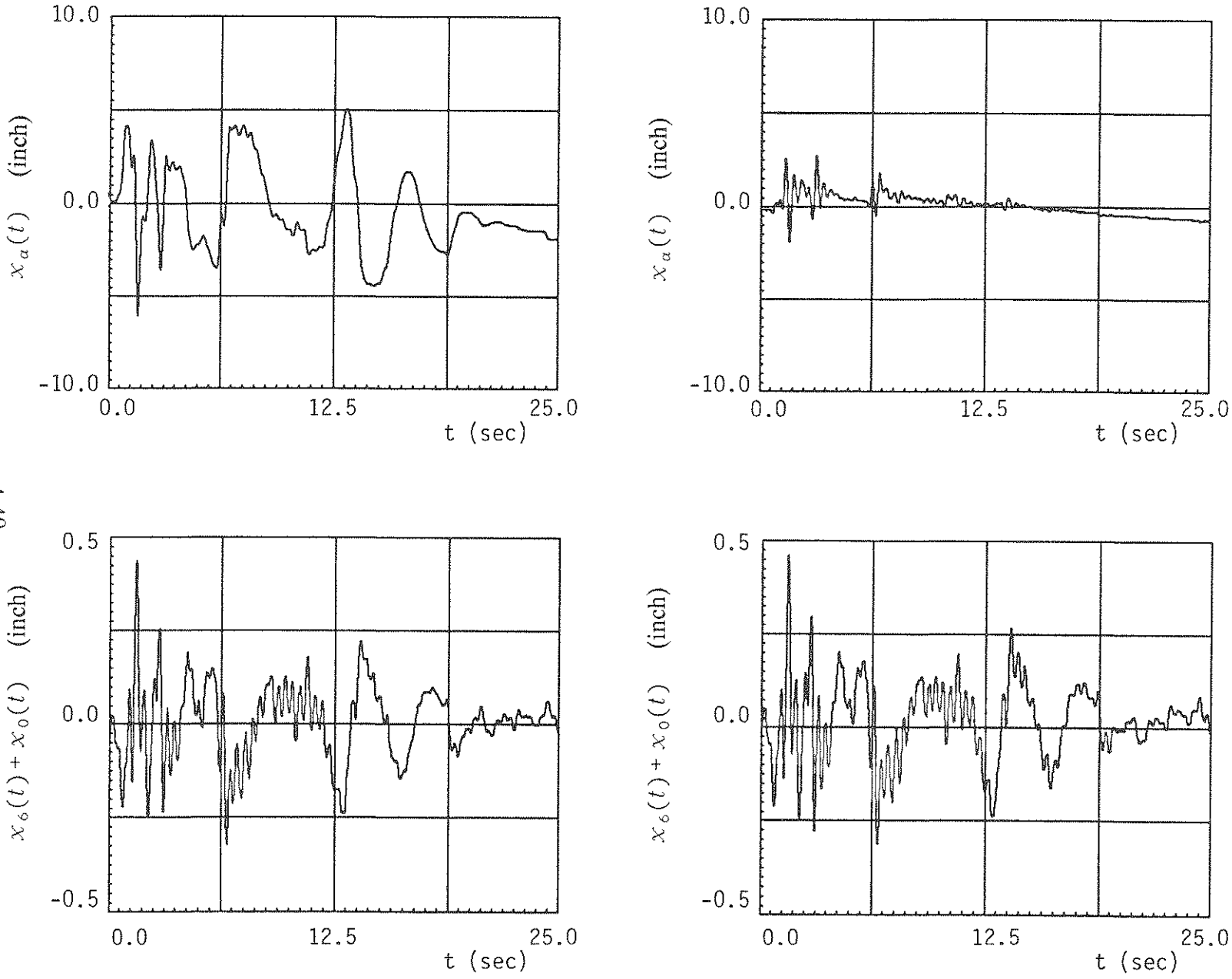

a) Control of the Absolute Displacement

b) Control of the Relative Displacement

Figure 4.27 - Comparison Between the Absolute Displacement Control and the Relative Displacement Control (El Centro 25% Excitation).

4.3.1.2.3 Comparison of Experimental Results With Theoretical Results For AMD

(A) *Comparison between experimental and theoretical results without control.* The simulations were carried out using the stiffness matrix and the damping matrix obtained from the identification studies using the banded white noise input as described in Section 4.1. A value of 1.4% critical damping ratio was used for the first mode of vibration of the model structure. Fig. 4.28 shows good agreement between experimental and theoretical responses to earthquake ground motion without control in the first seven seconds. In the following seconds, the experimental amplitudes become smaller than the analytical, due to the interaction of shaking table with the model structure at low amplitudes.

(B) *Comparison between experimental and theoretical results with control.* The relationship between the control force and the servo-currents of actuator are basically non-linear as shown by the modified Eq. 4.5(a). However, assuming that the current is always at equilibrium, the relation becomes linear (Eq. 4.5 (b)) (see Appendix A).

$$u = f(i, \dot{x}) \tag{4.5a}$$

$$u = (D_i + E_{\dot{x}}) \tag{4.5b}$$

where u, i and $\dot{x}$ show the control force, the servo-current of the actuator, and the relative velocity of the added mass, respectively. In the control simulations, this linearization methods, i.e., Eq. (4.5) (b), was used.

Moreover, the effects of the friction acting on the added mass were considered. The friction seems to have a significant influence on the experimental response. In the analytical simulations, a value of 150 kg was assumed for a Coulomb friction force based on the measured characteristics of the actuator used in the experiments.

The analytical response is in good agreement with the experimental results, when the KYB-M regulator (Type 2 in Table 2.4) is used in the control as shown in Fig. 4.29. The eminent peaks in the experimental time histories of the acceleration response and the control force are probably produced by the overshooting of the hydraulic piston caused by the abrupt directional change of the added mass.

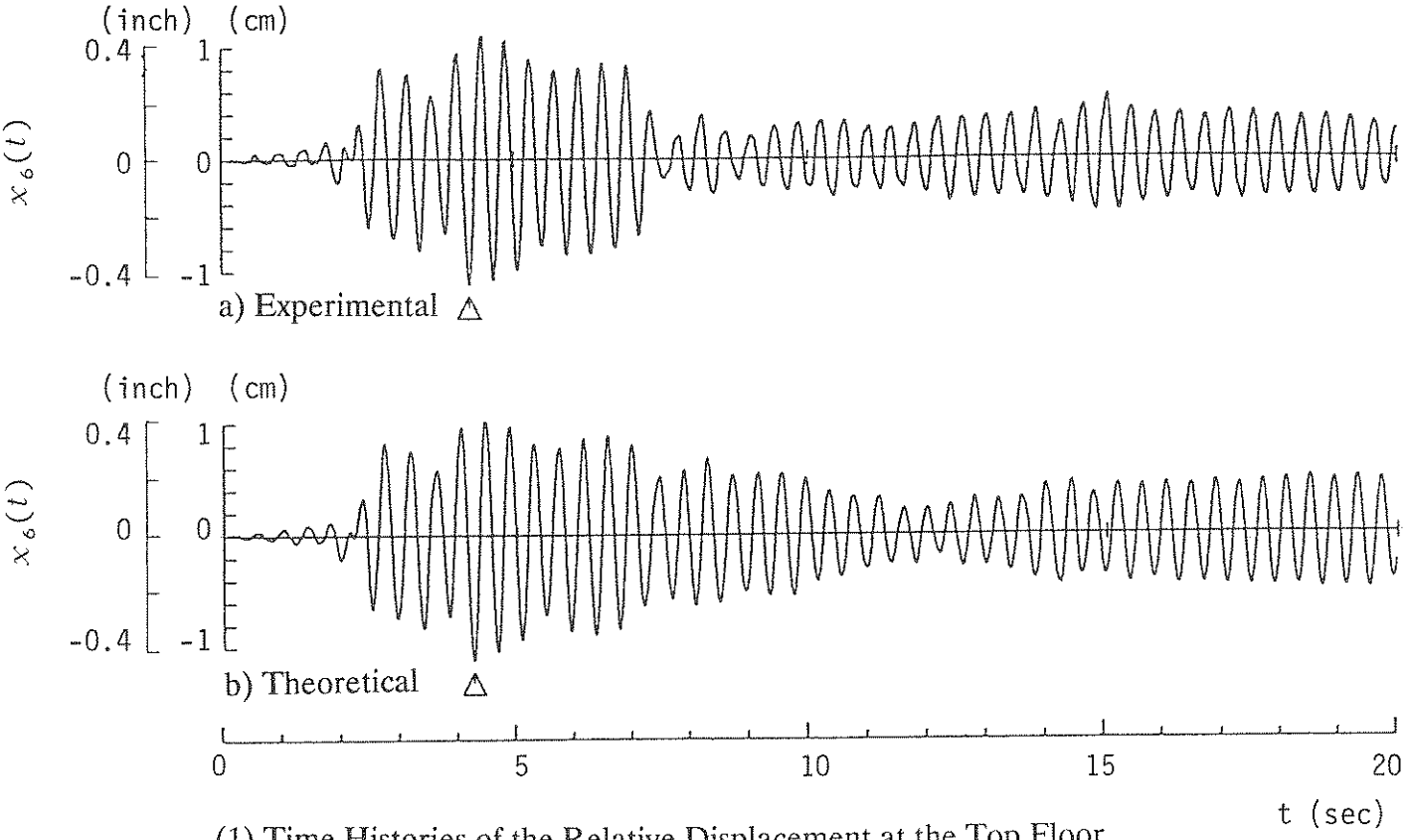

(1) Time Histories of the Relative Displacement at the Top Floor

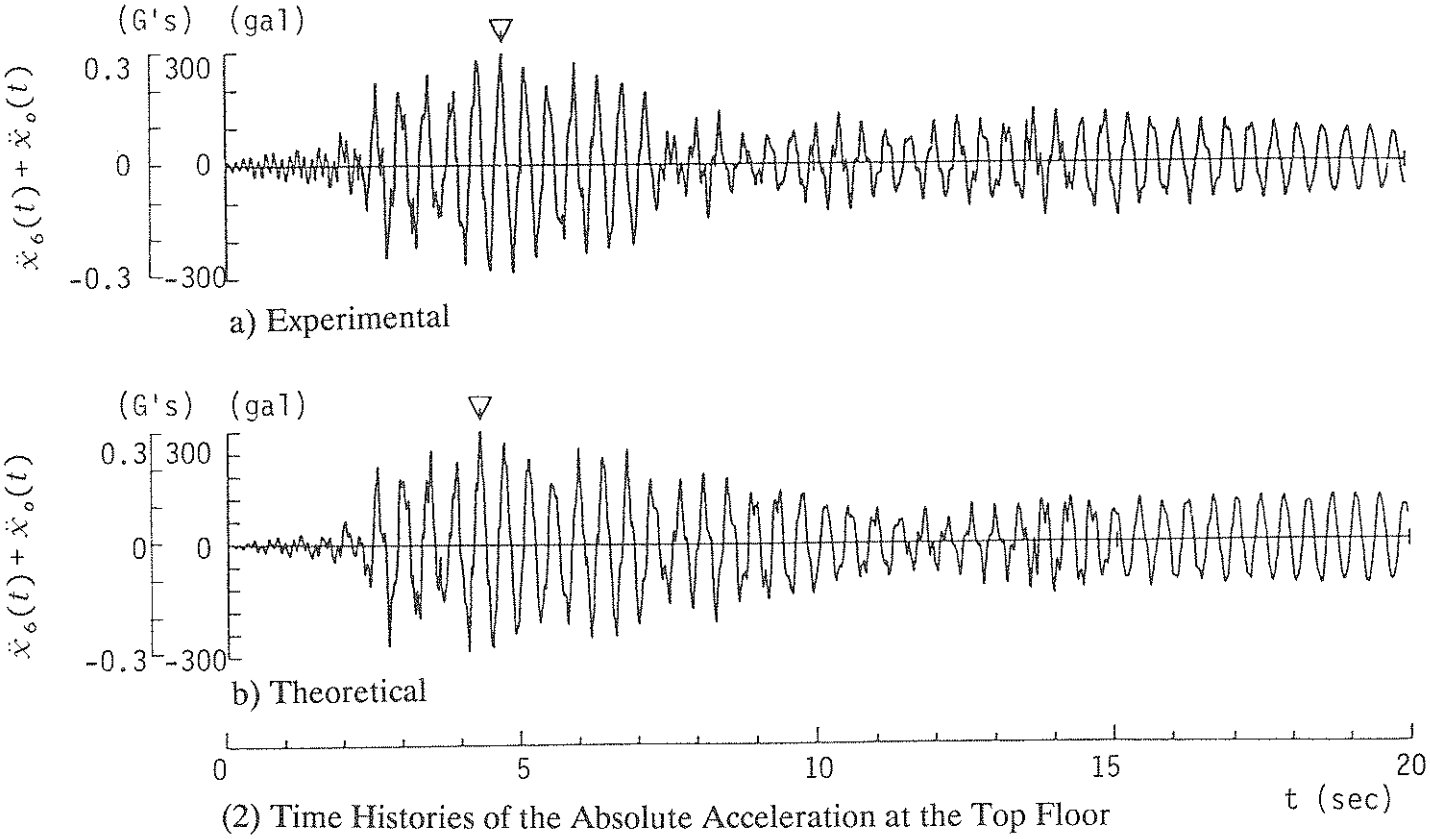

(2) Time Histories of the Absolute Acceleration at the Top Floor

Figure 4.28 - Experimental and Theoretical Results Without Control (El Centro 25% Excitation).

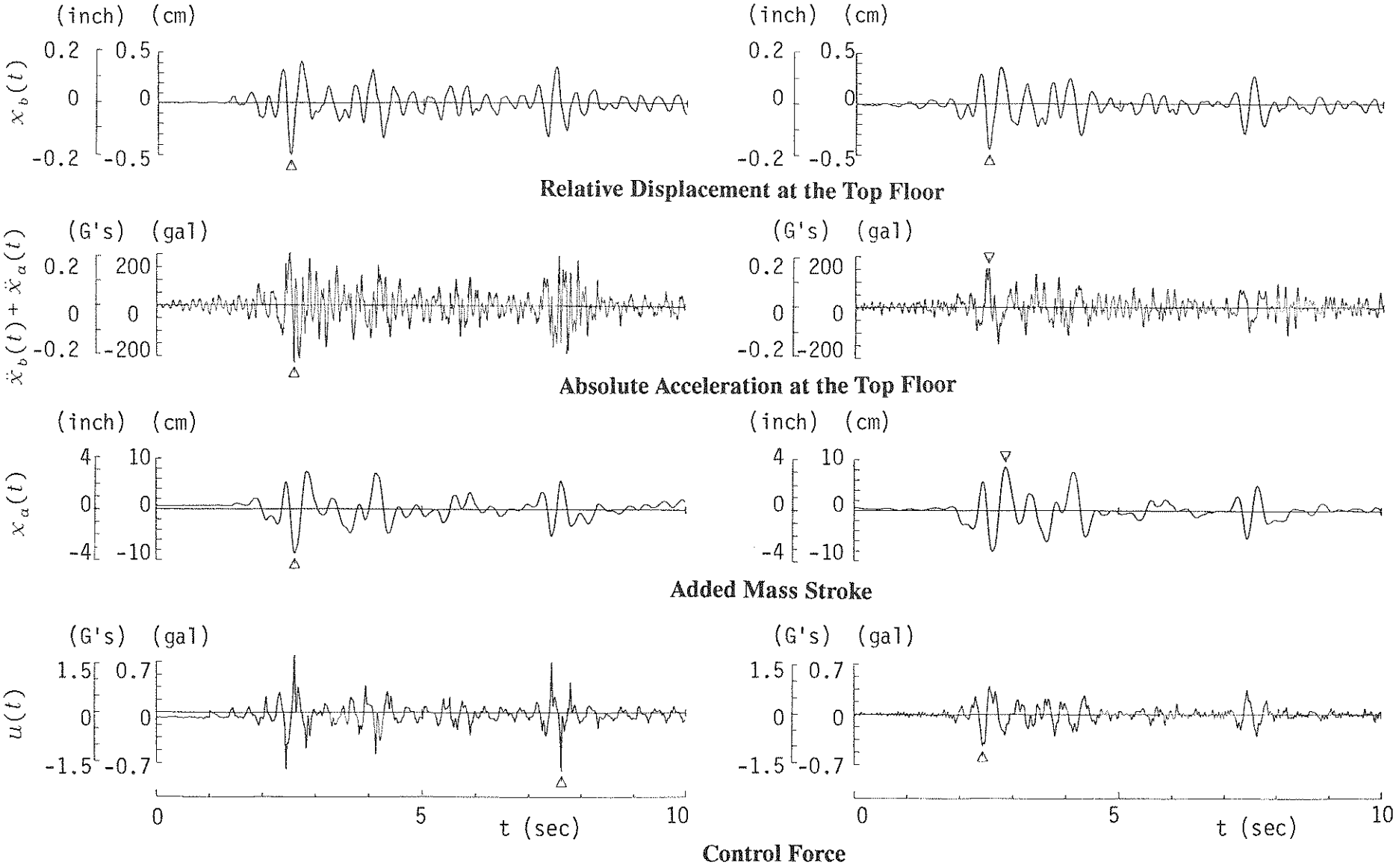

a) Experimental

b) Theoretical

Figure 4.29 - Comparison Between Experimental and Theoretical Results With Control (25% El Centro Excitation).

A comparison between the peak experimental and theoretical responses are summarized in Tables 4.5 and 4.6 for the 12 typical cases subjected to 25% El Centro excitation. Furthermore, concerning the peak values of relative displacement at each floor in these cases, the experimental and theoretical responses are shown in Figs. 4.30 (a) and (b), for comparison. Comparing the experimental results with the theoretical results, generally, the mass strokes and the control forces in the latter are larger than those in the former. The control effects in the latter are accordingly better than those in the former. This is because, in the analytical simulations, the friction acting on the added mass cannot be accurately estimated, and the experimental time delays in performing computations and executing the control forces as required are not taken into consideration.

The entire set of comparisons between the experimental and the theoretical results, are shown in Figs. 4.31 through 4.40 for the TAK-M regulator (No. 2 in Table 4.5). A good agreement could be seen in the entire set.

4.3.2 Response In "Weak" Direction

Following the experimental program described in Section 2.4 the structure was rotated 90° on the earthquake simulator and tested with various base motions. Both the ATS and AMD were installed on the structure. One of the configurations of the ATS, using the cables at the first floor, was installed and maintained inactive during the AMD testing. This was done to enable comparison of the two systems with same structural parameters, which are usually modified by the different configurations of the ATS.

4.3.2.1 Response With ATS Control

The experiments followed the schedule presented in Table 2.3 (see Section 2.4) using the cables (tendons) installed alone at the first floor or installed simultaneously at the third and first floors activated by independent actuators.

Following the identification studies which were presented in Section 4.1 the structure was shaken with three different earthquake base motions. 20% El Centro, 30% Hachinohe and 40% Miyagioki. The description of the motion was presented in Section 2.3, Table (2.1).

Table 4.5

Experimental Responses to 25% El Centro Excitation (Strong Direction)

No.	Control Conditions					Top Floor Relative Displ. [in.]	Top Floor Absolute Accel. [G's]	Base Shear Force [kips]	Max. Control Force [kips]	Max. Mass Stroke [in.]	Max. Control Power [Kw]
	Sensor Position	Objective Variables	Weight of Added Mass	Stiffness of Added Mass	Regulator Type						
0	Without Control					0.439	0.302	7.52	-	-	-
1	Top Floor	Relative Displ.	200 kg	-	TAK-S	0.200 (54.5)	0.242 (19.9)	3.76 (50.0)	1.45	3.70	4.25
2					TAK-M	0.235 (46.6)	0.238 (21.1)	4.84 (35.6)	0.856	2.37	1.09
3					KYB-S	0.188 (57.2)	0.285 (5.5)	4.34 (42.3)	2.56	3.69	5.73
4					KYB-M	0.199 (54.6)	0.226 (25.3)	3.71 (50.7)	1.74	3.45	3.86
5		Relative Accel.			TAK-M	0.240 (45.4)	0.250 (17.2)	4.82 (35.9)	0.678	1.98	0.976
6		Absolute Displ.			TAK-M	0.236 (46.3)	0.250 (17.1)	5.01 (33.4)	1.38	6.97	2.46
7	Top & 3rd Fl.	Relative Displ.			TAK-S	0.205 (53.4)	0.209 (30.7)	3.88 (48.4)	1.25	3.78	3.57
8					TAK-M	0.249 (43.3)	0.234 (22.4)	5.26 (30.1)	0.706	1.93	0.820
9	Top Floor		150 kg		KYB-M	0.206 (53.1)	0.225 (25.3)	4.03 (46.4)	1.57	4.05	4.61
10			250 kg		KYB-M	0.193 (56.1)	0.234 (22.6)	4.05 (46.1)	1.85	2.91	3.45
11			200 kg	Optimum	KYB-M	0.211 (51.9)	0.221 (26.8)	4.12 (45.2)	1.25	3.43	3.86
12				Half of Optimum	KYB-M	0.216 (50.9)	0.230 (23.9)	4.30 (42.8)	1.34	3.40	4.61

( ) Percentage of Reduction

Table 4.6

Theoretical Responses to 25% El Centro Excitation (Strong Direction)

No.	Control Conditions					Top Floor Relative Displ. [in.]	Top Floor Absolute Accel. [G's]	Base Shear Force [kips]	Max. Control Force [kips]	Max. Mass Stroke [in.]	Max. Control Power [Kw]
	Sensor Position	Objective Variables	Weight of Added Mass	Stiffness of Added Mass	Regulator Type						
0	Without Control					0.439	0.310	7.17	-	-	-
1	Top Floor	Relative Displ.	200 kg		TAK-S	0.128 (70.8)	0.129 (58.4)	2.42 (66.2)	1.60	4.39	5.86
2					TAK-M	0.191 (56.5)	0.160 (48.4)	3.55 (50.5)	1.11	3.21	2.56
3					KYB-S	0.147 (66.5)	0.177 (42.9)	2.49 (65.3)	1.59	3.86	5.53
4					KYB-M	0.174 (60.4)	0.177 (42.9)	2.65 (63.0)	1.30	3.37	3.55
5		Relative Accel.			TAK-M	0.202 (54.0)	0.187 (39.7)	3.40 (52.6)	0.977	3.32	2.35
6		Absolute Displ.			TAK-M	0.203 (53.8)	0.188 (39.4)	3.59 (49.9)	1.21	15.7	6.39
7	Top & 3rd Fl.	Relative Displ.			TAK-S	0.139 (68.3)	0.204 (34.2)	2.80 (60.9)	1.40	4.09	4.61
8					TAK-M	0.211 (51.9)	0.204 (34.2)	3.74 (47.8)	0.913	3.04	1.83
9	Top Floor		150 kg		KYB-M	0.169 (61.5)	0.158 (49.0)	2.61 (63.6)	1.18	4.70	4.54
10			250 kg		KYB-M	0.179 (59.2)	0.194 (37.4)	2.60 (63.7)	1.43	2.54	2.81
11			200 kg	Optimum	KYB-M	0.163 (62.9)	0.179 (42.3)	3.12 (56.5)	0.917	3.48	3.51
12				Half of Optimum	KYB-M	0.167 (62.0)	0.165 (46.8)	2.84 (60.4)	1.05	3.50	3.29

( ) Percentage of Reduction

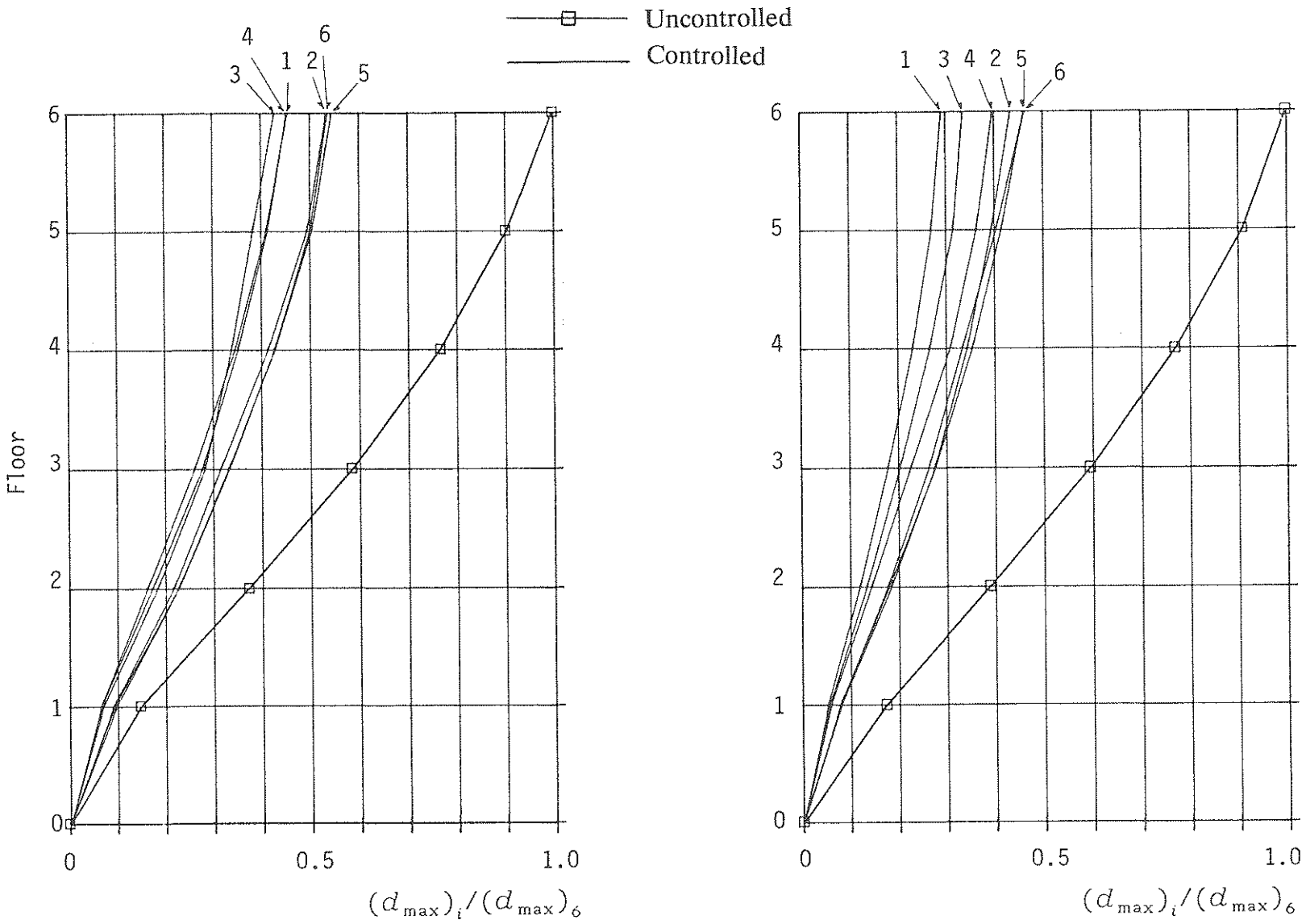

Figure 4.30(a) - The Peak Relative Displacement Under 25% El Centro Excitation.

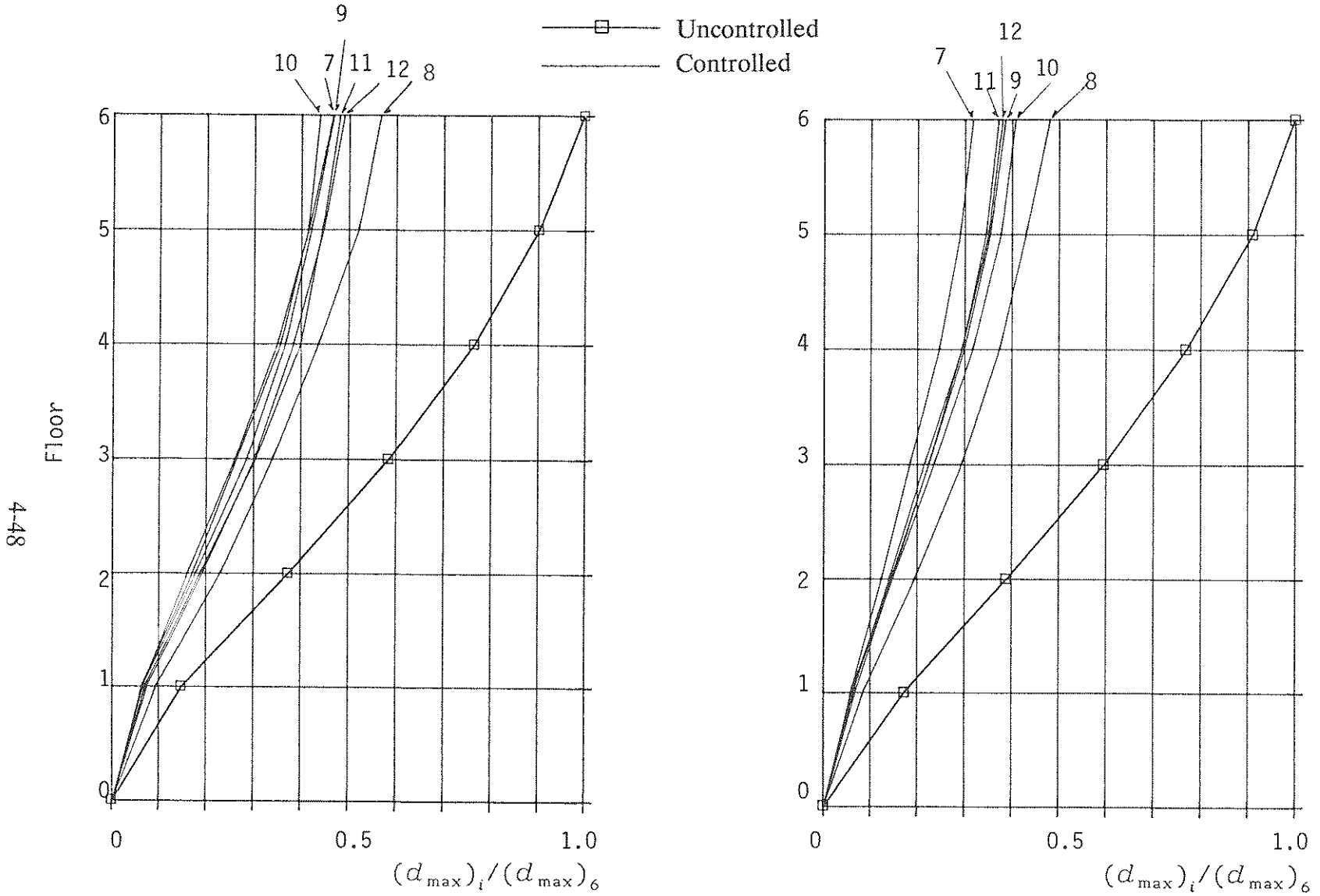

a) Experimental

b) Theoretical

Figure 4.30(b) - The Peak Relative Displacement Under 25% El Centro Excitation.

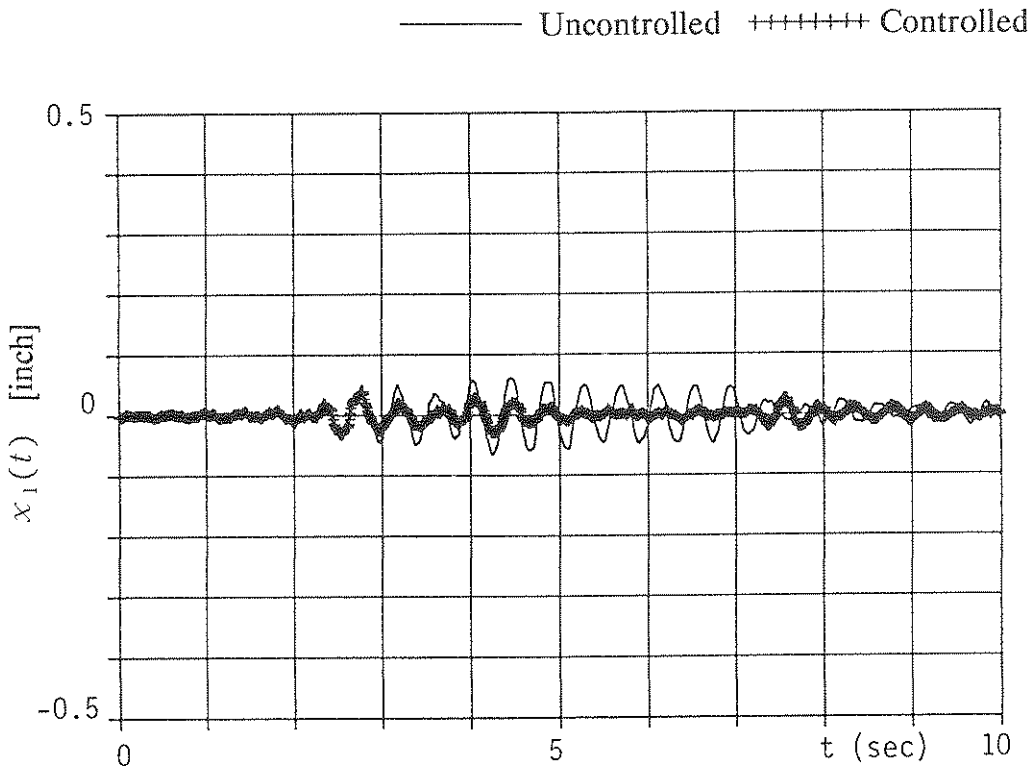

a) Experimental

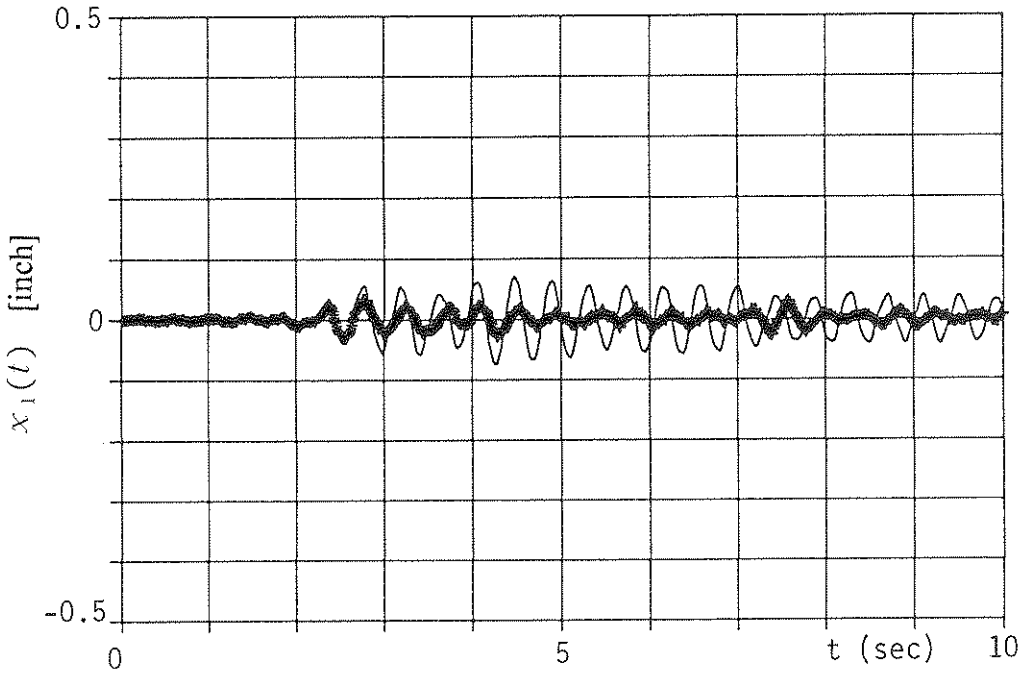

b) Theoretical

Figure 4.31 - First Floor Relative Displacement (25% El Centro).

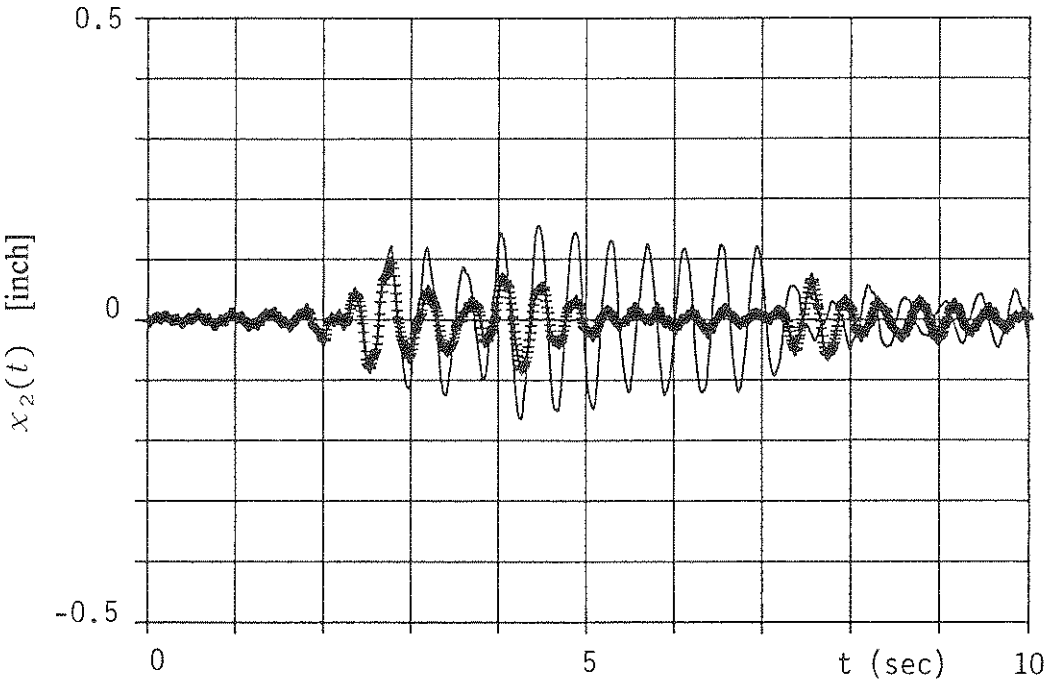

a) Experimental

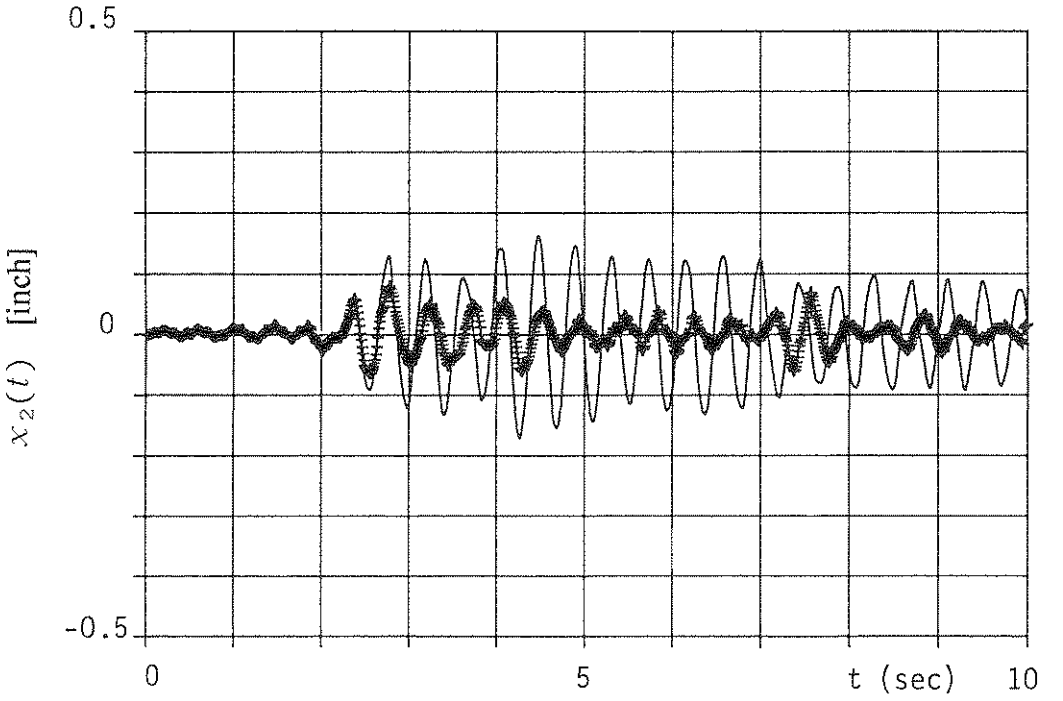

b) Theoretical

Figure 4.32 - Second Floor Relative Displacement (25% El Centro).

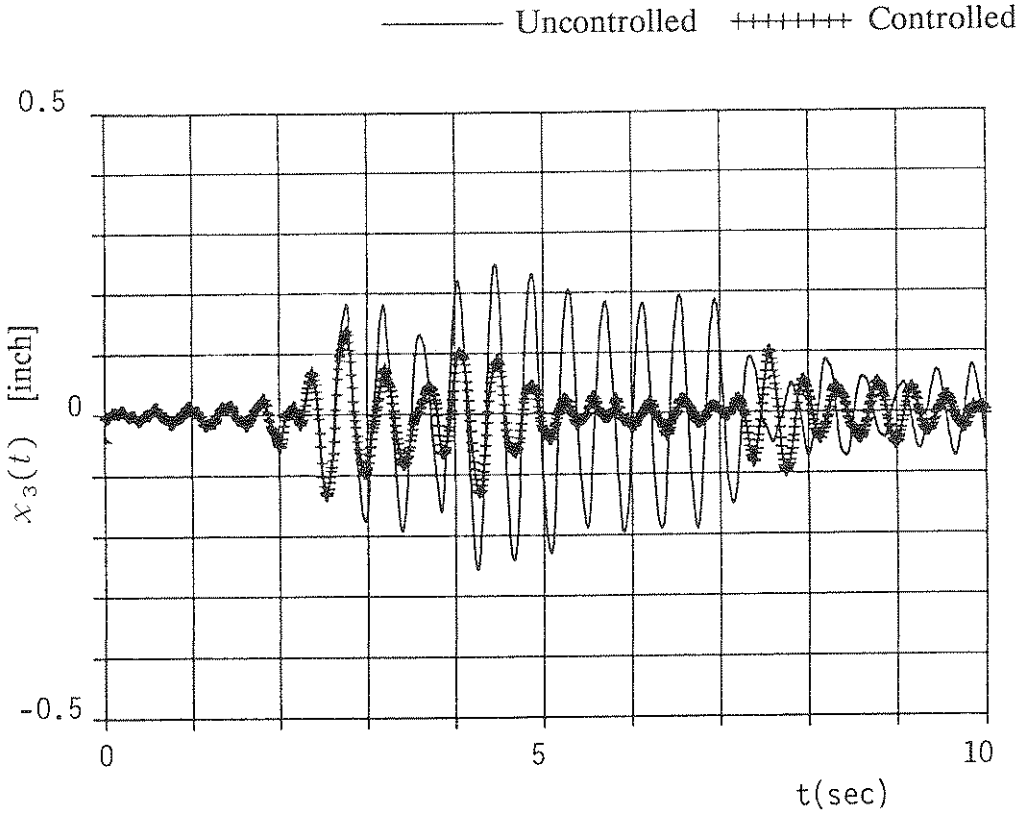

a) Experimental

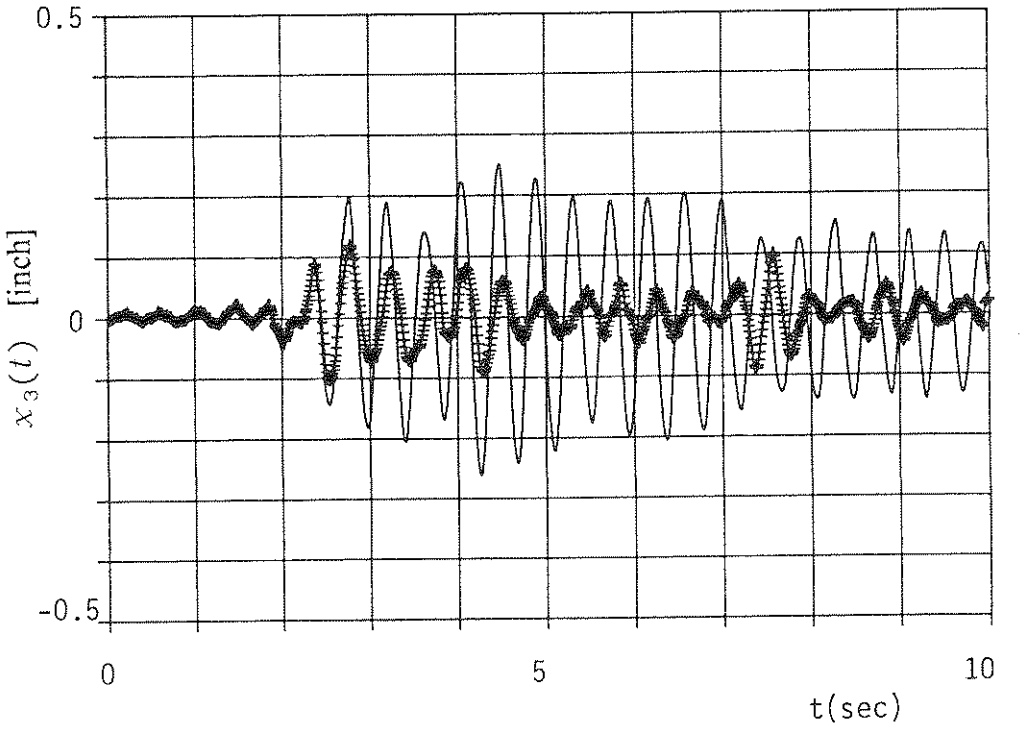

b) Theoretical

Figure 4.33 - Third Floor Relative Displacement (25% El Centro).

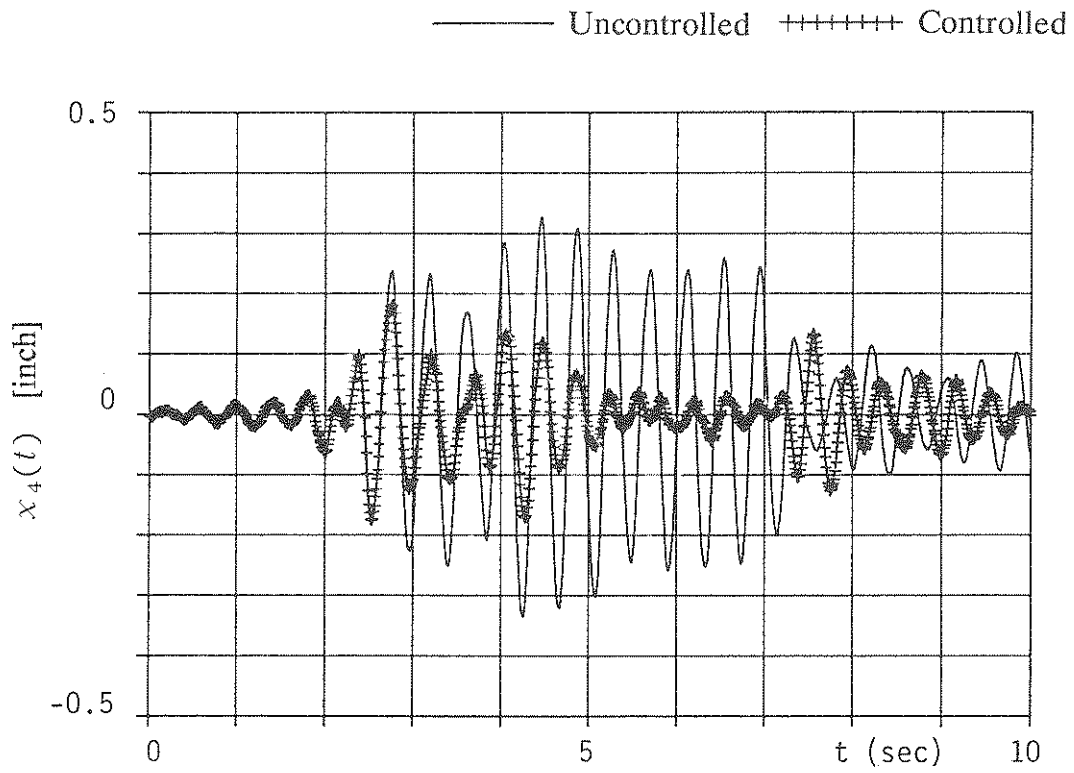

a) Experimental

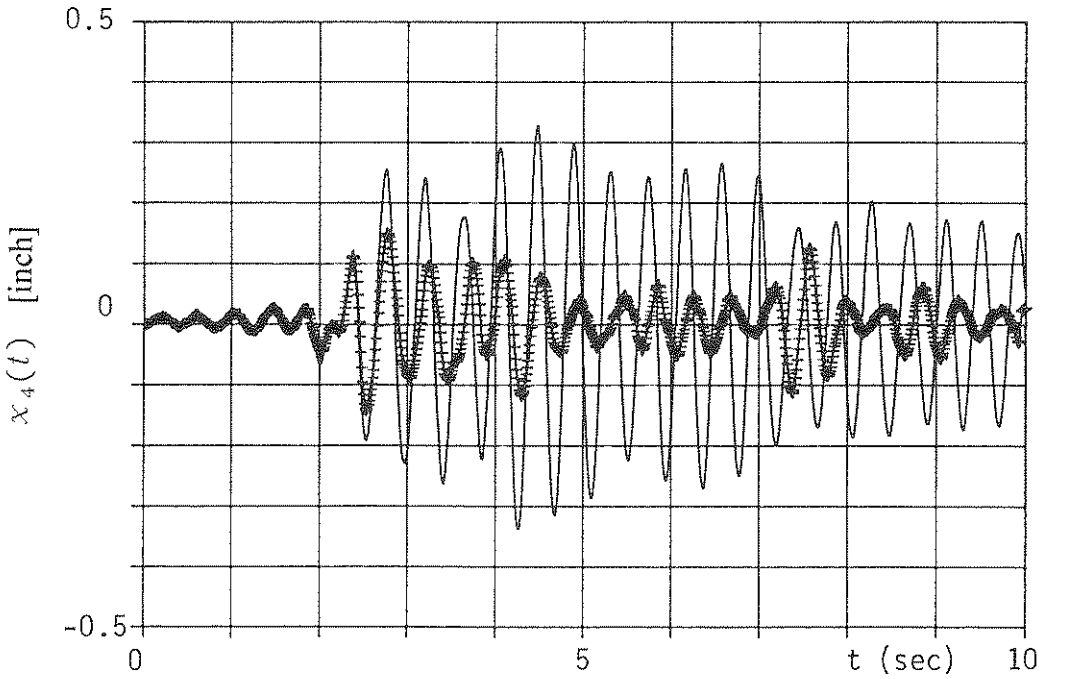

b) Theoretical

Figure 4.34 - Fourth Floor Relative Displacement (25% El Centro).

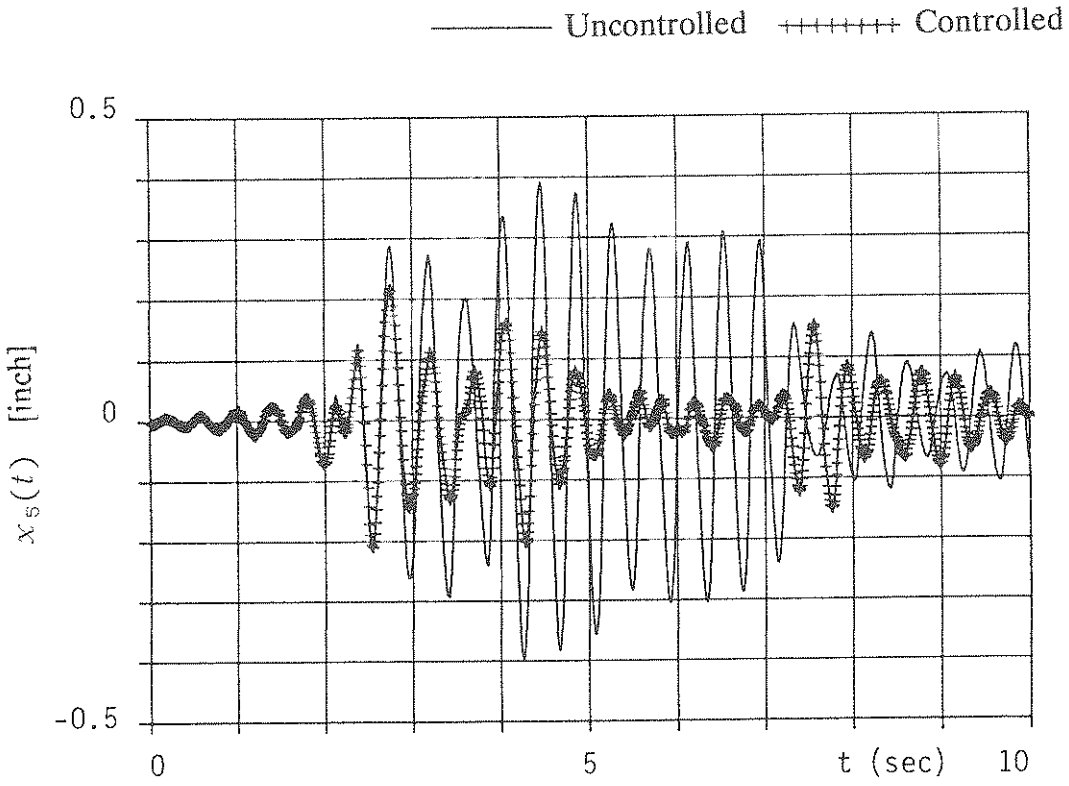

a) Experimental

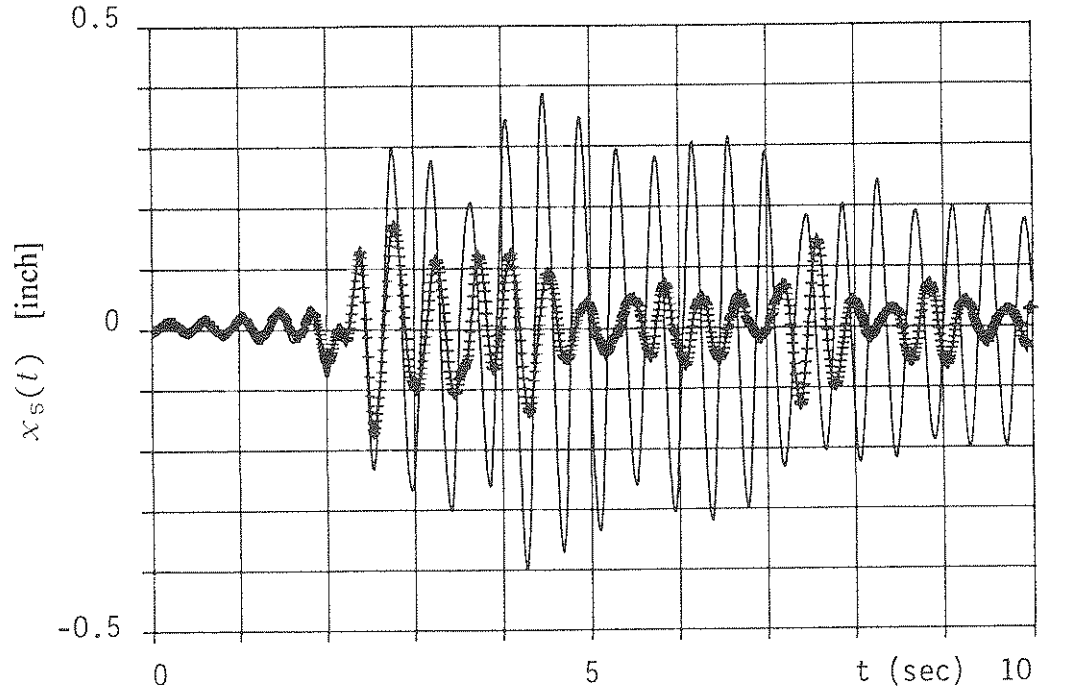

b) Theoretical

Figure 4.35 - Fifth Floor Relative Displacement (25% El Centro).

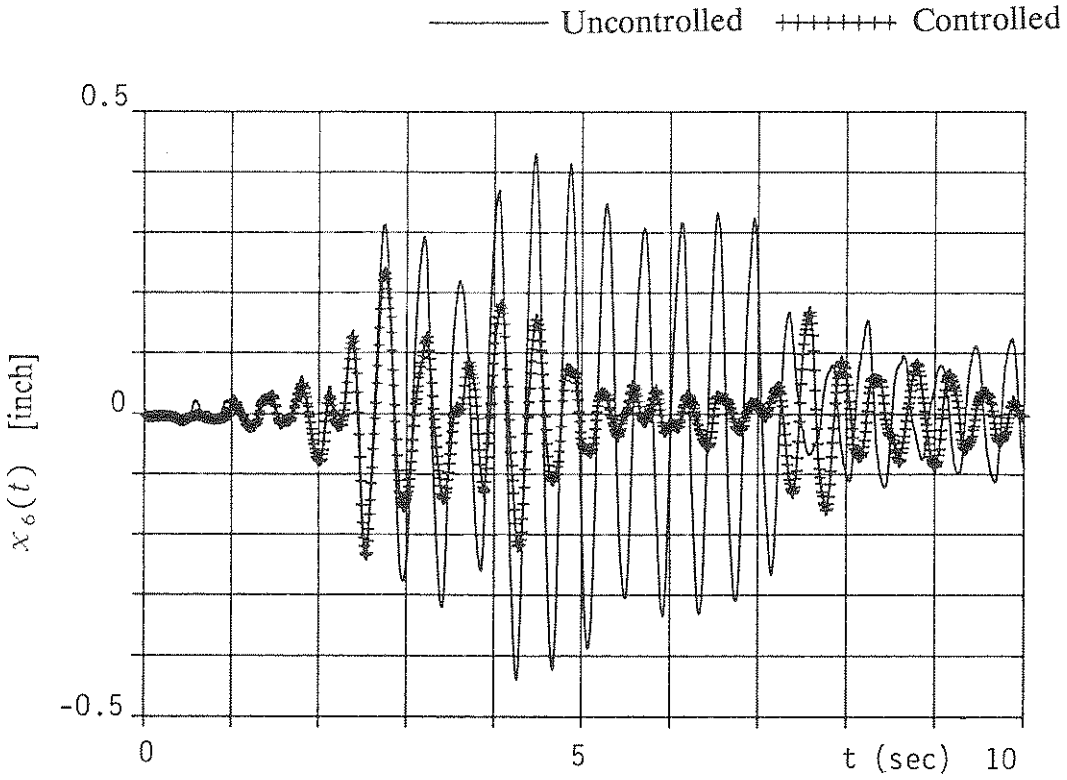

a) Experimental

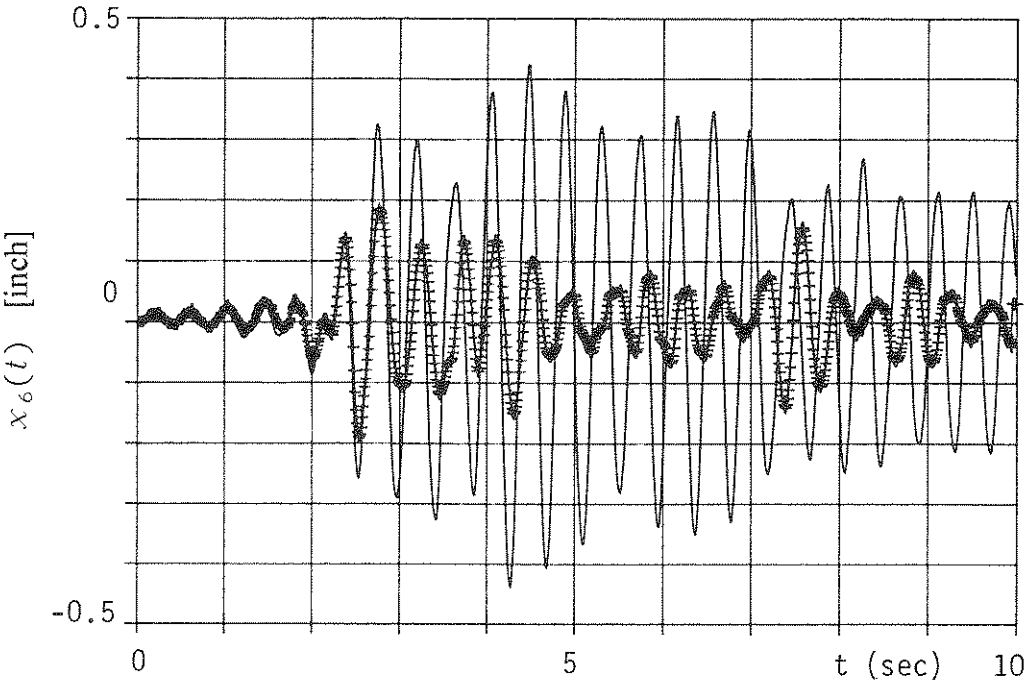

b) Theoretical

Figure 4.36 - Sixth Floor Relative Displacement (25% El Centro).

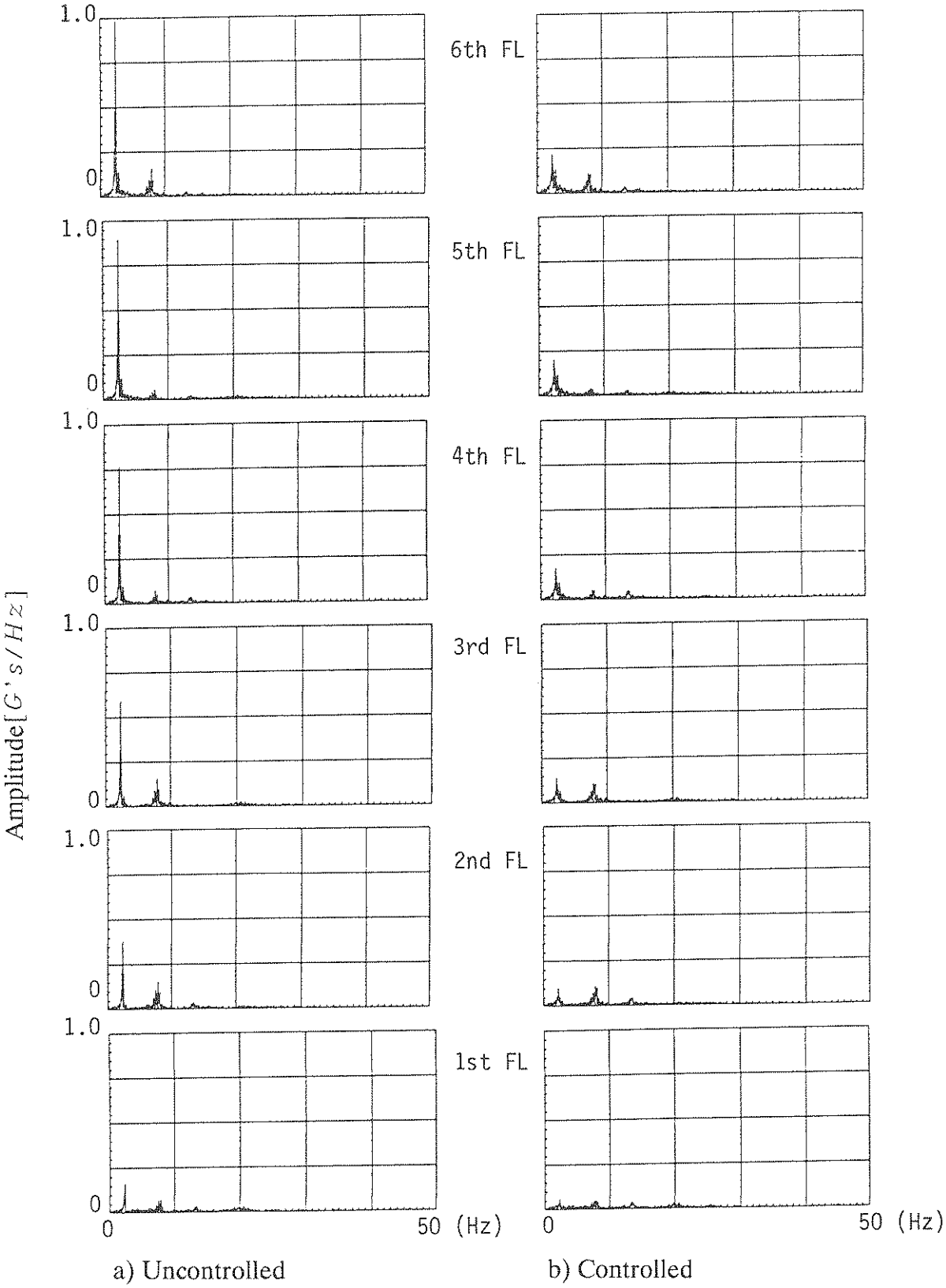

Figure 4.37 - Fourier Spectrum of Acceleration Responses.

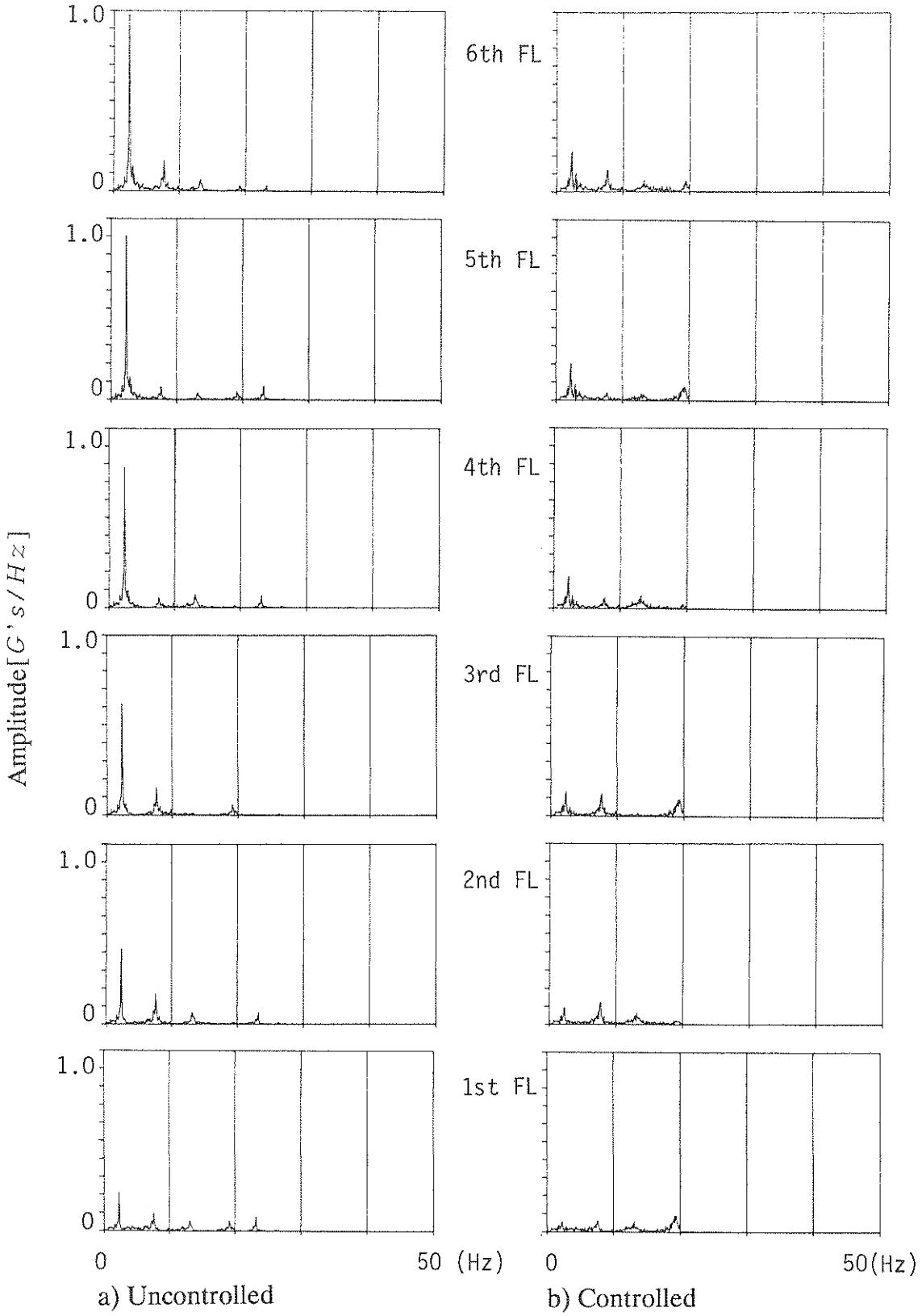

Figure 4.38 - Fourier Spectrum of Acceleration Responses (Simulation Under 25% El Centro).

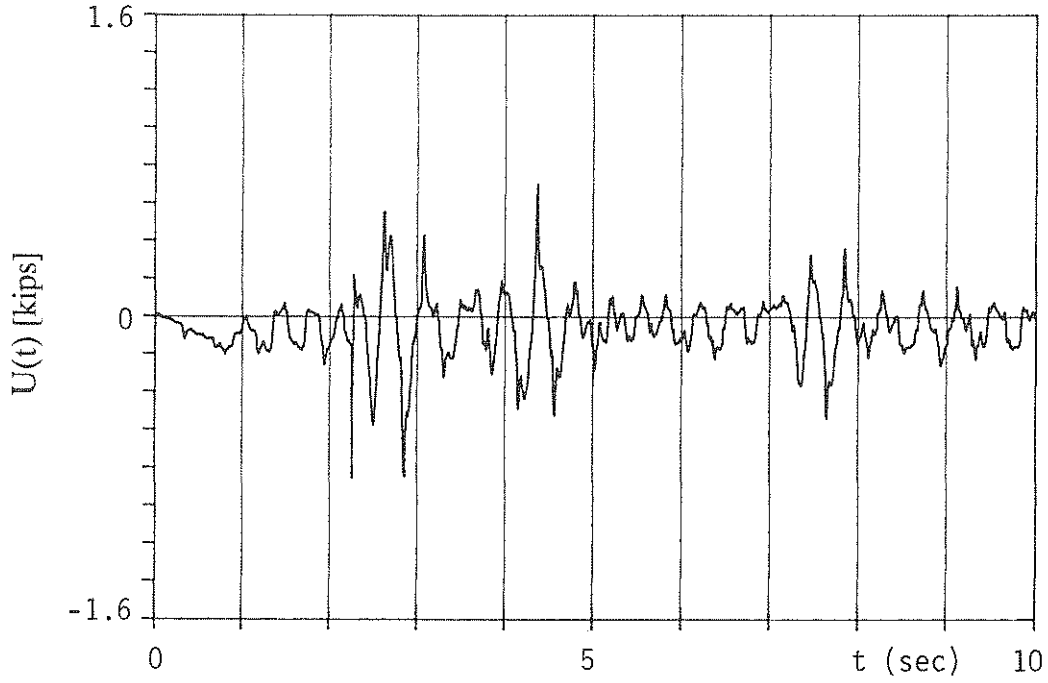

a) Time History

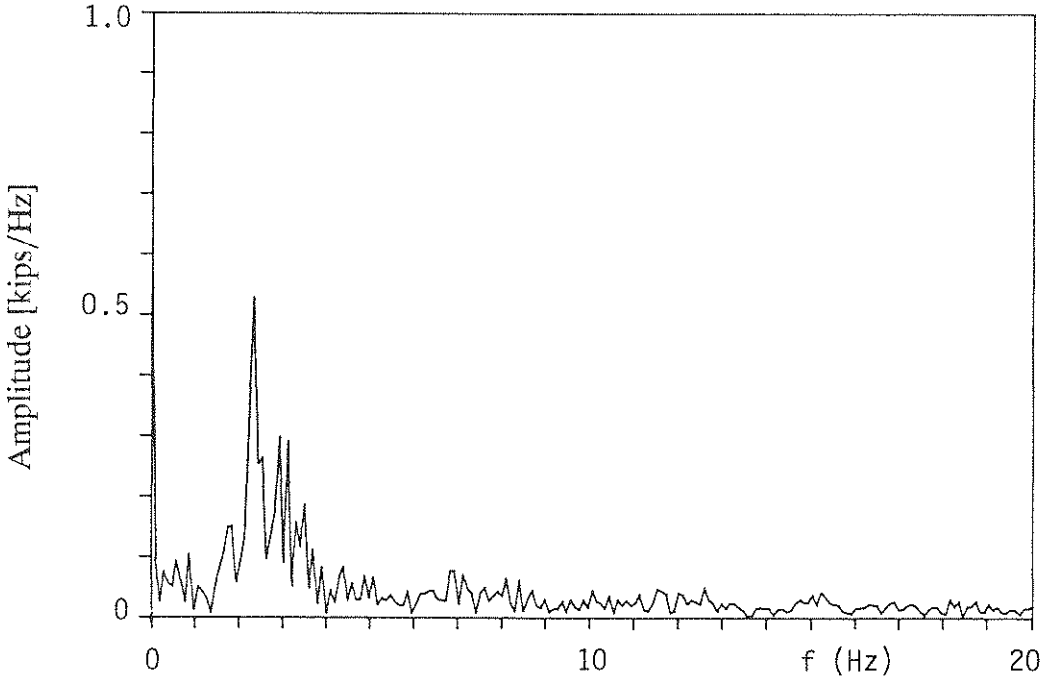

b) In Frequency Domain

Figure 4.39 - Control Force (Experimental Under 25% El Centro).

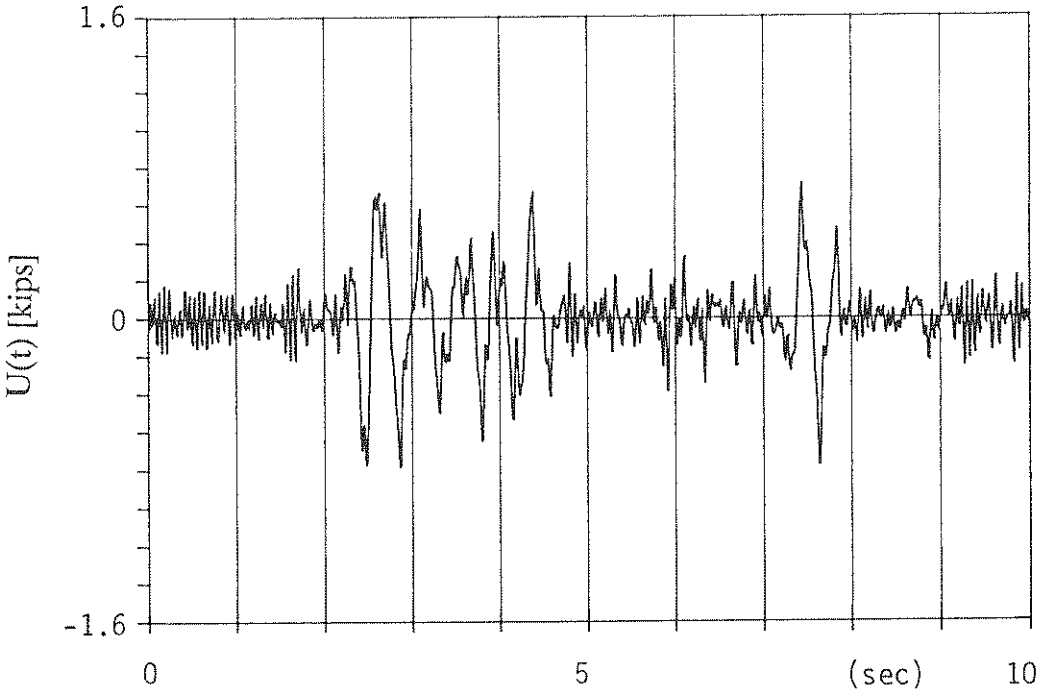

a) Time History

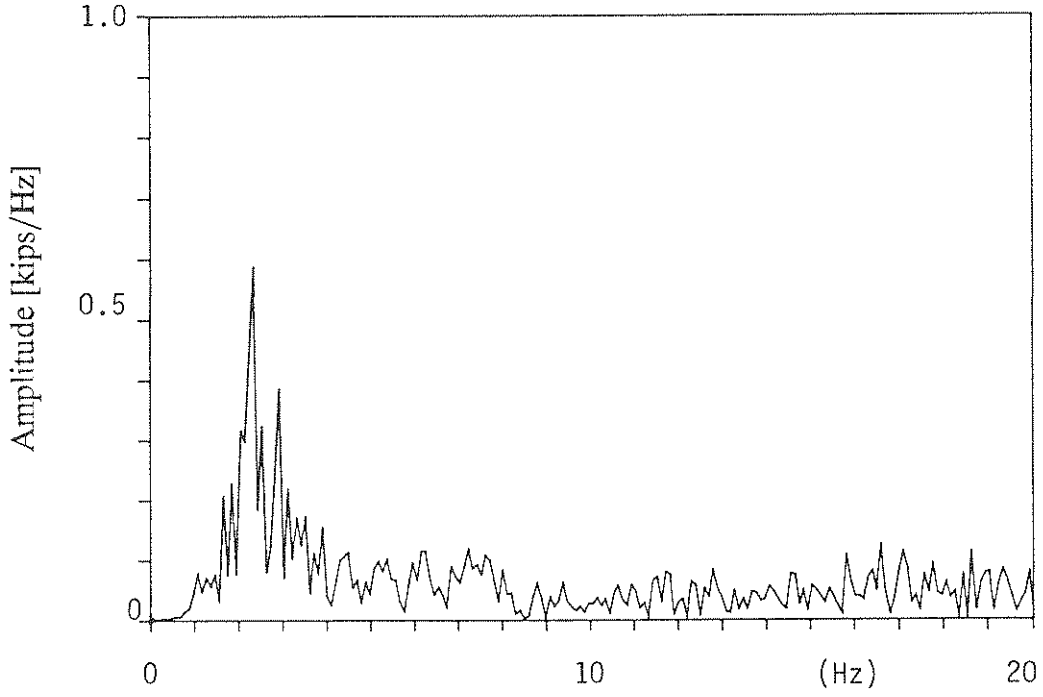

b) In Frequency Domain

Figure 4.40 - Control Force (Simulation Under 25% El Centro).

4.3.2.1.1 Control Parameters

As discussed previously in Section 3.1, the control efficiency is dependent on the parameter β . A better control is obtained with a reduction of β , however, the control force demand increases. The choice of β was determined analytically and adjusted experimentally to fit the demands for all cases. All cases (see Table 2.3 for designations) used $\beta = 4$ and $\beta = 8$ and case W2C3 used only $\beta = 8$. Lower values of β resulted in exceeding the actuators capacity in one case or another. Therefore, for sake of comparison, $\beta = 8$ was chosen to be the same for all experiments.

4.3.2.1.2 Structural Response and Comparison to Analytical Predictions

Using the model structure's parameters which were obtained from identification test (see Section 4.1), for each one of the experimental cases the theoretical analysis were made by using computer simulation. The peak structural responses for the experimental and theoretical cases are summarized in Table 4.7 for W1C1 cases and in Tables 4.8, 4.9, and 4.10 for W2 cases corresponding to the three earthquake excitations, respectively.

A few of typical time histories of relative displacement were shown in Figs. 4.41 through 4.43. The comparisons between experimental and theoretical peak relative displacements are shown in Figs. 4.44 through 4.50. Comparing these peak values of the responses, it can be noticed that the main differences appear in the time histories. The most probable reason for this discrepancy is the interaction between the shaking table and the controlled model structure, and the damping factors, as described in more detail in Section 4.3.1.1.3. The efficiency of control in all modes of vibration is evident from the frequency domain recordings for all ground motions except for the table-structure interaction influence lead to an increase in the second or third mode (see Figs. 4.51 through 4.53).

4.3.2.1.3 Comparison of Single Tendon System Versus Two Tendon System (Independent Control)

From theoretical analysis (see Figs. 4.45 through 4.49 and Figs. 4.54 through 4.56), it can be noticed that the case of two tendons independently controlled (W2C13) was producing the largest reductions. However, the experimental results show that the control efficiencies of W2C13 case were less than the single tendon case (W2C1), nevertheless , by a small margin. Comparing the control forces in experimental and theoretical response, it can be noticed

Table 4.7

Summary of Results in Weak Direction for One Actuator - On Tendon at First Floor (W1C1)

Excitation	Input	ElC. 20%		Hach. 30%		Miya. 40%	
Location of	Control Tendons	1st floor					
Case	No.	W1 C1					
Control	parameter	β = 4		β = 4		β = 4	
Experimental &	Theoretical	Exp.	Theo.	Exp.	Theo.	Exp.	Theo.
Ave. Reduction of Structural Response (%)	Relative Dspl.	31.5	18.3	20.7	26.6	28.2	42.1
	Storydrift	20.7	23.7	15.2	22.8	15.0	41.9
	Absolute Acc.		36.0		27.1		37.3
Max. Control	Force (Kips)	1.563	1.295	3.307	2.703	2.427	1.535
Max. Base Shear (kips)	Uncontrolled	2.876	2.128	5.725	4.379	3.487	3.041
	Controlled	2.543	1.549	4.912	3.042	3.301	1.678
	Reduction (%)	11.6	27.2	14.2	30.5	5.3	44.8
Max. Power	Requirements(Kw)	0.216	0.110	0.395	0.164	0.481	0.117

Table 4.8

Summary of Results in Weak Direction (W2) for 20% El Centro

Control cases		One Ctrl. Force						Two Ctrl. Force			
Location of	Control Tendons	1st floor				3rd floor		1&3 floor			
Case	No.	W2 C1				W2 C3		W2 C13			
Control	parameter	β = 8		β = 4		β = 8		β = 8		β = 4	
Experimental &	Theoretical	Exp.	Theo.	Exp.	Theo.	Exp.	Theo.	Exp.	Theo.	Exp.	Theo.
Ave. Reduction of Structural Response (%)	Relative Dspl.	30.7	22.0	34.9	28.6	12.3	10.7	25.2	27.2	33.8	35.6
	Storydrift	25.2	23.7	25.4	29.4	9.7	9.5	24.4	28.4	29.1	35.9
	Absolute Acc.		30.5		31.0		10.2		34.2		38.4
#1 Max. Control Force (Kips)		1.433	1.110	2.076	1.492	1.106	0.802	1.331	0.932	1.855	1.226
#2 Max. Control Force (Kips)								0.028	0.545	0.274	0.766
Max. Base Shear (kips)	Uncontrolled	3.935	2.843	3.935	2.843	3.935	2.843	3.945	2.843	3.945	2.843
	Controlled	2.912	1.893	2.663	1.704	3.738	2.559	3.196	1.739	2.782	1.541
	Reduction (%)	26.0	33.4	32.3	40.0	5.0	10.0	18.8	38.8	29.3	45.8
#1 Max. Power Supply (Kw)		0.099	0.056	0.265	0.104	0.161	0.026	0.081	0.041	0.174	0.076
#2 Max. Power Supply (Kw)								0.002	0.015	0.009	0.031

Table 4.9

Summary of Results in Weak Direction (W2) for 30% Hachinohe

Control cases		One Ctrl. Force						Two Ctrl. Force			
Location of Control Tendons		1st floor				3rd floor		1&3 floor			
Case No.		W2 C1				W2 C3		W2 C13			
Control parameter		β = 8		β = 4		β = 8		β = 8		β = 4	
Experimental & Theoretical		Exp.	Theo.	Exp.	Theo.	Exp.	Theo.	Exp.	Theo.	Exp.	Theo.
Ave. Reduction of Structural Response (%)	Relative Dspl.	31.6	29.6	39.2	37.9	16.9	21.0	24.5	35.5	33.7	45.0
	Storydrift	25.5	25.4	32.0	33.5	11.6	17.1	19.7	31.5	26.6	40.5
	Absolute Acc.		23.7		30.3		13.8		29.4		35.0
#1 Max. Control Force (Kips)		2.982	2.049	4.025	2.766	2.682	1.911	2.791	1.659	3.862	2.159
#2 Max. Control Force (Kips)								0.430	1.233	0.533	1.604
Max. Base Shear (kips)	Uncontrolled	7.687	5.870	7.687	5.870	7.687	5.870	7.687	5.870	7.687	5.870
	Controlled	5.340	4.043	4.392	3.501	6.633	4.575	5.810	2.649	5.083	3.245
	Reduction (%)	30.5	31.1	42.9	40.4	13.7	22.1	24.4	37.8	33.9	44.7
#1 Max. Power Supply (Kw)		0.300	0.044	0.689	0.083	0.257	0.039	0.263	0.031	0.607	0.053
#2 Max. Power Supply (Kw)								0.008	0.015	0.014	0.026

Table 4.10

Summary of Results in Weak Direction (W2) for 40% Miyagioki

Control cases		One Ctrl. Force						Two Ctrl. Force			
Location of Control Tendons		1st floor				3rd floor		1&3 floor			
Case No.		W2 C1				W2 C3		W2 C13			
Control parameter		β = 8		β = 4		β = 8		β = 8		β = 4	
Experimental & Theoretical		Exp.	Theo.	Exp.	Theo.	Exp.	Theo.	Exp.	Theo.	Exp.	Theo.
Ave. Reduction of Structural Response (%)	Relative Dspl.	23.9	28.8	32.5	37.0	10.0	17.3	19.5	34.4	27.4	43.4
	Storydrift	19.8	33.2	28.6	39.6	11.6	18.7	16.1	40.1	22.4	48.0
	Absolute Acc.		37.2		40.5		22.3		46.0		51.9
#1 Max. Control Force (Kips)		1.602	1.086	2.023	1.441	1.191	0.989	1.557	0.963	2.058	1.245
#2 Max. Control Force (Kips)								0.266	0.667	0.330	0.874
Max. Base Shear (kips)	Uncontrolled	4.336	3.850	4.336	3.850	4.336	3.850	4.336	3.850	4.336	3.850
	Controlled	3.394	2.290	2.798	2.081	3.854	3.145	3.503	2.148	2.991	1.941
	Reduction (%)	21.7	40.5	35.5	46.0	11.1	18.3	19.2	44.2	31.0	49.6
#1 Max. Power Supply (Kw)		0.124	0.024	0.269	0.042	0.047	0.016	0.137	0.019	0.271	0.032
#2 Max. Power Supply (Kw)								0.005	0.009	0.011	0.016

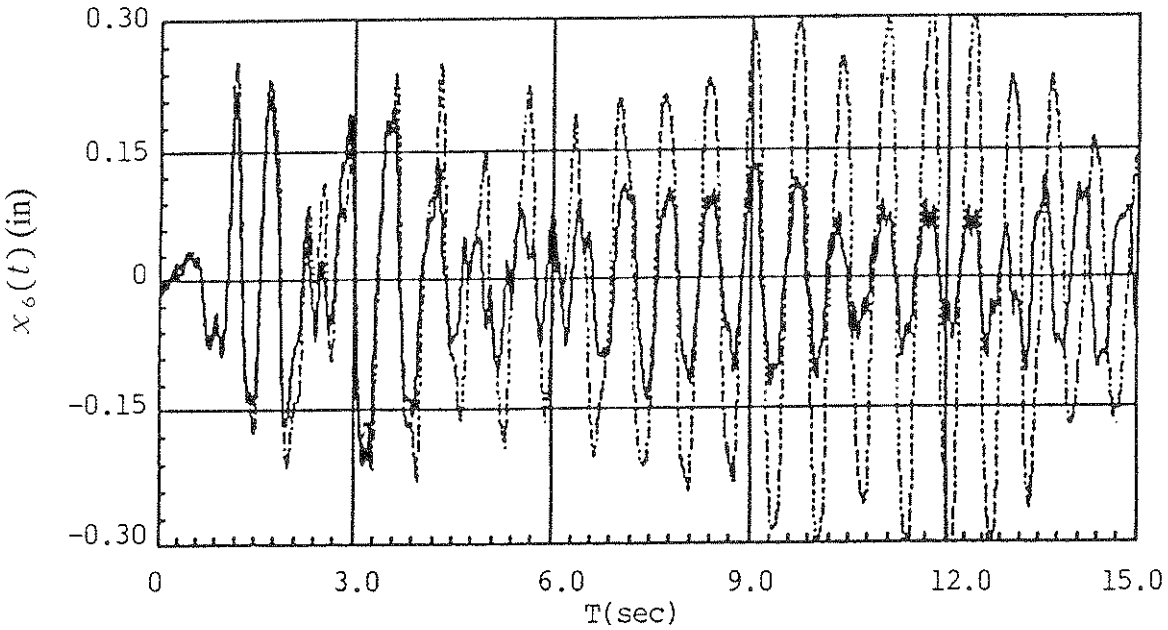

a) Experimental

----- No Control

—— With Control

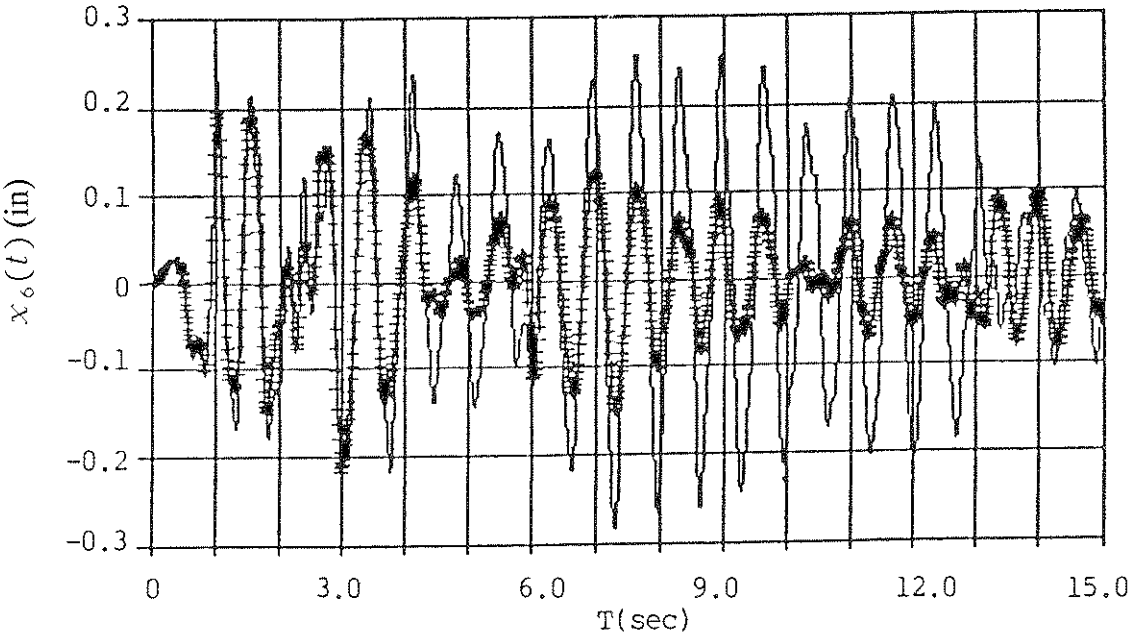

b) Theoretical

—— No Control

+++++ With Control

Figure 4.41 - Sixth Floor Relative Displacement in Weak Direction (El Centro).

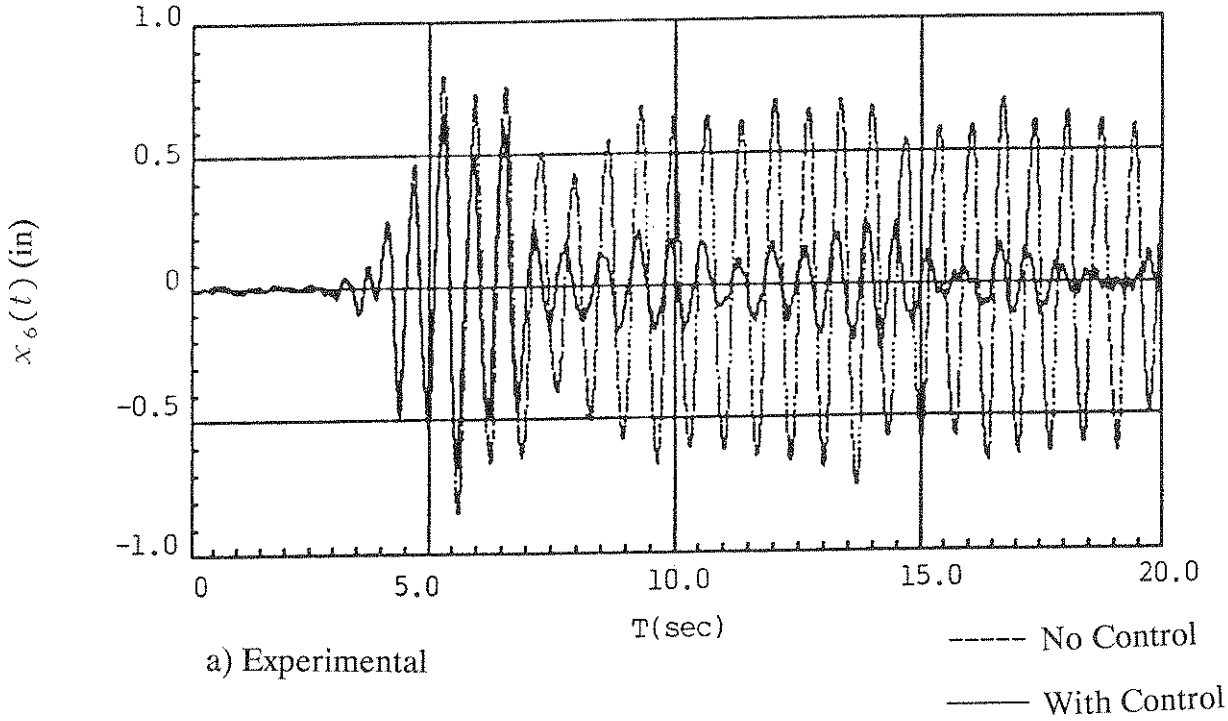

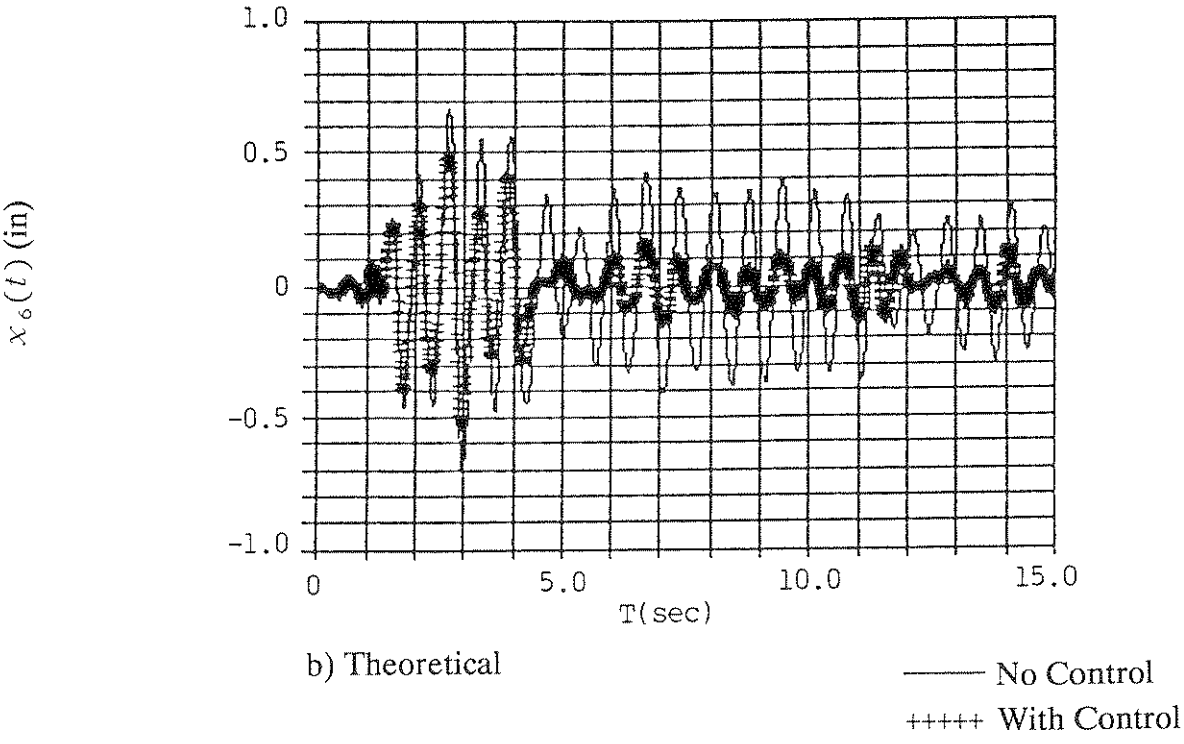

Figure 4.42 - Sixth Floor Relative Displacement in Weak Direction (Hachinohe).

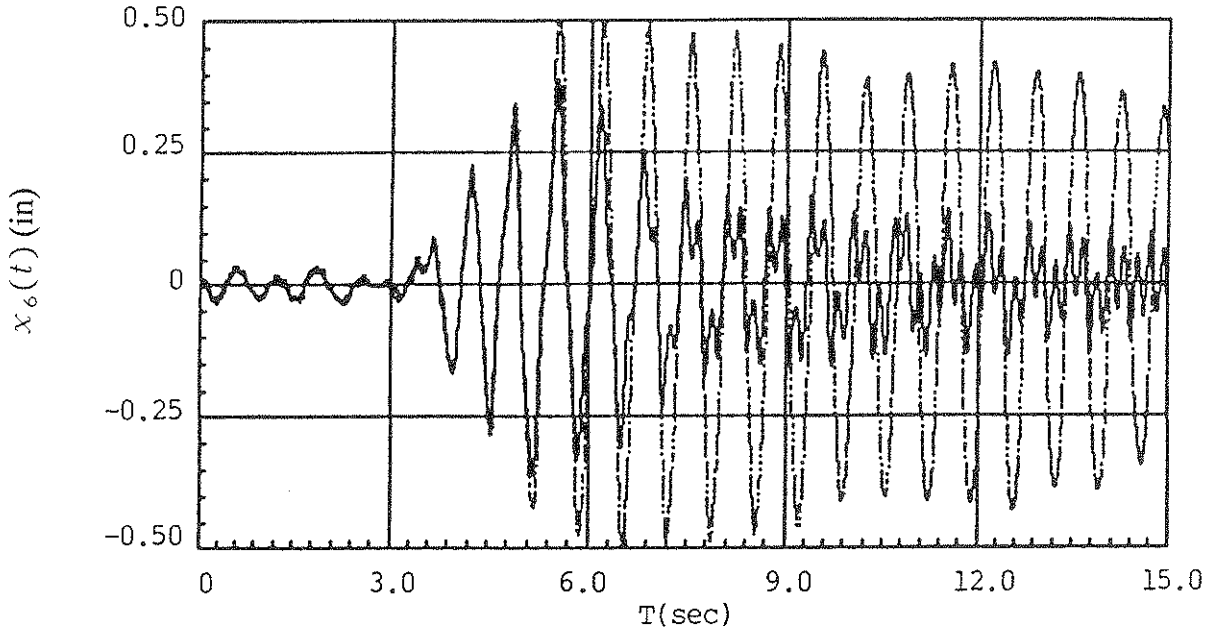

a) Experimental

----- No Control

——— With Control

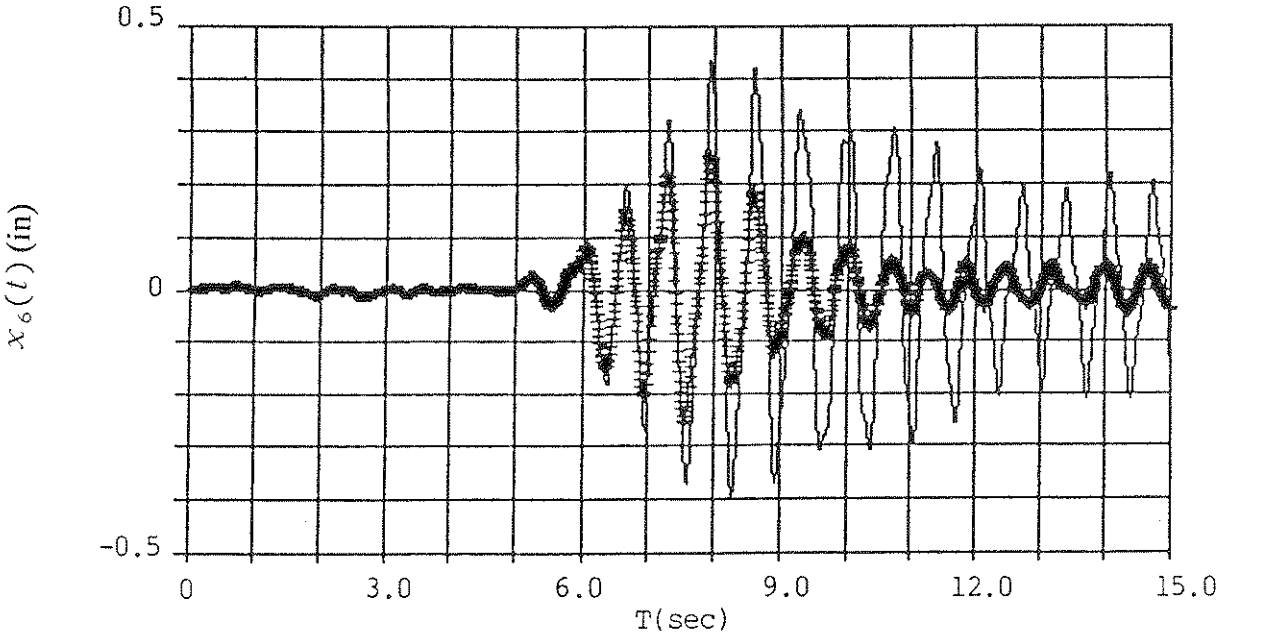

b) Theoretical

——— No Control

+++++ With Control

Figure 4.43 - Sixth Floor Relative Displacement in Weak Direction (Miyagioki).

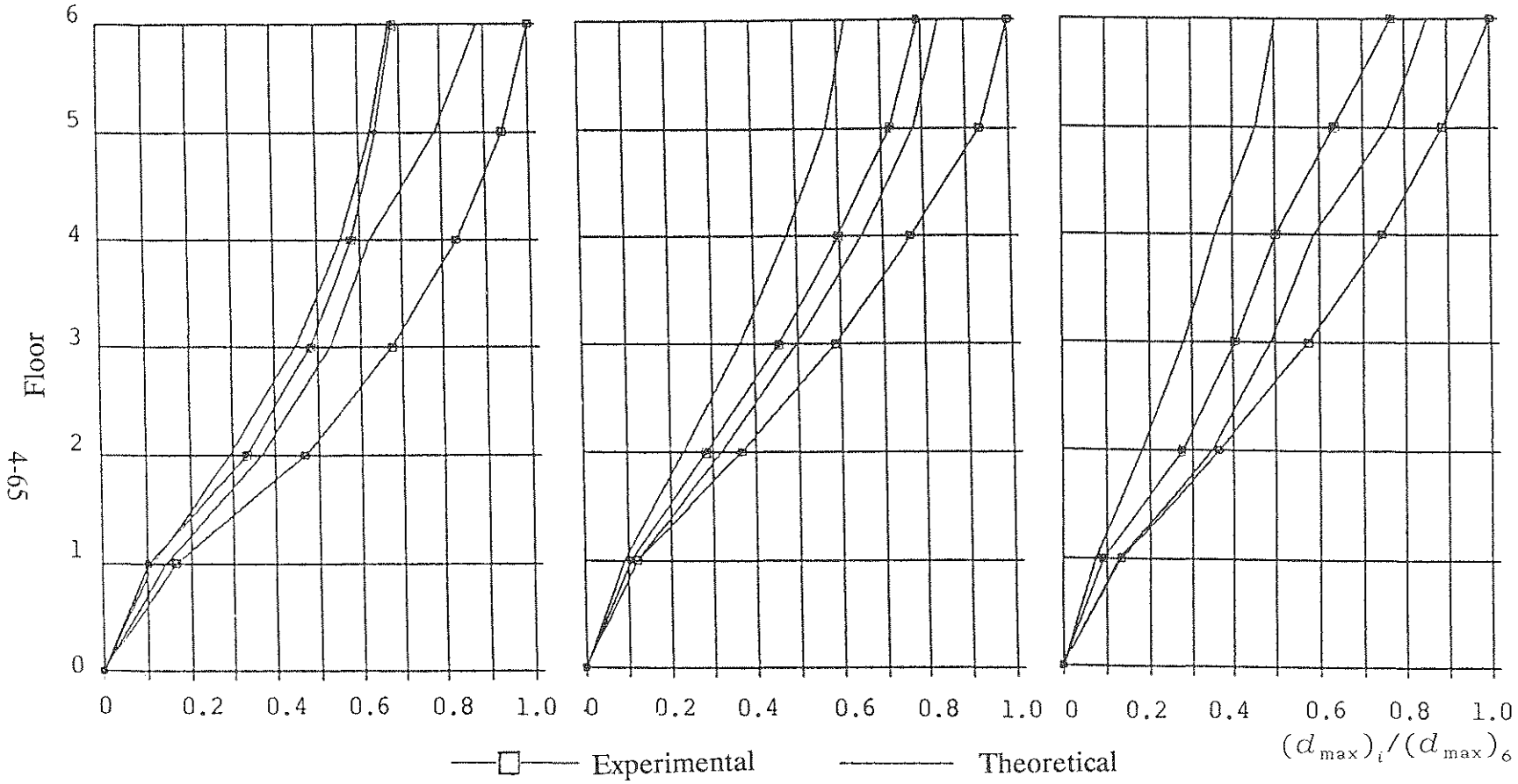

a) 20% El Centro b) 30% Hachinohe c) 40% Miyagioki

Figure 4.44 - Peak Relative Displacement For Case W1C1.

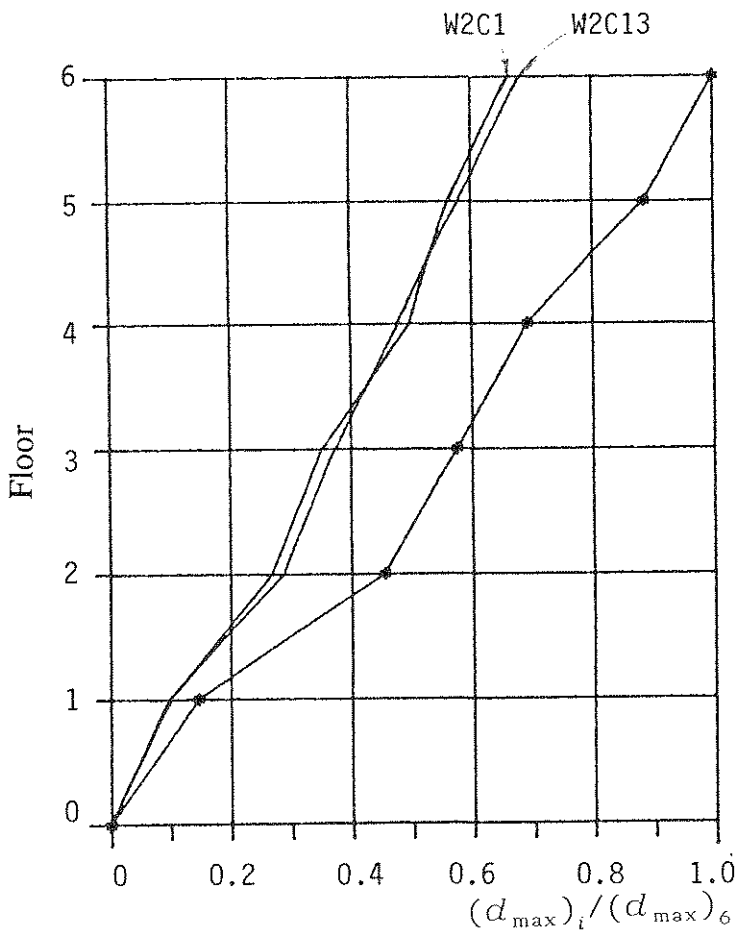

a) Experimental

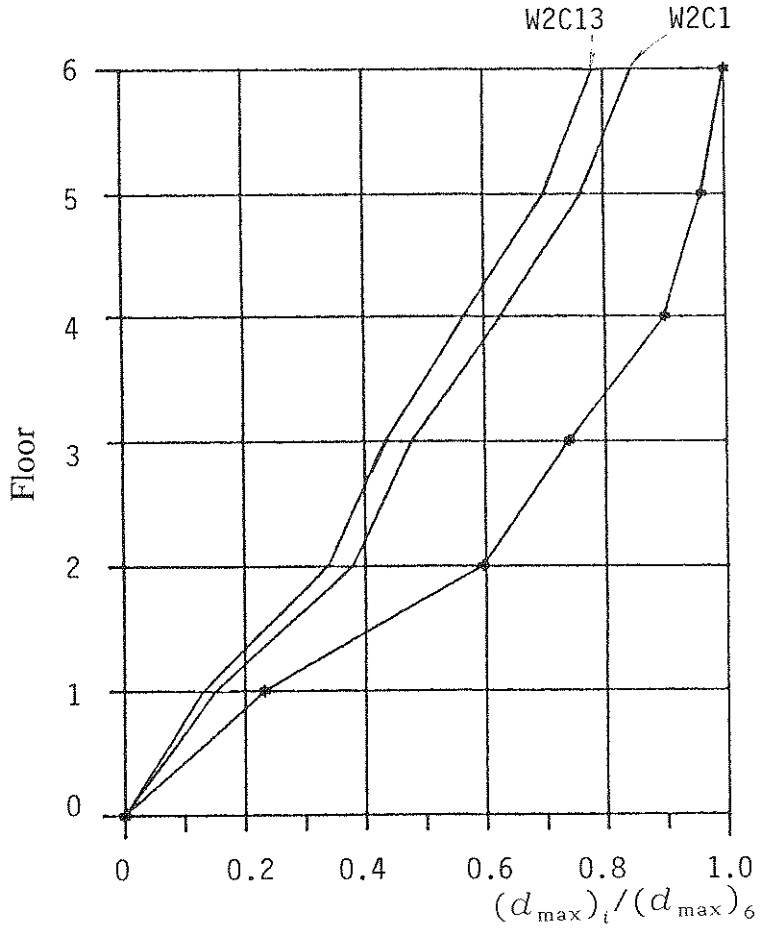

b) Theoretical

——— With Control

—●— Without Control

Figure 4.45 - The Peak Relative Displacement For 20% El Centro, $\beta = 4$

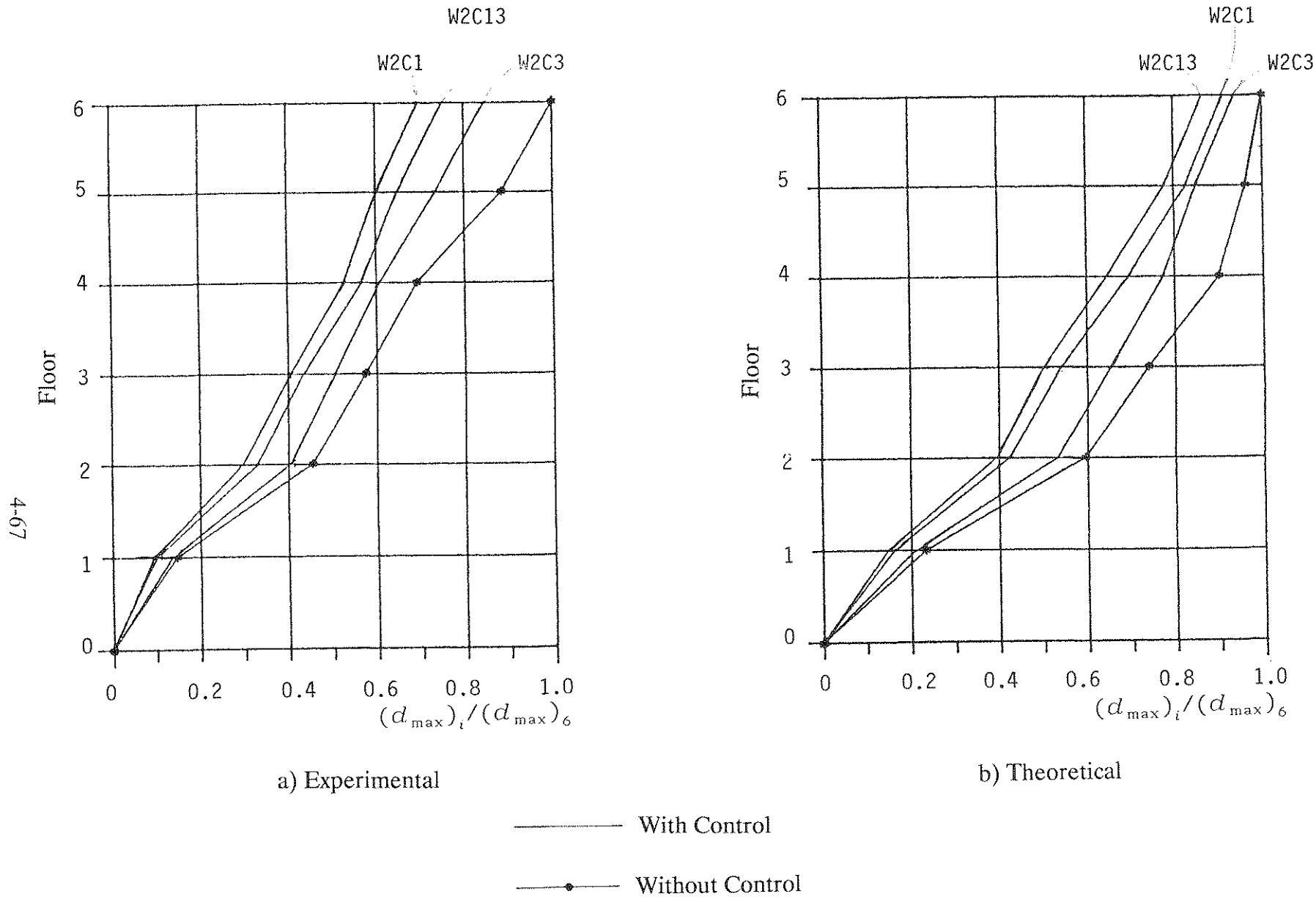

Figure 4.46 - The Peak Relative Displacement For 20% El Centro, $\beta = 8$.

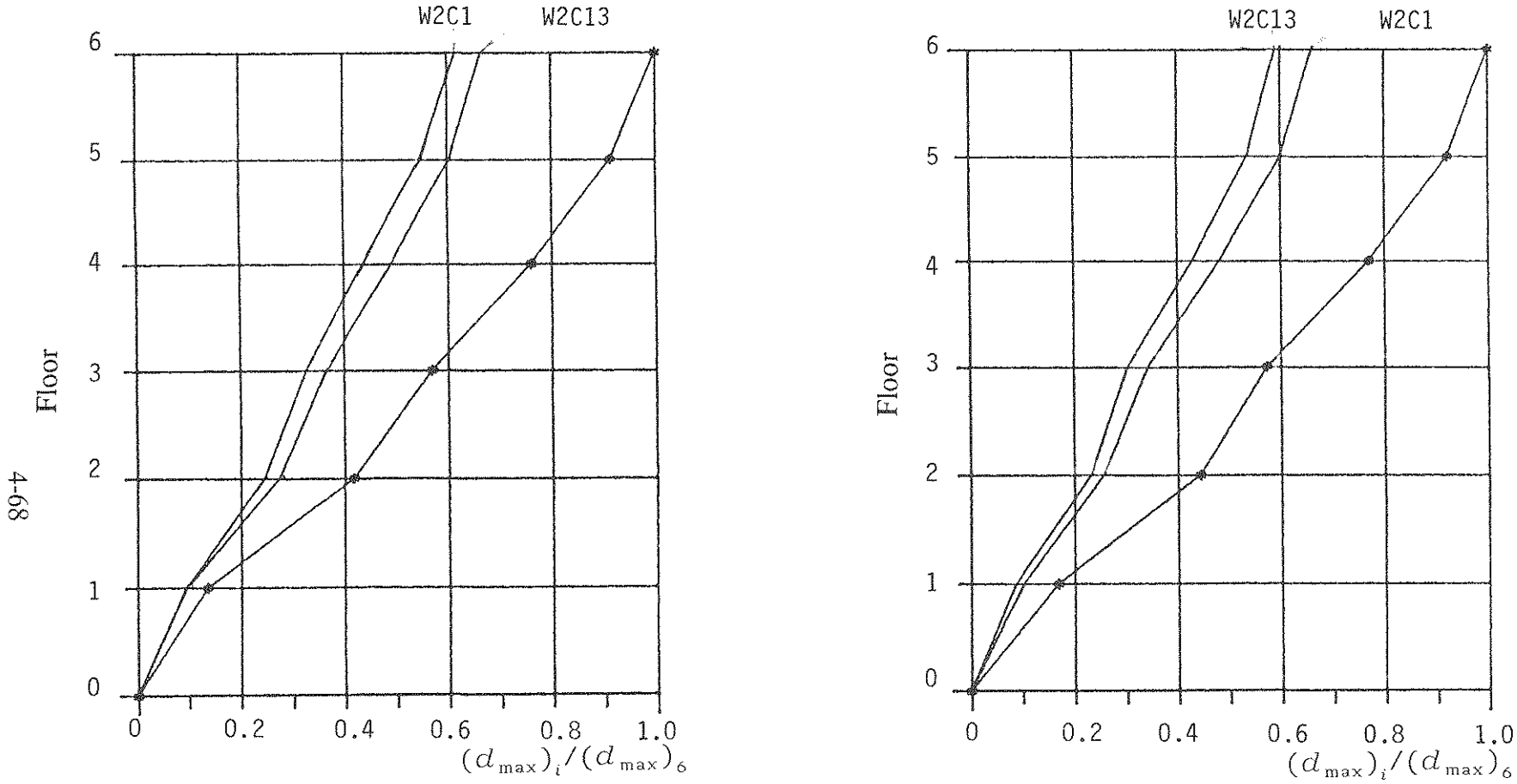

a) Experimental

b) Theoretical

——— With Control

———•——— Without Control

Figure 4.47 - The Peak Relative Displacement For 30% Hachinohe, $\beta = 4$.

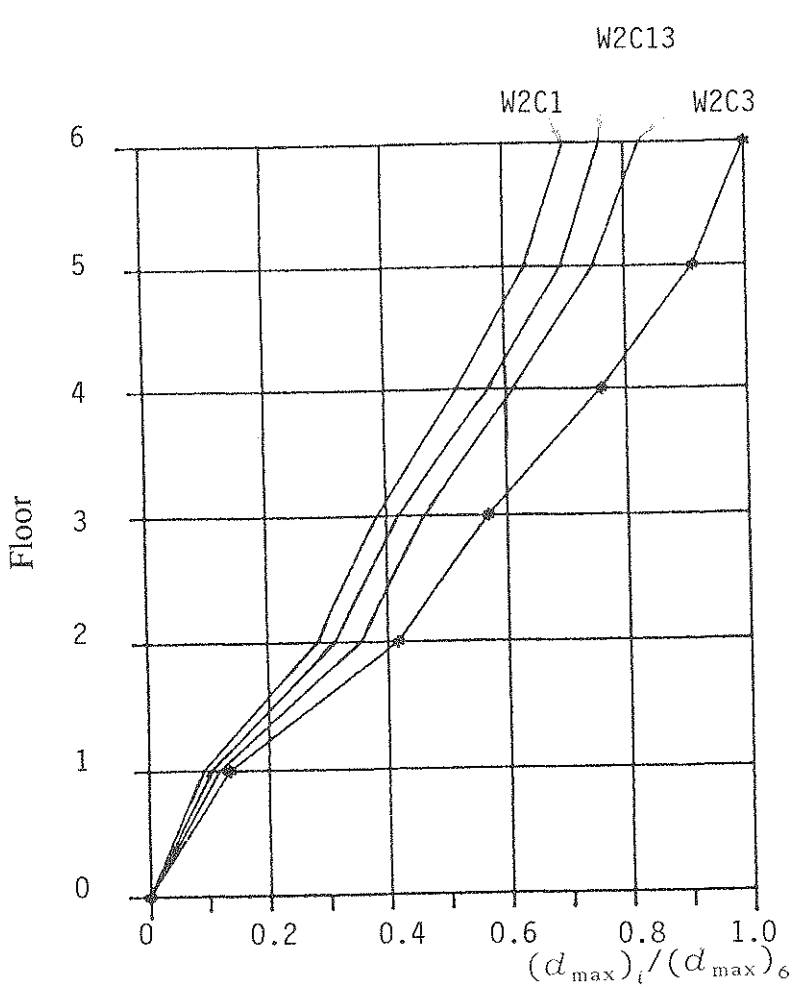

a) Experimental

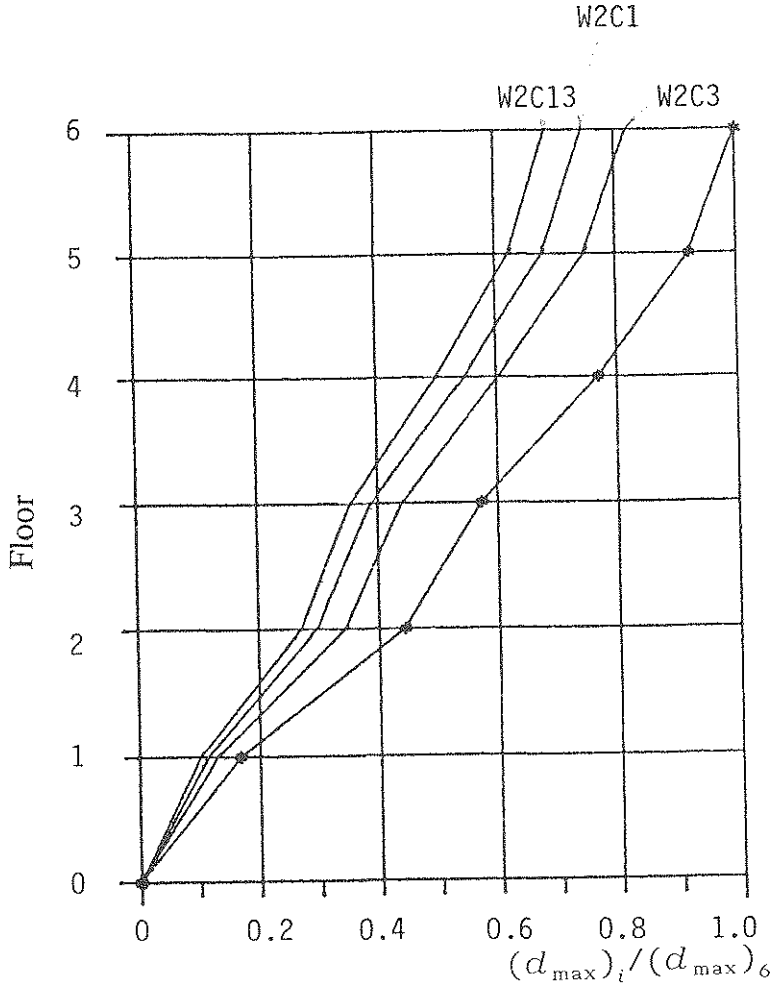

b) Theoretical

——— With Control

——*——— Without Control

Figure 4.48 - The Peak Relative Displacement For 30% Hachinohe, $\beta = 8$.

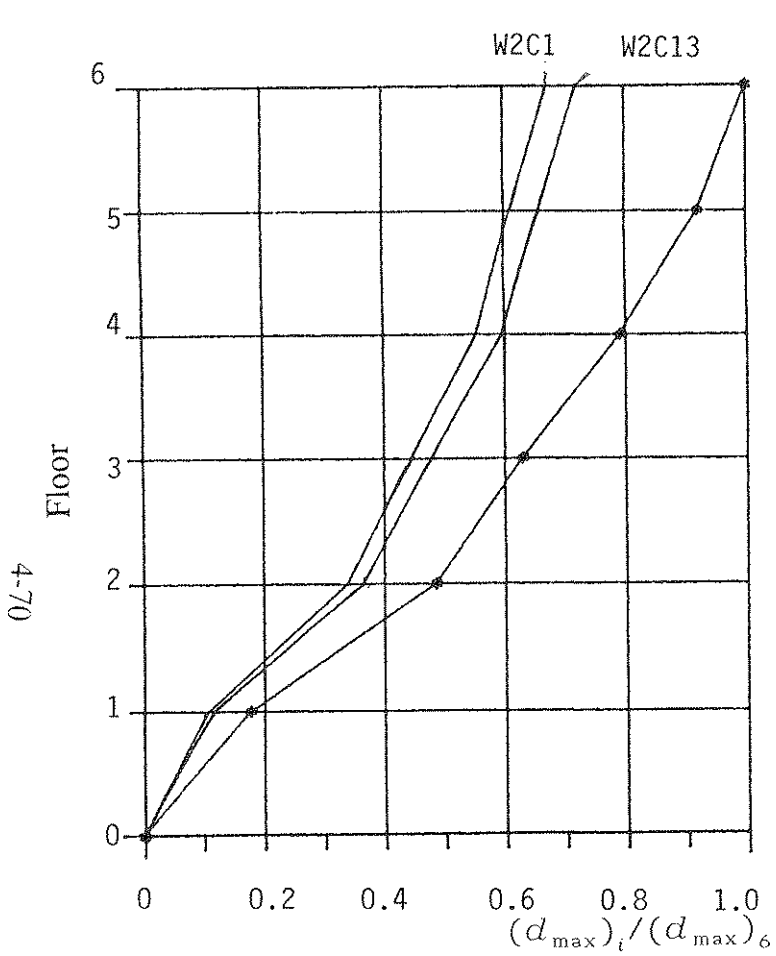

a) Experimental

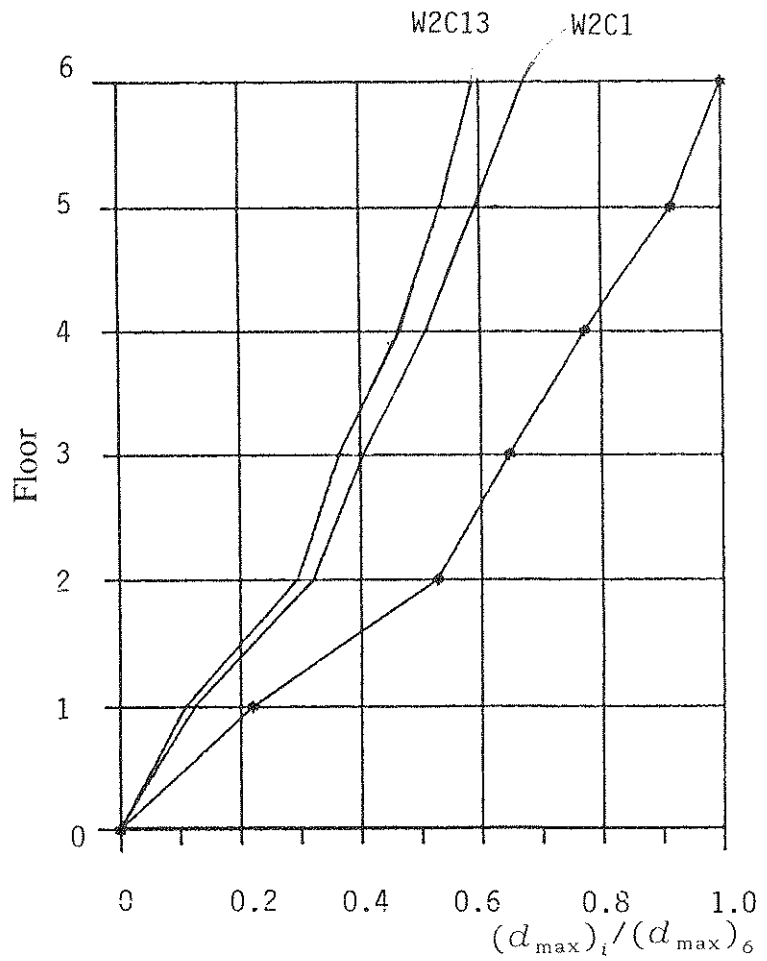

b) Theoretical

——— With Control

———●——— Without Control

Figure 4.49 - The Peak Relative Displacement For 40% Miyagioki, $\beta = 4$.

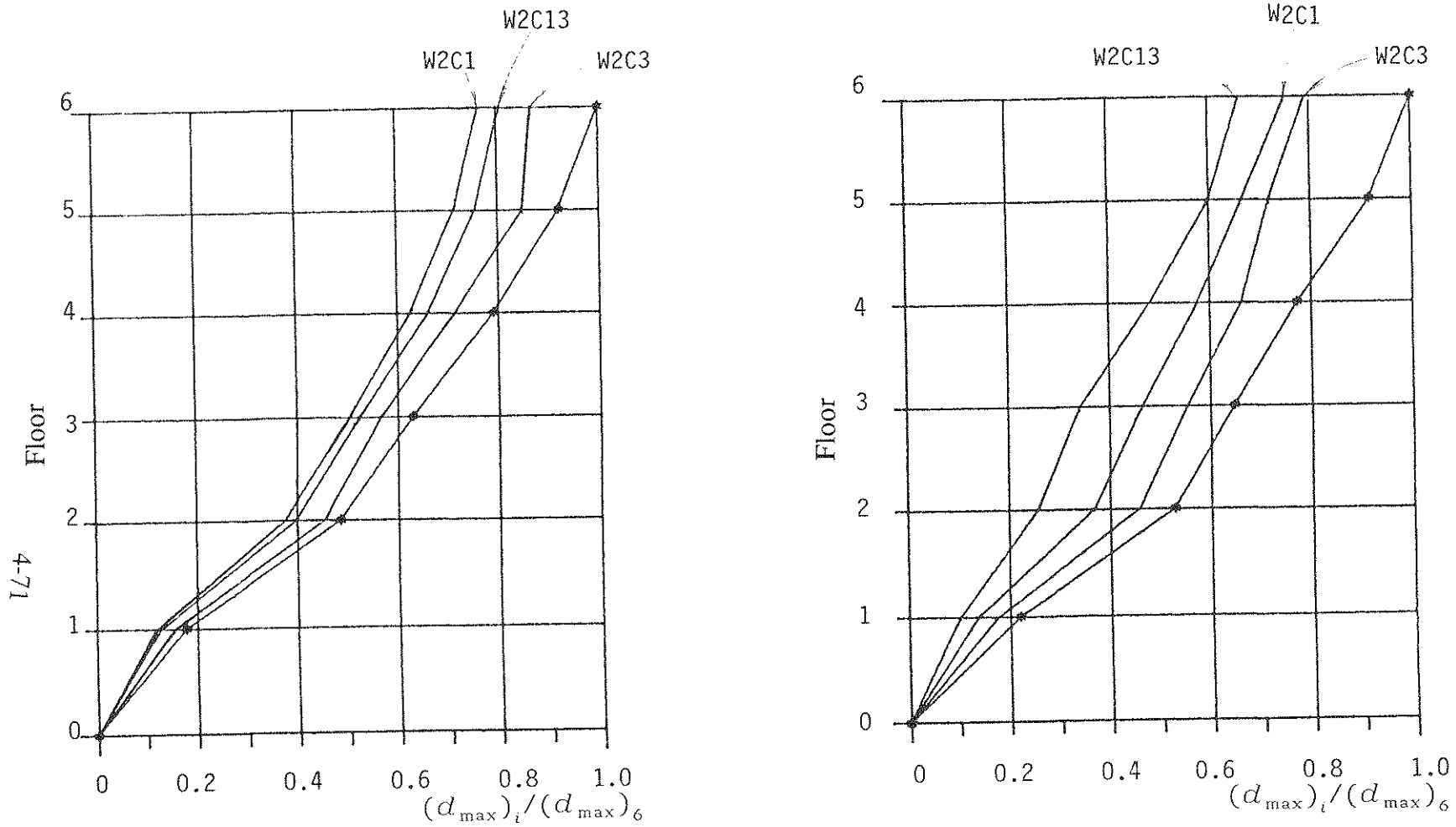

a) Experimental

b) Theoretical

——— With Control

——●—— Without Control

Figure 4.50 - The Peak Relative Displacement For 40% Miyagioki, $\beta = 8$

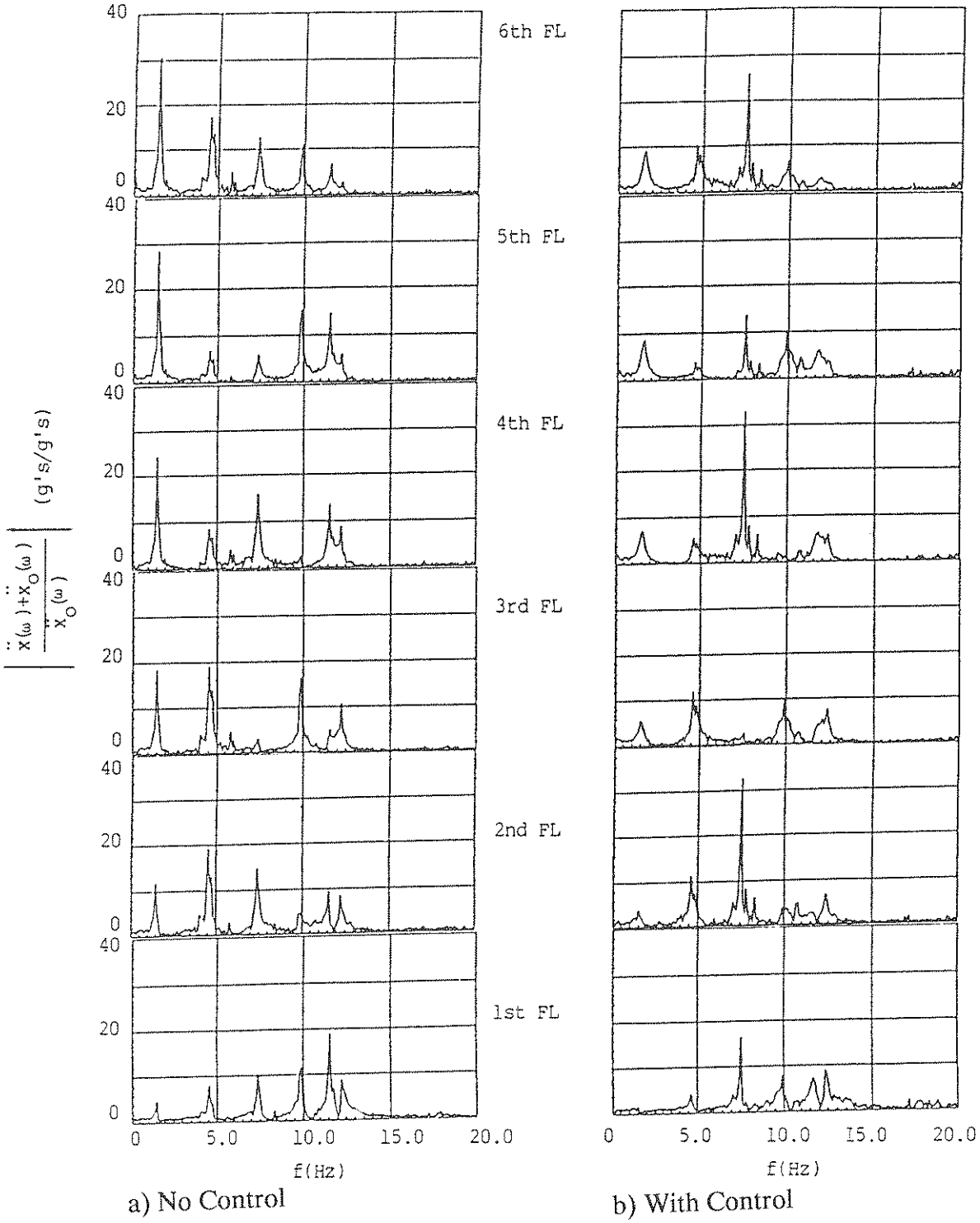

Figure 4.51 - Frequency Transfer Function of Absolute Acceleration in Weak Direction For 20% El Centro.

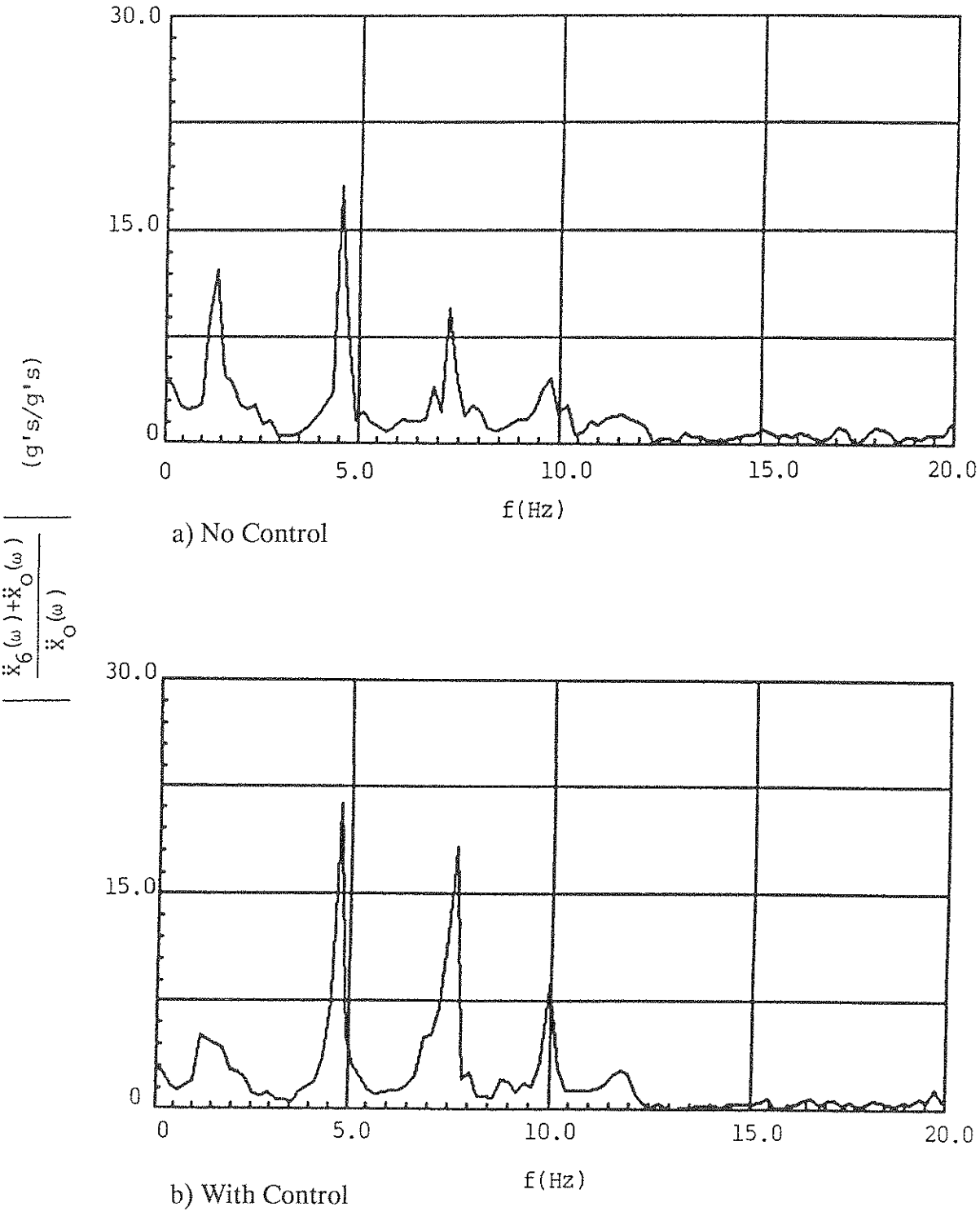

Figure 4.52 - Frequency Transfer Function of Sixth Floor Absolute Acceleration in Weak Direction For 30% Hachinohe.

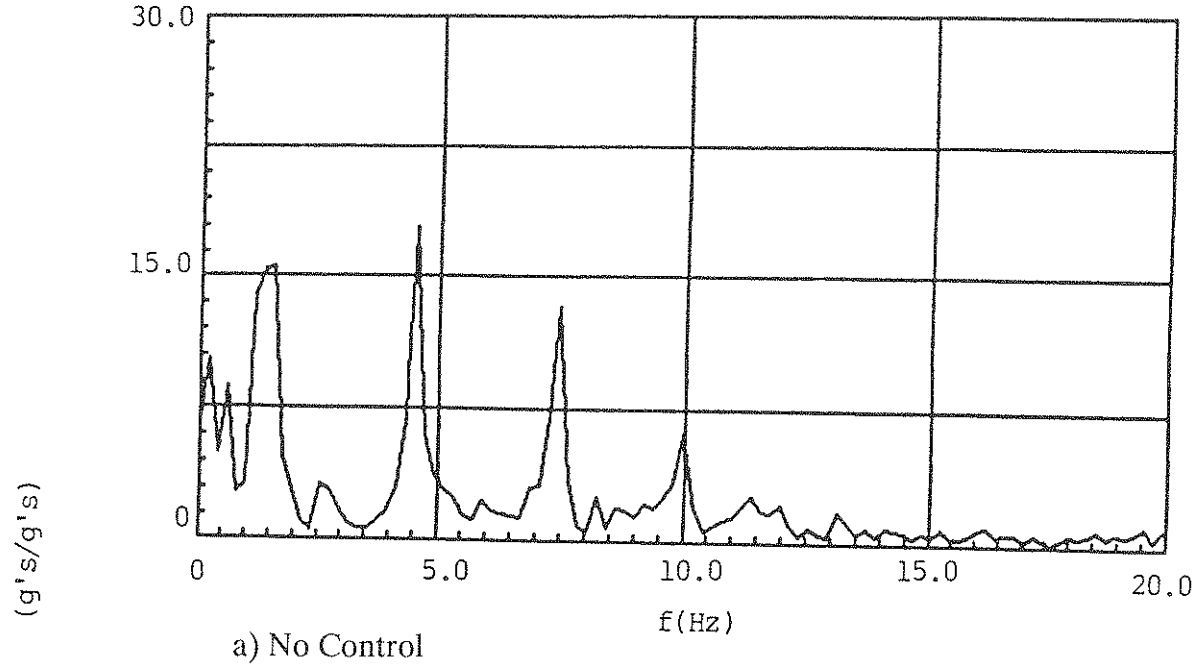

a) No Control

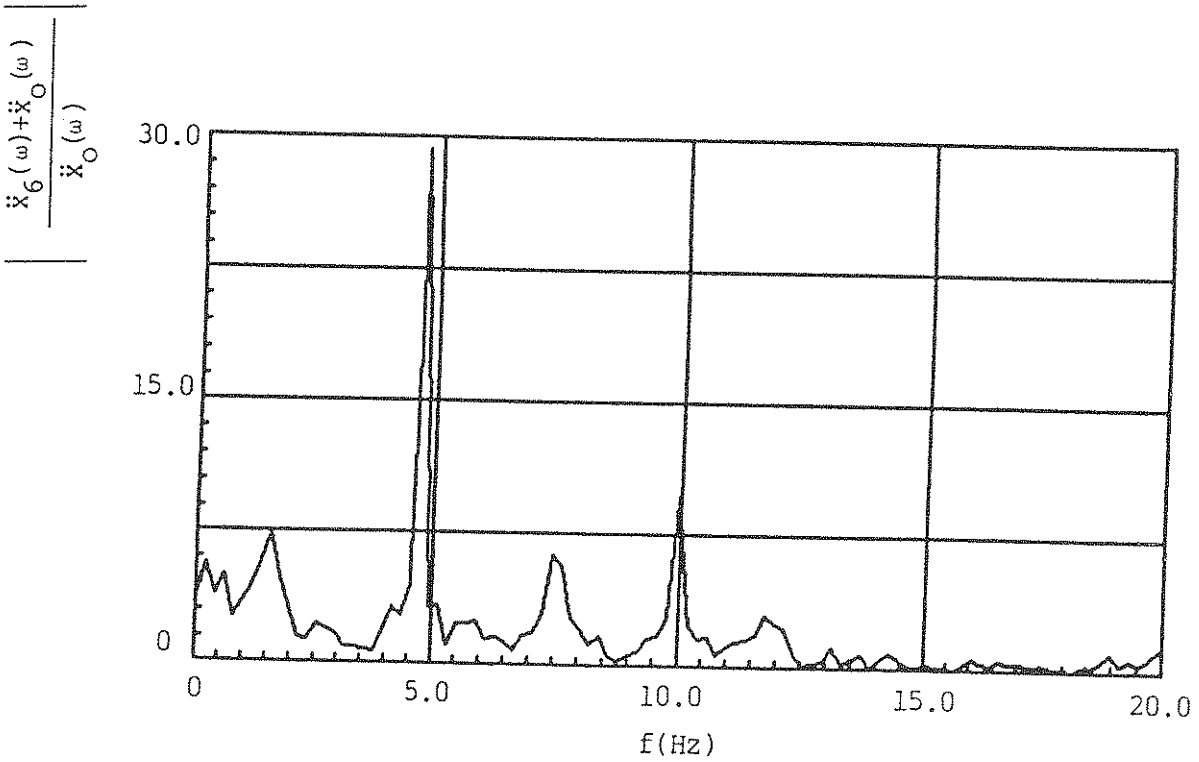

b) With Control

Figure 4.53 - Frequency Transfer Function of Sixth Floor Absolute Acceleration in Weak Direction For 40% Miyagioki.

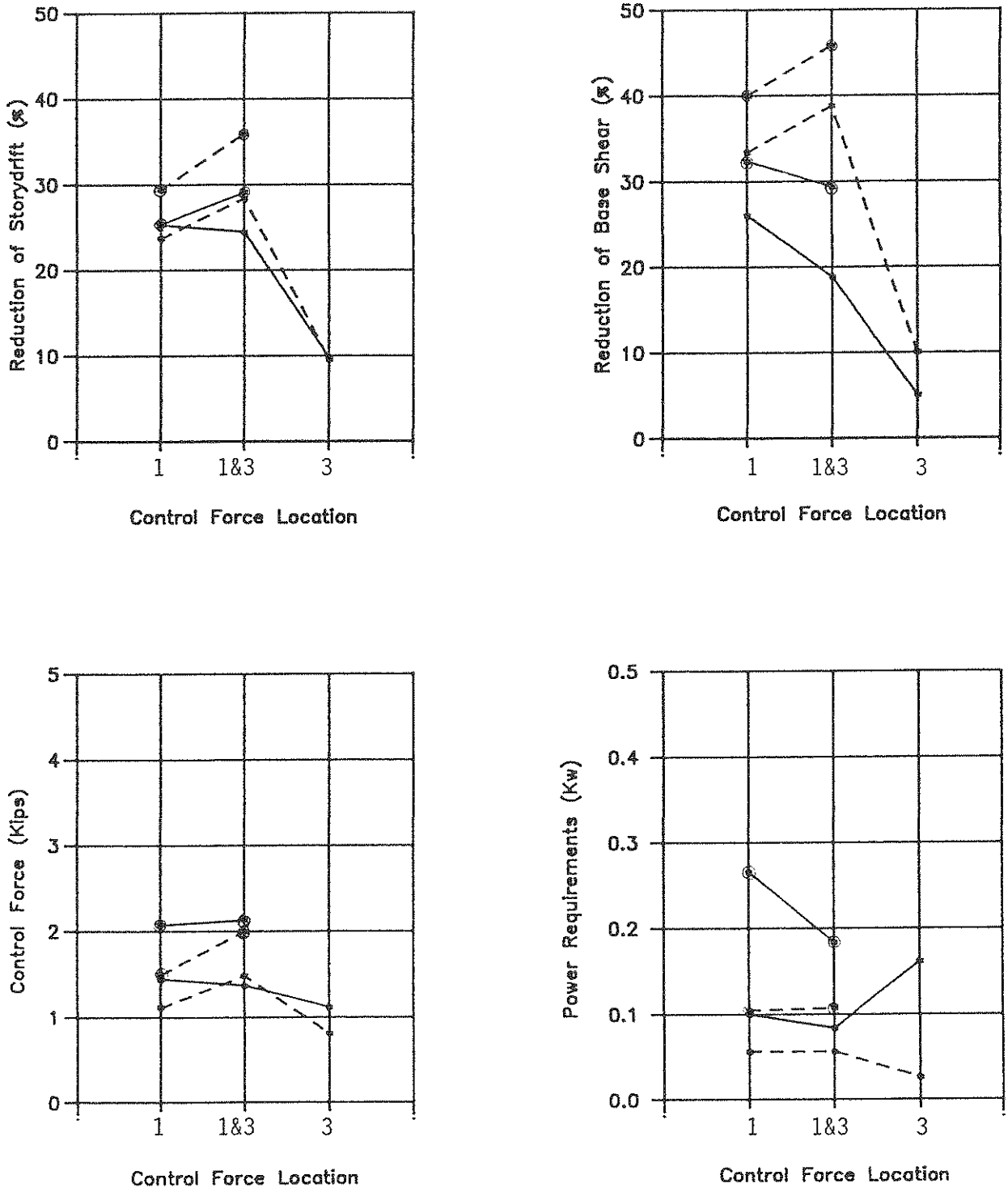

Figure 4.54 - Comparison of 1TS vs 2TS in Weak Direction for 20% El Centro.

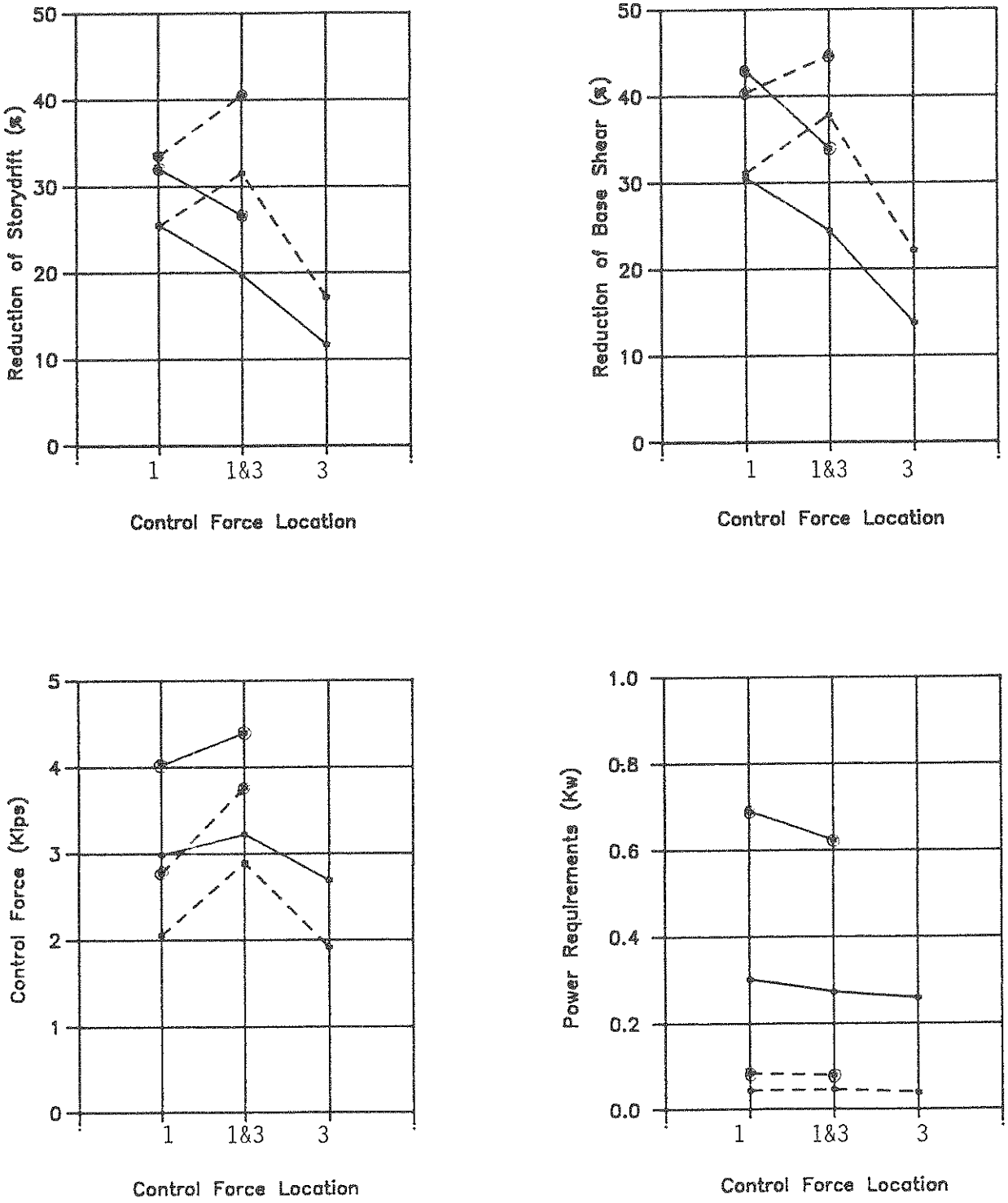

Figure 4.55 - Comparison of 1TS vs 2TSin Weak Direction For 30% Hachinohe.

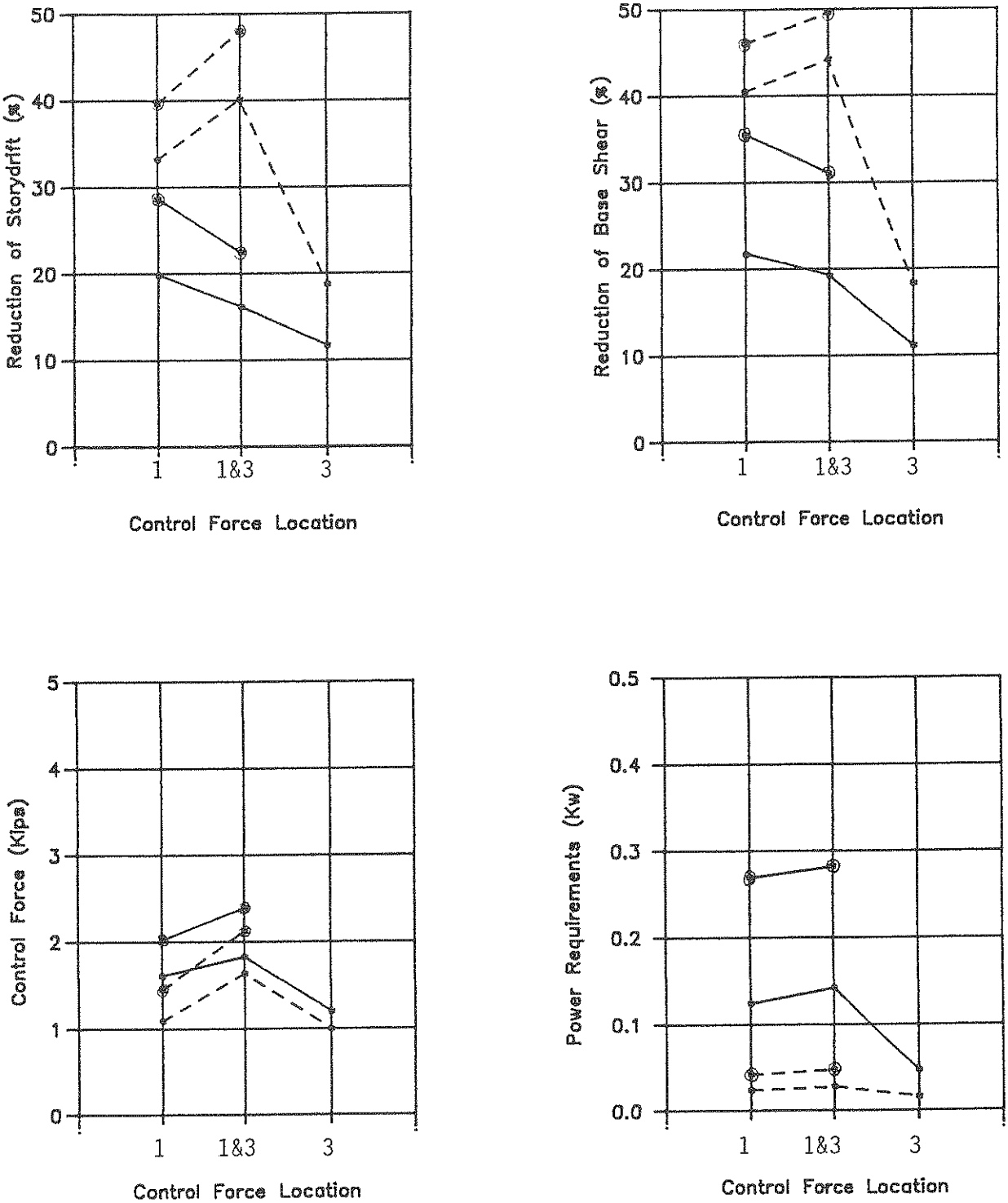

Figure 4.56 - Comparison of 1TS vs 2TSin Weak Direction For 40% Miyagioki.

(Fig. 4.54 through 4.56) that the control forces applied to the third floor in the experiments were substantially less than the theoretical. This is most likely due to errors of the actuator which could not be corrected during the limited times of testing. Therefore in these series of tests only a limited efficiency could be achieved for series W2C13.

In spite of the errors in the actuator operation during the experimental program, the case of two tendons activated independently (W2C13) produced reasonable reductions which indicate that this type of control is feasible. With additional improvements of the actuators operation, this case may be the most effective as indicated by the theoretical results.

4.3.2.1.4 Control Efficiency

The efficiency of control in the **weak direction** can be studied in Tables 4.8 through 4.10 and Figs. 4.54 through 4.56. The experimental reductions obtained for the three seismic excitations studied in the testing program, are 32 to 40% of the uncontrolled relative displacement, 25 to 32% of the story drift and 32 to 43% of the base shear.

The reduction of the absolute acceleration can be seen in Figs. 4.51 through 4.53 which show the absolute acceleration responses in frequency domain. It can be noticed in Fig. 4.51 that the acceleration was reduced in all modes except for the third mode which was increased due to the modification of the base excitation by the shaking table-model interaction. Most affected was the first mode which is dominant, so the total absolute acceleration was reduced by the control system. The theoretical results indicate that an average reduction of the absolute acceleration can be obtained from 35 to 52%.

In spite of the differences between the theoretical and experimental results which are as high as 20%, the experiential results show that the structural response is always under control for all control cases as initially predicted. Therefore, this device can be used for an efficient control.

4.3.2.2 Response With AMD Control

4.3.2.2.1 Samples of Experimental Results

To demonstrate the influence of the control system in the **weak direction** several samples of the experimental results were selected. Using the TAK-S regulator (Type 1 in Table 2.4) and

the 20% El Centro excitation, the relative displacement is substantially reduced at both sixth and third floors of the structure (see Fig. 4.57). At the same time, the absolute acceleration are also reduced, but not in the same ratios as the displacements (see Fig. 4.58). To achieve these reductions the active mass travels approximately four inches at peak, with accelerations of 0.75g producing control forces of 450 lbs (see Fig. 4.59).

When the same regulator is used for different base displacement, as indicated in the experimental program (see Section 2.3), the controlled response is always reduced leaving only a small vibration after several seconds (see Fig. 4.60). A comparison of the controlled peak displacements at all floors shows similar reductions of the response at all floors for all motions used (Fig. 4.61). In Fig. 4.61 there is a comparison of the regulator KYB-S (see Type 1 in Table 2.4) with the TAK-S regulator. Practically both regulators produce same response, i.e., a reduction of 30% to 40% at all floors.

Typical transfer functions of absolute acceleration response in respect to the base excitations are shown for the sixth and third floor response in Fig. 4.62 for the control identification studies performed with white noise excitations. The response with control, Fig. 4.62 (b) and 4.62 (c), show a good reduction in the first three modes, in particular, in the first mode, 1.46 Hz (for all algorithms) and more pronounced reduction for all three modes, 1.46, 4.59, and 7.42 Hz in the algorithm using two sensors control (see experimental program in Section 2.3). Little or no influence is observed for the higher modes. However the original accelerations are extremely small at these frequencies and their influence is negligible.

The percentage reduction at each peak of the relative displacement is shown in Fig. 4.63 (b). For the uncontrolled case, the occurrence of the maximum relative displacement at each floor is about 15 cycles behind that of the peak acceleration of El Centro excitation. The maximum value of the controlled case occurs at the same time as that of the input ground acceleration i.e., 15 cycles earlier than in the uncontrolled case. The control in the initial cycles is less effective, and the displacement response at one peak is even slightly amplified. However the effects of control are improved in latter cycles. All of the experimental results in the **weak direction** show identical tendencies for both AMD and ATS. Moreover, the response in the **strong direction** showed similar response.

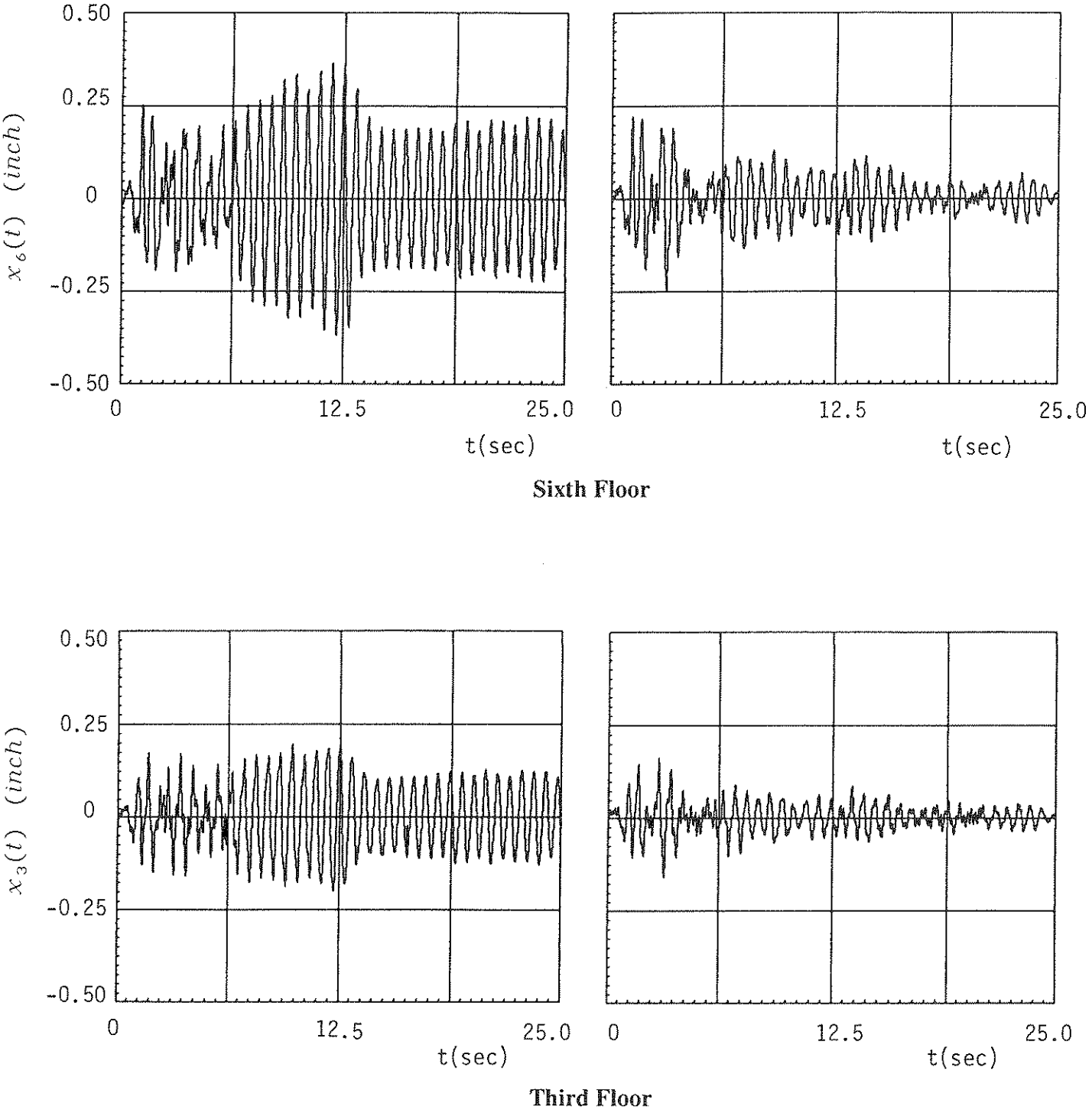

Figure 4.57 - Time Histories of the Relative Displacement (20% El Centro Excitation).

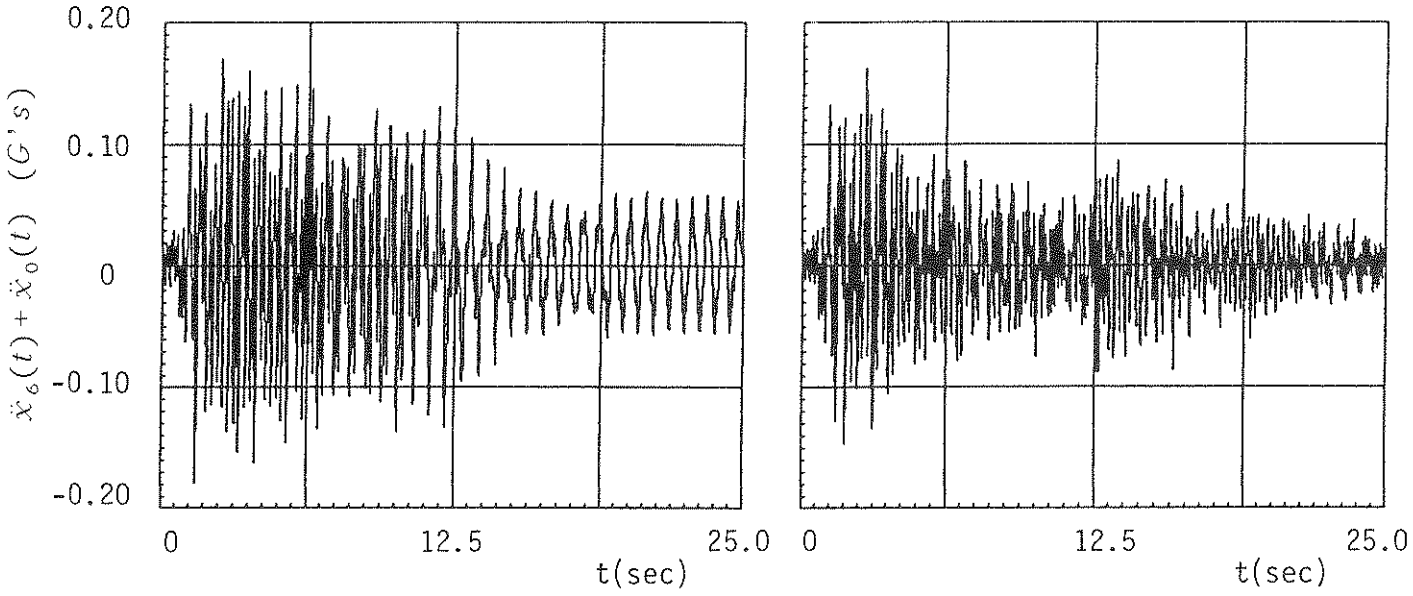

Sixth Floor

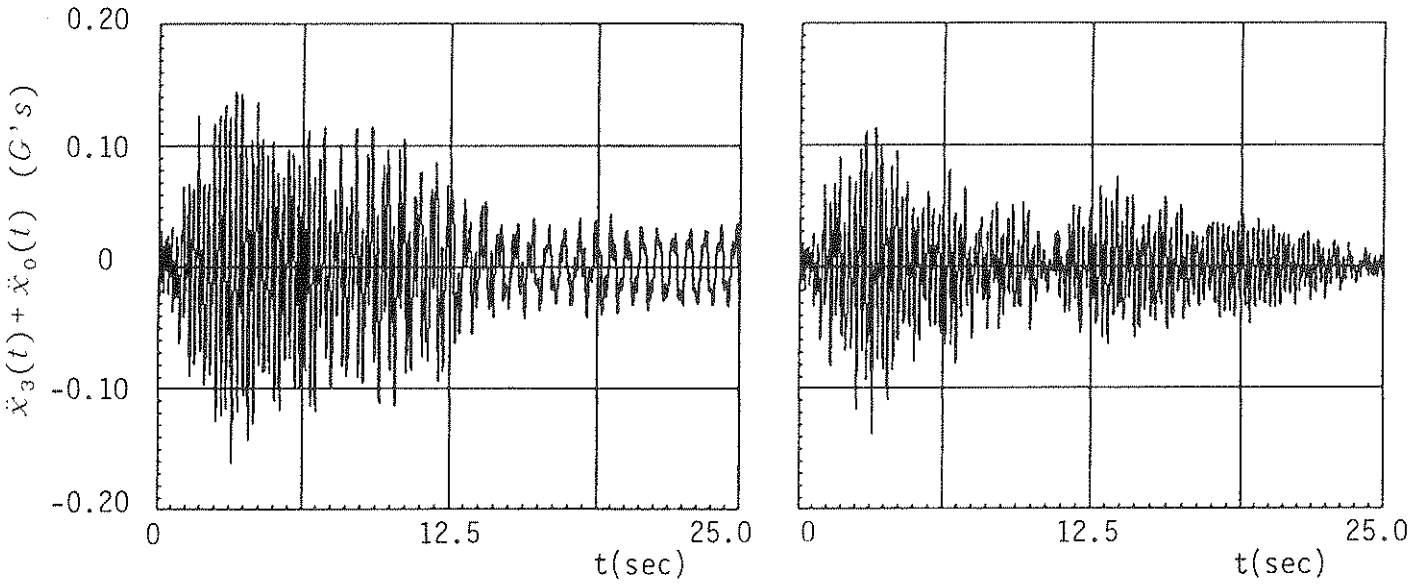

Third Floor

a) Without Control

b) With Control

Figure 4.58 - Time Histories of the Absolute Acceleration (20% El Centro Excitation).

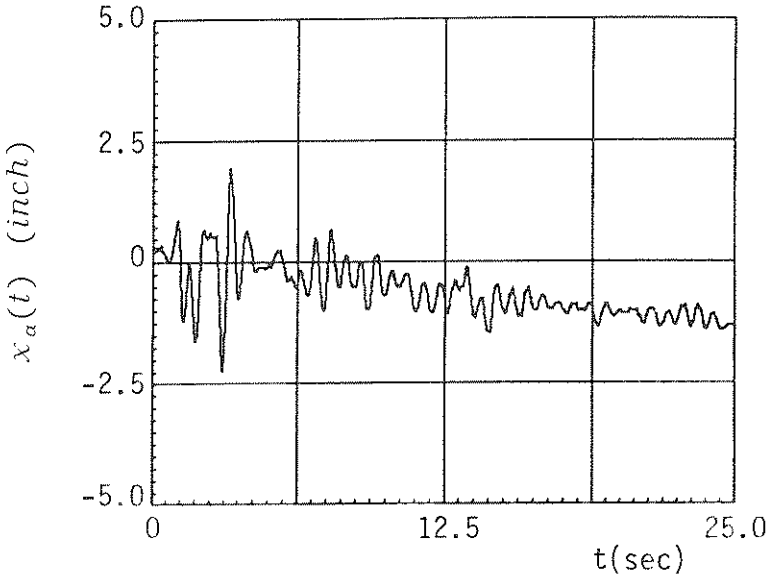

a) Mass Stroke

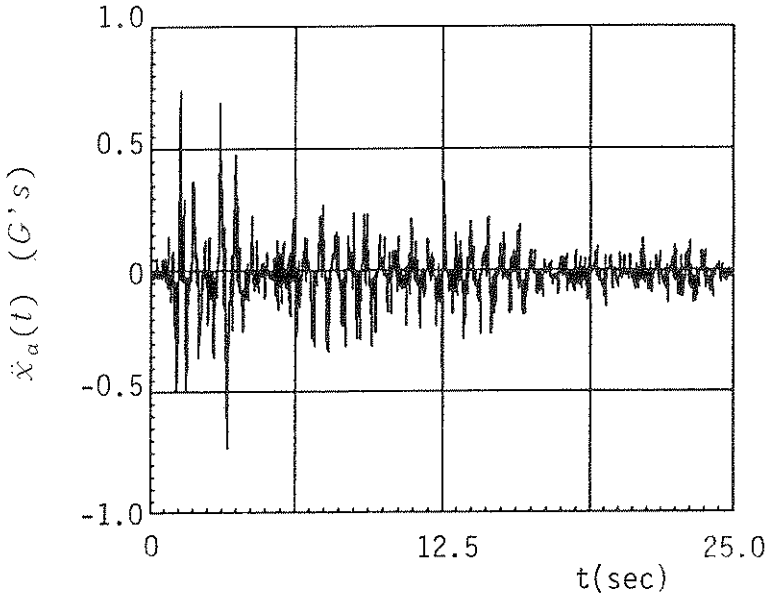

b) Mass Acceleration

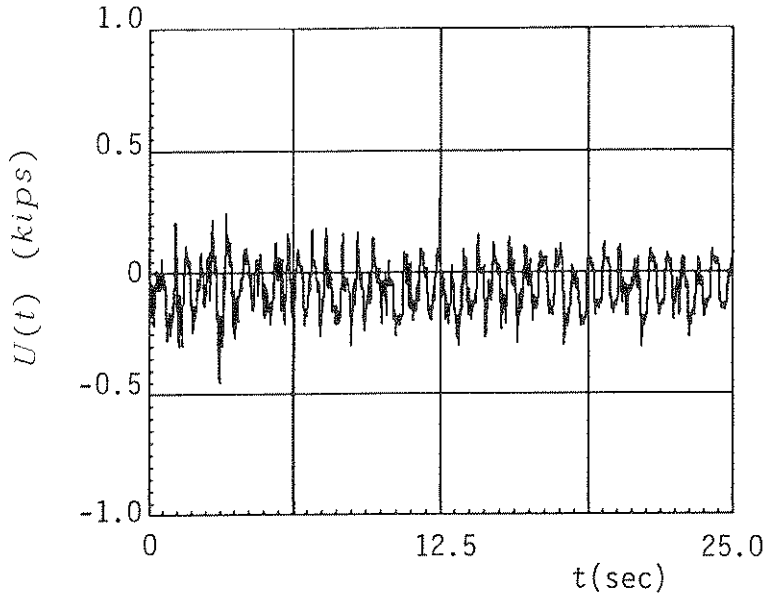

c) Control Force

Figure 4.59 - Time Histories Under Control (20% El Centro Excitation).

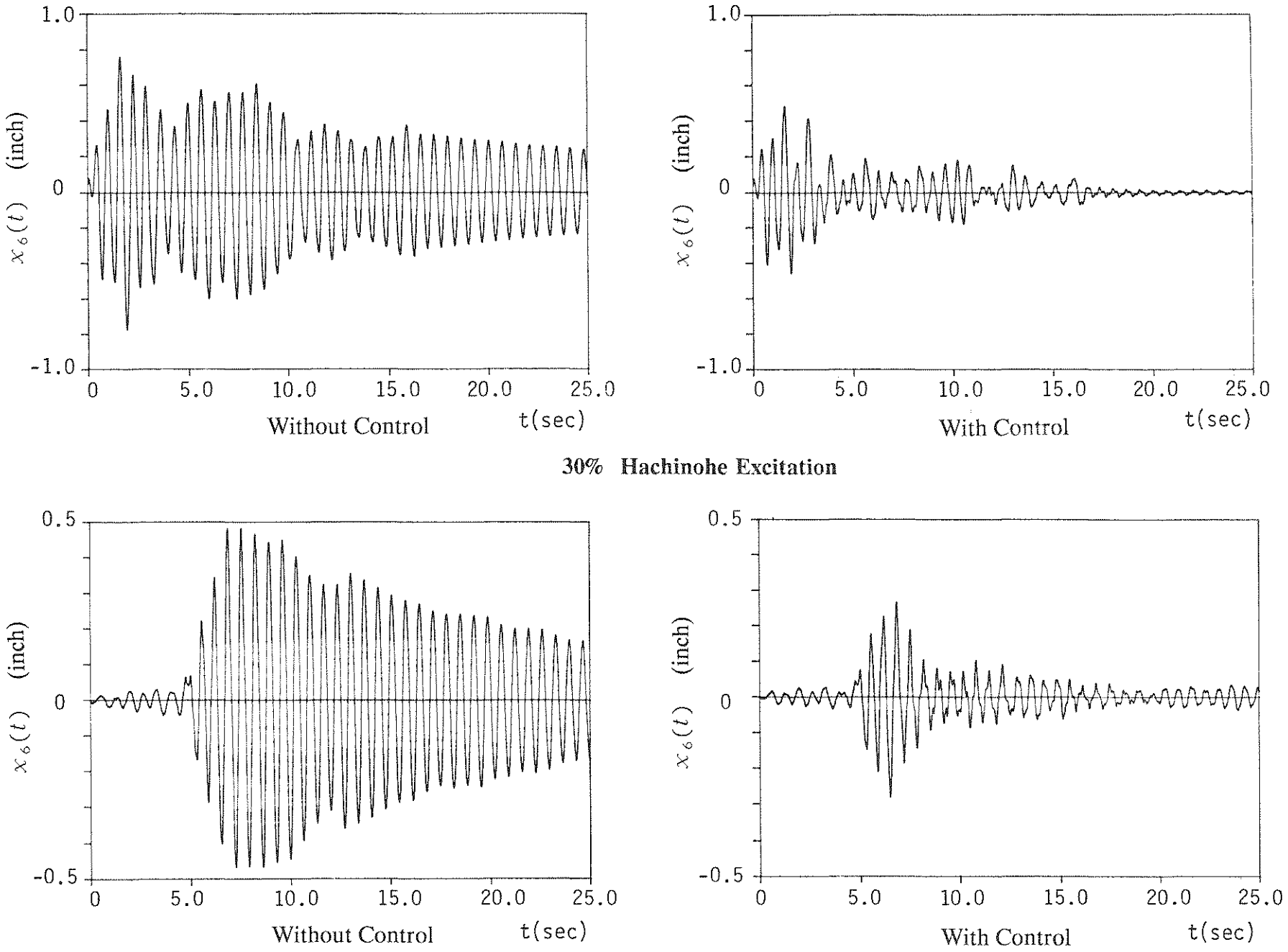

Figure 4.60 - Time Histories of the Relative Displacement at the Top Floor.

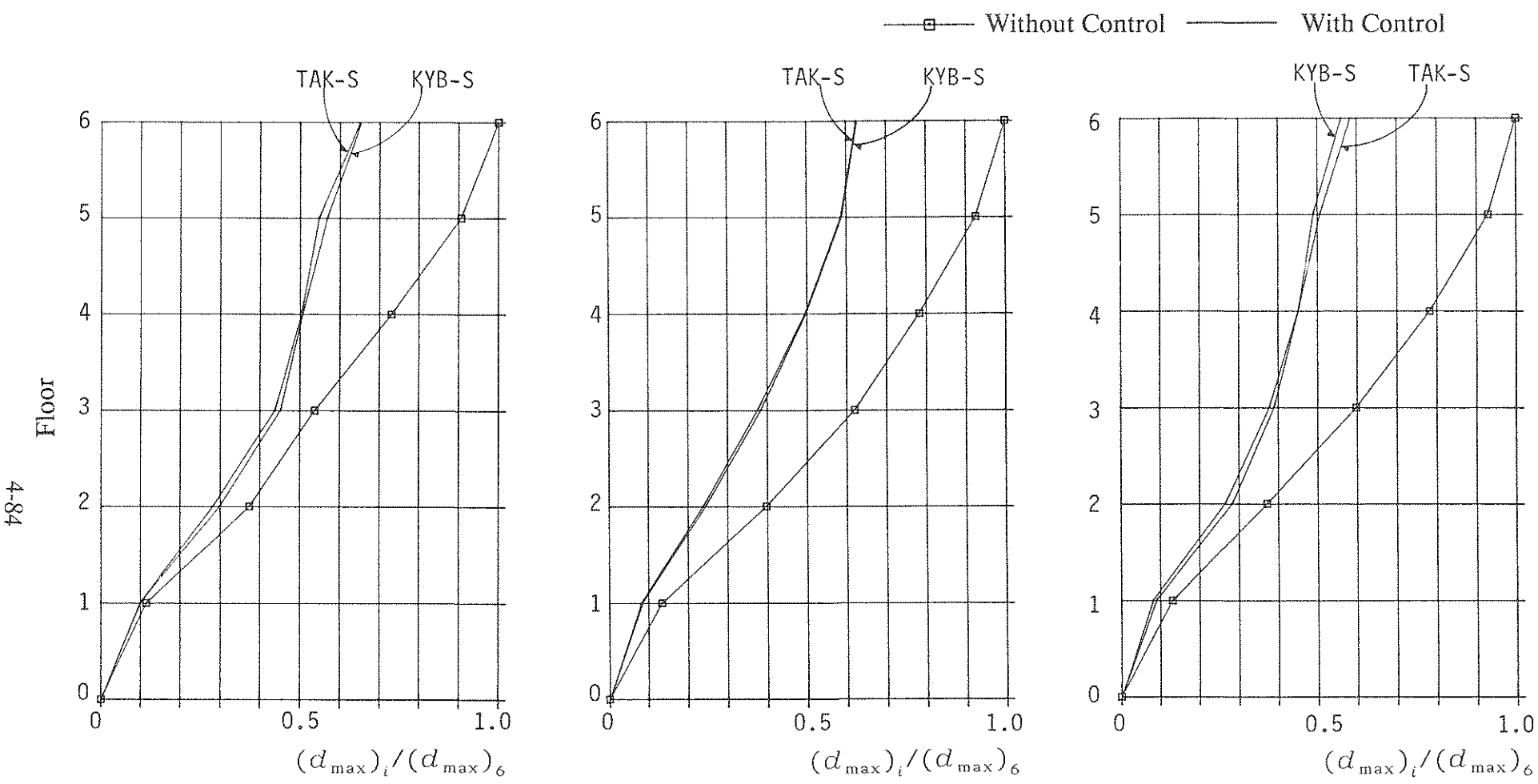

a) 20% El Centro Excitation

b) 30% Hachinohe Excitation

c) 40% Miyagioki Excitation

[Regulator Type: No. 1 in Table 2-4]

Figure 4.61 - The Peak Relative Displacements in Weak Direction.

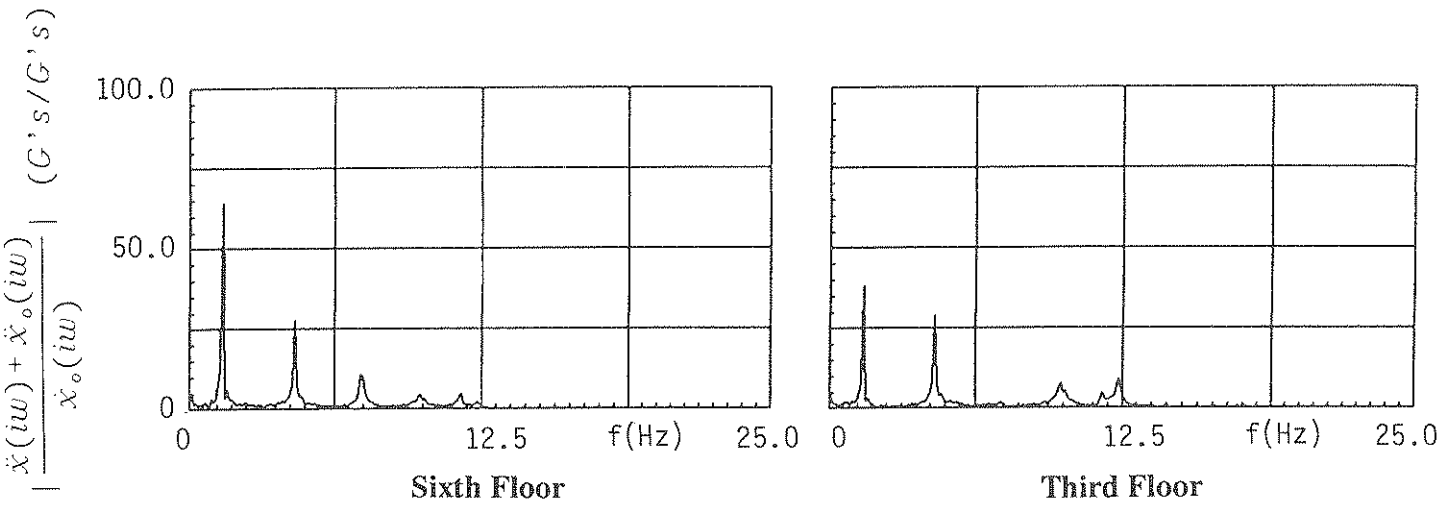

a) Uncontrolled

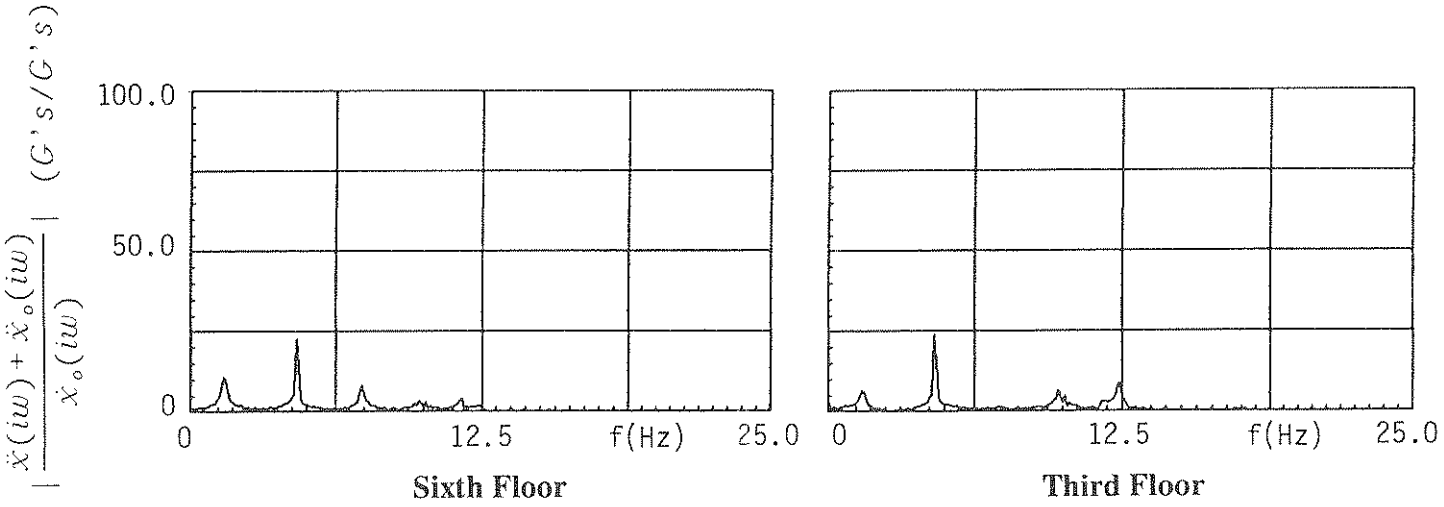

b) Controlled with the Top Floor Information

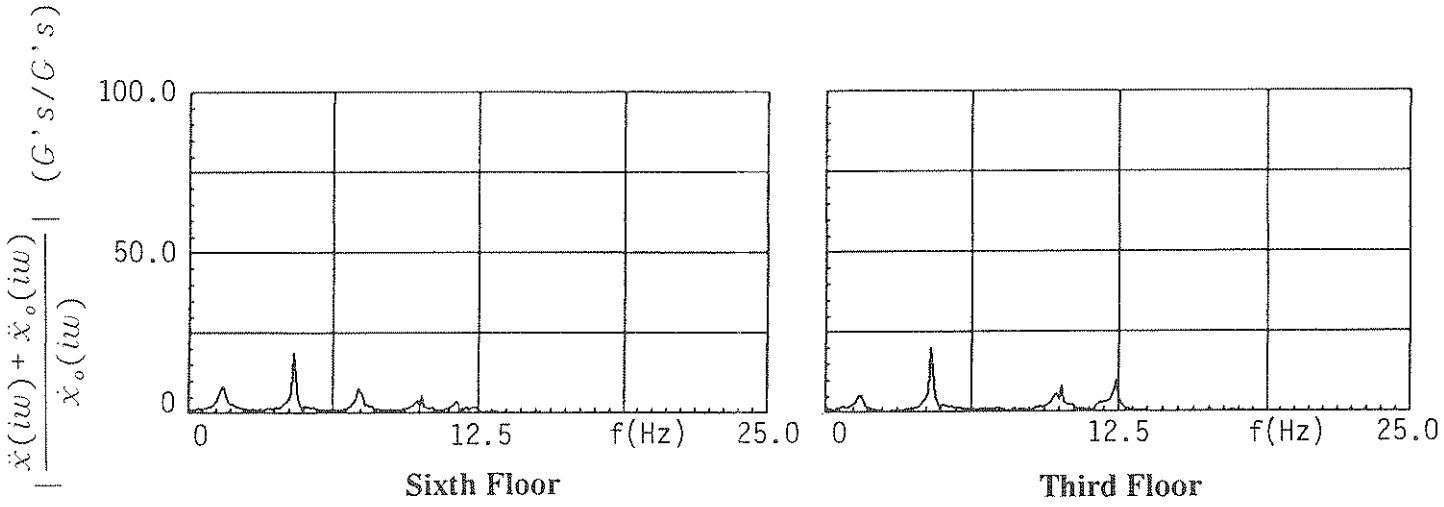

c) Controlled with the Top and the Third Floor Information

Figure 4.62 - Transfer Functions of the Absolute Acceleration in Weak Direction (White Noise 0.02 G Excitation).

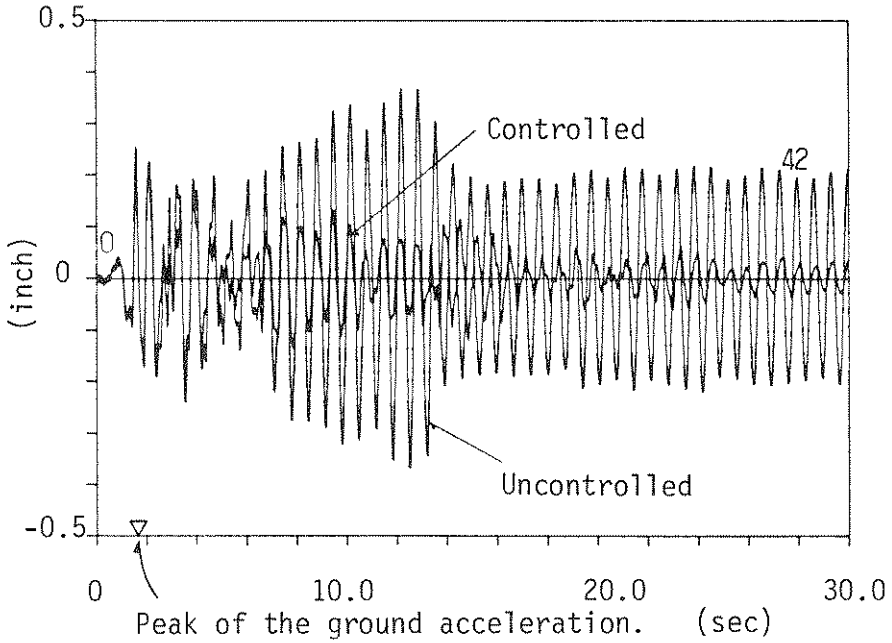

a) Displacement history

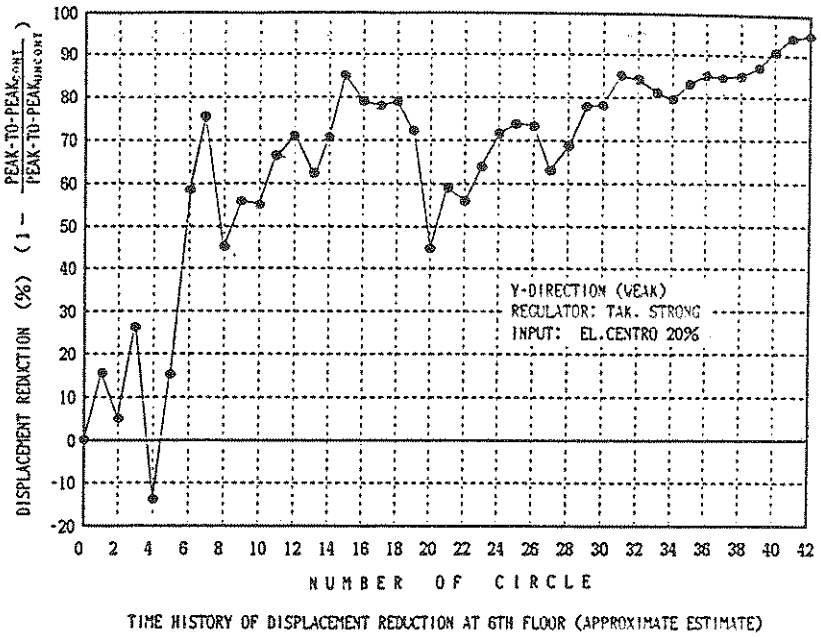

b) Peak reduction history

Figure 4.63 - Time Histories of the Relative Displacement at the Top Floor (20% El Centro Excitation).

4.3.2.2.2 Efficiency of Various Control Cases

The experimental results in the **weak direction** have almost identical tendencies to those in the **strong direction** discussed in Section 4.3.1.2.2. The influence of various weighting magnitudes used in different regulators are shown in Fig. 4.64 for the **weak direction** experiments. The relationship between the efficiency of control the active mass travel (stroke) or the control force are shown in Fig. 4.65 for all regulators. The efficiency of using two sensors for the control implementation is shown in Fig. 4.66, while the effect in varying the weight of the active mass is shown in Fig. 4.67. In addition, the effect of adding stiffness to the AMD is shown in Fig. 4.68 and changing the objective variables to velocity or acceleration instead of displacement are shown in Fig. 4.69. Same tendencies as discussed in Section 4.3.1.2.2 are valid also for the **weak direction** with the exception of several cases presented in the following.

Compared with the control in the **strong direction**, the control in the **weak direction** requires smaller control forces and, therefore, it is more sensitive to the unavoidable friction in the hydraulic actuator. As shown in Fig. 4.64, the experimental results with the "TAK-W" regulator, show different tendencies from those of the **strong direction**. This is due to the friction in the actuator which is approximately 60% of the maximum control force required.

Moreover, the control of the absolute acceleration is less effective than that in the **strong direction**. The reductions of the maximum acceleration could not be achieved using some regulators. This is probably due to the same reasons as previously described for the **strong direction** (Section 4.3.1.2.2). Particularly, since the model structure vibrates in the **weak direction** at lower modal frequencies than those in the **strong direction**, the higher modes of acceleration have much more influence on the control.

Contrary to the experimental results in the **strong direction**, the control efficiencies for the mass stroke and the control force, in the case using the measurements of responses at the top floor as control information, are better than those using both responses at the top and the third floors (see Figs. 4.64 and 4.66). Concerning the control efficiencies, there was no advantage in utilizing the third floor information, even though, as discussed on the experimental results under the banded white noise input, the third floor information made the control effects on the acceleration responses better.

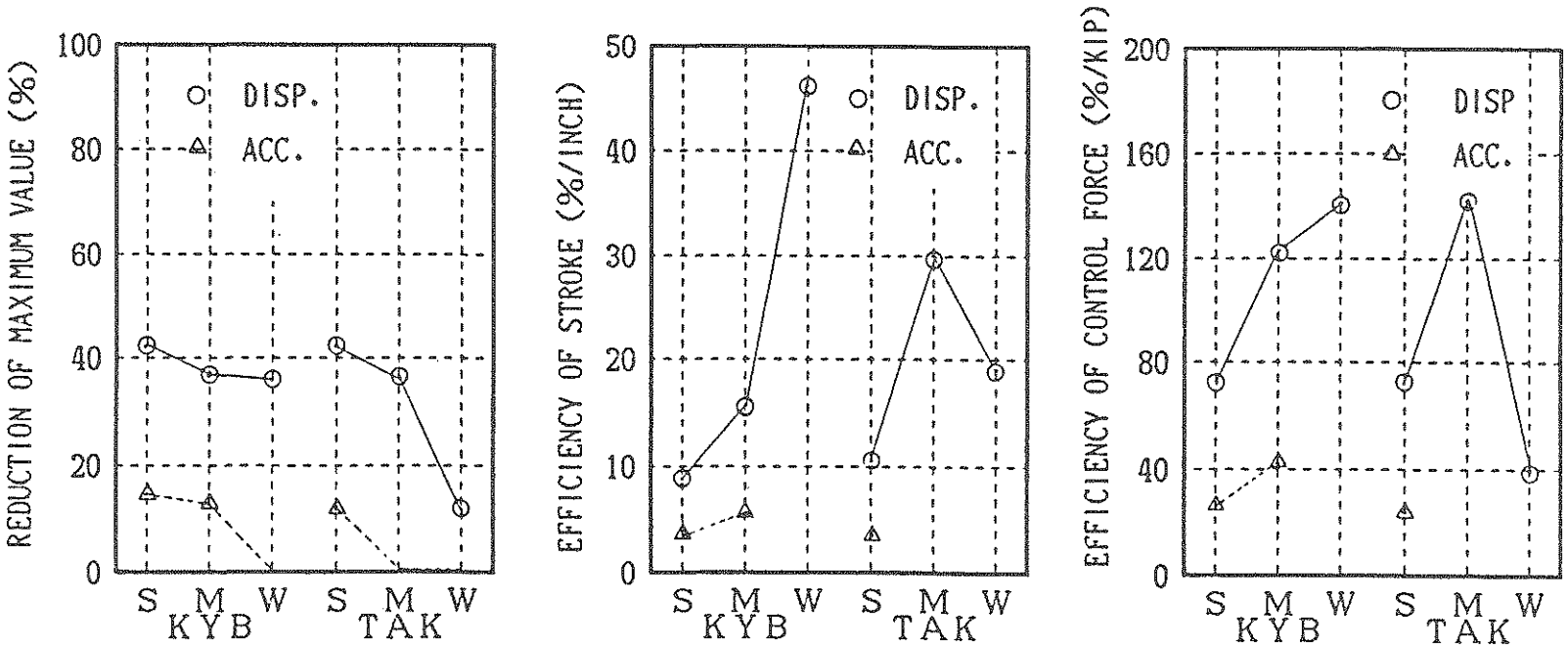

Sensor Position: The top floor

Objective Variable: The Relative Displacement at the Top Floor

Mass Weight: 200 (kg)

AMD STiffness: None

Figure 4.64 - Comparison by the Regulators Depending on the WeightingMagnitudes (20% El Centro Excitation).

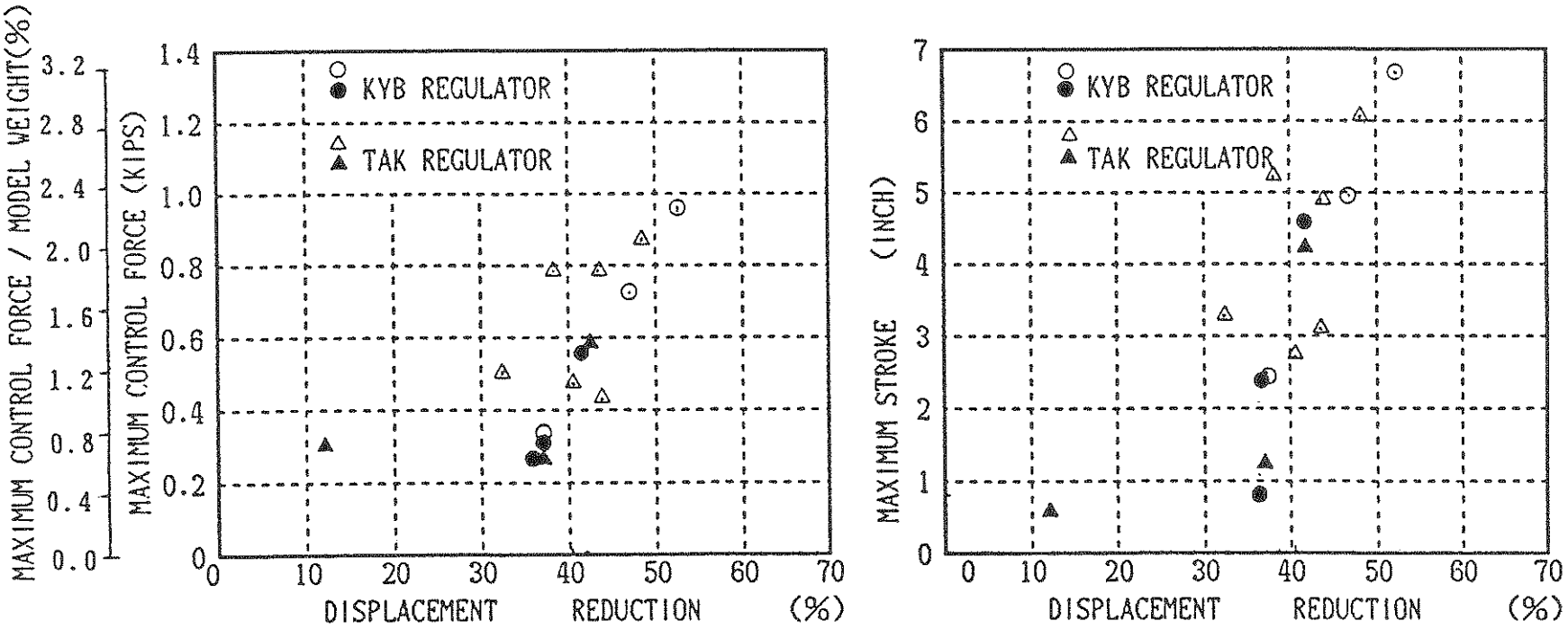

Figure 4.65 - Relationships Between the Displacement Reduction and the Maximum Control Forces or the Maximum Mass Stroke (20% El Centro Excitation).

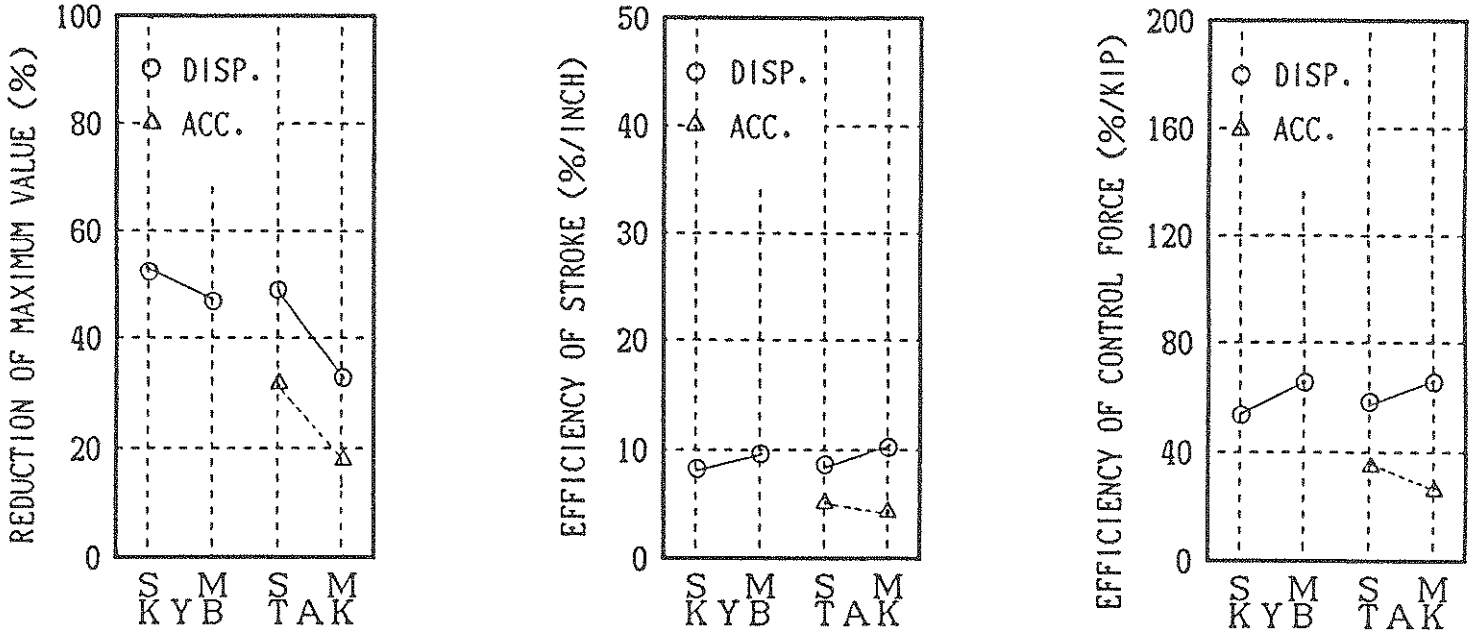

Sensor Position: The Top Floor and the Third Floors

Objective Variable: The Relative Displacements at the Top and the Third Floors

Mass Weight: 200 (kg)

AMD STiffness: None

Figure 4.66 - Effects of Using Both the Top (Sixth) and the Middle (Third) Floor Information (20% El Centro Excitation).

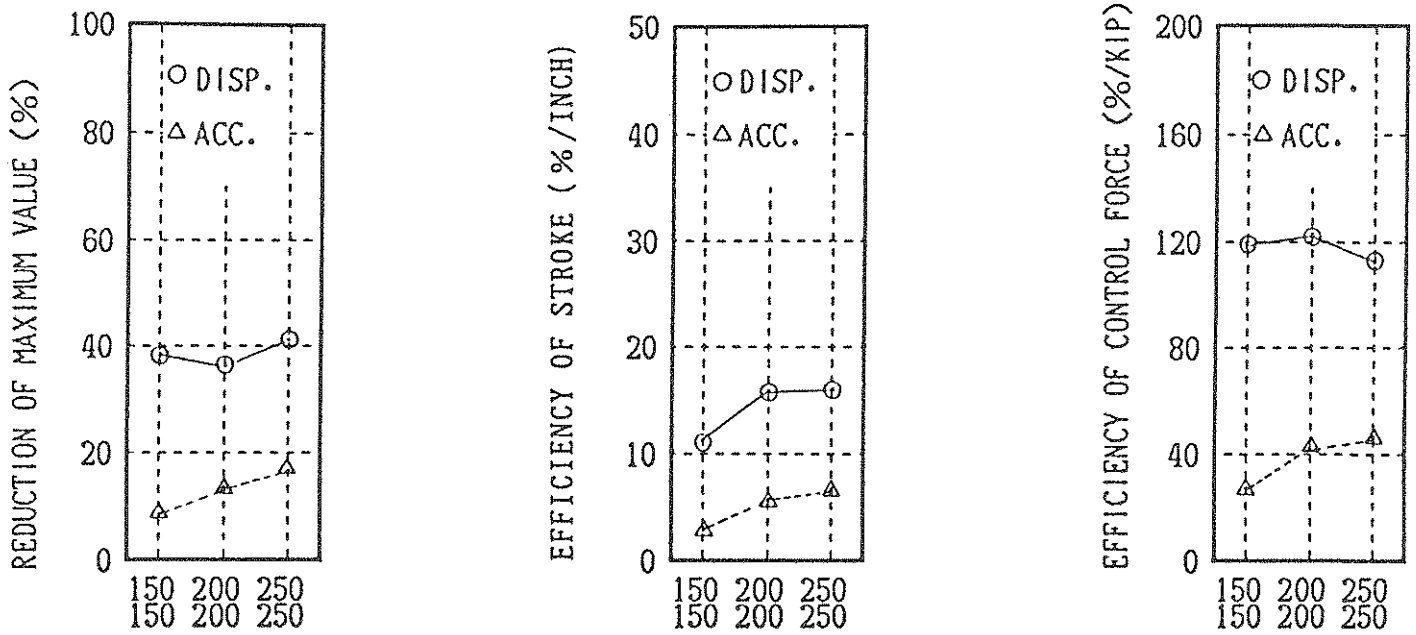

Sensor Position: The top floor

Objective Variable: The Relative Displacement at the Top Floor

AMD STiffness: None

Figure 4.67 - Effects of Changing the Mass Weight
(20% El Centro Excitation).

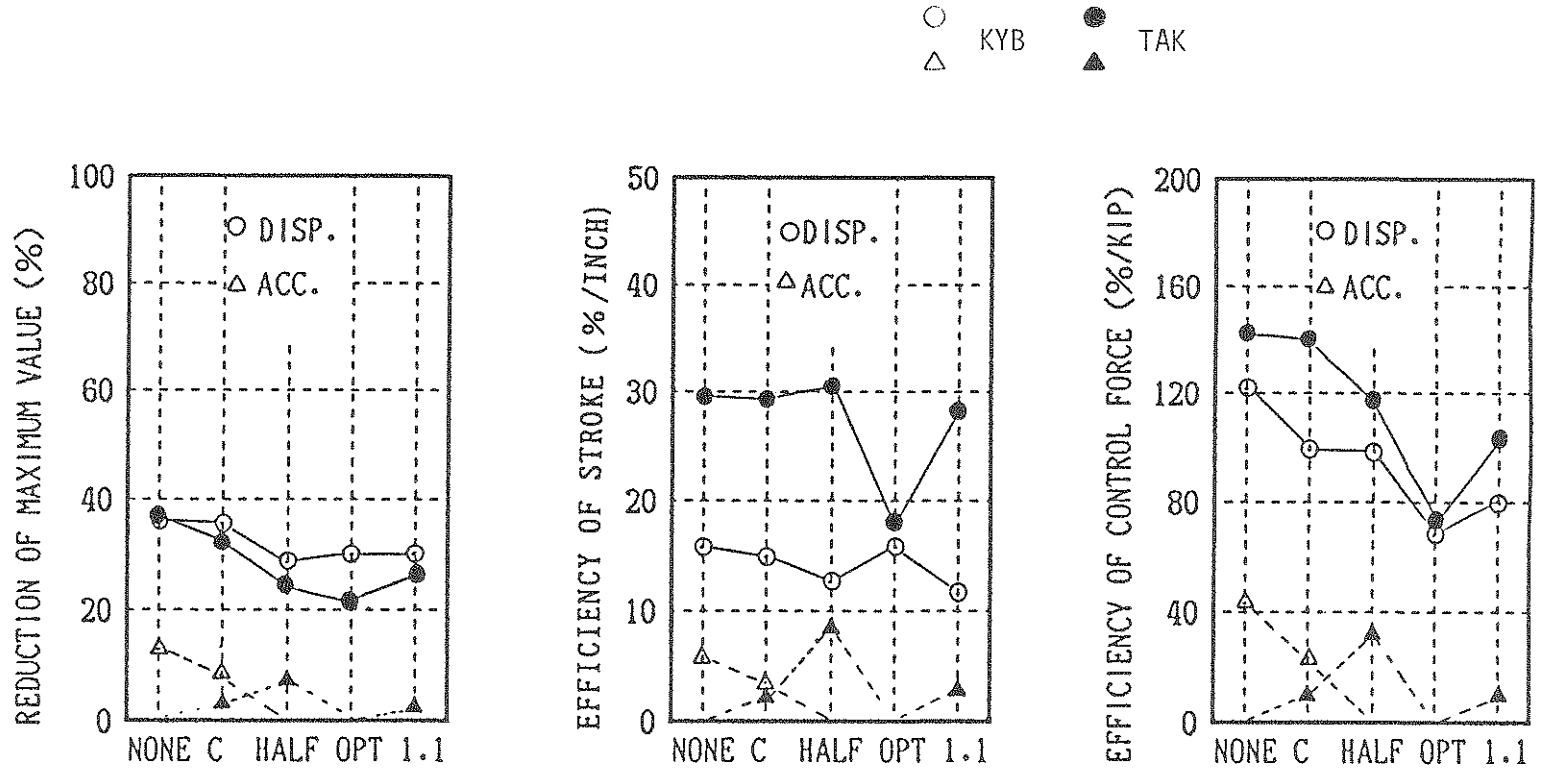

Sensor Position: The top floor

Objective Variable: The Relative Displacement at the Top Floor

Mass Weight: 200 (kg)

Figure 4.68 - Effects of Adding the Stiffness to the AMD (20% El Centro Excitation).

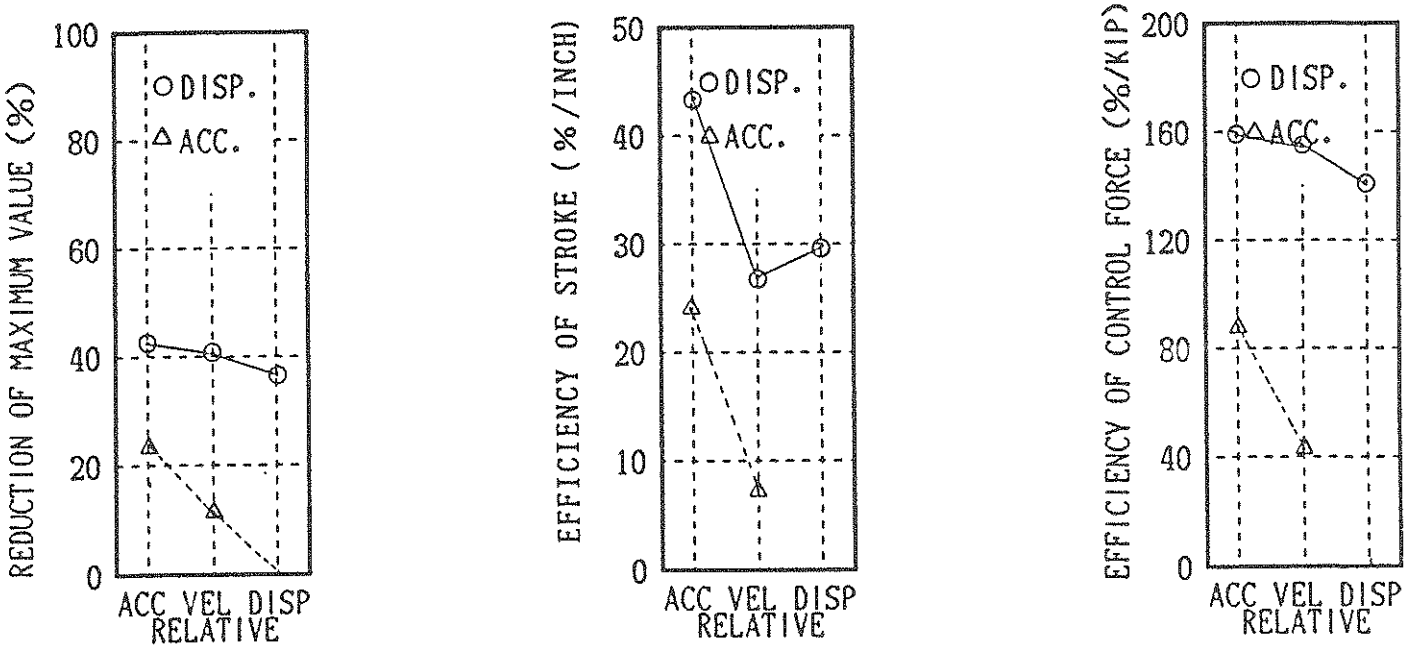

Sensor Position: The top floor

Mass Weight: 200 (kg)

AMD STiffness: None

Figure 4.69 - Comparison by the Objective Variables
(20% El Centro Excitation).

As shown in Fig. 4.68, the effects of the stiffness to the AMD were not obvious. This may arise from the reasons discussed below. Since the control forces required for the control in the **weak direction** were approximately one-third of those in the **strong direction**, the control results in the **weak direction** were more apt to be influenced by the friction of the hydraulic actuator. Moreover, with the gas spring attached to the AMD, the friction acting on the added mass increased by about 20%, as compared with that without the gas spring.

4.3.2.2.3 Comparison of Controlled Responses With Theoretical Prediction (in the weak direction)

(A) *Comparison between experimental and theoretical responses without control.* Similarly to the **strong direction**, the analytical simulations were carried out using the stiffness matrix and the damping matrix obtained from the identification studies made with the banded white noise excitation. The comparisons between the experimental and the theoretical responses without control, for earthquake motions of 20% El Centro, 30% Hachinoe and 40% Miyagioki are displayed in Figs. 4.70, 4.71, and 4.72, respectively. The theoretical responses show good agreement with the experimental responses, even though there are relatively large discrepancies between the experimental and theoretical acceleration responses during the 20% El Centrol excitation. These discrepancies occur in the last seconds of the earthquake where distortions in the input motion occurs due to model-structure interaction. For the other earthquakes these effects are less pronounced.

(B) *Comparison between experimental and theoretical responses with control.* Similarly in the analytical simulations for the **strong direction**, it was assumed that the relationship between the control forces and the servo-currents of actuator is always linear, and that it is a Coulomb friction of 150g acting on the added mass. The comparison between the experimental and the theoretical results controlled using the TAK-S regulator (Type 1 in Table 2.4), are illustrated in Fig. 4.73 through 4.75 for the various earthquake excitations. There is a good agreement between the experimental and the theoretical results, although the higher modes excited in the theoretical computations did not appear in the experimental responses.

The comparison between the maximum experimental and theoretical responses is summarized in Tables 4.11 through 4.16 for various regulators and different earthquake excitations. Furthermore, the peak relative displacements at every floor for the experimental and the theoretical responses are plotted in Figs. 4.76, 4.77 and 4.78, for the sake of comparison.

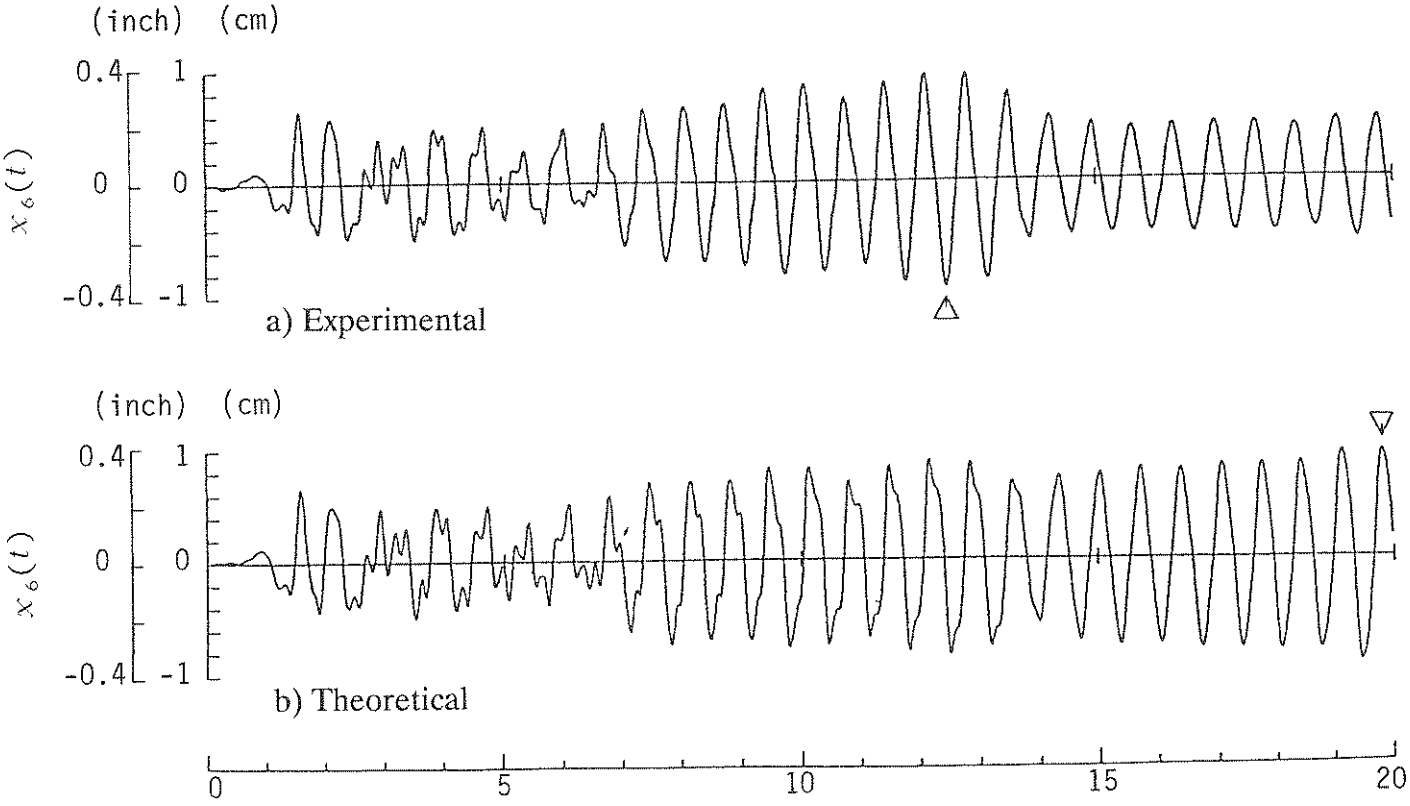

(1) Time Histories of the Relative Displacement at the Top Floor

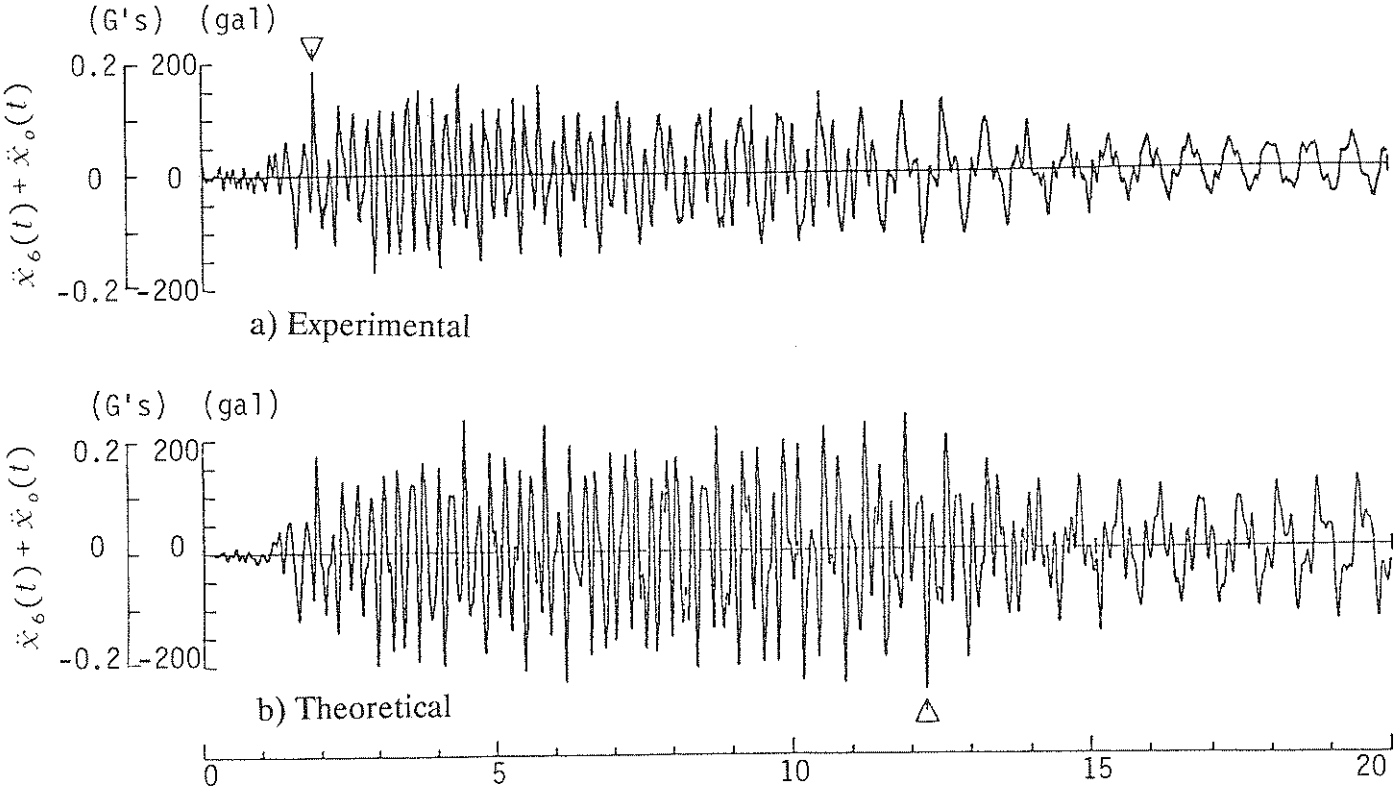

(2) Time Histories of the Absolute Acceleration at the Top Floor

Figure 4.70 -Comparison Between Experimental and Theoretical Results Without Control (20% El Centro Excitation).

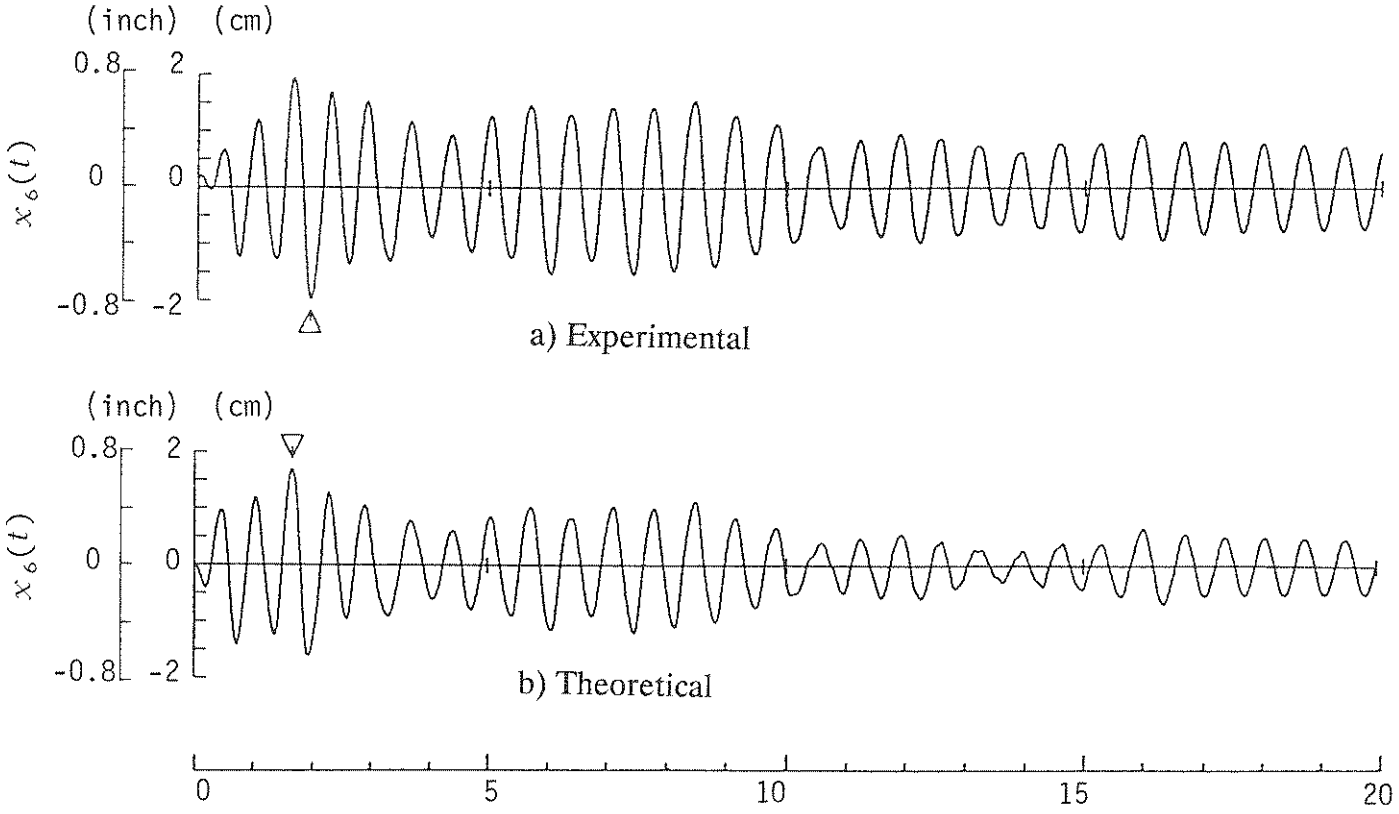

1) Time Histories of the Relative Displacement at the Top Floor

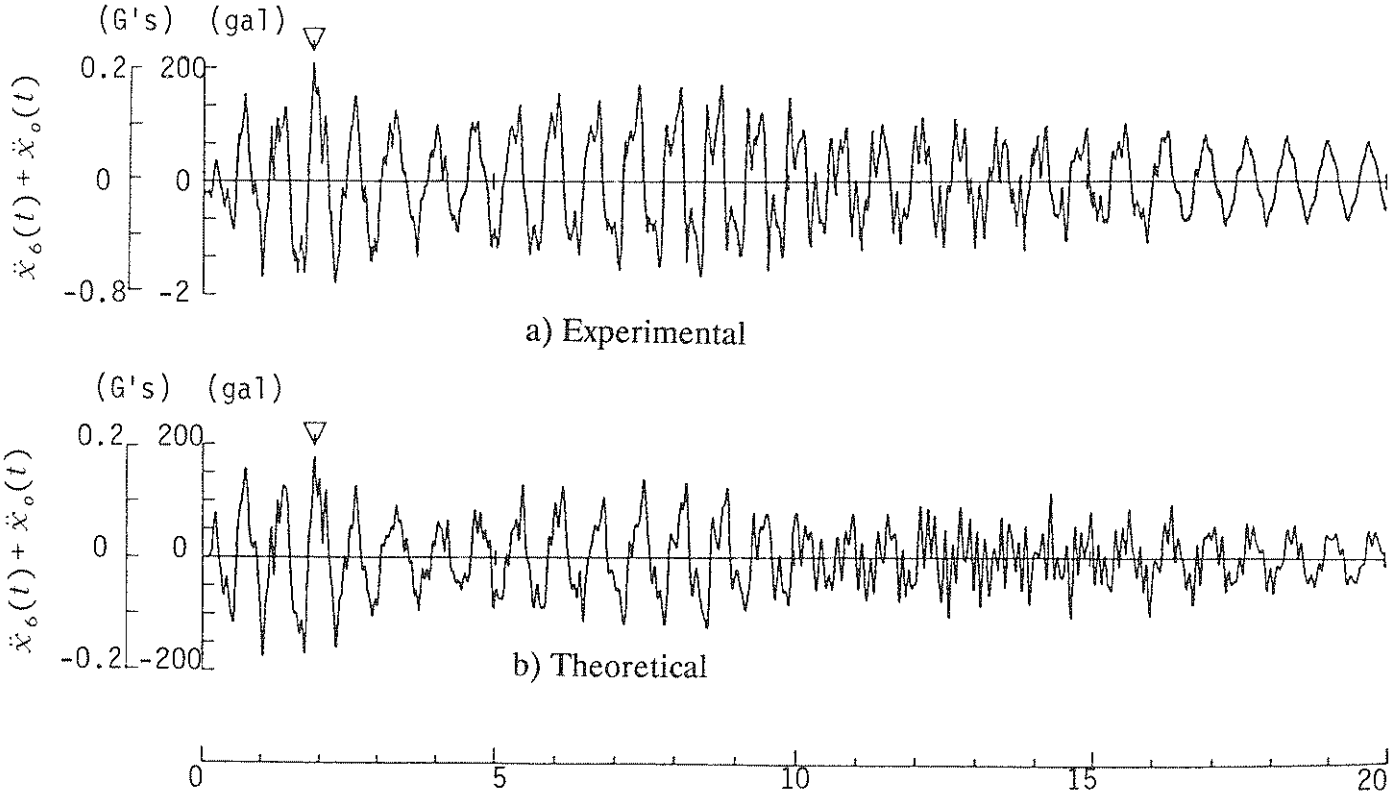

2) Time Histories of the Absolute Acceleration at the Top Floor

Figure 4.71 - Comparison Between Experimental and Theoretical Results Without Control (30% Hachinohe Excitation).

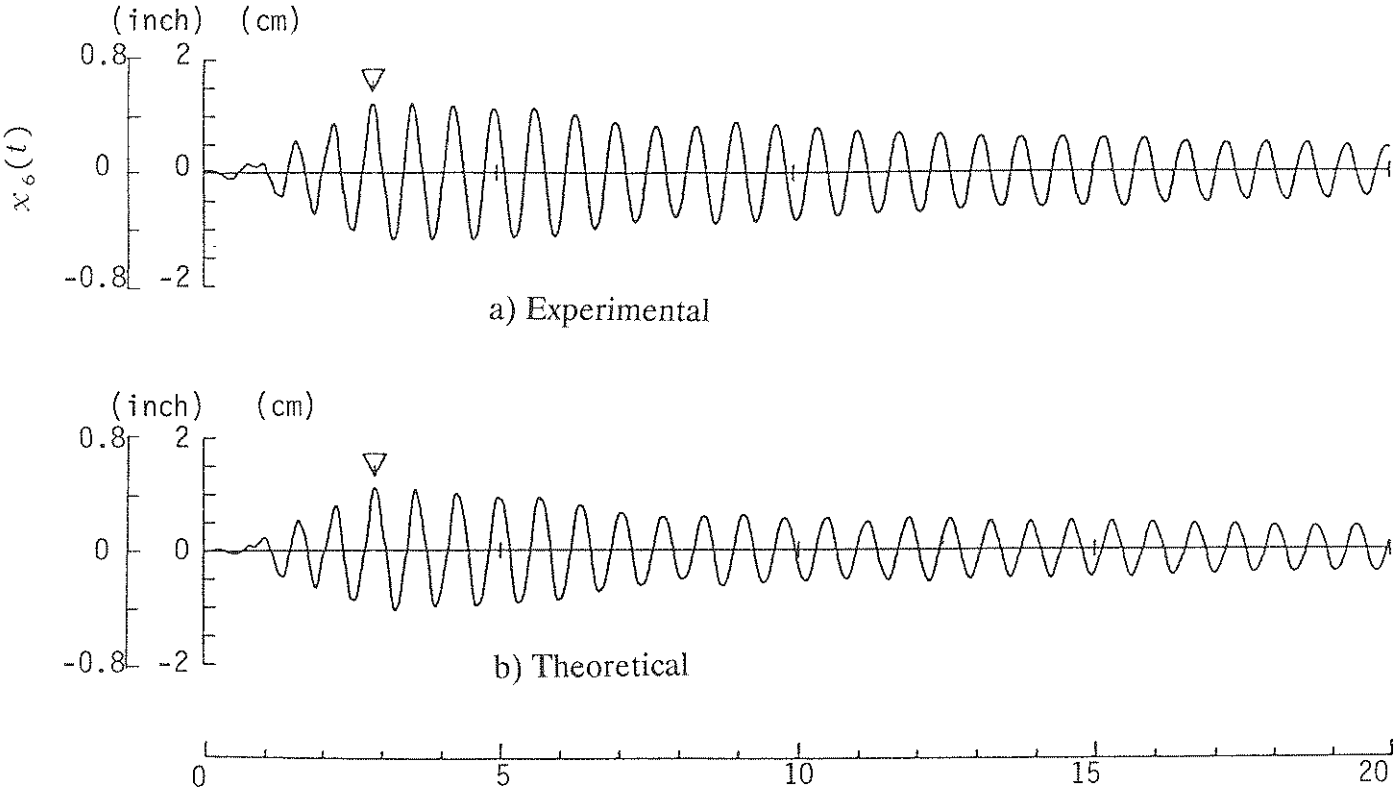

1) Time Histories of the Relative Displacement at the Top Floor

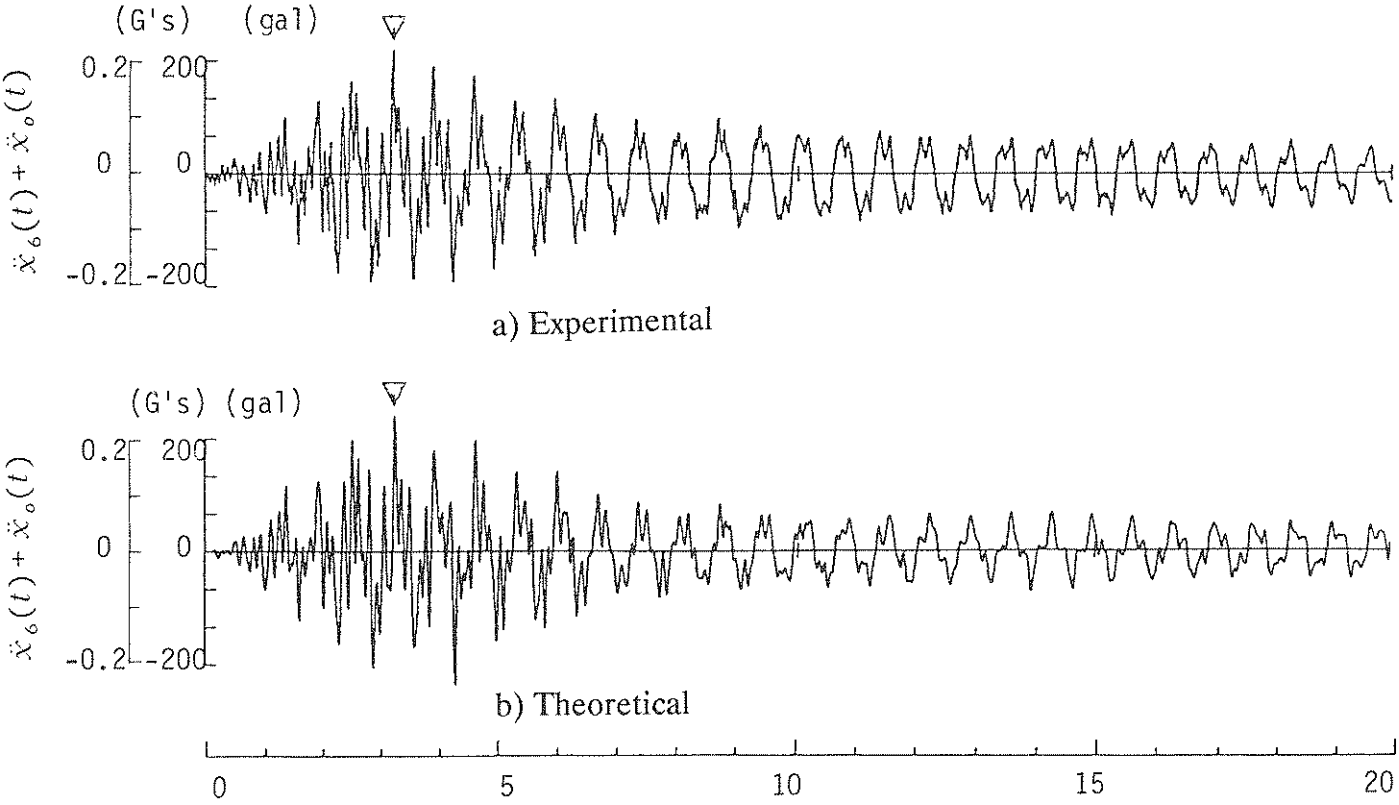

2) Time Histories of the Absolute Acceleration at the Top Floor

Figure 4.72 - Comparison Between Experimental and Theoretical Results Without Control (40% Miyagioki Excitation).

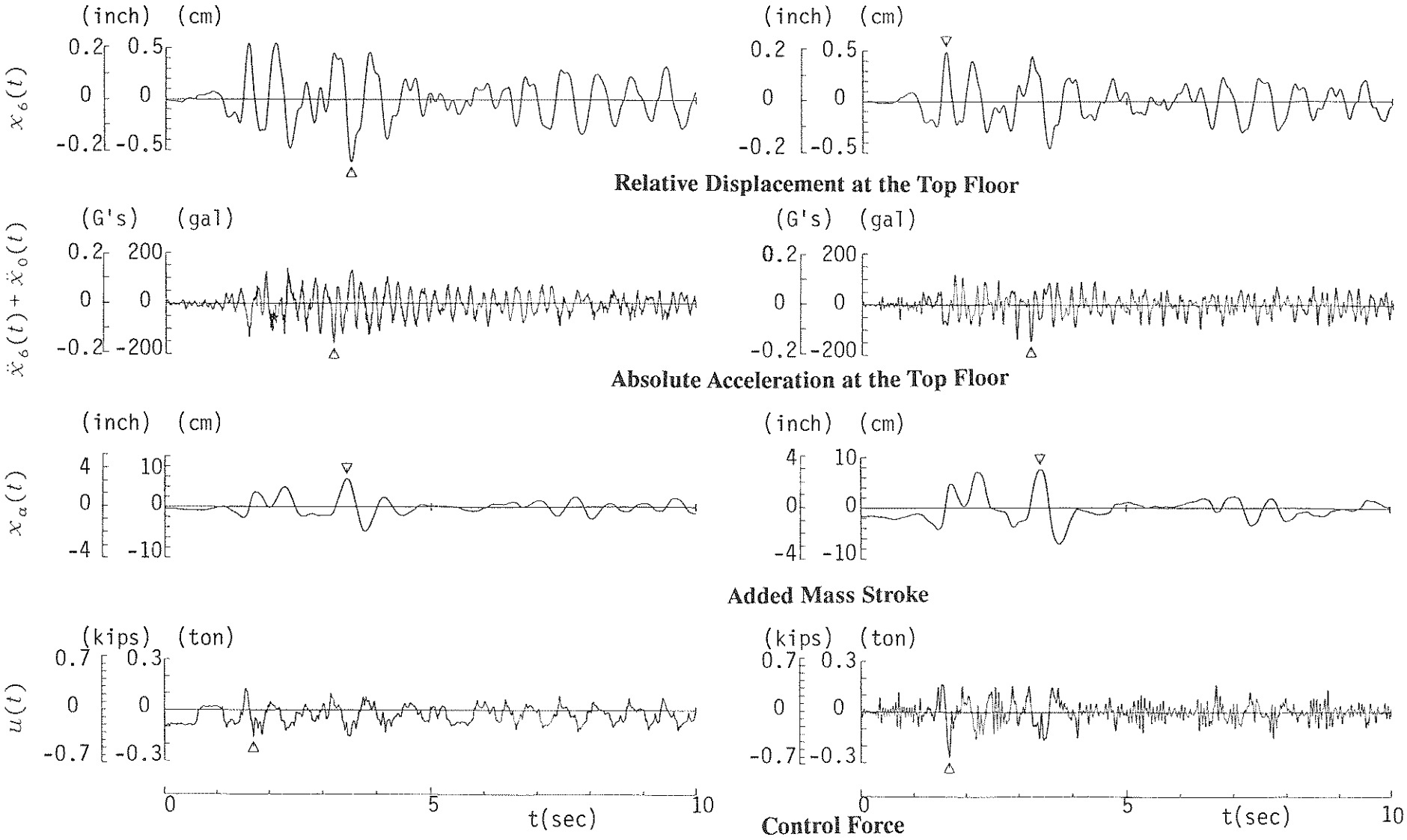

a) Experimental

b) Theoretical

Figure 4.73 - Comparison Between Experimental and Theoretical Results With Control (20% El Centro Excitation).

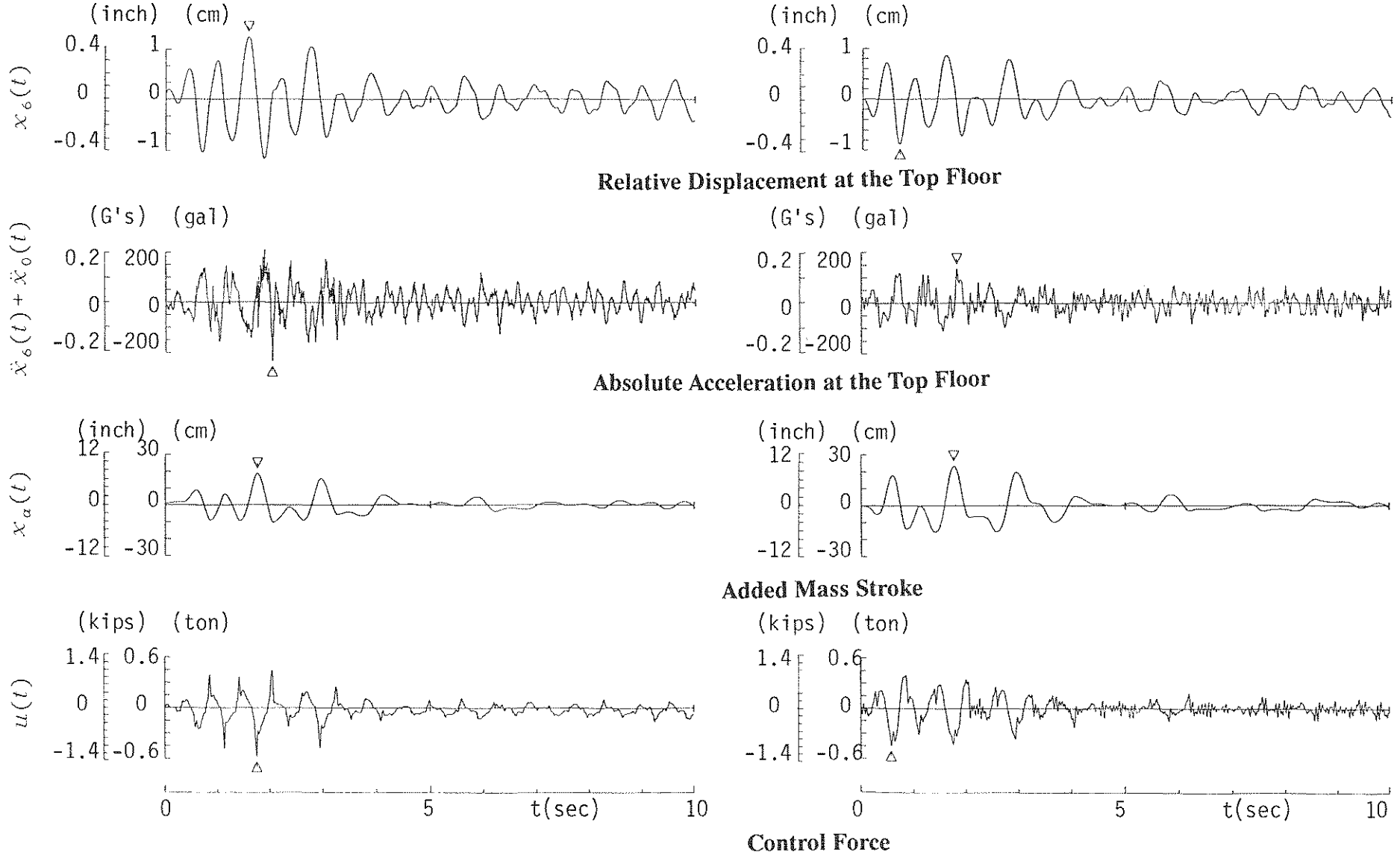

a) Experimental

b) Theoretical

Figure 4.74 - Comparison Between Experimental and Theoretical Results With Control (30% Hachinohe Excitation).

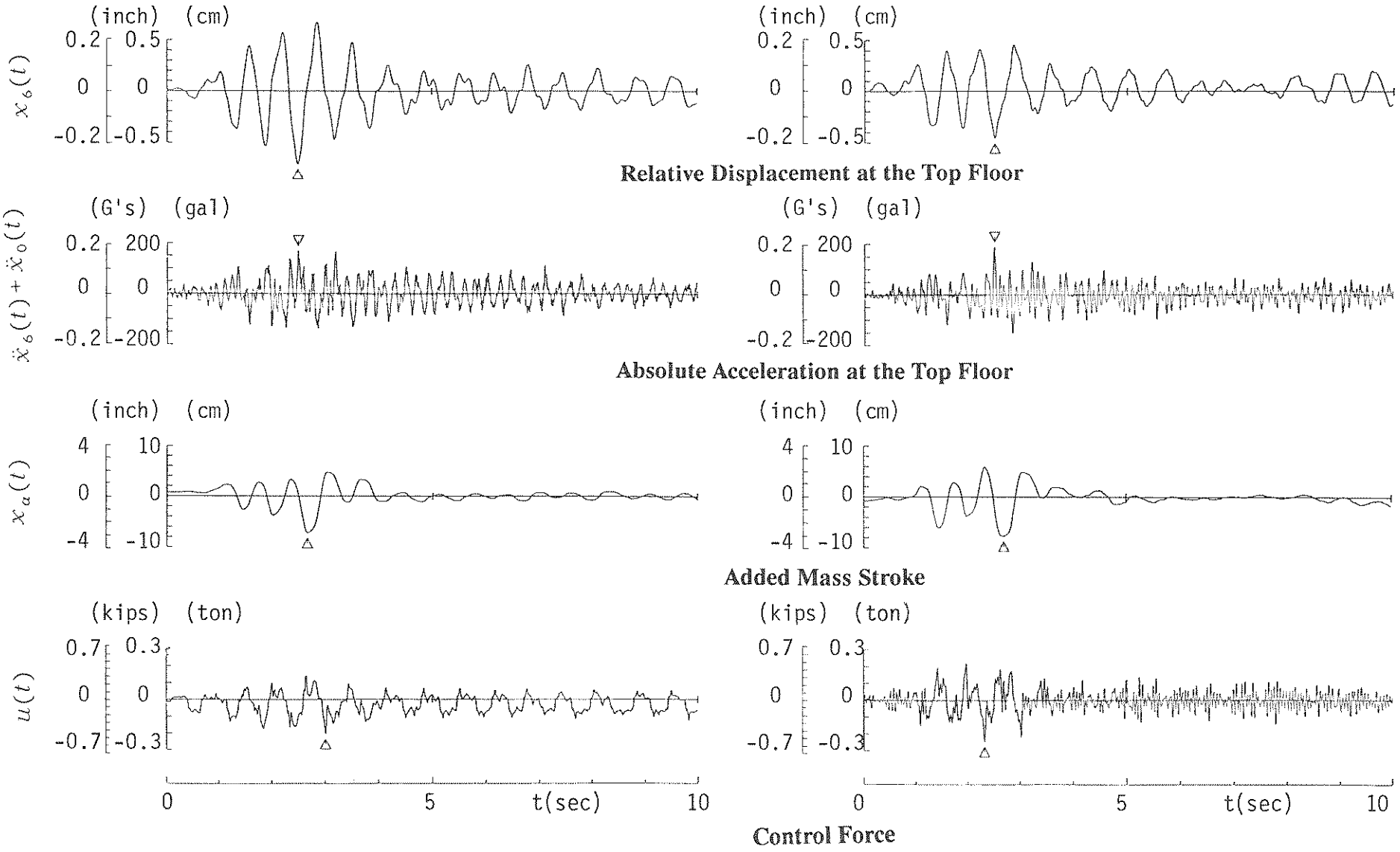

a) Experimental

b) Theoretical

Figure 4.75 - Comparison Between Experimental and Theoretical Results With Control (40% Miyagioki Excitation).

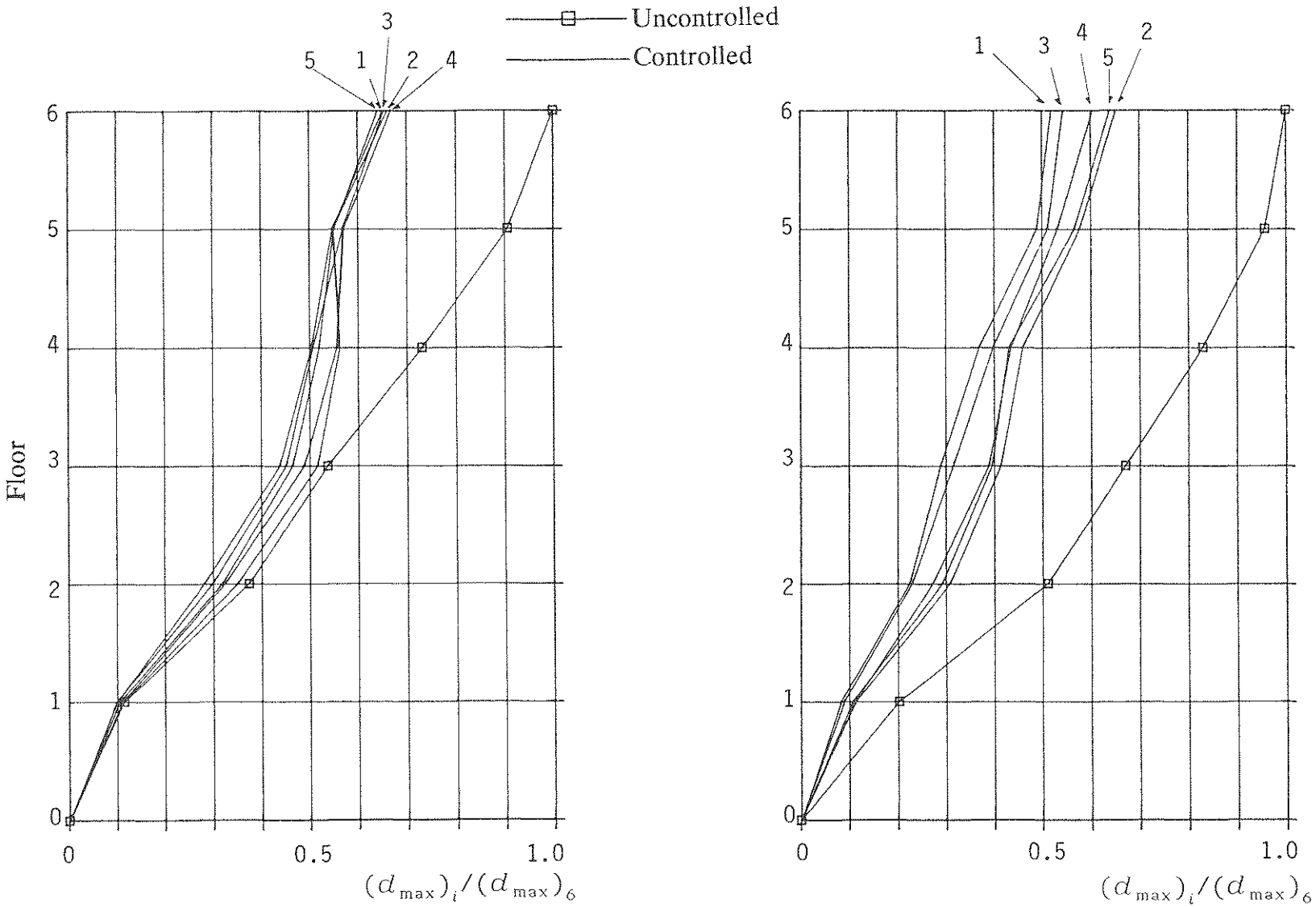

Figure 4.76(a) - The Peak Relative Displacement Under 20% El Centro Excitation.

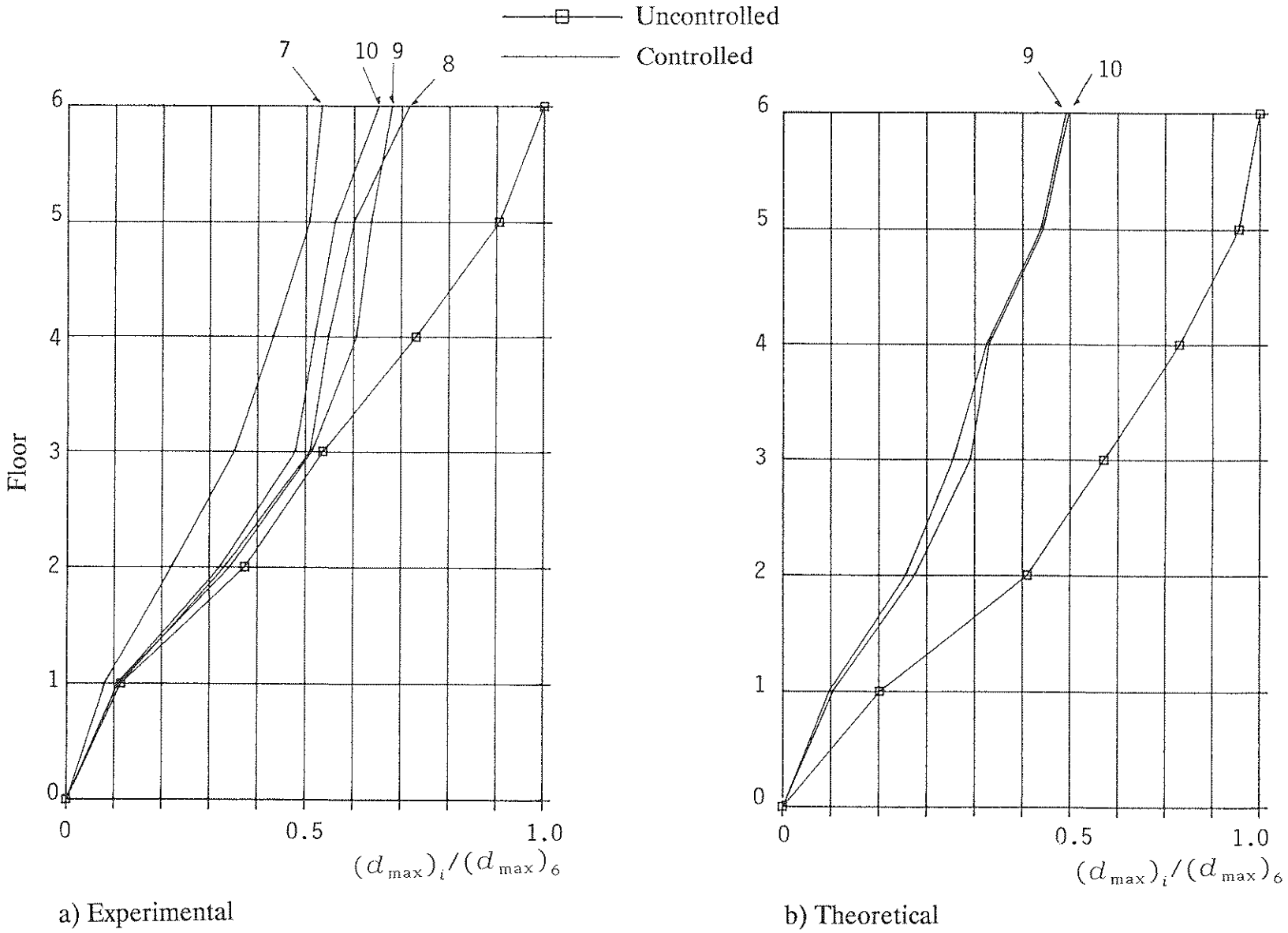

Figure 4.76(b) - The Peak Relative Displacement Under 20% El Centro Excitation.

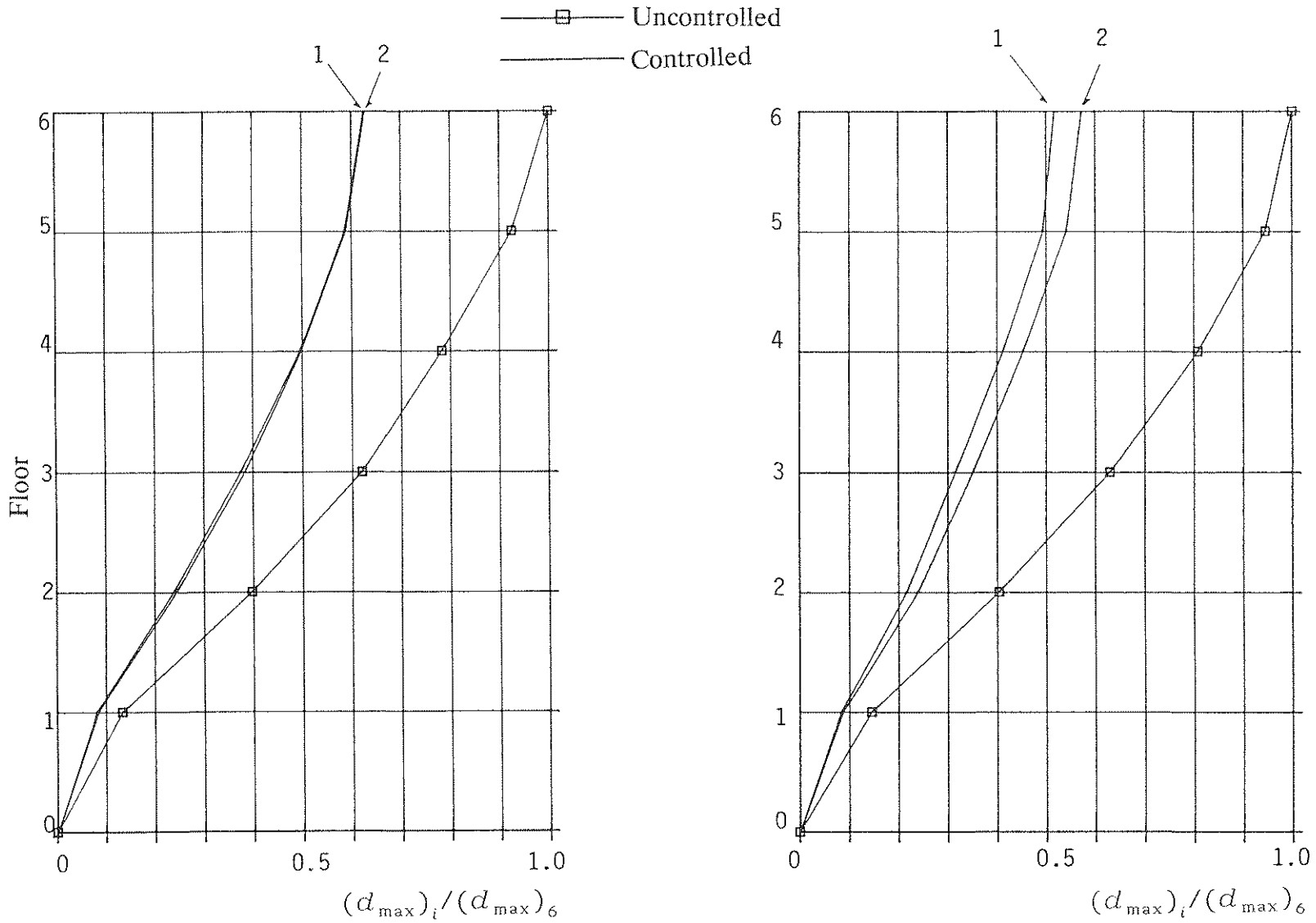

Figure 4.77 - The Peak Relative Displacement Under 30% Hachinohe Excitation.

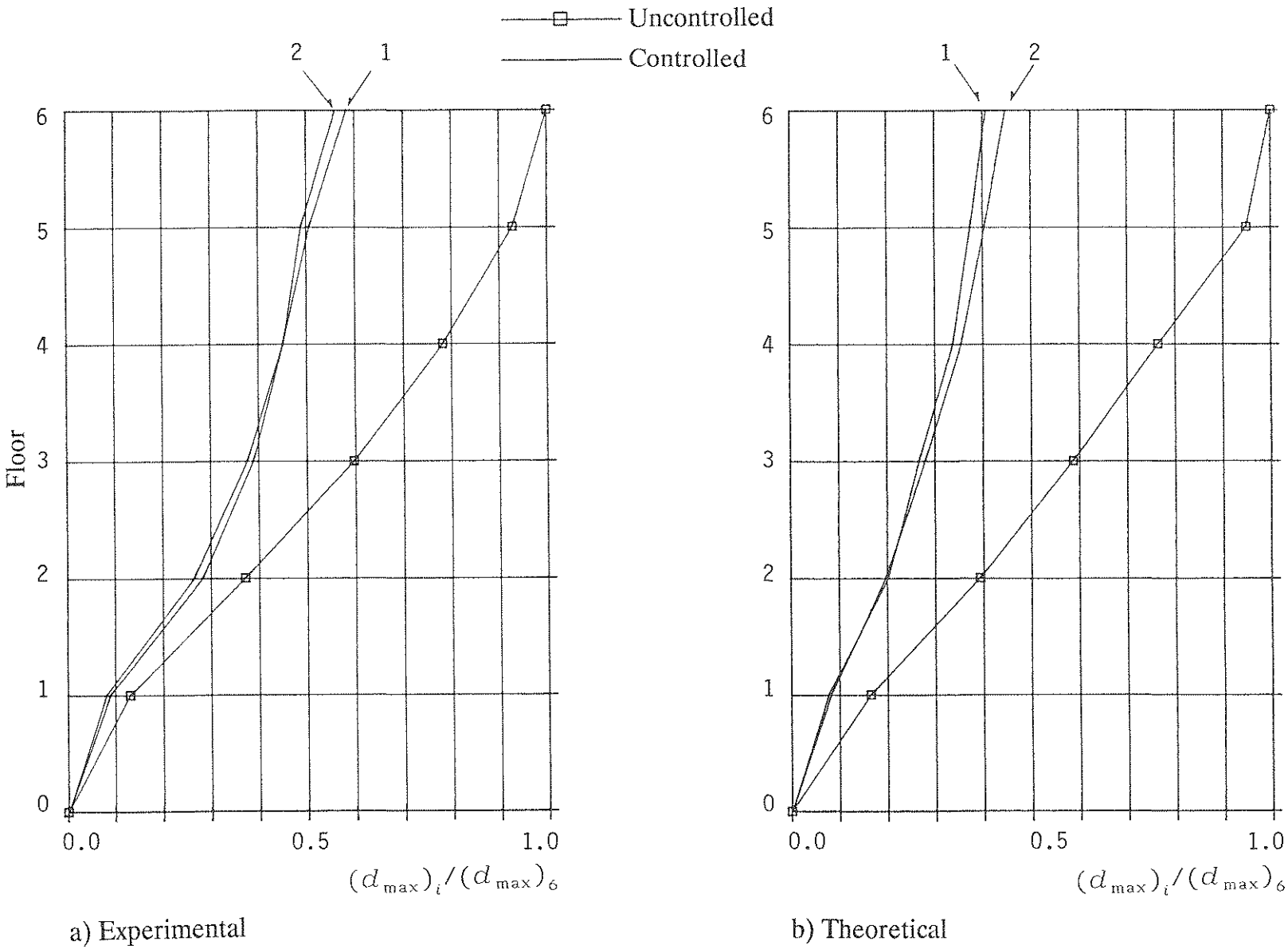

Figure 4.78 - The Peak Relative Displacement Under 40% Miyagioki Excitation.

Table 4.11

Experimental Responses to 20% El Centro Excitation (Weak Direction)

No.	Control Conditions					Top Floor Relative Displ. [in.]	Top Floor Absolute Accel. [G's]	Base Shear Force [kips]	Max. Control Force [kips]	Max. Mass Stroke [in.]	Max. Control Power [Kw]
	Sensor Position	Objective Variables	Weight of Added Mass	Stiffness of Added Mass	Regulator Type						
0	Without Control					0.368	0.183	2.73	-	-	-
1	Top Floor	Relative Displ.	200 kg	-	TAK-S	0.240 (34.9)	0.156 (14.8)	2.14 (21.7)	0.347	2.20	0.561
2					TAK-M	0.243 (33.9)	0.202 (-)	2.64 (3.3)	0.446	0.736	0.218
3					KYB-S	0.241 (34.6)	0.156 (14.8)	2.36 (13.5)	0.446	2.32	0.700
4					KYB-M	0.246 (33.2)	0.160 (12.6)	2.51 (8.1)	0.503	1.51	0.392
5		Relative Accel.			TAK-M	0.236 (35.9)	0.141 (23.0)	2.28 (16.4)	0.277	0.591	0.0975
6		Absolute Displ.			TAK-M	-	-	-	-	-	-
7	Top & 3rd Fl.	Relative Displ.			TAK-S	0.196 (46.8)	0.127 (30.6)	1.81 (33.6)	0.568	3.69	0.911
8					TAK-M	0.264 (28.4)	0.160 (12.6)	2.43 (11.0)	0.729	1.88	0.559
9	Top Floor		150 kg		KYB-M	0.251 (32.0)	0.168 (8.2)	2.53 (7.9)	0.319	2.07	0.530
10			250kg		KYB-M	0.240 (34.8)	0.154 (15.8)	2.43 (10.9)	0.500	1.41	0.427
11			200 kg	Optimum	KYB-M	-	-	-	-	-	-
12				Half of Optimum	KYB-M	-	-	-	-	-	-

( ) Percentage of Reduction

Table 4.12

Theoretical Responses to 20% El Centro Excitation (Weak Direction)

No.	Control Conditions					Top Floor Relative Displ. [in.]	Top Floor Absolute Accel. [G's]	Base Shear Force [kips]	Max. Control Force [kips]	Max. Mass Stroke [in.]	Max. Control Power [Kw]
	Sensor Position	Objective Variables	Weight of Added Mass	Stiffness of Added Mass	Regulator Type						
0	Without Control					0.370	0.253	3.57	-	-	-
1	Top Floor	Relative Displ.	200 kg	-	TAK-S	0.192 (48.1)	0.150 (40.7)	1.48 (58.5)	0.706	2.99	1.13
2					TAK-M	0.241 (34.9)	0.187 (26.1)	2.02 (43.4)	0.481	1.50	0.309
3					KYB-S	0.201 (45.7)	0.172 (32.0)	1.62 (54.6)	0.710	2.60	0.946
4					KYB-M	0.224 (39.5)	0.175 (30.8)	1.99 (44.2)	0.604	1.98	0.503
5		Relative Accel.			TAK-M	0.237 (35.9)	0.187 (26.1)	1.97 (44.8)	0.481	0.996	0.255
6		Absolute Displ.			TAK-M	-	-	-	-	-	-
7	Top & 3rd Fl.	Relative Displ.			TAK-S	*	*	*	*	*	*
8					TAK-M	*	*	*	*	*	*
9	Top Floor		150 kg		KYB-M	0.219 (40.8)	0.142 (43.9)	1.72 (51.8)	0.549	2.80	0.739
10			250 kg		KYB-M	0.221 (40.3)	0.199 (21.3)	1.85 (48.2)	0.650	1.41	0.331
11			200 kg	Optimum	KYB-M	-	-	-	-	-	-
12				Half of Optimum	KYB-M	-	-	-	-	-	-

( ) Percentage of reduction * divergent

Table 4.13

Experimental Responses to 30% Hachinohe EW Excitation (Weak Direction)

No.	Control Conditions					Top Floor Relative Displ. [in.]	Top Floor Absolute Accel. [G's]	Base Shear Force [kips]	Max. Control Force [kips]	Max. Mass Stroke [in.]	Max. Control Power [Kw]
	Sensor Position	Objective Variables	Weight of Added Mass	Stiffness of Added Mass	Regulator Type						
0	Without Control					0.775	0.216	5.19	-	-	-
1	Top Floor	Relative Displ.	200 kg	-	TAK-S	0.484 (37.5)	0.242 (-)	3.49 (32.8)	1.28	7.36	2.44
2					KYB-S	0.487 (37.2)	0.210 (3.0)	3.47 (33.2)	1.22	7.02	2.81

( ) Percentage of Reduction

Table 4.14

Theoretical Responses to 30% Hachinohe EW Excitation (Weak Direction)

No.	Control Conditions					Top Floor Relative Displ. [in.]	Top Floor Absolute Accel. [G's]	Base Shear Force [kips]	Max. Control Force [kips]	Max. Mass Stroke [in.]	Max. Control Power [Kw]
	Sensor Position	Objective Variables	Weight of Added Mass	Stiffness of Added Mass	Regulator Type						
0	Without Control					0.665	0.181	4.36	-	-	-
1	Top Floor	Relative Displ.	200 kg	-	TAK-S	0.344 (48.3)	0.130 (28.2)	2.55 (41.5)	1.17	9.14	4.90
2					KYB-S	0.381 (42.7)	0.135 (25.4)	2.66 (40.0)	1.08	8.04	3.70

( ) Percentage of Reduction

Table 4.15

Experimental Responses to 40% Miyagioki EW Excitation (Weak Direction)

No.	Control Conditions					Top Floor Relative Displ. [in.]	Top Floor Absolute Accel. [G's]	Base Shear Force [kips]	Max. Control Force [kips]	Max. Mass Stroke [in.]	Max. Control Power [Kw]
	Sensor Position	Objective Variables	Weight of Added Mass	Stiffness of Added Mass	Regulator Type						
0	Without Control					0.483	0.223	3.39	-	-	-
1	Top Floor	Relative Displ.	200 kg	-	TAK-S	0.282 (41.6)	0.174 (22.0)	2.42 (28.6)	0.451	2.83	0.590
2					KYB-S	0.271 (43.9)	0.228 (-)	2.49 (26.6)	0.724	2.93	0.679

( ) Percentage of Reduction

Table 4.16

Theoretical Responses to 40% Miyagioki EW Excitation (Weak Direction)

No.	Control Conditions					Top Floor Relative Displ. [in.]	Top Floor Absolute Accel. [G's]	Base Shear Force [kips]	Max. Control Force [kips]	Max. Mass Stroke [in.]	Max. Control Power [Kw]
	Sensor Position	Objective Variables	Weight of Added Mass	Stiffness of Added Mass	Regulator Type						
0	Without Control					0.441	0.243	3.47	-	-	-
1	Top Floor	Relative Displ.	200 kg	-	TAK-S	0.180 (59.2)	0.184 (24.3)	1.63 (53.0)	0.730	3.04	0.832
2					KYB-S	0.198 (55.1)	0.207 (14.8)	1.82 (47.6)	0.703	2.67	0.798

( ) Percentage of Reduction

Although not identical, the experimental and the theoretical results show similar tendencies to those in the strong direction. The control effects produced by the analytical simulations for the various earthquake excitations are generally overestimated due to the reasons previously discussed for the **strong direction** in Section 4.3.1.2.3.

Figures 4-79 through 4-88 show good agreement of the true response of the structure the TAK-S (No. 1 in Table 4-11), a typical control regulator. Figure 4-79 through 4-88 show good agreement of the true and frequency response of the structure controlled by the AMD using the TAK-S/No. 1 Table 4-11, a typical control regulator. Both the experimental and the analytical responses show the reduction of responses and identical trends although some differences are present.

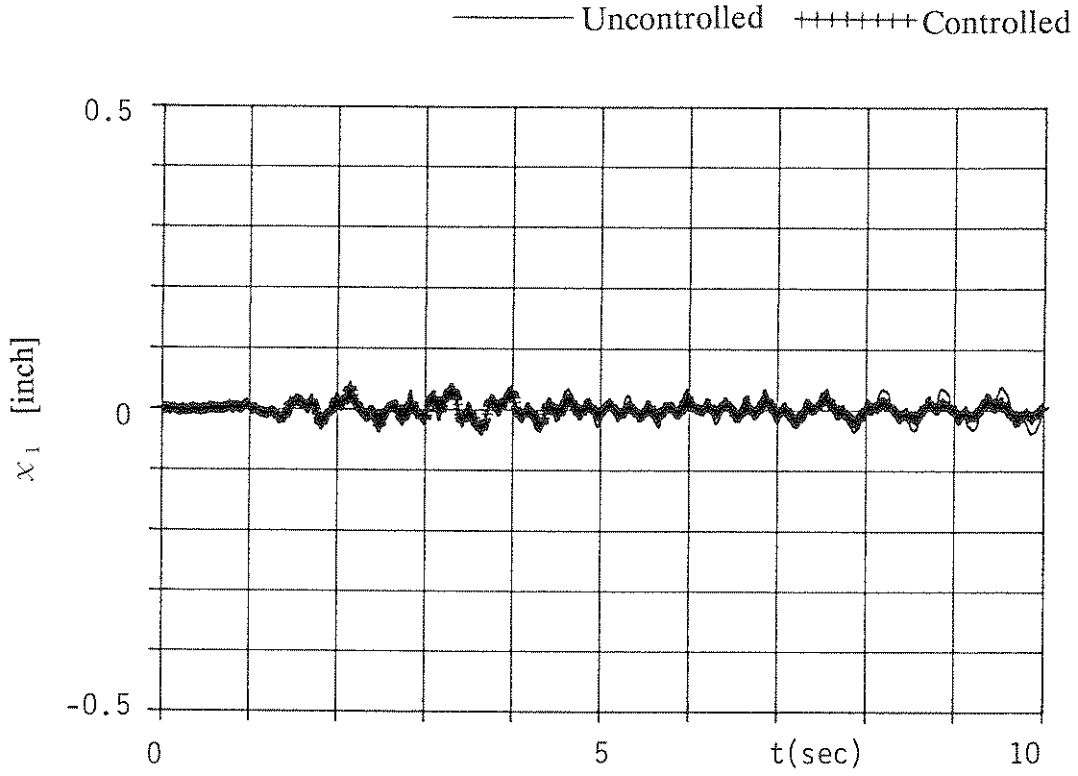

a) Experimental

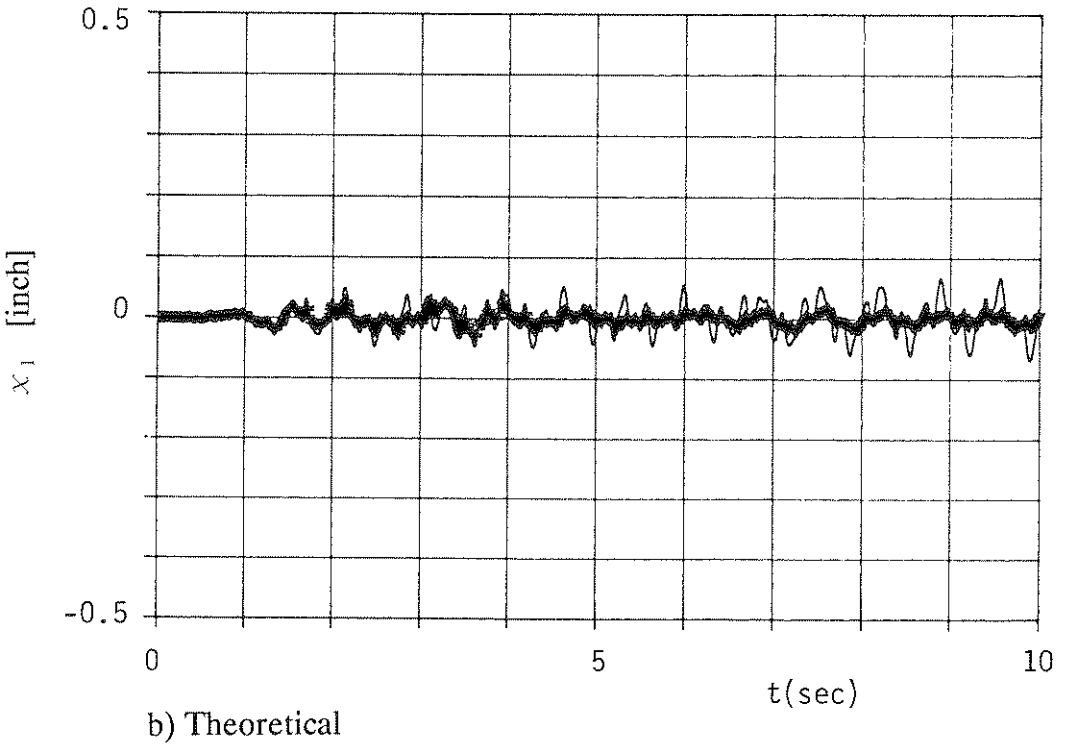

b) Theoretical

Figure 4.79 - First Floor Relative Displacement (20% El Centro).

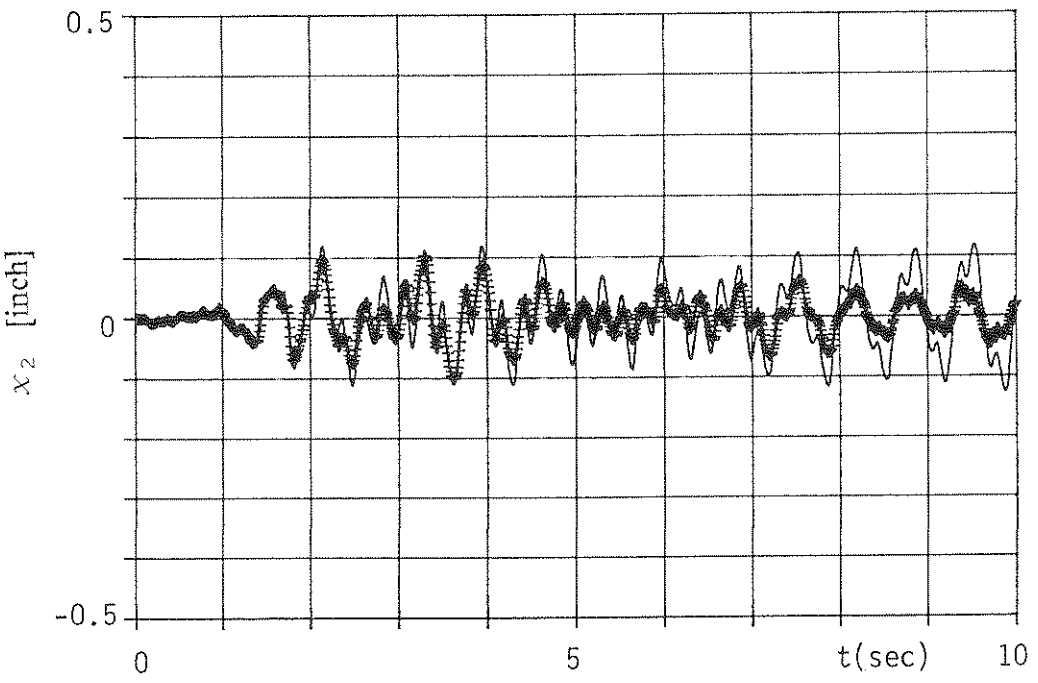

a) Experimental

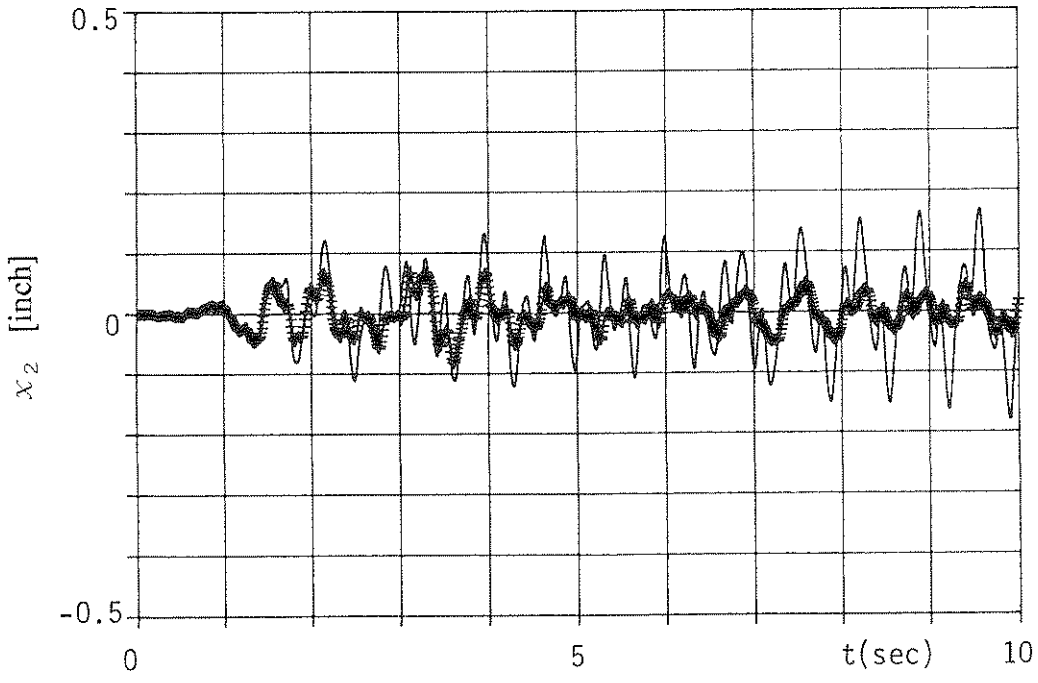

b) Theoretical

Figure 4.80 - Second Floor Relative Displacement (20% El Centro).

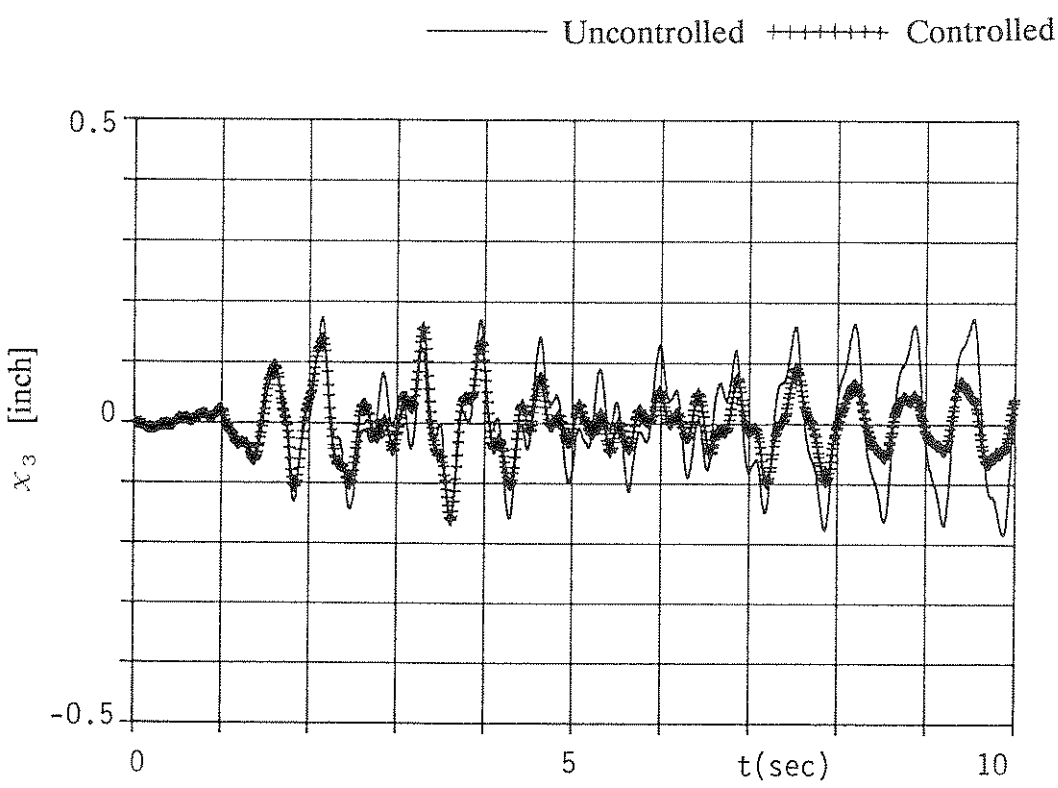

a) Experimental

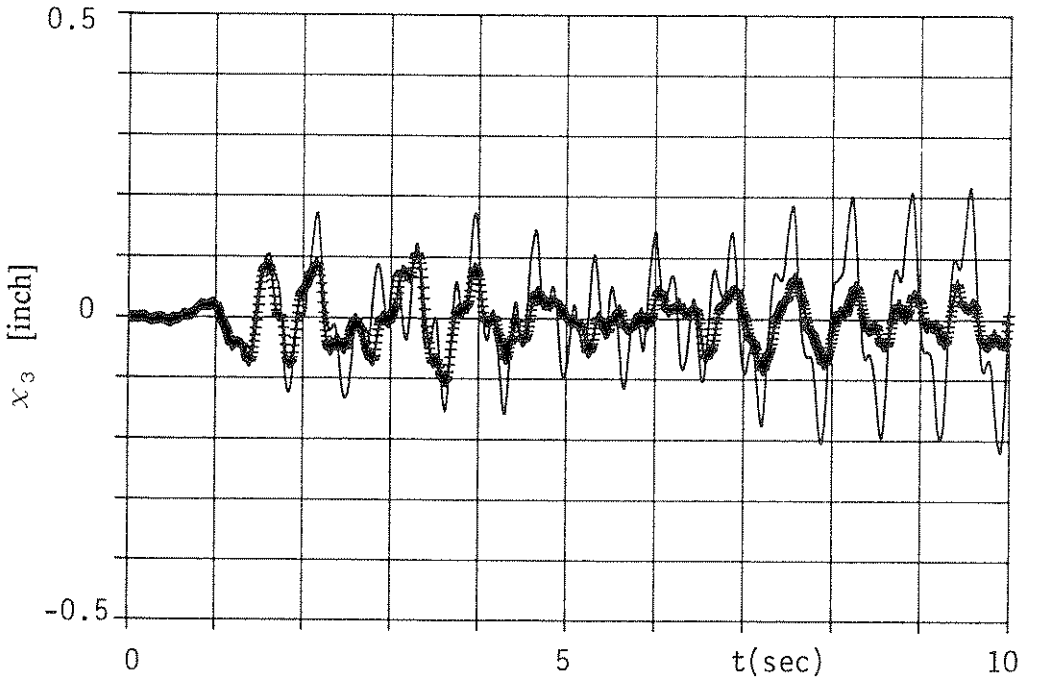

b) Theoretical

Figure 4.81 - Third Floor Relative Displacement (20% El Centro).

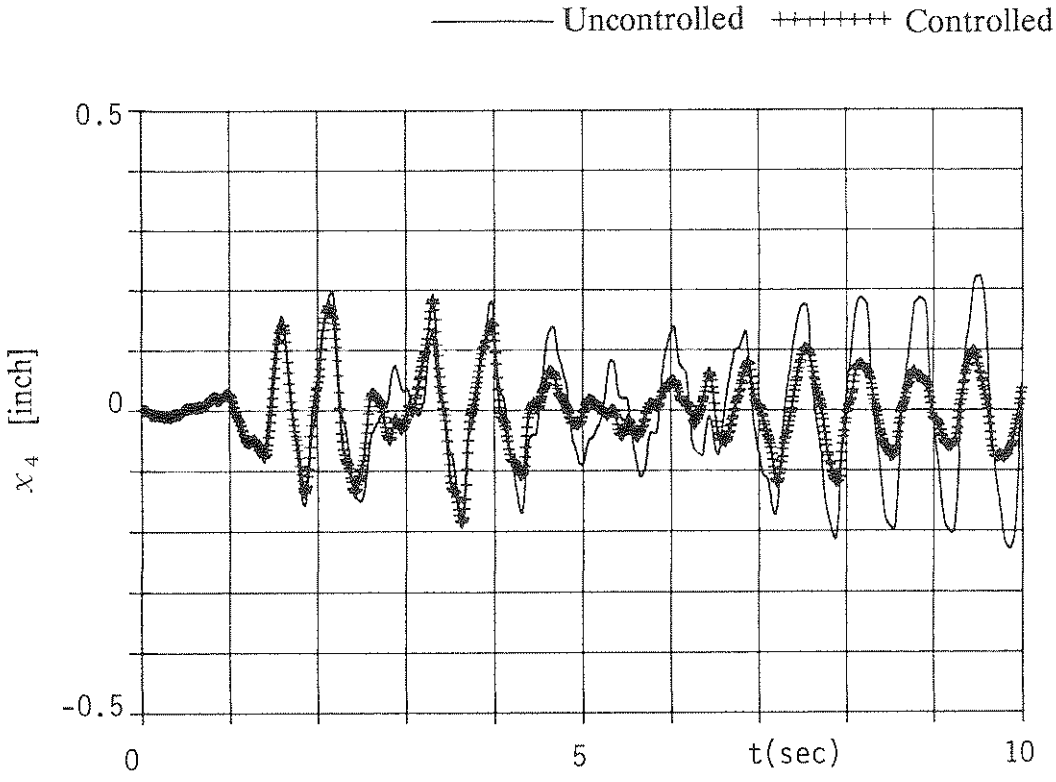

a) Experimental

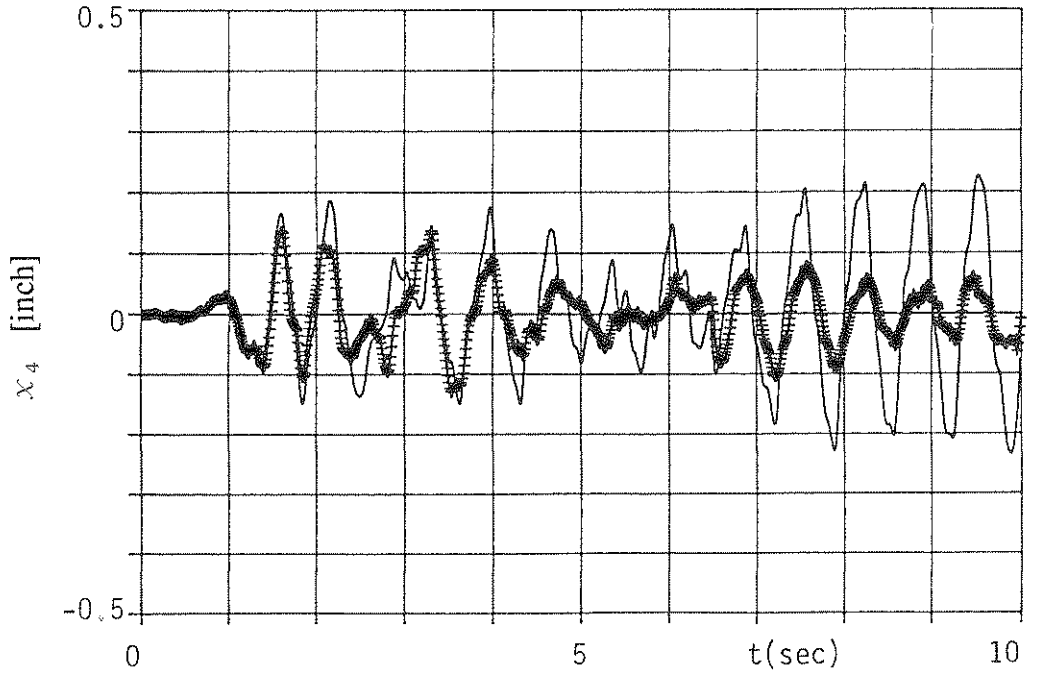

b) Theoretical

Figure 4.82 - Fourth Floor Relative Displacement (20% El Centro).

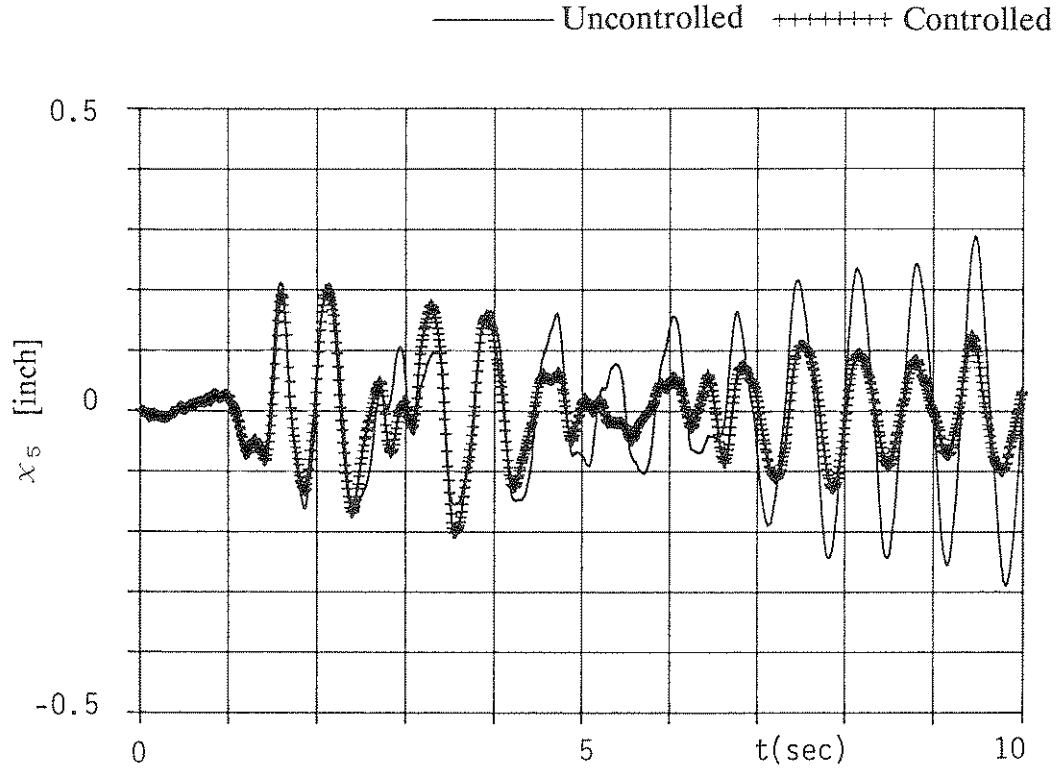

a) Experimental

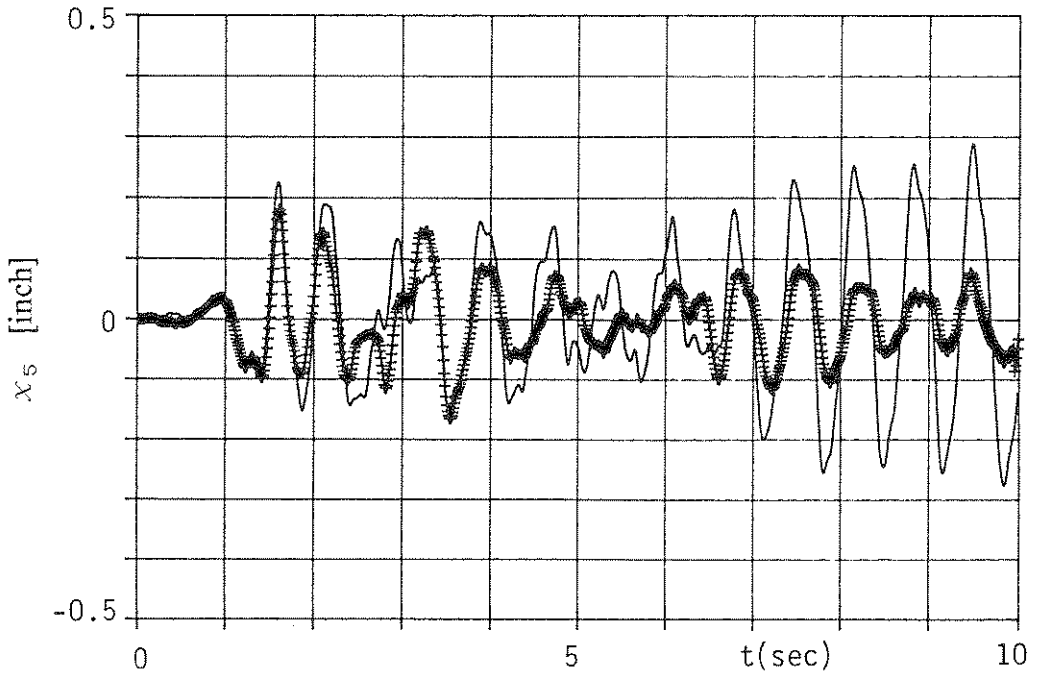

b) Theoretical

Figure 4.83 - Fifth Floor Relative Displacement (20% El Centro).

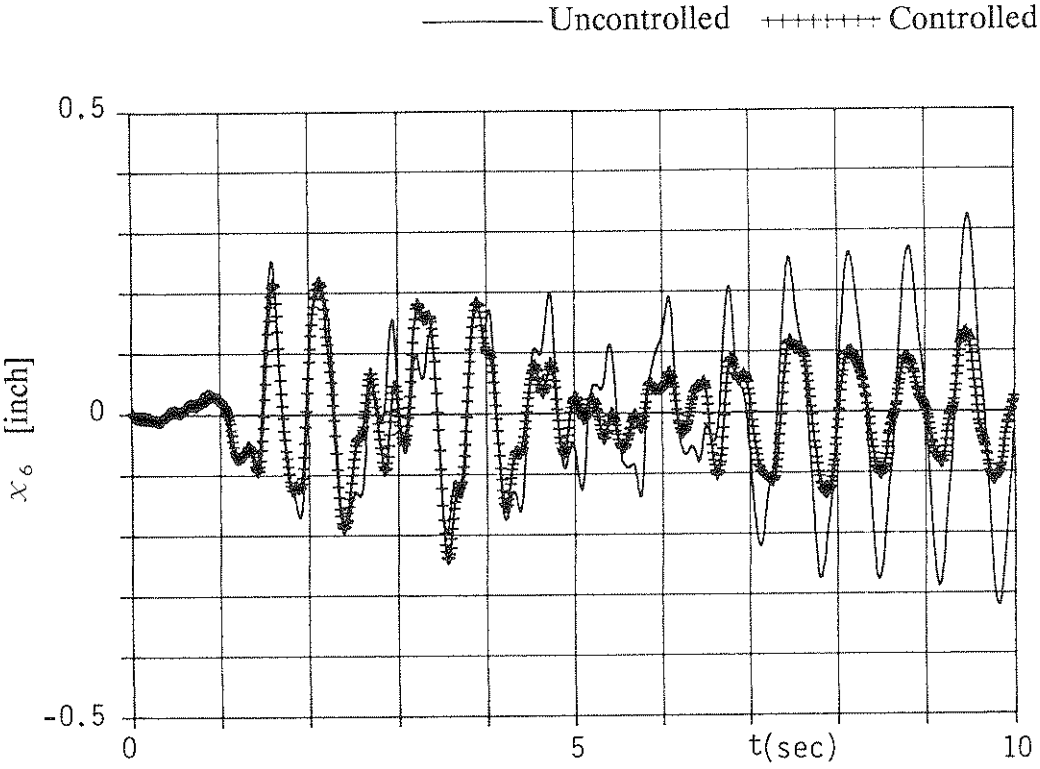

a) Experimental

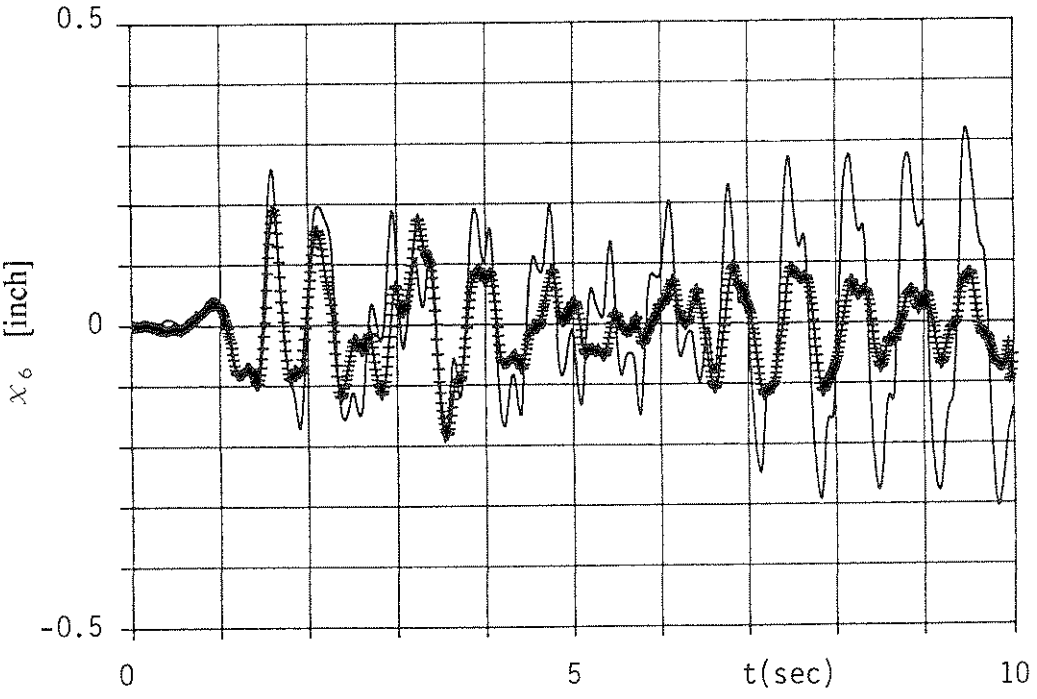

b)Theoretical

Figure 4.84 - Sixth Floor Relative Displacement (20% El Centro).

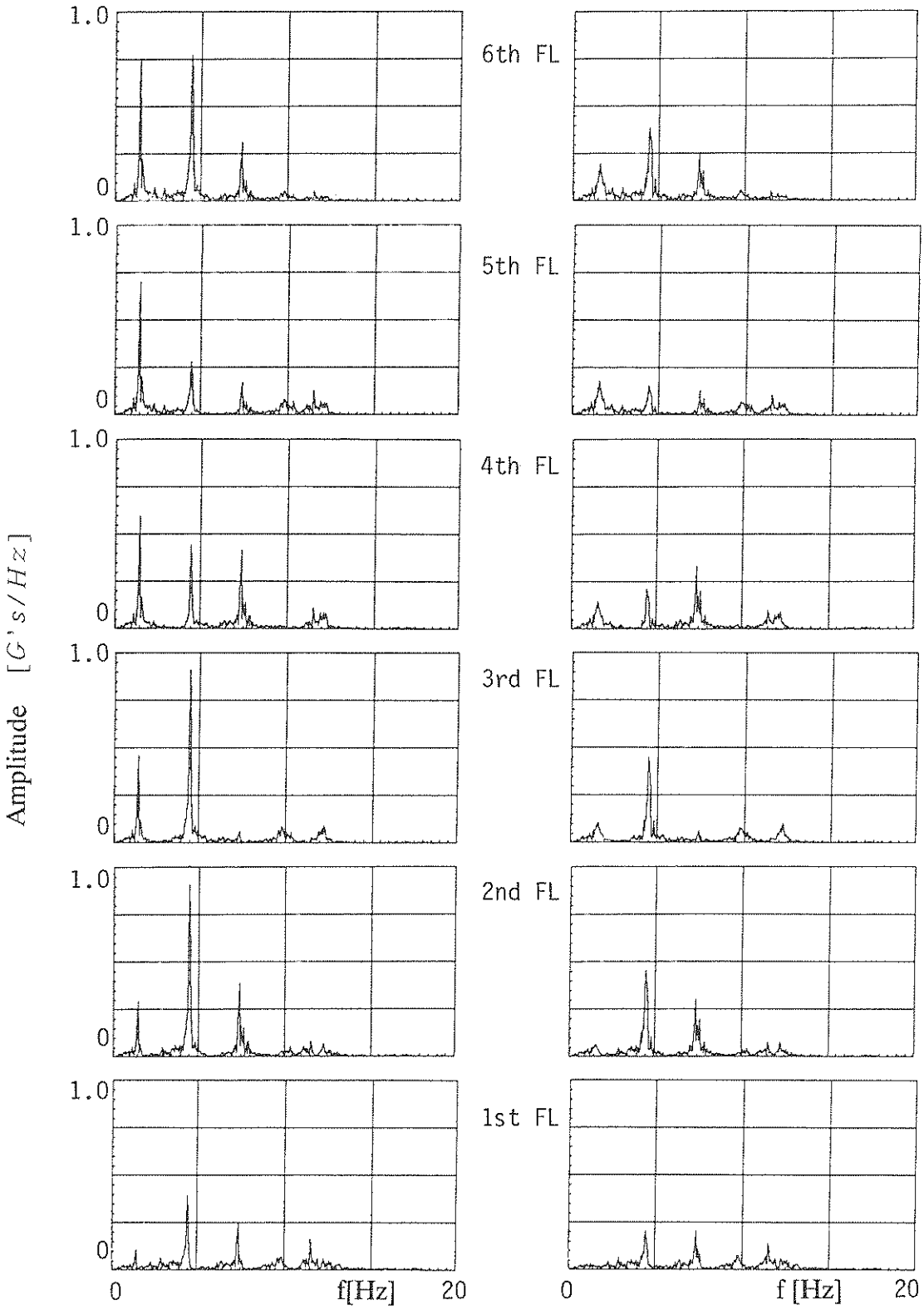

a) Uncontrolled b) Controlled

Figure 4.85 - Fourier Spectrum of Acceleration Responses (Experiment Under 20% ElCentro).

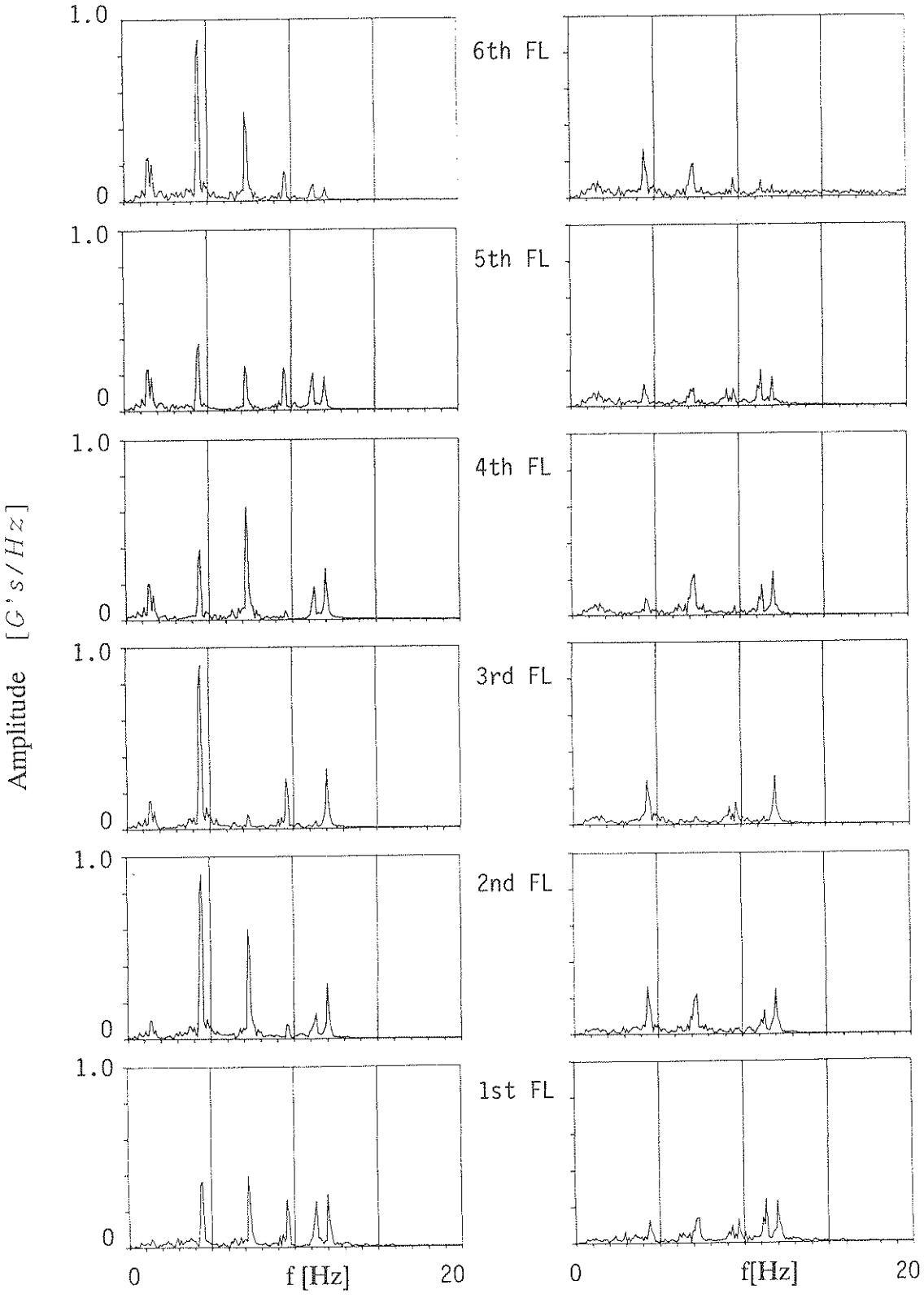

Figure 4.86 - Fourier Spectrum of Acceleration Responses (Simulation Under 20% El Centro).

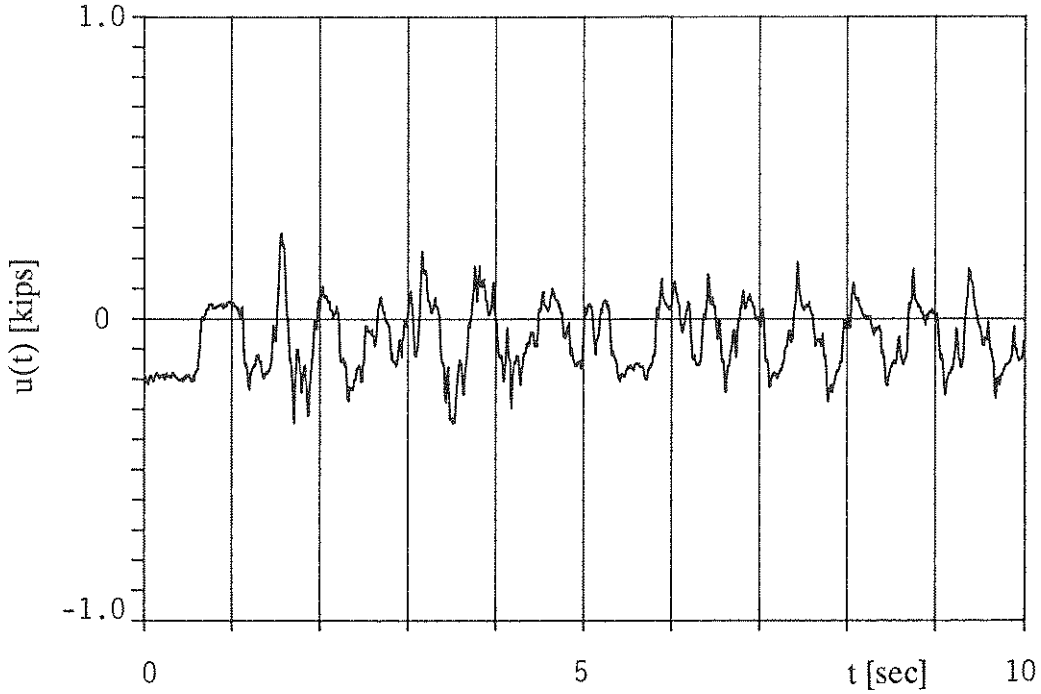

a) Time History

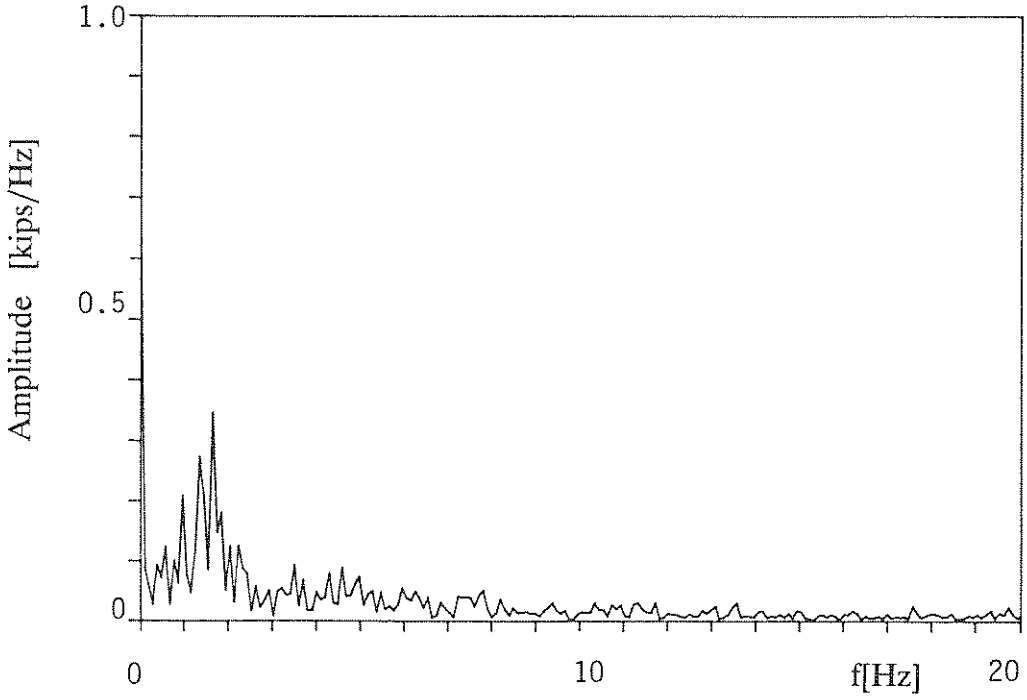

b) Frequency Domain

Figure 4.87 - Control Force (Experiment Under 20% El Centro).

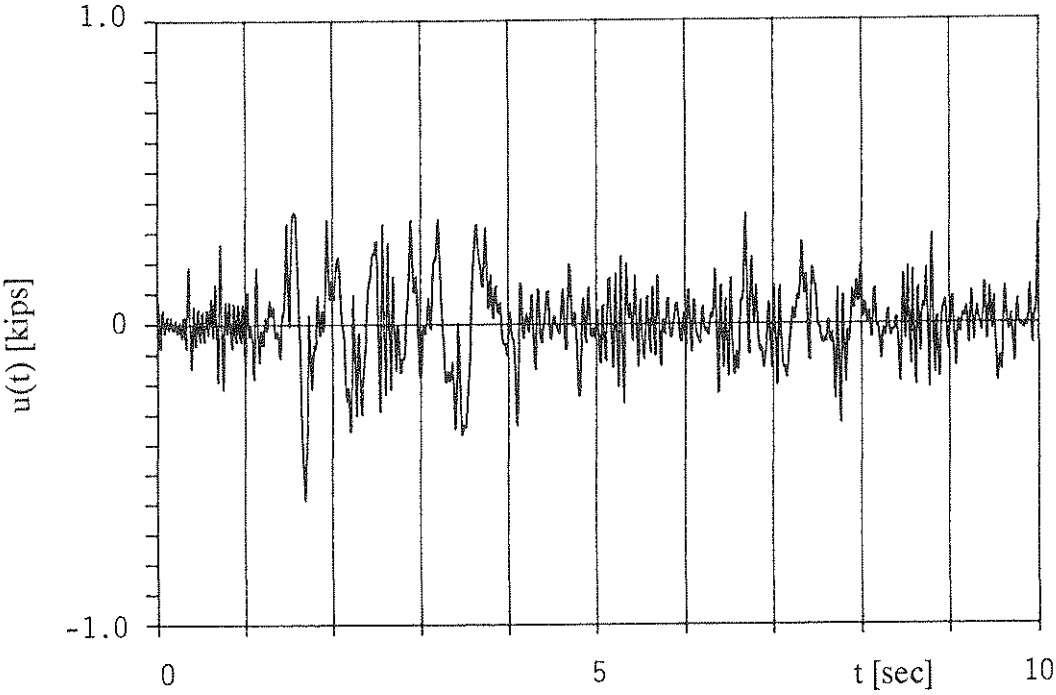

a) Time History

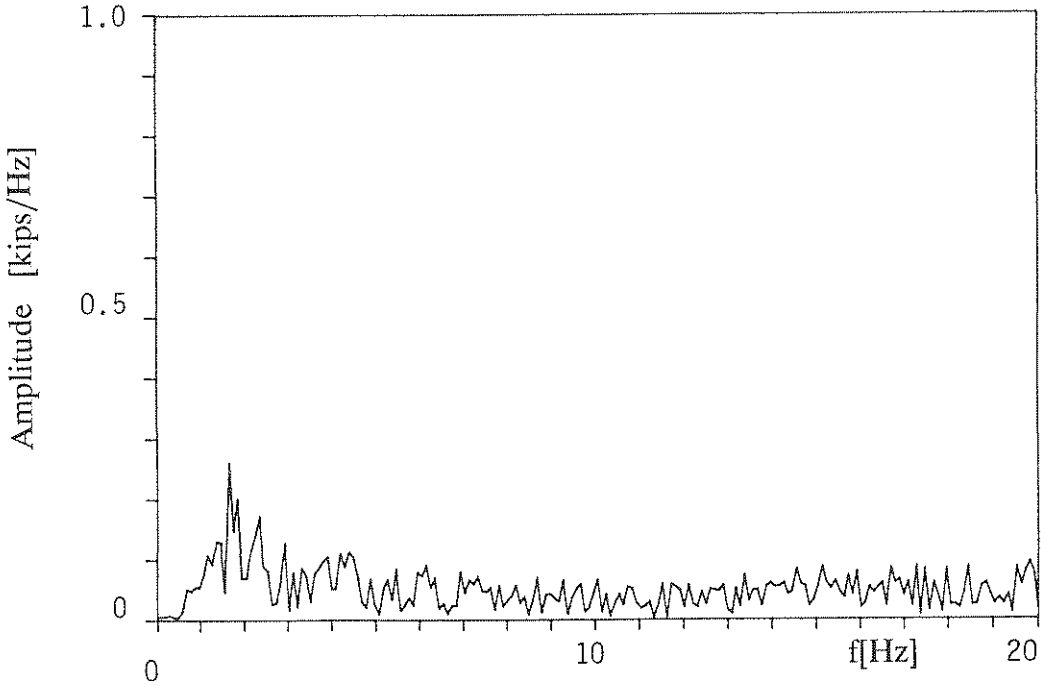

b) Frequency Domain

Figure 4.88 - Control Force (Simulation Under 20% El Centro).

SECTION 5
ACTIVE MASS DAMPER - ACTIVE TENDON PERFORMANCE COMPARISONS

One of the advantages of testing two different active systems using the same structural model is that their performance characteristics can be realistically compared. For comparison purposes, the performance quantities of interest are the maximum top-floor maximum relative displacement, maximum top-floor absolute acceleration, and maximum base shear. Peak control force and peak power required are also of interest from the viewpoint of control requirements. Accordingly, a comparison of these quantities for the AMD and the tendon system was carried out and is shown in Figs. 5.1 and 5.2 in the strong direction and in Figs. 5.3 and 5.4 in the weak direction. The performance is based on the responses to all earthquake motion accelerograms used in the experimental program (see Section 2.4). The ranges of these performance and control values cover 12 cases for the AMD and five cases for the ATS in the **strong direction** and, in the **weak direction**, 13 cases for the AMD and six cases for the ATS.

First of all, the discrepancies between the simulation and experimental results are noted; their causes have been discussed in Section 4 concerning the experimental results. In terms of the performance quantities, it is seen that both systems have similar ranges of effectiveness. The AMD performed better in the strong direction partly due to its robustness and partly due to significant first-mode contribution to the over-all structural dynamics, which can be controlled effectively by the AMD system. In the weak direction, differences in control effectiveness are less distinct. One common feature, shared by both active systems, is that there was only modest reduction in the maximum top-floor absolute acceleration. As alluded to earlier, this may be a result of the fact that acceleration reduction was not explicitly called for in the performance criterion used. A revision of the control law may lead to better performance in this regard.

As shown in Figs. 5.1 through 5.4, significant differences do exist in the maximum control force and maximum power required. Larger control forces are generally required in the case of the active tendon system, while larger power is required for operating the AMD. These considerations may play a significant role when an active control system is to be designed for actual structural applications.

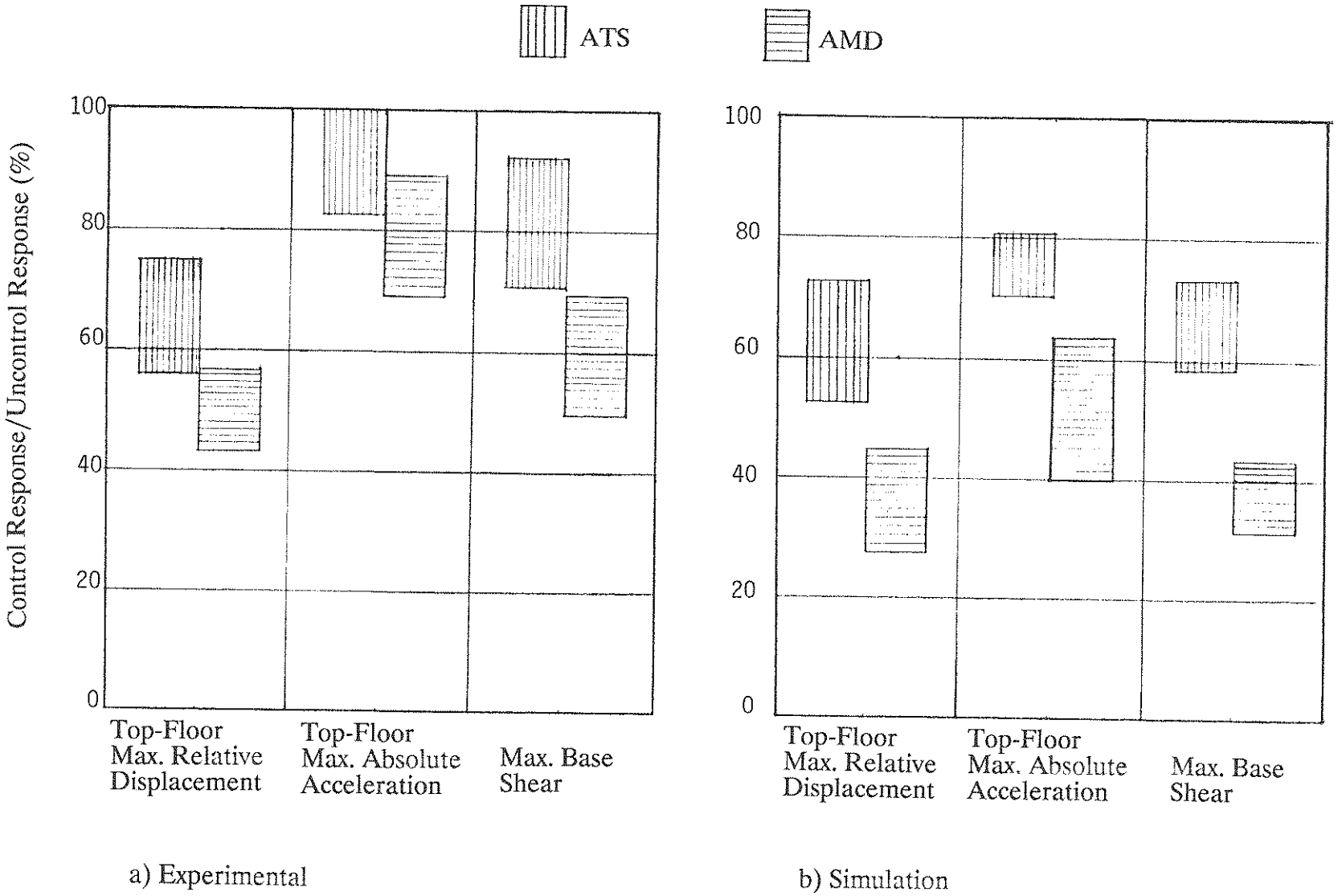

Figure 5.1 - Response Parameters In Strong Direction.

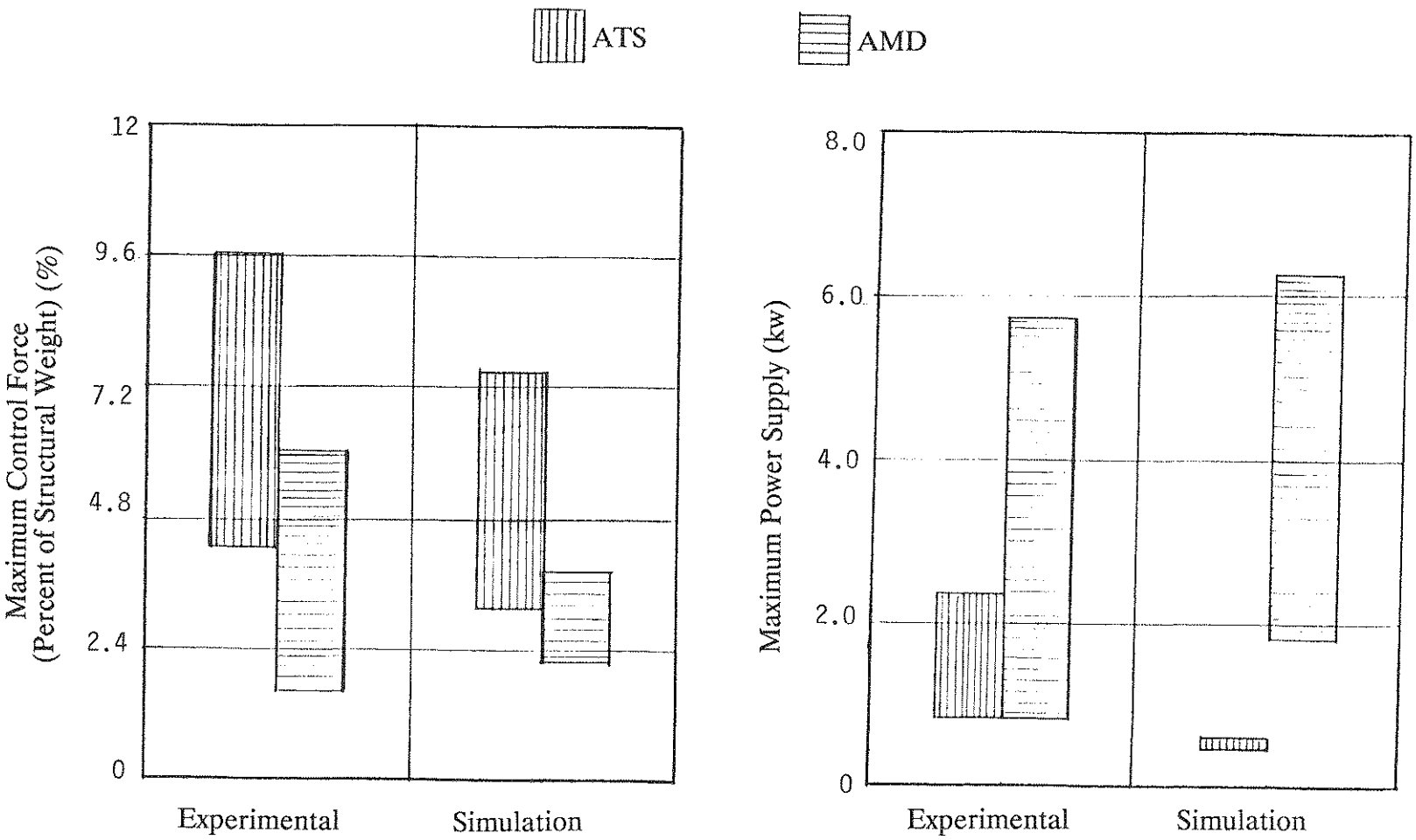

a) Maximum Control Force

b) Maximum Power Supply

Figure 5.2 - Control Parameter in Strong Direction.

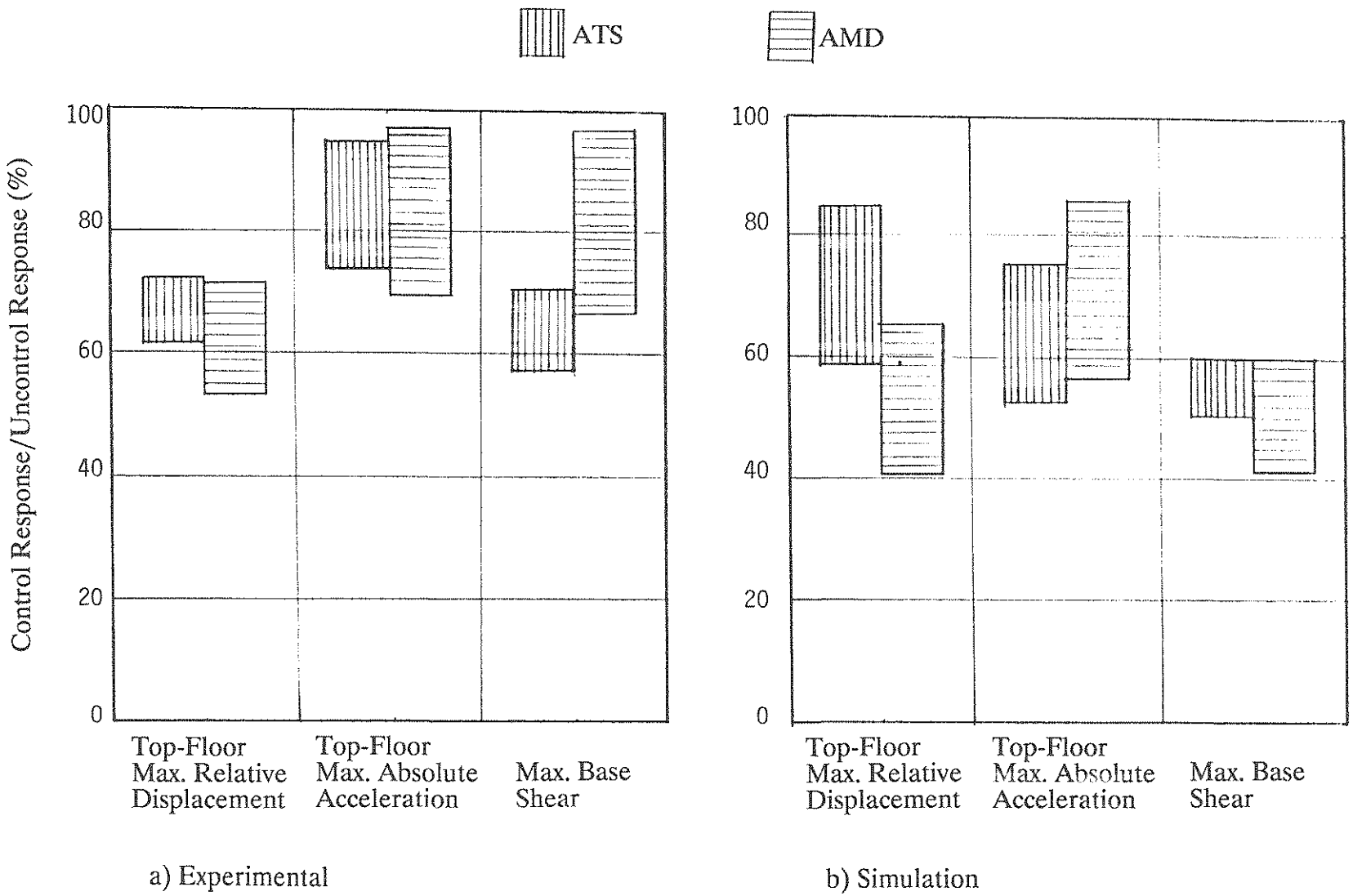

Figure 5.3 - Response Parameters in Weak Direction.

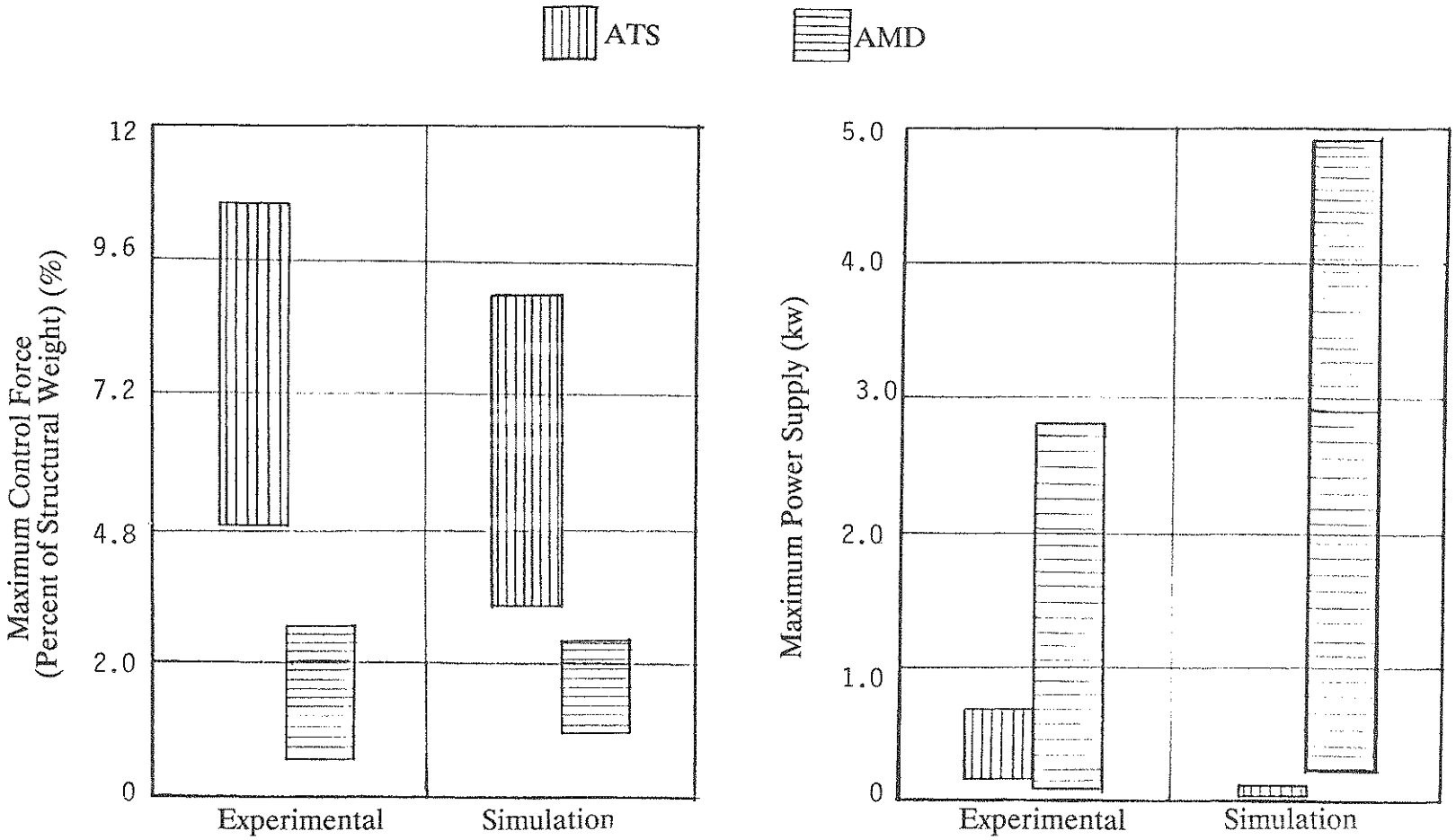

a) Maximum Control Force

b) Maximum Power Supply

Figure 5.4 - Control Parameters in Weak Direction.

Time constraints did not allow more extensive experimentation of greater variety of control laws and control configurations. Moreover, considerations such maintenance also need to be considered for a more complete evaluation of relative merits of the AMD and the active tendon system.

In closing, it should be noted that the experimental and the analytical studies show that both AMD and ATS are effective in reducing the dynamic response during earthquakes. While the ATS lies a better potential in reducing the response of higher modes of vibration, the AMD showed his efficiency for several lower modes only. For all practical purposes this is not a deficiency since the AMD is capable to control the lower modes which are usually excited by earthquake and wind gusts.

SECTION 6
CONCLUDING REMARKS

As indicated in the Introduction, this series of experiments represents a last phase of the active control experimental program carried out in the laboratory using a model structure. Several significant features of these experiments are noteworthy. They include:

(a) A substantially larger and heavier six-story structural model was used, thus allowing the active control systems to operate in an even more realistic dynamic environment.

(b) Multiple tendon control was made possible, providing opportunities to investigate a wide variety of control configurations.

(c) An active mass damper system was tested in conjunction with the active tendon system, allowing a realistic performance comparison of these two systems.

In the active tendon case, the following arrangements were included in the experimental study:

(a) A single actuator is placed at the base with diagonal tendons connected to a single floor.

(b) A single actuator is placed at the base with tendons connected simultaneously to two floors, thus applying proportional control to the structure.

(c) Two actuators are placed at different locations of the structure with two sets of tendons acting independently.

A comparison of the single-force control case and the proportional control case was made in the strong direction. The independent control case was attempted in the weak direction, but was not totally successful due to errors accumulated in the actuator dynamics. However, these experimental results again give evidence that tendon control is viable in structural control applications. Moreover, the single-force control case was found to be as effective as other control configurations in terms of control effectiveness and control system requirements. These results confirm that a simple active control system can be effective in response control of complex structures under earthquake - type excitations.

Encouraging results were also obtained using the active mass damper system. Robustness of the AMD system was demonstrated and it was further shown that sensor information at the top floor and at the base was sufficient to insure desired control efficiency.

Experimental results obtained using the AMD system also provide invaluable information for control system design. An increase in the added mass, for example, would reduce the mass stroke and the power supply required. Other design considerations which can substantially improve the AMD performance and design include regular conditions, sensor configurations, and gas spring stiffness.

Finally, it is noted that plans are underway for full-scale testing and demonstration of an active mass damper and an active tendon system. These systems are to be installed in a six-story, 600-ton symmetric building, which is being erected in Tokyo, Japan.

The tentative design of the active tendon system consists of two orthogonal sets of active bracings with tendons attached to the first floor. It is designed to provide motion control in either of the two directions.

The AMD system is also a biaxial unit. It is of the pendulum type with a fail-safe regulator. It weights 6 tons, approximately 1/100 of the structural weight, and has a maximum stroke of ± 1.0 in with a maximum control force of 10 tons.

The planned research tasks upon completion of the installation are:

(a) Calibration of the control systems by using one of the systems as motion inducer and the other as motion controller. Even without actual seismic motion, much of the performance characteristics can be assessed using this calibration method. During the calibration period, several feasible control algorithms will be evaluated and control parameters refined on the basis of knowledge gained in the laboratory.

(b) One of the systems will be deactivated in order to allow the assessment of the other system under actual ground excitation. A total five-year observation period is planned.

SECTION 7
REFERENCES

Abdel-Rohman, M. and Leipholz, H.H.E. (1983), "Active Control of Tall Buildings", ASCE J. Struct. Eng., Vol. 109, pp. 628-645.

Abdel-Rohman, M. (1984), "Effectiveness of Active TMD for Building Control, Trans. Can. Soc. Mech. Eng., Vol. 8, pp. 179-184.

Abdel-Rhoman, M., (1987), "Feasibility of Active Control of Tall Buildings Against Wind," ASCE J. Struc. Eng., Vol. 113, pp. 349-362.

Abdel-Rohman, M. (1987), "Control by Pole Assignment Method", ASCE J. Eng. Mechn. Div., Vol. 104, pp. 1157-1175.

Aizawa, S., Yamaguchi, I., Kinoshila, K., Yamaguchi, N., Hayamizu, Y., Fukao, Y., Minewaki, S., Abe, H., and Haniuda, N. (1987), "An Experimental Study on Active Mass Damper (Part I. Algorithm, Part 2. Experiments of Four-Story Model and Part 3. Simulation)" (in Japanese), Annual Meeting of Architectural Institute of Japan, pp. 899-904.

Bouten, H. and Meyr, H. (1987), "Control Design for ADC Grider", in Structural Control, Martinus Nijhoff, Amsterdam, pp. 669-693.

Chang, J.C.H. and Soong, T.T. (1980), "The Use of Aerodynamic Appendages for Tall Building Control", in Structural Control (ed. H.H.E. Leipholz), North Holland, Amsterdam, pp. 199-210.

Chung, L.L., Reinhorn, A.M. and Soong, T.T. (1986), "An Experimental Study of Active Structural Control", in Dynamic Response of Structures (ed. G.C. Hart and R.B. Nelson), ASCE, New York, pp. 795-802.

Chung, L.L., Lin, R.C., Soong, T.T. and Reinhorn, A.M. (1988), Experimental Study of Active Control of MDOF Structures Under Seismic Excitations", Report NCEER-88-0025, NCEER/SUNY Buffalo.

Chung, L.L., Reinhorn, A.M., and Soong, T.T. (1988), "Experiments on Active Control of Seismic Structures", J. Engr. Mech. ASCE, Vol. 114(2), pp. 241-256.

Chung, L.L., Lin, R.C., Soong, T.T. and Reinhorn, A.M. (1989), "Experimental Study of Active Control for MDOF Seismic Structures", ASCE J. Eng. Mech. Div., Vol. 115, no. 8, pp. 1609-1627.

ENR (1977), "Tuned Mass Damper Steady Sway of Skyscraper in Wind", Eng. News Record, August pp. 28-29.

Fukao, Y., Abe, H., Aizawa, S., Hayamizu, Y., Yamaguchi, I., and Kinoshita, K. (1988), "An Analytical Study on Active Mass Damper" (in Japanese), Annual Meeting of Architectural Institute of Japan, pp. 529-530.

Fukao, Y., Abe, H., Kinoshita, K., Haniuda, N. (1989), "An Experimental Research on Active Mass Damper (Part 1. Effect of Various Parameters on Damping Efficiency, and Part 2. Comparison with Test Results and Simulations)", (in Japanese), Annual Meeting of Architectural Institute of Japan, pp. 2254.2255.

Hrovat, D., Barak, P. and Robins, M. (1983), "Semi-Active vs. Passive or Active Tuned Mass Dampers for Structural control, ASCE J. Eng. Mech. Div., Vol. 109, pp. 691-701.

Juang, J.N., Sae-Ung, S. and Yang, J.N. (1980), "Active Control of Large Building Structures", in Structural Control (ed. H.H.E. Leipholz),North-Holland, Amsterdam, pp. 663-676.

Kobori, T., Kanayama, H. and Kamagata, S. (1987), "Dynamic Intelligent Building as active Seismic Response Controlled Structures", Proc. Annual Meeting Arch. Inst. Japan, Tokyo.

Kuroiwa, H. and Aizawa, S. (May 1987) Private Communications.

Lin, R.C., Soong, T.T. and Reinhorn, A.M. (1987), "Active Stochastic Control of Seismic Structures", Proc. US-Japan Joint Seminars on Stochastic Structural Mechanics, Boca Raton, FL.

Lin, R.C., Soong, T.T. and Reinhorn, A.M. (1987), "Experimental Evaluation of Instantaneous Optimal Algorithms For Structural Control", Report NCEER-87-0002, (PB88-134341/AS) NCEER/SUNY Buffalo.

Lund, R.A. (1980), "Active Damping of Large Structures in Winds, in Structural Control (ed. H.H.E. Leipholz), North-Holland, Amsterdam, pp. 459-470.

McGreevy S., Soong, T.T. and Reinhorn, A.M., (1988), "An Experimental Study of Time Delay Compensation in Active Structural Control" Proceedings of 6th International Modal Analysis Conference and Exhibits, Vol. I, PP. 733-739, Orlando Florida.

Nissim Isaac, (1978), "Improvement of Structure Bearing Capacity Through Controlled Constraints", M.S. Thesis, Technion-Israel Institute of Technology, Haifa, May.

Okada, Y. and Okashita, R. "Adaptive Control of an Active Mass Damper to Reduce Structural Vibration", Current Topics in Structural Mechanics - 1989, PVP Vol. 179, H. Chung (ed.), pp. 129-134.

Petersen, N.R. (1980), "Design of Large Scale Tuned Mass Dampers", in Structural Control, (ed. H.H.E. Leipholz), North-Holland, Amsterdam, 1980, pp. 581-596.

Prucz, Z. and Soong, T.T. (1983), "On Reliability and Active Control of Tension Leg Platforms", in Recent Advances in Engineering Mechanics and Their Impact on Civil Engineering Practice (ed. W.F. Chen and A.D.M. Lewis), pp. 903-906.

Reinhorn, A.M., Manolis, G.D. and Wen, C.Y. (1985), "Active Control of Inelastic Structures", Proceeding Second Int. Symp. on Structural Control
University of Waterloo, Canada, July 15-17.

Reinhorn and Manolis (1985), "Current State of Knowledge on structural Control", The Shock and Vibration Digest, Vol. 17, No. 10, October.

Reinhorn, A.M., Soong, T.T. and Manolis, G.D. (1986), "Disaster Prevention of Deep Water Offshore Structures By Means of Active Control", Proc. ASME Fifth Int. OMAE Conf., Tokyo, Japan, pp. 33-44.

Reinhorn, A.M., Manolis, G.D. and Wen, C.Y. (1987), "Active Control of Inelastic Structures", ASCE J. Eng. Mech. Div., Vol. 113, No., pp. 315-333.

Reinhorn and Manolis (1989), "Recent Advances in Structural Control", The Shock and Vibration Digest, Vol. 21, No. 1, January.

Rodellar, J., Chung, L.L., Soong, T.T., Reinhorn, A.M., (1987), "Experimental Digital Predictive Control of Structures", Vibration Control and Active Vibration Suppression, D. Inman and J. Simmons (eds.) ASME, New York, Vol DE-4, pp. 115-120.

Rodellar, J. Chung, L.L., Soong, T.T. and Reinhorn, A., (1989), "Experimental Digital Control of Structures", ASCE J. Eng. Mech. Div., Vol. 115, no. 6, pp. 1245-1261.

Roorda, J. (1975), "Tendon Control in Tall Structures", ASCE J. Struct. Div., Vol. 101, pp. 505-521.

Roorda, J. (1980), "Experiments in Feedback Control of Structures", in Structural Control, North Holland, Amsterdam, pp. 621-661.

Sae-Ung, S. and Yao, J.T.P. (1978), "Active Control of Building Structures", ASCE J. Eng. Mech. Div., Vol. 104, pp. 335-350.

Sage, A.P. and White, C.C. (1977), Optimal System Control, second edition, Prentice Hall, New York.

Samali, B., Yang, J.N. and Lin, S.C. (1985), "Control of Lateral-Torsional Motion of Buildings Under Seismic Load", ASCE J. Struct. Eng., Vol. 111, pp. 2165-2180.

Samali, B., Yang, J.N. and Yeh, C.T. (1985), "Control of Coupled Lateral Torsional Motion of Wind-Excited Buildings", ASCE J. Eng. Mech. Div., Vol. 111, pp. 777-796.

Soong, T.T., Reinhorn, A.M. and Yang, J.N. (1987), "A Standardized Model for Structural Control Experiments and Some Experimental Results", in Structural Control H.H.E. Leipholz, (ed.) Martinus Nijhoff, Amsterdam, pp. 669-693.

Soong, T.T. (1988), "Active Structural Control in Civil Engineering", Journal of Engineering Structures, Vol. 10, pp. 74-84.

Wiesner, K.B. (1986), "The Role of Damping Systems", Proc. 3rd Int. Conf. Tall Bldg., Chicago.

Yang J.N. and Giannopoulos, F. (1978), "Active Tendon Control of Structures", ASCE J. Eng. Mechn. Div., Vol. 104, pp. 551-568.

Yang, J.N. and Giannopoulus, F. (1979) (a), "Active Control and Stability of Cable-Stayed Bridge", ASCE J. Eng. Mech. Div., Vol. 105, pp. 677-694.

Yang, J.N. and Giannopoulus, F. (1979) (b), "Active Control of Two-Cable-Stayed Bridge", ASCE J. Eng. Mech. Div., Vol. 105, pp. 795-810.

Yang, J.N. (1982), "Control of Tall Buildings Under Earthquake Excitations", ASCE J. Eng. Mech. Div., Vol. 108, pp. 50-68.

Yang, J.N. and Lin, M.J. (1983), "Building Critical-Mode Control: Nonstationary Earthquakes", ASCE J. Eng. Mech. Div., Vol. 109, 1375-1389.

Yang, J.N. and Samali, B., (1983), "Control of Tall Buildings in Along-Wind Motion", ASCE J. Struct. Div., Vol. 109, pp. 50-68.

Yao, J.T.P. (1972), "Concept of Structural Control", ASCE J. Stru. Div., Vol. 98, pp. 1567-1574.

APPENDIX A
SERVO-CURRENT IN AMD ALGORITHM

The equation of motion of the SDOF model structure, added mass and control force shown in Fig. 3.2 can be written as:

$$m_s(\ddot{x}_s + \ddot{x}_0) + c_s\dot{x}_s + k_s x_s = F - U \qquad (A-1)$$

$$m_a(\ddot{x}_a + \ddot{x}_0) = U \qquad (A-2)$$

$$U = A_c(P_1 - P_2) - c_a(\dot{x}_a - \dot{x}_s) - k_a(x_a - x_s) \qquad (A-3)$$

where m_s, k_s and c_s are, respectively, the mass, stiffness and damping coefficient of the model structure: m_a, k_a and c_a are those of the active mass damper: x_s and x_a represent the relative displacement (to the ground) of the structure and added mass, respectively: $\ddot{x}_0$ is the ground acceleration. A_c is the effective area of cylinder and P_1, P_2 are the cylinder pressure of actuator.

The equations of continuity for the cylinder have the forms as follows:

$$V_1/K\dot{P}_1 = Q_1 - A_c(\dot{x}_a - \dot{x}_s) - Q_3 - Q_5 \qquad (A-4)$$

$$V_2/K\dot{P}_2 = -Q_2 + A_c(\dot{x}_a - \dot{x}_s) - Q_4 - Q_5 \qquad (A-5)$$

where $Q_3 = R_1P_1$, $Q_4 = R_1P_2$ and $Q_5 = R_2(P_1 - P_2)$; V_1 and V_2 are the cylinder volume, R_1 and R_2 are, respectively, the coefficient for inner and outer leaking of the cylinder; K is the compressibility of oil and $Q_1 \sim Q_5$ are the oil flow shown in Fig. 3.2.

The characteristics of servo-valve are expressed as follows:

$$Q_1 = (i/I_r)\cdot Q_r\sqrt{(P_s - P_1)/35} \quad (i \geq 0) \qquad (A-6)$$

$$Q_2 = (i/I_r)\cdot Q_r\sqrt{P_2/35} \quad (i \geq 0) \qquad (A-7)$$

$$Q_1 = (i/I_r)\cdot Q_r\sqrt{P_1/35} \quad (i<0) \qquad (A-8)$$

$$Q_2 = (i/I_r)\cdot Q_r\sqrt{(P_s-P_2)/35} \quad (i<0) \qquad (A-9)$$

where i is the servo-current, I_r, Q_r is the rated current, the rated flow of the servo-valve, respectively, and P_s is the supplied pressure.

Linearizing Eq. (A-3) through (A-9) near at equilibrium, one obtains the equation as follows:

$$\Delta U = \frac{2A_c\alpha}{\gamma}\Delta i - \left(\frac{2A_c^2}{\gamma}+c_a\right)\Delta\dot{x}_a' - k_a\Delta x_a' \qquad (A-10)$$

where $x_a' = x_a - x_s$, $\alpha = k/\sqrt{2}$, $\gamma = \beta + R_1 + 2R_2$,

$$\beta = \frac{ki_o}{\sqrt{2}P_s}, \qquad k = \frac{Q_r}{I_r}\sqrt{\frac{P_s}{35}},$$

and i_o is the servo-current at equilibrium.

APPENDIX B
SAMPLE COMPUTER PROGRAM FOR ATS

```
'''''''''''''''''''''''''''''''''''''''''''''''''''''''''''''''''''''''''''''''''''''
'  THIS PROGRAM IS PROVIDED TO EXECUTE ON-LINE CALCULATION OF FEEDBACK CONTROL
'  MOVEMENT(s) OF THE ACTUATOR(s) ACCORDING TO CLOSED-LOOP CONTROL ALGORITHM.
'  FEEDBACK STATES ARE ACQUIRED FROM 14 CHANNELS. THE ACQUISITION SYSTEM IS
'  ABLE TO TAKE DATA OF MAXIMUM 8 CHANNELS SIMULTANEOUSLY. THE FREQUENCY OF
'  DATA ACQUISITION CAN BE ADJUSTED BY CHANGING THE PARAMETERS PDRL & PDRH.
'
'''''''''''''''''''''''''''''''''''''''''''''''''''''''''''''''''''''''''''''''''''''
   DEFINT A-Z: DEFSNG V,G,F,k: DIM ADL(8), ADH(8),G(30) :GO TO 20

'~~~~~~~~~~~~~~~~~~~~~~~~~~~~~~~~~~~~~~~~~~~~~~~~~'
'  CONVERTING ANALOG SIGNAL TO DIGITAL VALUES     '
'                                                 '
'~~~~~~~~~~~~~~~~~~~~~~~~~~~~~~~~~~~~~~~~~~~~~~~~~'
10 C.R=B.A+1: S.R=B.A+1: D.R=B.A: OUT C.R,CSTP: TEMP=INP(D.R)
   WAIT S.R,C.W : OUT C.R,CLR: WAIT S.R,C.W: OUT C.R,CLR
   WAIT S.R,W.W,W.W: OUT D.R,PRDL: WAIT S.R,W.W,W.W: OUT D.R,PRDH
   WAIT S.R,C.W: OUT C.R,CSAD: WAIT S.R,W.W,W.W: OUT D.R,ADGAIN
   WAIT S.R,W.W,W.W: OUT D.R,ADST: WAIT S.R,W.W,W.W: OUT D.R,ADEN
   WAIT S.R,W.W,W.W: OUT D.R,NCVL: WAIT S.R,W.W,W.W: OUT D.R,NCVH
   WAIT S.R,C.W: OUT C.R,CRAD

'~~~~~~~~~~~~~~~~~~~~~~~~~~~~~~~~~~~~~~~~~~~~~~~~~~~~~~~~~~~~'
'  RESTORING DIGITAL DATA IN TWO PARTS : ADL(L) & ADH(L)     '
'                                                            '
'~~~~~~~~~~~~~~~~~~~~~~~~~~~~~~~~~~~~~~~~~~~~~~~~~~~~~~~~~~~~'
   FOR L= 1 TO NCVL:
   WAIT S.R,R.W: ADL(L)=INP(D.R)
   WAIT S.R,R.W: ADH(L)=INP(D.R)
   NEXT L

'~~~~~~~~~~~~~~~~~~~~~~~~~~~~~~~~~~~~~~~~~~~~~~~~~~~~~~~~~~~~~~~~~~~~~~~~~~~~'
'  CALCULATING FEEDBACK STATES BY MULTIPLYING STATE VARIABLES WITH           '
'  CORRESPONDING GAIN FACTORS                                                '
'                                                                            '
'~~~~~~~~~~~~~~~~~~~~~~~~~~~~~~~~~~~~~~~~~~~~~~~~~~~~~~~~~~~~~~~~~~~~~~~~~~~~'
   FOR I=1 TO NCVL
   F1=F1+G(I+B1)*(ADH(I)*256+ADL(I))
   F2=F2+G(I+B1+15)*(ADH(I)*256+ADL(I))
   NEXT I

   IF ADEN=7 THEN  B1=8: ADEN=5: NCVL=6: B.A=&H2EC: GOTO 10

'~~~~~~~~~~~~~~~~~~~~~~~~~~~~~~~~~~~~~~~~~~~~~~~~~~~~~~~~~~~~~~~~~'
'  CONVERTING THE CALCULATED OUTPUT STATES TO ANALOG SIGNALS      '
'  AND IN TURN FEED BACK TO THE HYDRAULIC ACTUATOR                '
'                                                                 '
'~~~~~~~~~~~~~~~~~~~~~~~~~~~~~~~~~~~~~~~~~~~~~~~~~~~~~~~~~~~~~~~~~'
   FIN1=2.*F1-F01:F01=F1:FIN2=2.*F2-F02:F02=F2

'~~~~~~~~~~~~~~~~~~~~~~~~~~'
'  OUTPUT TO 1st ACTUATOR  '
'                          '
'~~~~~~~~~~~~~~~~~~~~~~~~~~'
   HIGH=INT(FIN1/256): LOW=INT(FIN1-HIGH*256):DACSLCT=0: TEMP=INP(D.R)
   WAIT S.R, C.W: OUT C.R, CLR: WAIT S.R, C.W: OUT C.R,CDAOUT
```

```
   WAIT S.R, W.W, W.W: OUT D.R,DACSLCT: WAIT S.R, W.W, W.W: OUT D.R, LOW
   WAIT S.R, W.W, W.W: OUT D.R, HIGH :F1=G(15)

'~~~~~~~~~~~~~~~~~~~~~~~~~~~'
'  OUTPUT TO 2nd ACTUATOR   '
'                           '
'~~~~~~~~~~~~~~~~~~~~~~~~~~~'
   HIGH=INT(FIN2/256): LOW=INT(FIN2-HIGH*256):DACSLCT=1: TEMP=INP(D.R)
   WAIT S.R, C.W: OUT C.R, CLR: WAIT S.R, C.W: OUT C.R,CDAOUT
   WAIT S.R, W.W, W.W: OUT D.R,DACSLCT: WAIT S.R, W.W, W.W: OUT D.R, LOW
   WAIT S.R, W.W, W.W: OUT D.R, HIGH :F2=G(30)

'~~~~~~~~~~~~~~~~~~~~~~~~~~~~~~'
'  INITIALIZING PARAMETERS     '
'                              '
'~~~~~~~~~~~~~~~~~~~~~~~~~~~~~~'
   ADEN=7: NCVL=8: B.A=&H2EE: B1=0: GOTO 10

'~~~~~~~~~~~~~~~~'
'  GAIN FACTORS  '
'                '
'~~~~~~~~~~~~~~~~'
20 KU=-.25:G(1)=(.16/KU)*.642: G(2)=.16/KU*(-.7656):G(3)=.16/KU*(-0.005295):
   G(4)=.2/KU*(-0.00649):G(5)=.2/KU*(0.00183):G(6)=.2/KU*.2088 :
   G(7)=(-0.0754)/KU*.2:G(8)=25.32/KU*(-.0305): G(9)=15./KU*(.0115):
   G(10)=14.75/KU*.00705:G(11)=19.63/KU*.00552: G(12)=18.48/KU*(.005603):
   G(13)=14.96/KU*(-.001113): G(14)=19.70/KU*.00194:G(15)=2048:G(30)=2048:
   G(16)=.16/KU*(-.1307):G(17)=.16/KU*(-.0428):G(18)=.16/KU*(.8978):
   G(19)=.2/KU*(-.6656):G(20)=.2/KU*(-.2001):G(21)=.2/KU*(.0789):
   G(22)=.2/KU*(.0626):G(23)=.16/KU*(-.01018):G(24)=.16/KU*(-.00256):
   G(25)=.16/KU*(-.00438):G(26)=.2/KU*(.00796):G(27)=.2/KU*(.003496):
   G(28)=.2/KU*(.00469):G(29)=.2/KU*(.000958):

'~~~~~~~~~~~~~~~~~~~~~~~~~~~'
'  INITIALIZING PARAMETERS  '
'                           '
'~~~~~~~~~~~~~~~~~~~~~~~~~~~'
   PRDL=120 : ADGAIN=0:  PRDH=0: C.W=&H4:W.W=&H2:R.W=&H5:CSTP=&HF:CLR=&H1:
   CLK=&H3:CSAD=&HD:CRAD=&HE:CDAOUT=&H8 :ADEN=7: NCVL=8: B.A=&H2EE:

'~~~~~~~~~~~~~~~~~~~~~~~~~~~~~~~~~~~~~~~~~~~~~~~~~~~~~~~~~~~~~~~~~~~~~~~~~~~~~~~'
'  TAKING INITIAL READINGS AND ADJUSTING OFFSET OF OUTPUT SIGNAL  '
'                                                                '
'~~~~~~~~~~~~~~~~~~~~~~~~~~~~~~~~~~~~~~~~~~~~~~~~~~~~~~~~~~~~~~~~~~~~~~~~~~~~~~~'
25 C.R=B.A+1: S.R=B.A+1: D.R=B.A: OUT C.R,CSTP: TEMP=INP(D.R)
   WAIT S.R,C.W: OUT C.R,CLR: WAIT S.R,C.W: OUT C.R,CLK
   WAIT S.R,W.W,W.W: OUT D.R,PRDL: WAIT S.R,W.W,W.W: OUT D.R,PRDH
   WAIT S.R,C.W: OUT C.R,CSAD: WAIT S.R,W.W,W.W: OUT D.R,ADGAIN
   WAIT S.R,W.W,W.W: OUT D.R,ADST: WAIT S.R,W.W,W.W: OUT D.R,ADEN
   WAIT S.R,W.W,W.W: OUT D.R,NCVL: WAIT S.R,W.W,W.W: OUT D.R,NCVH
   WAIT S.R,C.W: OUT C.R,CRAD

   FOR L= 1 TO NCVL
   WAIT S.R,R.W: ADL(L)=INP(D.R)
   WAIT S.R,R.W: ADH(L)=INP(D.R)
   NEXT L
```

```
FOR I=1 TO NCVL
G(15)=G(15)-G(I+B1)*(ADH(I)*256+ADL(I))
G(30)=G(30)-G(I+B1+15)*(ADH(I)*256+ADL(I))
NEXT I

IF ADEN=7 THEN
B1=8: ADEN=5: NCVL=6: B.A=&H2EC: GOTO 25
ADEN=7: NCVL=8: B.A=&H2EE: B1=0
G(15)=G(15)-2048*.012/10
G(30)=G(30)-2048*.03/10
F1=G(15):F2=G(30): GO TO 10
```

NATIONAL CENTER FOR EARTHQUAKE ENGINEERING RESEARCH
LIST OF PUBLISHED TECHNICAL REPORTS

The National Center for Earthquake Engineering Research (NCEER) publishes technical reports on a variety of subjects related to earthquake engineering written by authors funded through NCEER. These reports are available from both NCEER's Publications Department and the National Technical Information Service (NTIS). Requests for reports should be directed to the Publications Department, National Center for Earthquake Engineering Research, State University of New York at Buffalo, Red Jacket Quadrangle, Buffalo, New York 14261. Reports can also be requested through NTIS, 5285 Port Royal Road, Springfield, Virginia 22161. NTIS accession numbers are shown in parenthesis, if available.

NCEER-87-0001 "First-Year Program in Research, Education and Technology Transfer," 3/5/87, (PB88-134275/AS).

NCEER-87-0002 "Experimental Evaluation of Instantaneous Optimal Algorithms for Structural Control," by R.C. Lin, T.T. Soong and A.M. Reinhorn, 4/20/87, (PB88-134341/AS).

NCEER-87-0003 "Experimentation Using the Earthquake Simulation Facilities at University at Buffalo," by A.M. Reinhorn and R.L. Ketter, to be published.

NCEER-87-0004 "The System Characteristics and Performance of a Shaking Table," by J.S. Hwang, K.C. Chang and G.C. Lee, 6/1/87, (PB88-134259/AS).

NCEER-87-0005 "A Finite Element Formulation for Nonlinear Viscoplastic Material Using a Q Model," by O. Gyebi and G. Dasgupta, 11/2/87, (PB88-213764/AS).

NCEER-87-0006 "Symbolic Manipulation Program (SMP) - Algebraic Codes for Two and Three Dimensional Finite Element Formulations," by X. Lee and G. Dasgupta, 11/9/87, (PB88-219522/AS).

NCEER-87-0007 "Instantaneous Optimal Control Laws for Tall Buildings Under Seismic Excitations," by J.N. Yang, A. Akbarpour and P. Ghaemmaghami, 6/10/87, (PB88-134333/AS).

NCEER-87-0008 "IDARC: Inelastic Damage Analysis of Reinforced Concrete Frame - Shear-Wall Structures," by Y.J. Park, A.M. Reinhorn and S.K. Kunnath, 7/20/87, (PB88-134325/AS).

NCEER-87-0009 "Liquefaction Potential for New York State: A Preliminary Report on Sites in Manhattan and Buffalo," by M. Budhu, V. Vijayakumar, R.F. Giese and L. Baumgras, 8/31/87, (PB88-163704/AS). This report is available only through NTIS (see address given above).

NCEER-87-0010 "Vertical and Torsional Vibration of Foundations in Inhomogeneous Media," by A.S. Veletsos and K.W. Dotson, 6/1/87, (PB88-134291/AS).

NCEER-87-0011 "Seismic Probabilistic Risk Assessment and Seismic Margins Studies for Nuclear Power Plants," by Howard H.M. Hwang, 6/15/87, (PB88-134267/AS). This report is available only through NTIS (see address given above).

NCEER-87-0012 "Parametric Studies of Frequency Response of Secondary Systems Under Ground-Acceleration Excitations," by Y. Yong and Y.K. Lin, 6/10/87, (PB88-134309/AS).

NCEER-87-0013 "Frequency Response of Secondary Systems Under Seismic Excitation," by J.A. HoLung, J. Cai and Y.K. Lin, 7/31/87, (PB88-134317/AS).

NCEER-87-0014 "Modelling Earthquake Ground Motions in Seismically Active Regions Using Parametric Time Series Methods," by G.W. Ellis and A.S. Cakmak, 8/25/87, (PB88-134283/AS).

NCEER-87-0015 "Detection and Assessment of Seismic Structural Damage," by E. DiPasquale and A.S. Cakmak, 8/25/87, (PB88-163712/AS).

NCEER-87-0016 "Pipeline Experiment at Parkfield, California," by J. Isenberg and E. Richardson, 9/15/87, (PB88-163720/AS).

NCEER-87-0017 "Digital Simulation of Seismic Ground Motion," by M. Shinozuka, G. Deodatis and T. Harada, 8/31/87, (PB88-155197/AS). This report is available only through NTIS (see address given above).

NCEER-87-0018 "Practical Considerations for Structural Control: System Uncertainty, System Time Delay and Truncation of Small Control Forces," J.N. Yang and A. Akbarpour, 8/10/87, (PB88-163738/AS).

NCEER-87-0019 "Modal Analysis of Nonclassically Damped Structural Systems Using Canonical Transformation," by J.N. Yang, S. Sarkani and F.X. Long, 9/27/87, (PB88-187851/AS).

NCEER-87-0020 "A Nonstationary Solution in Random Vibration Theory," by J.R. Red-Horse and P.D. Spanos, 11/3/87, (PB88-163746/AS).

NCEER-87-0021 "Horizontal Impedances for Radially Inhomogeneous Viscoelastic Soil Layers," by A.S. Veletsos and K.W. Dotson, 10/15/87, (PB88-150859/AS).

NCEER-87-0022 "Seismic Damage Assessment of Reinforced Concrete Members," by Y.S. Chung, C. Meyer and M. Shinozuka, 10/9/87, (PB88-150867/AS). This report is available only through NTIS (see address given above).

NCEER-87-0023 "Active Structural Control in Civil Engineering," by T.T. Soong, 11/11/87, (PB88-187778/AS).

NCEER-87-0024 Vertical and Torsional Impedances for Radially Inhomogeneous Viscoelastic Soil Layers," by K.W. Dotson and A.S. Veletsos, 12/87, (PB88-187786/AS).

NCEER-87-0025 "Proceedings from the Symposium on Seismic Hazards, Ground Motions, Soil-Liquefaction and Engineering Practice in Eastern North America," October 20-22, 1987, edited by K.H. Jacob, 12/87, (PB88-188115/AS).

NCEER-87-0026 "Report on the Whittier-Narrows, California, Earthquake of October 1, 1987," by J. Pantelic and A. Reinhorn, 11/87, (PB88-187752/AS). This report is available only through NTIS (see address given above).

NCEER-87-0027 "Design of a Modular Program for Transient Nonlinear Analysis of Large 3-D Building Structures," by S. Srivastav and J.F. Abel, 12/30/87, (PB88-187950/AS).

NCEER-87-0028 "Second-Year Program in Research, Education and Technology Transfer," 3/8/88, (PB88-219480/AS).

NCEER-88-0001 "Workshop on Seismic Computer Analysis and Design of Buildings With Interactive Graphics," by W. McGuire, J.F. Abel and C.H. Conley, 1/18/88, (PB88-187760/AS).

NCEER-88-0002 "Optimal Control of Nonlinear Flexible Structures," by J.N. Yang, F.X. Long and D. Wong, 1/22/88, (PB88-213772/AS).

NCEER-88-0003 "Substructuring Techniques in the Time Domain for Primary-Secondary Structural Systems," by G.D. Manolis and G. Juhn, 2/10/88, (PB88-213780/AS).

NCEER-88-0004 "Iterative Seismic Analysis of Primary-Secondary Systems," by A. Singhal, L.D. Lutes and P.D. Spanos, 2/23/88, (PB88-213798/AS).

NCEER-88-0005 "Stochastic Finite Element Expansion for Random Media," by P.D. Spanos and R. Ghanem, 3/14/88, (PB88-213806/AS).

NCEER-88-0006 "Combining Structural Optimization and Structural Control," by F.Y. Cheng and C.P. Pantelides, 1/10/88, (PB88-213814/AS).

NCEER-88-0007 "Seismic Performance Assessment of Code-Designed Structures," by H.H-M. Hwang, J-W. Jaw and H-J. Shau, 3/20/88, (PB88-219423/AS).

NCEER-88-0008 "Reliability Analysis of Code-Designed Structures Under Natural Hazards," by H.H-M. Hwang, H. Ushiba and M. Shinozuka, 2/29/88, (PB88-229471/AS).

NCEER-88-0009 "Seismic Fragility Analysis of Shear Wall Structures," by J-W Jaw and H.H-M. Hwang, 4/30/88, (PB89-102867/AS).

NCEER-88-0010 "Base Isolation of a Multi-Story Building Under a Harmonic Ground Motion - A Comparison of Performances of Various Systems," by F-G Fan, G. Ahmadi and I.G. Tadjbakhsh, 5/18/88, (PB89-122238/AS).

NCEER-88-0011 "Seismic Floor Response Spectra for a Combined System by Green's Functions," by F.M. Lavelle, L.A. Bergman and P.D. Spanos, 5/1/88, (PB89-102875/AS).

NCEER-88-0012 "A New Solution Technique for Randomly Excited Hysteretic Structures," by G.Q. Cai and Y.K. Lin, 5/16/88, (PB89-102883/AS).

NCEER-88-0013 "A Study of Radiation Damping and Soil-Structure Interaction Effects in the Centrifuge," by K. Weissman, supervised by J.H. Prevost, 5/24/88, (PB89-144703/AS).

NCEER-88-0014 "Parameter Identification and Implementation of a Kinematic Plasticity Model for Frictional Soils," by J.H. Prevost and D.V. Griffiths, to be published.

NCEER-88-0015 "Two- and Three- Dimensional Dynamic Finite Element Analyses of the Long Valley Dam," by D.V. Griffiths and J.H. Prevost, 6/17/88, (PB89-144711/AS).

NCEER-88-0016 "Damage Assessment of Reinforced Concrete Structures in Eastern United States," by A.M. Reinhorn, M.J. Seidel, S.K. Kunnath and Y.J. Park, 6/15/88, (PB89-122220/AS).

NCEER-88-0017 "Dynamic Compliance of Vertically Loaded Strip Foundations in Multilayered Viscoelastic Soils," by S. Ahmad and A.S.M. Israil, 6/17/88, (PB89-102891/AS).

NCEER-88-0018 "An Experimental Study of Seismic Structural Response With Added Viscoelastic Dampers," by R.C. Lin, Z. Liang, T.T. Soong and R.H. Zhang, 6/30/88, (PB89-122212/AS).

NCEER-88-0019 "Experimental Investigation of Primary - Secondary System Interaction," by G.D. Manolis, G. Juhn and A.M. Reinhorn, 5/27/88, (PB89-122204/AS).

NCEER-88-0020 "A Response Spectrum Approach For Analysis of Nonclassically Damped Structures," by J.N. Yang, S. Sarkani and F.X. Long, 4/22/88, (PB89-102909/AS).

NCEER-88-0021 "Seismic Interaction of Structures and Soils: Stochastic Approach," by A.S. Veletsos and A.M. Prasad, 7/21/88, (PB89-122196/AS).

NCEER-88-0022 "Identification of the Serviceability Limit State and Detection of Seismic Structural Damage," by E. DiPasquale and A.S. Cakmak, 6/15/88, (PB89-122188/AS).

NCEER-88-0023 "Multi-Hazard Risk Analysis: Case of a Simple Offshore Structure," by B.K. Bhartia and E.H. Vanmarcke, 7/21/88, (PB89-145213/AS).

NCEER-88-0024 "Automated Seismic Design of Reinforced Concrete Buildings," by Y.S. Chung, C. Meyer and M. Shinozuka, 7/5/88, (PB89-122170/AS).

NCEER-88-0025 "Experimental Study of Active Control of MDOF Structures Under Seismic Excitations," by L.L. Chung, R.C. Lin, T.T. Soong and A.M. Reinhorn, 7/10/88, (PB89-122600/AS).

NCEER-88-0026 "Earthquake Simulation Tests of a Low-Rise Metal Structure," by J.S. Hwang, K.C. Chang, G.C. Lee and R.L. Ketter, 8/1/88, (PB89-102917/AS).

NCEER-88-0027 "Systems Study of Urban Response and Reconstruction Due to Catastrophic Earthquakes," by F. Kozin and H.K. Zhou, 9/22/88, to be published.

NCEER-88-0028 "Seismic Fragility Analysis of Plane Frame Structures," by H.H-M. Hwang and Y.K. Low, 7/31/88, (PB89-131445/AS).

NCEER-88-0029 "Response Analysis of Stochastic Structures," by A. Kardara, C. Bucher and M. Shinozuka, 9/22/88, (PB89-174429/AS).

NCEER-88-0030 "Nonnormal Accelerations Due to Yielding in a Primary Structure," by D.C.K. Chen and L.D. Lutes, 9/19/88, (PB89-131437/AS).

NCEER-88-0031 "Design Approaches for Soil-Structure Interaction," by A.S. Veletsos, A.M. Prasad and Y. Tang, 12/30/88, (PB89-174437/AS).

NCEER-88-0032 "A Re-evaluation of Design Spectra for Seismic Damage Control," by C.J. Turkstra and A.G. Tallin, 11/7/88, (PB89-145221/AS).

NCEER-88-0033 "The Behavior and Design of Noncontact Lap Splices Subjected to Repeated Inelastic Tensile Loading," by V.E. Sagan, P. Gergely and R.N. White, 12/8/88, (PB89-163737/AS).

NCEER-88-0034 "Seismic Response of Pile Foundations," by S.M. Mamoon, P.K. Banerjee and S. Ahmad, 11/1/88, (PB89-145239/AS).

NCEER-88-0035 "Modeling of R/C Building Structures With Flexible Floor Diaphragms (IDARC2)," by A.M. Reinhorn, S.K. Kunnath and N. Panahshahi, 9/7/88, (PB89-207153/AS).

NCEER-88-0036 "Solution of the Dam-Reservoir Interaction Problem Using a Combination of FEM, BEM with Particular Integrals, Modal Analysis, and Substructuring," by C-S. Tsai, G.C. Lee and R.L. Ketter, 12/31/88, (PB89-207146/AS).

NCEER-88-0037 "Optimal Placement of Actuators for Structural Control," by F.Y. Cheng and C.P. Pantelides, 8/15/88, (PB89-162846/AS).

NCEER-88-0038 "Teflon Bearings in Aseismic Base Isolation: Experimental Studies and Mathematical Modeling," by A. Mokha, M.C. Constantinou and A.M. Reinhorn, 12/5/88, (PB89-218457/AS).

NCEER-88-0039 "Seismic Behavior of Flat Slab High-Rise Buildings in the New York City Area," by P. Weidlinger and M. Ettouney, 10/15/88.

NCEER-88-0040 "Evaluation of the Earthquake Resistance of Existing Buildings in New York City," by P. Weidlinger and M. Ettouney, 10/15/88, to be published.

NCEER-88-0041 "Small-Scale Modeling Techniques for Reinforced Concrete Structures Subjected to Seismic Loads," by W. Kim, A. El-Attar and R.N. White, 11/22/88, (PB89-189625/AS).

NCEER-88-0042 "Modeling Strong Ground Motion from Multiple Event Earthquakes," by G.W. Ellis and A.S. Cakmak, 10/15/88, (PB89-174445/AS).

NCEER-88-0043 "Nonstationary Models of Seismic Ground Acceleration," by M. Grigoriu, S.E. Ruiz and E. Rosenblueth, 7/15/88, (PB89-189617/AS).

NCEER-88-0044 "SARCF User's Guide: Seismic Analysis of Reinforced Concrete Frames," by Y.S. Chung, C. Meyer and M. Shinozuka, 11/9/88, (PB89-174452/AS).

NCEER-88-0045 "First Expert Panel Meeting on Disaster Research and Planning," edited by J. Pantelic and J. Stoyle, 9/15/88, (PB89-174460/AS).

NCEER-88-0046 "Preliminary Studies of the Effect of Degrading Infill Walls on the Nonlinear Seismic Response of Steel Frames," by C.Z. Chrysostomou, P. Gergely and J.F. Abel, 12/19/88, (PB89-208383/AS).

NCEER-88-0047 "Reinforced Concrete Frame Component Testing Facility - Design, Construction, Instrumentation and Operation," by S.P. Pessiki, C. Conley, T. Bond, P. Gergely and R.N. White, 12/16/88, (PB89-174478/AS).

NCEER-89-0001 "Effects of Protective Cushion and Soil Compliancy on the Response of Equipment Within a Seismically Excited Building," by J.A. HoLung, 2/16/89, (PB89-207179/AS).

NCEER-89-0002 "Statistical Evaluation of Response Modification Factors for Reinforced Concrete Structures," by H.H-M. Hwang and J-W. Jaw, 2/17/89, (PB89-207187/AS).

NCEER-89-0003 "Hysteretic Columns Under Random Excitation," by G-Q. Cai and Y.K. Lin, 1/9/89, (PB89-196513/AS).

NCEER-89-0004 "Experimental Study of 'Elephant Foot Bulge' Instability of Thin-Walled Metal Tanks," by Z-H. Jia and R.L. Ketter, 2/22/89, (PB89-207195/AS).

NCEER-89-0005 "Experiment on Performance of Buried Pipelines Across San Andreas Fault," by J. Isenberg, E. Richardson and T.D. O'Rourke, 3/10/89, (PB89-218440/AS).

NCEER-89-0006 "A Knowledge-Based Approach to Structural Design of Earthquake-Resistant Buildings," by M. Subramani, P. Gergely, C.H. Conley, J.F. Abel and A.H. Zaghw, 1/15/89, (PB89-218465/AS).

NCEER-89-0007 "Liquefaction Hazards and Their Effects on Buried Pipelines," by T.D. O'Rourke and P.A. Lane, 2/1/89, (PB89-218481).

NCEER-89-0008 "Fundamentals of System Identification in Structural Dynamics," by H. Imai, C-B. Yun, O. Maruyama and M. Shinozuka, 1/26/89, (PB89-207211/AS).

NCEER-89-0009 "Effects of the 1985 Michoacan Earthquake on Water Systems and Other Buried Lifelines in Mexico," by A.G. Ayala and M.J. O'Rourke, 3/8/89, (PB89-207229/AS).

NCEER-89-0010 "NCEER Bibliography of Earthquake Education Materials," by K.E.K. Ross, 3/10/89, (PB89-218473/AS).

NCEER-89-0011 "Inelastic Three-Dimensional Response Analysis of Reinforced Concrete Building Structures (IDARC-3D), Part I - Modeling," by S.K. Kunnath and A.M. Reinhorn, 4/17/89.

NCEER-89-0012 "Recommended Modifications to ATC-14," by C.D. Poland and J.O. Malley, 4/12/89.

NCEER-89-0013 "Repair and Strengthening of Beam-to-Column Connections Subjected to Earthquake Loading," by M. Corazao and A.J. Durrani, 2/28/89.

NCEER-89-0014 "Program EXKAL2 for Identification of Structural Dynamic Systems," by O. Maruyama, C-B. Yun, M. Hoshiya and M. Shinozuka, 5/19/89.

NCEER-89-0015 "Response of Frames With Bolted Semi-Rigid Connections, Part I - Experimental Study and Analytical Predictions," by P.J. DiCorso, A.M. Reinhorn, J.R. Dickerson, J.B. Radziminski and W.L. Harper, 6/1/89, to be published.

NCEER-89-0016 "ARMA Monte Carlo Simulation in Probabilistic Structural Analysis," by P.D. Spanos and M.P. Mignolet, 7/10/89.

NCEER-89-0017 "Preliminary Proceedings of the Conference on Disaster Preparedness - The Place of Earthquake Education in Our Schools, July 9-11, 1989," 6/23/89.

NCEER-89-0018 "Multidimensional Models of Hysteretic Material Behavior for Vibration Analysis of Shape Memory Energy Absorbing Devices, by E.J. Graesser and F.A. Cozzarelli, 6/7/89.

NCEER-89-0019 "Nonlinear Dynamic Analysis of Three-Dimensional Base Isolated Structures (3D-BASIS)," by S. Nagarajaiah, A.M. Reinhorn and M.C. Constantinou, 8/3/89.

NCEER-89-0020 "Structural Control Considering Time-Rate of Control Forces and Control Rate Constraints," by F.Y. Cheng and C.P. Pantelides, 8/3/89.

NCEER-89-0021 "Subsurface Conditions of Memphis and Shelby County," by K.W. Ng, T-S. Chang and H-H.M. Hwang, 7/26/89.

NCEER-89-0022 "Seismic Wave Propagation Effects on Straight Jointed Buried Pipelines," by K. Elhmadi and M.J. O'Rourke, 8/24/89.

NCEER-89-0023 "Workshop on Serviceability Analysis of Water Delivery Systems," edited by M. Grigoriu, 3/6/89.

NCEER-89-0024 "Shaking Table Study of a 1/5 Scale Steel Frame Composed of Tapered Members," by K.C. Chang, J.S. Hwang and G.C. Lee, 9/18/89.

NCEER-89-0025 "DYNA1D: A Computer Program for Nonlinear Seismic Site Response Analysis - Technical Documentation," by Jean H. Prevost, 9/14/89.

NCEER-89-0026 "1:4 Scale Model Studies of Active Tendon Systems and Active Mass Dampers for Aseismic Protection," by A.M. Reinhorn, T.T. Soong, R.C. Lin, Y.P. Yang, Y. Fukao, H. Abe and M. Nakai, 9/15/89.